Engineered Methods for Maturation of iPS-Derived Hepatocytes

By
Hamisha Ardalani

A dissertation submitted in partial fulfillment of
the requirements for the degree of:

Doctor of Philosophy
(Biomedical Engineering)

at the
University of Wisconsin-Madison
2019

Date of final oral examination: September 3rd, 2019

The dissertation is approved by the following members of the Final Oral Committee:

William L. Murphy, Professor, Biomedical Engineering (Advisor, Chair)
James A. Thomson, Professor, Cellular and Regenerative Biology (Advisor)
David Beebe, Professor, Biomedical Engineering
Christopher A. Bradfield, Professor, Molecular and Environmental Toxicology
Naomi C. Chesler, Professor, Biomedical Engineering

Abstract

Although the advent of iPS/ES-derived hepatocytes in the past decade has helped to bridge the gap between clinical demands and primary human hepatocyte (PHH) availability, those cells exhibit a fetal phenotype rather than a mature phenotype and therefore is not entirely on par with PHH. In order to create the mature iPS-derived hepatocytes (iHEP), we created an in vitro model with the focus on two significant areas known to play an important role on iHEP maturation: (i) cell-cell interaction (homotypic and heterotypic) and (ii) cell-extracellular matrix (ECM) interactions; both in the 3D culture context. We show that 3D culture of iHEPs and their co-culture with human sinusoidal endothelial cells (sECs) improves their maturity. In addition, co-culture of ECs self-organized into capillary-like structures within the hepatic 3D cultures, mimicking aspects of an *in vivo* architecture. Although iHEPs in 3D co-cultured with ECs are significantly more mature than iHEPs in monoculture, they express fetal markers and do not approach the maturity of adult PHHs. To further promote iHEP differentiation towards the adult PHH phenotype, alternative approaches should be explored, such as stimulation with the culture of iHEP aggregates in ECMs. However, the first step towards that goal is finding an ECM that is not only supportive of ECs to go through angiogenesis but also is supportive of iHEP metabolic functions and enzyme activities. To mimic aspect of cell-ECM interactions in vitro, we used synthetic biomaterials, which can serve as a powerful tool to deconstruct the microenvironmental influence on stem cell fate. We show that PEG hydrogels tethered with an adhesive peptide sequence (RGD), which promotes integrin-mediated cell adhesions, and matrix metalloproteinase-degradable crosslinker (KCGGPQGIWGQGCK) can be used to manipulate the ECM parameters to elicit responses that mimic the in vivo vasculogenesis and is also supportive of metabolic function of iPS-derived hepatocyte cultured in 3D aggregate format.

To my family.

Acknowledgments

"The seeds you plant with love and belief, they never perish". I started this journey with love and so much belief, there were times I doubted myself but the love of science kept me going; and there were countless times that I was despaired by experiments not working but the belief of my family, friends and mentors in me kept me en-route and assured me at the finish line of this marathon of PhD the seeds I planted at the start of this marathon and nurtured with love and occasionally hatred, belief and disbelief would finally blossom. To everyone who helped me on this journey I am forever grateful and am truly indebted to. I can't possibly pay you back, but I can promise to not let the blossomed seeds to perish and would try to grow this plant by paying it forward.

I'd like to start by thanking my dear advisors, Dr. William Murphy and Dr. James Thomson for their support, mentorship and encouragement throughout my entire PhD. The opportunities and resources that I have been granted in their labs are unmatched and I would have been ill-equipped to seize them without their mentorship. I appreciate their trust in me and the freedom they gave me to pursue variety of projects that drive my curiosity. I'd also like to thank my committee members: Drs. David Beebe, Christopher Bradfield, and Naomi Chesler, who have all been supportive.

I would also like to express my gratitude to every current and past member of the Thomson and Murphy lab who have supported me scientifically, professionally and personally throughout the graduate school. In particular, I would like to thank Dr. Kate Barteau, Dr. Eric Nguyen, Dr. Mike Schwartz, Dr. Angie Xie, Dr. Gaurav Kaushik, Victoria Harms, Ulrika Muller and Jim Melonda from the Murphy lab. Dr. Srikumar Sengupta, Jessica Antosiewics-Bourget, Jenifer Bollin and Erin Syth from the Thomson lab. Mitch Probasco for patiently teaching me the ins and

outs of axolotls when I started working voluntarily in the Thomson lab. Lauren Bischel for teaching me the basics of microfluidics. Morten Seirup is a wonderful friend, officemate and peer; I am grateful for the scientific and political discussions that we have had. Dr. Vernella Vickerman, is a wonderful friend and mentor; I am grateful for her mentorship and support both as a friend and as a colleague during the rollercoaster ride of graduate school.

I'd also like to express my gratitude to Dr. Ron Stewart for his great mentorship when I was working with the axolotls and his willingness to talk science. I'd also like to thank Dr. Amir Assadi, who not only was a great scientific mentor during my early days at UW but also a great second dad whom I am deeply indebted to. Thanks to my dear friend, Dr. Pegah Mehrpouya who was in trenches of PhD with me and was always willing to lend a kind ear or serve as a welcome distraction and to celebrate and share her experience with me.

Most importantly, I have been most fortunate to have the support and wisdom of my dear sister and my role model, Dr. Newsha Ardalani, whom I strove to achieve the examples set by her in the family; and my wonderful brother-in-law Dr. Tony Nowatzki and his parents in this journey. Last and foremost, I am thankful to my parents, Shokoufeh and Parviz, for the educational opportunities that they have provided me throughout my entire life. They always made sure my sister and I get the high-caliber education and have access to the best opportunities. They made sacrifices that at the time I might have not appreciated nor understood. Without my parents and their sacrifices, I would not be where I am today. Though we are thousands of miles away, I always had felt their unconditional love and unwavering support very near and dear to my heart, and for that I am eternally grateful.

Table of Contents

List of Figures

List of Tables

List of Movies

Chapter 1: Introduction

1.1 Background and Significance

Pluripotent stem cell-derived liver cells are a promising cell source for *in vitro* liver models and tissue-engineering applications. However, these cells do not replicate the function of primary human hepatocytes (PHH). Hepatocyte-like cells differentiated from pluripotent stem cells have lower synthetic ability and metabolic enzyme activity compared to primary hepatocytes, and unlike primary hepatocytes they consistently express immature hepatic markers such as α-fetoprotein (AFP). On the other hand, the use of PHH in applications such as drug toxicity screening [1] is limited due to donor to donor variability, limited supply, tendency to de-differentiate and rapid loss of hepatocyte-specific functions in conventional 2D monolayer cultures [2–4]. Therefore, there is a need for new approaches to mature induced pluripotent stem cell (iPS)-derived or embryonic stem cell (ES)-derived hepatocytes [5–7] as a substitute for PHH.

Early attempts to mature iPS/ES-derived hepatocytes were focused on two-dimensional (2D) differentiation protocols and use of chemical and small molecules [5–8]. More recent studies have demonstrated that three-dimensional (3D) culture better recapitulated the complex 3D interactions between cell-cell and cell-extracellular matrix (ECM) in the liver [9,10]. 3D cell culture systems, such as collagen matrices [11], micropatterned formats [12] or spheroid culture [13–15], have been used to recreate cell-cell junctions and mimic liver architecture more effectively than traditional sandwich cultures, leading to enhanced iPS-derived hepatocyte function. Limitations of these previous cell cultures include limited scalability, drug absorption/adsorption to the ECM, and batch-to-batch differences in 3D ECMs [16]. 3D spheroids may circumvent these limitations. However, 3D spheroid cultures that include non-parenchymal cells (NPCs) have typically been conducted with primary mouse cells [15], which do not

recapitulate human liver physiology. This thesis describes methods that mimic aspects of the liver lobule during liver development, including the 3D structure, heterotypic cell-cell interactions and cell-ECM interactions. We show the effect of those factors on metabolic function and CYP450 enzyme activity of the iPS-derived hepatocytes. Our 3D culture platform is compatible with standard assay plates and automation, which makes the approach suitable for high-throughput drug toxicity screening. Moreover, the media is serum-free and chemically defined. It is important for studies in which binding of drugs or drug metabolites to serum proteins may confound the interpretation of data. Unlike previous studies, our 3D co-cultured platform used cells all from human origin, and this is important due to differences in drug metabolism and toxicity pathways between rodents and humans [17–20].

To mimic the aspect of cell-ECM interactions in vitro, we used synthetic biomaterials, which can serve as a powerful tool to deconstruct the microenvironmental influence on stem cell fate. Here, we used chemically-defined poly (ethylene glycol) (PEG)-based hydrogels. PEG is an attractive biomaterial substrate because of its inherent ability to resist nonspecific protein adsorption and cell attachment [21] by virtue of its structured interaction with water [22,23]. Additionally, PEG is routinely used as a biomaterial substrate because of the numerous chemistries available for crosslinking and attachment of tethered macromolecules [24]. We show that PEG hydrogels tethered with Arg-Gly-Glu (RGD) an adhesive peptide sequence, which promotes integrin-mediated cell adhesions, and matrix metalloproteinase-degradable crosslinker (KCGGPQGIWGQGCK) can be used to manipulate the ECM parameters to elicit responses that mimic the in vivo vasculogenesis and is also supportive of metabolic function of iPS-derived hepatocyte cultured in 3D aggregate format.

1.2 Summary of the Work

Chapter 2 of this thesis provides a comprehensive overview of the different stages of liver development, the effect of sinusoidal endothelial cells (sECs), extracellular matrix (ECM) and integrin-binding ligands on hepatocyte maturation, and how this information can be used to produce more mature induced pluripotent stem (iPS) or embryonic stem (ES) derived cells. Since endothelial cells and vascular development plays an important role in organ development and in particular liver development, Chapter 3 of this thesis provides an overview of the structure of blood vessels and key signaling molecules, which play significant role in vasculogenesis, angiogenesis and maturation of nascent blood, role of ECM and recent advances in making tissue-engineered blood vessels (both macro- and micro-vessels) *ex vivo*.

Chapter 4 focuses on the effect of 3D culture and liver non-parenchymal cells on maturation of iPS derived hepatocytes. We show that 3D culture of iPS-derived hepatocytes and their co-culture with human sinusoidal endothelial cells (sECs) improves their maturity. In addition, co-culture of ECs formed endothelial networks within the hepatic 3D cultures, mimicking aspects of an *in vivo* architecture. Although iHEPs in 3D co-cultured with ECs were significantly more mature than iHEPs in monoculture, they express fetal markers and do not approach the maturity of adult PHHs. To further promote iHEP differentiation towards the adult PHH phenotype, alternative approaches should be explored, such as stimulation with small molecules or culturing iHEP aggregates in ECMs. Such ECM should be supportive of the functions of both ECs and iHEPs.

Chapter 5 then describes a chemically defined synthetic PEG hydrogel, that allows iPS-derived endothelial cells to self-organize into capillary networks through mechanisms consistent with *in vivo* vascular morphogenesis. We show that capillary tubules with patent lumens are stable for at least 14 days when endothelial cells, without the support of mural cells, are encapsulated in PEG hydrogels and are polymerized within the passive flow microfluidic device. This suggests that lack of mural cells does not entirely account for the regression of vascular networks in vitro.

In Chapter 6, we then used the PEG formulation identified in Chapter 5 and show that PEG hydrogels at 50% crosslinking density with the shear modulus of 785±40 Pa and no adhesive peptides supports iHEP aggregate metabolic functions and enzyme activities, similar to naturally derived ECM such as Matrigel. Finally, in Chapter 7 we summarize our findings, address limitations of our studies, and suggest avenues to pursue in future extensions of this work. Collectively, this thesis describes methods to improve metabolic function and enzyme activity of iPS derived hepatocyte, and highlights how 3D culture, cell-cell, and cell-ECM interactions can affect the metabolic function of iPS-derived hepatocytes.

1.3 References

[1] I.M. Arias, ed., The liver: biology and pathobiology, 5. ed., 1. impr, Wiley-Blackwell, Chichester, 2009.

[2] G. Elaut, T. Henkens, P. Papeleu, S. Snykers, M. Vinken, T. Vanhaecke, V. Rogiers, Molecular mechanisms underlying the dedifferentiation process of isolated hepatocytes and their cultures, Curr. Drug Metab. 7 (2006) 629–660.

[3] J. Fraczek, J. Bolleyn, T. Vanhaecke, V. Rogiers, M. Vinken, Primary hepatocyte cultures for pharmaco-toxicological studies: at the busy crossroad of various anti-dedifferentiation strategies, Arch. Toxicol. 87 (2013) 577–610. doi:10.1007/s00204-012-0983-3.

[4] T.D. Boyer, M.P. Manns, A.J. Sanyal, D. Zakim, eds., Zakim and Boyer's hepatology: a textbook of liver disease, 6th ed, Saunders/Elsevier, Philadelphia, PA, 2012.

[5] K. Si-Tayeb, F.K. Noto, M. Nagaoka, J. Li, M.A. Battle, C. Duris, P.E. North, S. Dalton, S.A. Duncan, Highly efficient generation of human hepatocyte-like cells from induced pluripotent stem cells, Hepatology. 51 (2010) 297–305. doi:10.1002/hep.23354.

[6] Z. Song, J. Cai, Y. Liu, D. Zhao, J. Yong, S. Duo, X. Song, Y. Guo, Y. Zhao, H. Qin, X. Yin, C. Wu, J. Che, S. Lu, M. Ding, H. Deng, Efficient generation of hepatocyte-like cells from human induced pluripotent stem cells, Cell Research. 19 (2009) 1233–1242. doi:10.1038/cr.2009.107.

[7] T. Touboul, N.R.F. Hannan, S. Corbineau, A. Martinez, C. Martinet, S. Branchereau, S. Mainot, H. Strick-Marchand, R. Pedersen, J. Di Santo, A. Weber, L. Vallier, Generation of functional hepatocytes from human embryonic stem cells under chemically defined conditions that recapitulate liver development, Hepatology. 51 (2010) 1754–1765. doi:10.1002/hep.23506.

[8] J. Shan, R.E. Schwartz, N.T. Ross, D.J. Logan, D. Thomas, S.A. Duncan, T.E. North, W. Goessling, A.E. Carpenter, S.N. Bhatia, Identification of small molecules for human hepatocyte expansion and iPS differentiation, Nature Chemical Biology. 9 (2013) 514–520. doi:10.1038/nchembio.1270.

[9] T. Takebe, K. Sekine, M. Enomura, H. Koike, M. Kimura, T. Ogaeri, R.-R. Zhang, Y. Ueno, Y.-W. Zheng, N. Koike, S. Aoyama, Y. Adachi, H. Taniguchi, Vascularized and functional human liver from an iPSC-derived organ bud transplant, Nature. 499 (2013) 481–484. doi:10.1038/nature12271.

[10] T. Takebe, R.-R. Zhang, H. Koike, M. Kimura, E. Yoshizawa, M. Enomura, N. Koike, K. Sekine, H. Taniguchi, Generation of a vascularized and functional human liver from an iPSC-derived organ bud transplant, Nature Protocols. 9 (2014) 396–409. doi:10.1038/nprot.2014.020.

[11] R.L. Gieseck III, N.R.F. Hannan, R. Bort, N.A. Hanley, R.A.L. Drake, G.W.W. Cameron, T.A. Wynn, L. Vallier, Maturation of Induced Pluripotent Stem Cell Derived Hepatocytes by 3D-Culture, PLoS ONE. 9 (2014) e86372. doi:10.1371/journal.pone.0086372.

[12] D.R. Berger, B.R. Ware, M.D. Davidson, S.R. Allsup, S.R. Khetani, Enhancing the functional maturity of induced pluripotent stem cell-derived human hepatocytes by controlled presentation of cell-cell interactions in vitro, Hepatology. 61 (2015) 1370–1381. doi:10.1002/hep.27621.

[13] K. Takayama, K. Kawabata, Y. Nagamoto, K. Kishimoto, K. Tashiro, F. Sakurai, M. Tachibana, K. Kanda, T. Hayakawa, M.K. Furue, H. Mizuguchi, 3D spheroid culture of hESC/hiPSC-derived hepatocyte-like cells for drug toxicity testing, Biomaterials. 34 (2013) 1781–1789. doi:10.1016/j.biomaterials.2012.11.029.

[14] S. Sengupta, B.P. Johnson, S.A. Swanson, R. Stewart, C.A. Bradfield, J.A. Thomson, Aggregate Culture of Human Embryonic Stem Cell-Derived Hepatocytes in Suspension Are an Improved In Vitro Model for Drug Metabolism and Toxicity Testing, Toxicological Sciences. 140 (2014) 236–245. doi:10.1093/toxsci/kfu069.

[15] W. Song, Y.-C. Lu, A.S. Frankel, D. An, R.E. Schwartz, M. Ma, Engraftment of human induced pluripotent stem cell-derived hepatocytes in immunocompetent mice via 3D co-aggregation and encapsulation, Scientific Reports. 5 (2015). doi:10.1038/srep16884.

[16] P. Godoy, N.J. Hewitt, U. Albrecht, M.E. Andersen, N. Ansari, S. Bhattacharya, J.G. Bode, J. et al. , Recent advances in 2D and 3D in vitro systems using primary hepatocytes, alternative hepatocyte sources and non-parenchymal liver cells and their use in investigating mechanisms of hepatotoxicity, cell signaling and ADME, Archives of Toxicology. 87 (2013) 1315–1530. doi:10.1007/s00204-013-1078-5.

[17] C. Lu, A.P. Li, Species comparison in P450 induction: effects of dexamethasone, omeprazole, and rifampin on P450 isoforms 1A and 3A in primary cultured hepatocytes from

man, Sprague-Dawley rat, minipig, and beagle dog, Chem. Biol. Interact. 134 (2001) 271–281.
[18] H. Shih, G.V. Pickwell, D.K. Guenette, B. Bilir, L.C. Quattrochi, Species differences in hepatocyte induction of CYP1A1 and CYP1A2 by omeprazole, Human & Experimental Toxicology. 18 (1999) 95–105. doi:10.1177/096032719901800206.
[19] D.R. Nelson, Cytochrome P450 and the individuality of species, Arch. Biochem. Biophys. 369 (1999) 1–10. doi:10.1006/abbi.1999.1352.
[20] H. Olson, G. Betton, D. Robinson, K. Thomas, A. Monro, G. Kolaja, P. Lilly, J. Sanders, G. Sipes, W. Bracken, M. Dorato, K. Van Deun, P. Smith, B. Berger, A. Heller, Concordance of the Toxicity of Pharmaceuticals in Humans and in Animals, Regulatory Toxicology and Pharmacology. 32 (2000) 56–67. doi:10.1006/rtph.2000.1399.
[21] K. Holmberg, K. Bergström, C. Brink, E. Österberg, F. Tiberg, J.M. Harris, Effects on protein adsorption, bacterial adhesion and contact angle of grafting PEG chains to polystyrene, Journal of Adhesion Science and Technology. 7 (1993) 503–517. doi:10.1163/156856193X00826.
[22] Z. Yang, J.A. Galloway, H. Yu, Protein Interactions with Poly(ethylene glycol) Self-Assembled Monolayers on Glass Substrates: Diffusion and Adsorption, Langmuir. 15 (1999) 8405–8411. doi:10.1021/la990260y.
[23] J.M. Harris, E.C. Struck, M.G. Case, M.S. Paley, M. Yalpani, J.M. Van Alstine, D.E. Brooks, Synthesis and characterization of poly(ethylene glycol) derivatives, J. Polym. Sci. Polym. Chem. Ed. 22 (1984) 341–352. doi:10.1002/pol.1984.170220207.
[24] J. Zhu, Bioactive modification of poly(ethylene glycol) hydrogels for tissue engineering, Biomaterials. 31 (2010) 4639–4656. doi:10.1016/j.biomaterials.2010.02.044.

Chapter 2: Endothelial cells and hepatocytes in the liver: From organogenesis to in vitro liver models

Hamisha Ardalani, James A. Thomson, William L. Murphy. "Endothelial cells and hepatocytes in the liver: From organogenesis to in vitro liver models." In Preparation.

2.1 Introduction

Development of pluripotent stem cell derived liver cells, in particular hepatocytes and endothelial cells, points to a promising source of cells for use in *in vitro* liver models, therapies and tissue-engineering applications. However, thus far, attempts to make mature adult liver cells *ex vivo* have been unsuccessful. Here, we review different stages of liver development, the effect of sinusoidal endothelial cells (sECs), extracellular matrix (ECM) and integrin bindings on hepatocyte maturation, and how this information can be used to produce more mature induced pluripotent stem (iPS) or embryonic stem (ES) derived cells.

In Section 2.2 and 2.3, we discuss the role of endothelial cells in organ development with a focus on the liver. Next, we review the role of specialized liver endothelial cells referred to as sECs in hepatocyte maturation and liver disease initiation, in Section 2.3 and 2.4, respectively. After explaining the importance of vasculogenesis and angiogenesis in hepatocyte maturation and liver development, we review vascular models *in vitro* established in the field in Section 2.5. As type of cells used in liver models *in vitro* impacts significantly the relevancy of those models or studies to human liver physiology, we review different types of non-parenchymal cells used in the field as well as discuss the importance of iPS/ES derived cells in Section 2.6. Moreover, the liver research community faces the problem of iPS/ES derived hepatocyte cell immaturity, thus we review strategies for developing a hepatocyte closer to primary human hepatocytes in Section 2.7.

As changes in ECM components occurs in parallel to maturation of cells across the liver lobule, we review the change of ECM and integrin ligands during fetal liver development and in the adult liver in Section 2.8. Different types of biomaterials used for culturing liver cells are discussed in Section 2.9.

2.2 Role of endothelial cells in organ development

The role of endothelial cells in organ development was recognized thousands of years ago by Aristotle (384-322 B.C.). By observing the development of the chick embryo, he noticed that each part of the embryo is located in the vicinity of the vascular structure. Thus, he concluded that vascular architecture in the embryo functions as a “frame” or “model” which shapes the body structure of the growing organism [1]. Aristotle was right; and now we know blood vessels that perfuse all tissues in the body mediate a vital metabolic exchange between tissue and blood. Indeed, it is the endothelium of the blood vessels that enables this exchange. In the following sections, we discuss the role of endothelial cells in organ development and, more specifically, their role in the liver.

2.2.1 Ability of endothelial cells to promote organ development

Apart from the apparent role of endothelial cells in vascular development, there is emerging evidence that endothelial cells play an important part in organ development and cell differentiation even before blood flow is established in the organ. Endothelial cells are active in embryo patterning, organ differentiation, and postnatal tissue modeling. There is a reciprocal signal interaction between endothelial cells and surrounding cells that results in organ development, homeostasis, and tissue patterning, while endothelial cells acquire specific characteristics and phenotype based on signals received from their microenvironment [2–5].

The role of endothelial cells in the development of different organs is evidenced by experiments such as knock-out results or other forms of cellular interventions. Often, disruption of blood vessel architecture results in disruption of specific tissue type as a consequence of the loss of endothelial cell signaling. For example, when VEGF signaling is disrupted in mouse kidney glomerular epithelium, it results in capillary depletion and a dramatic decrease in number of nephrons [6,7]. In another example, overexpression of VEGF in lung mesenchyme results in an increase in size of central pulmonary vessels and a decrease in number of terminal buds, as well as inhibition of type I alveolar cell differentiation [8].

2.2.2 Why is liver a good model to investigate role of endothelial cells in organ development?

Since liver vasculature is necessary for early hematopoietic tissue function, it is a good model to study the role of endothelial cells in organ development. Moreover, when the liver bud is forming during liver development, and prior to blood circulation, endothelial precursor cells interact with developing hepatic epithelium and the septum transversum; this close contact with blood vessels continues as hepatoblast cells migrate into the stroma. In the following section, we discuss the emergence and development of hepatic sinusoids in humans along with their instructive vascular niche role in hepatocyte differentiation and maturation.

2.3 What is role of vascularization in hepatogenesis and hepatocyte maturation?

Endothelial cells induce organogenesis before the development of circulation during embryo development; oxygen and nutrients are delivered to the tissue through passive conduits formed by endothelial cells. Endothelial cells also set up an instructive vascular niche that can stimulate organ regeneration [9]. Here, we specifically discuss the emergence and development

of hepatic sinusoids in humans along with their instructive vascular niche roles in hepatocyte differentiation, maturation, and metabolic zonation.

2.3.1 Endothelial and vascular emergence during liver development and its connection to hepatocyte maturation

Sinusoids are the smallest blood vessels of the liver and are the first blood vessels to form during hepatogenesis. Sinusoids transfer blood from a hepatic artery and portal vein throughout the liver lobules. Sinusoidal endothelial cells play an essential role in the transfer of solutes and soluble macro-molecules between serum and hepatocytes [10]. Sinusoids are mainly formed through angiogenesis from existing blood vessels in the septum transversum mesenchyme [11]. However, some studies suggest the formation of sinusoids may be facilitated by the introduction of endothelial cells originated from mesothelial precursors, at least in avian embryos [12].

Early structural differentiation of hepatic sinusoids occurs between 5- and 12-weeks' gestation in humans. At 5 weeks' gestation where the hepatic sinusoids are still primitive, the foregut (endoderm) forms the liver primordium. Liver primordium is essentially hepatoblasts arranged in thick cords separated by vascular spaces. The liver primordium starts to grow into the septum transversum (mesoderm) in which the hepatic sinusoids are developing (Fig. 2.1a). Initially, at 5 weeks' gestation in humans, the endothelial lining is continuous with a basement membrane and shows no fenestrations. Around 12 weeks' gestation, fenestrations appear with diaphragms which later disappear during development; mature sinusoidal endothelial cells are fenestrated (ranging from 50-200 nm) to facilitate transfer of molecules from the surface of hepatocytes to the sinusoidal lumen [13]. During this period (5 to 12 weeks' gestation), liver sinusoidal endothelial cells gradually lose cell markers of continuous endothelial cells such as

CD31(PECAM-1), CD34 and 1F10 antigen and acquire adult sinusoidal markers such as CD4, CD32 and ICAM-1, VAP1, Stabilin 1 and 2, L-SIGN, Reelin and Von Willebrand factor (Fig. 2. 1b) [14–16]. Blood flow velocity in the sinusoids is estimated to be around 407-452 μm/s, which is significantly slower than the velocity of flow in other capillaries (599-1000 μm/s) [17]. Since endothelial cells are in contact with hepatocytes early on in liver development, it raises the question of whether or not sECs have any role in liver morphogenesis and hepatic differentiation. Mouse studies have verified critical role of endothelial cells in liver development by a null mutation in the mouse's vascular endothelial growth factor receptor gene (VEGFR-2 or FLK-1), which resulted in embryos that lack endothelial cells and hepatoblast that failed to delaminate in the embryo [18]. Liver bud growth was arrested as a result of angiogenesis repression, suggesting that endothelial cells provide important paracrine signals in addition to the physical factors to promote hepatoblast migration and proliferation. Moreover, endothelial cells are essential for biliary duct epithelium differentiation through activation of the NOTCH signaling pathway. The communication between endothelial cells and hepatoblasts is reciprocal as deletion of HNF4-alpha, a critical nuclear receptor for hepatoblasts, results in endothelial cells loss, in addition to loss in hepatocyte polarity [19].

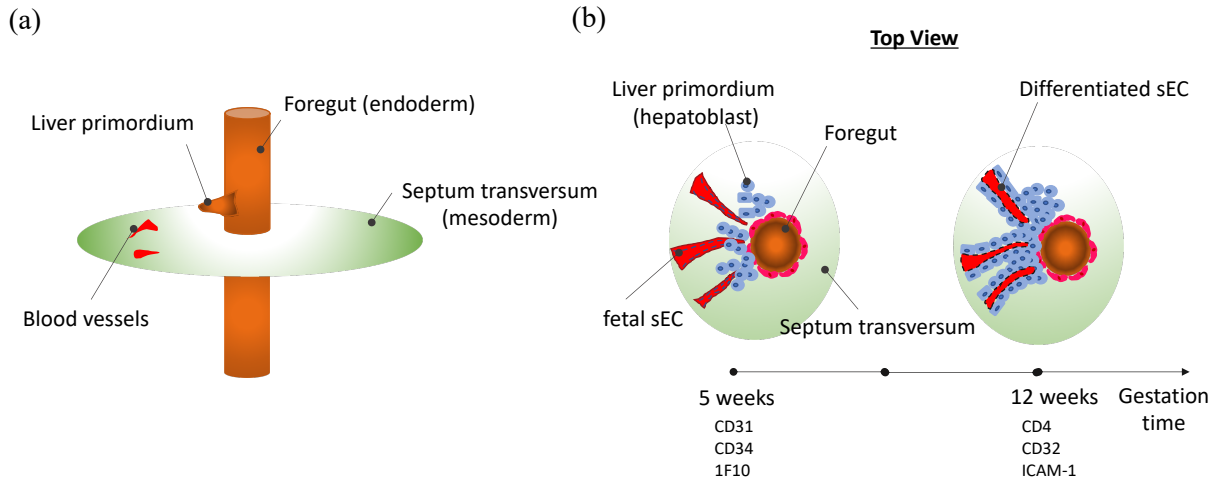

Figure 2.1 Formation of sinusoids during human embryogenesis. Adapted and re-drawn from Poisson, J. et al.[15] **(a)** Early emergence of primitive sECs when liver primordium is formed at 5 weeks' gestation. Liver primordium starts to grow into the septum transversum (mesoderm) in which the hepatic sinusoids are developing. **(b)** Top view of Fig 2.1a. At 5 weeks' gestation in humans, the endothelial lining is continuous with a basement membrane and shows no fenestrations. Around 12 weeks' gestation, fenestrations appear, and the basement membrane starts to disappear. Sinusoidal endothelial cells gradually lose cell markers of continuous endothelial cells and acquire adult sinusoidal markers.

2.3.2 Role of sinusoidal endothelial cells on hepatocyte zonation?

As mentioned earlier in Section 2.3.1, sECs are fenestrated. The size of fenestrae differs from 50-200 nm depending on the location [13]. sECs in the periportal area have larger fenestrae but fewer fenestrae per sieve plate. Sieve plates are group of 10-100 fenestrae aggregated together. sECs in the perivenous area have smaller fenestrae but they are more numerous per sieve plate. Perhaps this is attributed to the increasing need for oxygen exchange due to a decrease in oxygen tension from the periportal region (P_{O2}=60-70 mmHg or 10-12%) to the perivenous region (P_{O2}=25-35 mmHg or 3-5%) in the liver acinus [20,21]. In addition to sECs structural heterogeneity along the liver lobule, hepatocytes show heterogeneity in their metabolic capacity along the liver lobule. Metabolically, the liver acinus is divided into 3 different zones: zone 1,

periportal zone (highly oxygenated); zone 2, transition zone (intermediate oxygen level); and zone 3, perivenous zone (least oxygenated). For example, albumin and urea synthesis, oxidative phosphorylation, and gluconeogenesis are elevated in zone 1; while glycolysis, lipogenesis and xenobiotic metabolism are increased in zone 3. Many factors like O_2 and hormone gradients, ECM composition, and non-parenchymal cell distribution contribute to hepatic zonation [21,22]. Specifically, the oxygen gradient is important in creating metabolic gradients along the liver lobule.

The direct relationship between sECs and hepatocyte zonation has not been studied yet. A number of reports have indicated that beta-catenin, hedgehog signaling, and the oxygen gradient contribute to metabolic zonation [22–24]. Here, we focus on the oxygen gradient effect on the metabolic zonation of the liver and its relationship to sECs. Hypoxia-inducible factor (HIF) is an important transcription factor found at high levels in the oxygen-poor zone of the liver (perivenous zone) and is an important player in the establishment of hepatic zonation [25]. HIF can regulate many genes, such as VEGF, in response to the oxygen gradient in the liver [26]. VEGF produced by epithelial cells is essential for vascular development and morphogenesis of hepatic sinusoids. It is shown that lack of VEGF from liver epithelial lineage during mid-gestational development disturbs zonal endothelial cells, hepatocyte cell differentiation, and formation of proper 3D vascular and zonal architecture [27]. Moreover, HIF can regulate metabolic liver functions such as insulin regulation, gluconeogenesis, lipogenesis and ketone bodies [28]. It also plays a vital role in structural maintenance of the liver, as HIF-1A deficiency in mice results in the extension of hepatic lobule, enhanced lobular oxygen consumption, and increased content of mitochondrial DNA [29]. Thus, crosstalk between hepatocytes and sECs are responsible for proper zonation of the liver.

2.4 Role of sinusoidal endothelial cells in liver diseases

The essential role of sinusoidal endothelial cells for proper liver development is discussed earlier in Sections 2.2 and 2.3. Here, we discuss its role in initiating diseases associated with the liver. The role of liver sECs in chronic liver disease is established through these four primary processes: 1) capillarization of sinusoids, 2) angiogenesis, 3) angiocrine signals, and 4) vasoconstriction [15].

Capillarization happens when sECs dedifferentiate, lose their fenestrae, and develop the basement membrane. It is an early event in an injured liver, occurring before hepatic stellate cells and macrophages are activated [30,31].

Angiogenesis is the development of new vessels from preexisting vessels that happens during liver fibrogenesis. Liver fibrosis and angiogenesis are correlated events. As fibrosis enhances hepatic angiogenesis and angiogenesis enhances liver fibrosis [32]. Angiocrine signals are the paracrine factors that sECs produce for maintenance of organ homeostasis, provides the balance between self-renewal and differentiation of stem cells, organ regeneration, and tumor growth. Ding et al. have insightful review of the role of angiocrine signals produced by sECs in liver fibrosis and liver regeneration [33].

2.4.1 Role of sinusoidal endothelial cells in chronic liver diseases

Endothelial dysfunction is evidenced in chronic liver disease and advanced cirrhosis. In a healthy liver, exposure of sECs to physiological shear stress activates transcription factor such as Kruppel factor 2 (KLF2), that leads to the upregulation of vasodilating agents (nitric oxide [NO]) and downregulation of vasoconstricting agents (endothelin-1). Vasodilation helps attenuate the increase in blood pressure. Moreover, NO produced by sECs maintains the quiescence state of hepatic stellate cells. However, in a chronic liver disease like cirrhosis, sECs are capillarized which

leads to activation of hSCs and the production of collagen and fibrosis. This change means sECs are no longer sensitive to the shear stress and, instead of dilating when shear stress increases, they constrict, and the vasoconstriction leads to intrahepatic resistance [15,34].

2.4.2 Role of sinusoidal endothelial cells in hepatocellular carcinoma

Hepatocellular carcinoma (HCC) usually happens in the context of chronic liver disease. It is associated with changes in sECs within and around the tumor. sEC markers (Stabilin-1 and 2, LYVE-1 and CD32b) are lost during tumor progression. sECs derived from HCC have higher expression of integrins and lower expression of ICAM-1 compared to normal human liver sECs. They also have higher angiogenic, pro-coagulant, and fibrinolytic capacities compared to healthy human liver sECs.

2.4.3 Role of sinusoidal endothelial cells in liver regeneration

As mentioned earlier (Section 2.2.1), endothelial cells play a significant role in organ development, so it is not surprising that LSECs play an essential role in liver regeneration [9,33]. Liver regeneration occurs after acute liver injuries or partial hepatectomy. After resection of the liver, shear stress increases on sECs because the portal flow per gram of tissue immediately increases in the early stages. An increase in shear stress on sECs leads to the release of NO, sensitizing hepatocyte to hepatocyte growth factor (HGF) and encouraging hepatocyte proliferation. In later stages, sECs also start to proliferate. The proliferation of sECs is caused by upregulation of angiopoietin-2 and VEGFR2/VEGFA pathways [15].

2.4.4 Role of sinusoidal endothelial cells in inflammation and infection

Since sECs are a barrier between blood and liver, they play a key factor in restricting or enabling the entrance of leucocytes (or white blood cells) to the liver. The role of sECs in enabling entrance of leucocytes to the liver is as follows: sECs express ICAM-1 and VAP-1 (vascular adhesion protein-1) which allows leucocytes to adhere to ECs [35], and inflammation leads to overexpression of ICAM-1and VAP-1, allowing trans-endothelial migration of leucocytes or white blood cells (Specifically, Stablin-1 is known to induce T-cell trans-endothelial migration) [36]; The role of sECs in inhibiting entrance of leucocytes to the liver is as follows: sECs can inhibit the entrance of leucocytes by modulating lymphocyte behavior. Antigen presentation by sECs leads to tolerance induction in $CD8^+$ cells (Subcategory of T Cells) [37]. Moreover, sECs can induce differentiation of T-cells into immunosuppressive regulatory T cells (Treg) [38]. sECs can also modulate the anti-inflammatory actions in the liver by the increase in IL-10 in Th1 cells, an anti-inflammatory cytokine [39]. Also, the expression of Lectin on the surface of sECs makes them a vulnerable target for pathogens, like hepatitis B and C viruses; thus they can induce infection in hepatocytes [40].

2.5 *In vitro* liver vascular models

Unlike other tissues like cornea and skin that can absorb nutrients and oxygen from their environments by diffusion, liver tissues are highly vascularized and metabolically more demanding, making diffusion insufficient for delivery of nutrients and oxygen to all the cells. In fact, the liver contains more than 100 billion hepatocytes positioned within 50 μm of the sinusoids [41]. Thus, incorporating endothelial cells that can form connected, perfusable vasculature is an important aspect often underscored in developed *in vitro* liver models.

A variety of approaches have been developed to promote vascularization in *in vitro* human liver models. Those approaches can be categorized into three different categories: 1) self-

assembled spheroids/organoids, 2) bio-printed livers, and 3) engineered liver tissues or liver-on-a-chip. We have summarized the benefits and limitations of each category in Table 2.1. We have also included studies using endothelial cells in each category and reviewed whether or not endothelial cells could form any connected vasculature reminiscent of liver sinusoids.

As discussed in Section 2.3.2, liver acinus has three different zones with different oxygen tensions. There are very few *in vitro* liver models that can recapitulate the metabolic zonation and gradient in oxygen tension. For example, Allen et al. created a bioreactor platform where they control the oxygen gradient along the area in which hepatocytes are cultured [42]. D. L. Taylor group created multiple generations of a liver on a chip platform called LAMP, Liver Acinus Micro Physiology system, in which they create different metabolic zones by controlling oxygen tension [21,43]. Such *in vitro* liver models with the ability to recapitulate the complex cellular microenvironment and structural organization of the liver are useful for investigating the role of zonation in physiology, toxicology, and disease progression.

Table 2.1. In vitro liver models

Model	Connected Vasculature	Benefits	Limitations
Self-assembled spheroids/organoids Cells and origin Human: upcyte^{R}*hepatocytes, upcyte^{R} sECs, upcyte^{R} MSCs[44] Human: hepatic endoderm cells, HUVECs, MSCs[45,46] Human: hepatocytes, KCs, sECs[47] Human: hepatocytes, HUVECs, hSCs[48]	No Yes No No	• Easy to make • High throughput	• No control over cell distribution • In the absence of perfusable vasculature, cellular necrosis can happen in the core of organoids if the diameter is bigger than 250-300 μM
Bio-printed liver Cells and origin Human: HepG2, HUVECs[49] Human: hepatocytes, mouse: fibroblast [50] Human: hepatocytes, human dermal fibroblast, HUVECs[51] Mouse: sECs, KCs, hSCs, hepatocytes[52]	No Yes† Yes Yes	• Allows for spatial control over cell layout to mimic the exact liver architecture • Automated and reproducible	• Low throughput • Complex and expensive instruments • Require a large number of cells • In the absence of perfusable vasculature, it can develop necrosis.
Engineered liver tissue and liver-on-a-chip Cells and origin Rat: hSC, sECs, hepatocytes [53] Rat: hSC, sEC, hepatocytes[54] Human: iPS-derived hepatocyte and TMNK1(sEC line)[55] Human: HUVEC-D, THP-1 (monocyte as KC), LX-2 (immortalized hSC line), hepatocytes[21] Human: sECs, THP-1 (monocyte as KC), LX-2 (immortalized hSC line), hepatocytes[43]	No No No No Yes	• Allows for control over the fluid flow properties • Constant change of the nutrient and waste	• Low throughput • Perfusion requires fluid pumps and control systems • Large dead volumes due to the tubing system • Potential binding of drugs and bio-chemicals to the tubing

*Upcyte® cells are genetically engineered cell strains derived from primary human cells by lentiviral transduction of genes or gene combinations inducing transient proliferation capacity.

†Although Kizawa et al. did not add endothelial cells during construction of the bio-printed tissue, they observed vascular network structure. The authors assumed the structures are due to heterogeneity in the commercially available primary hepatocyte.

Abbreviations: KC, Kupffer cell; hSC: hepatic stellate cell; sEC, sinusoidal endothelial cell; MSC, mesenchymal stem cell; HUVEC, human umbilical vein endothelial cells; HUVEC-D, human dermal microvascular endothelial cells

2.6 Cells used in liver models and the importance of iPS/ES derived cells

The source of cells used in *in vitro* liver models has a significant impact on observed biological responses as well as the relevancy of those models to human liver physiology. In the following section, we review sources of non-parenchymal cells used in *in vitro* liver models and the recent advances in generating those cells from ES or iPS cells.

2.6.1 Why are sinusoidal endothelial cells rarely used in in vitro liver models?

There are multiple reasons why sECs are not commonly used in *in vitro* liver models, including rapid disappearance of fenestrae, development of basement membrane, and change in expression of cell surface markers after sECs are cultured as monolayers. There is also a lack of consensus among research groups regarding identification and isolation of sECs. There is no single marker specific to sECs, and combinations of markers are necessary for their identification. For example, Ding et al. group identified sECs by VEGFR3^{+} CD34^{-} VEGFR2^{+} VE-cadherin^{+} Factor VIII^{+} CD45^{-} [33], and Lalor et al. identified sECs by CD31^{+}, LYVE-1^{+}, L-SIGN^{+}, Stablin-1^{+}, CD34^{-}, PROX1^{-} [56]. Particularly, the expression of CD31 (classical endothelial cell surface marker) by sECs is controversial; some studies report its expression in sECs evidenced by immunohistochemistry, while other studies report its absence in flow cytometry data [10]. As a result, not only is it difficult to acquire a pure population of sECs but also the rapid de-differentiation of sECs is an issue after the *in vitro* culture. Studies have shown that co-culture of sECs with both hepatocytes and fibroblasts and the use of coated plates with an ECM derived from

Space of Disse have allowed sECs to keep their differentiated state [57]. Since sECs are exposed to lower oxygen pressures along the liver lobule *in vivo* (90 -30 mmHg), culturing them in atmospheric oxygen pressure (160 mmHg) has an adverse effect on their survival. It is shown that culturing sECs at 5% O_2 instead of the commonly used 20% O_2 would improve sECs survival in culture [58].

On the other hand, manufactured immortalized sEC lines are not exact replicas of actual sECs. For example, TMNK-1 and iSEC cell lines, immortalized by viral transfection, do not have fenestrae [59,60]. Moreover, the immortality of the produced cell lines makes them susceptible to react differently than primary sECs in response to external factors such as stress. Poisson and colleagues have an insightful review of different sEC lines [15]. Because of the limitations that sECs have, other endothelial cell sources such as human umbilical vein endothelial cells (HUVECs) are used by researchers in place of sECs.

2.6.2 State of the field on iPS/ES derived sECs, hSCs, Kupffer cells and Cholangiocytes

Koui and colleagues recently published a study reported generation of liver sinusoidal endothelial progenitors from human iPS cells. They showed that cultured cells maintain high expression of sEC progenitor markers: *FLK1, CD34, CD31, CDH5, STAB2, and LYVE1*. Additionally, they showed successful cryopreservation of the cells without phenotypic changes [61]. In another study, Coll and colleagues showed successful generation of hepatic stellate cells from human iPS cells. They showed that derived hSCs are between the quiescence and activated states by looking at the gene expression profiles. Moreover, functional assays showed the hSCs could accumulate retinyl esters in lipid droplets and become activated in response to stimuli like mediators of wound healing [62]. Also, recently developed protocol by Buchrieser and colleagues for deriving monocyte from pluripotent stem cells could be a potential model for Kupffer cells

[63]. Successful generation of Cholangiocytes or biliary epithelial cells derived from pluripotent stem cells with some degree of functionality like bile acid transfer and alkaline phosphate activity was reported in multiple papers as well [64–66].

2.6.3 What is the importance of using iPS/ES derived cells in in vitro liver models?

Since liver is an essential organ in drug testing, animals are often used as part of the drug development process. However, results from animals are often misleading due to differences in levels and substrate specificity of liver enzymes between animals and humans. Forty to fifty percent of all failures in clinical drug development are due to unexpected toxicity and pharmacokinetic problems [65]; this is due to the fact that hepatic clearance and chemical profiles of metabolites of animal models are not a good representative of human profiles. Human cell systems, like human hepatocytes, immortalized cell lines, and liver microsomes, are also not adequate to replace animal models. For instance, isolated human hepatocytes lose expression of key enzymes such as CYP450 after isolation and rapidly de-differentiate. Cell lines that are derived from tumors [67–69] often do not have the correct morphology and polarization for vectorial drug transport (transport of a molecule or an ion across an epithelium or endothelium in a certain direction) from plasma to the bile [70]. Microsomes, vesicles formed from the endoplasmic reticulum and contain phase I enzymes, lack complete drug metabolizing enzymes and transporters for all types of drugs. Therefore, there is a need for new sources of cells. The ideal source of cells is from stem cells, which could be expanded for large clonal populations and be differentiated to any cell line, including hepatocytes. Pluripotent cells currently available for research are either human embryonic stem cells (hESCs) or induced pluripotent stem cells (iPSCs). The former is isolated from inner cell mass of the human blastocyst (5 days post-fertilization) [71], and the latter is programmed from human somatic cells [72,73].

Pluripotent stem cells are attractive models for studying liver development and disease. First, researchers have the option of choosing their desired genetic background and then differentiate them to the cell type of interest. Second, the advent of new genome engineering methods, such as CRISPR/Cas9, has made it easy to introduce the relevant mutations into the genome of pluripotent cells and, thus, allowed researchers to study liver development or to model rare inborn errors in hepatic metabolism. Third, differentiation protocols are amenable to automation and use of high-throughput screening methods which allows investigators to explore multiple experimental parameters to enhance understanding of liver development and diseases [74].

2.7 Strategies to mature iPS/ ES derived hepatocytes

Although the advent of iPS/ES derived hepatocytes in the past decade has helped to bridge the gap between clinical demands and primary human hepatocyte (PHH) availability, those cells exhibit a fetal phenotype rather than a mature phenotype and therefore is not entirely on par with PHH [75]. In the following section, we discuss the mature versus fetal phenotype of hepatocytes and review the strategies to maturing iPS/ES derived hepatocytes.

2.7.1 What is considered a mature hepatocyte? What is considered fetal hepatocyte?

Morphologically, mature hepatocytes are polarized, which is shown by the expression of gap and adherent junction proteins. Gap junction (Connexin 32) and tight junctions (ZO1) in the apical tip of the lateral membrane; adherent junctions (E-cadherin) at lateral membrane; adaptor proteins (α- and β-catenin) at basolateral membrane are essential features of mature polarized hepatocytes [70,76]. These junction proteins are involved in cell engraftment and membrane transports (e.g., multidrug resistance proteins and bile acid transporters) [70]. ATP-binding

cassette (ABC) transporters are known to mature after birth. The expression level of ABCB11, also known as the bile-salt export pump (BSEP) increases with maturity. Another feature of mature hepatocytes is polyploidy which is the presence of two or more nuclei in the fraction of cells [77–79].

In contrast, fetal hepatocytes display a high level of Alpha-fetoprotein (AFP), glutathione S-transferases π (GSTp), heat shock protein (HSP) 47 and low level of CYP2A6, CYP3A4, and alcohol dehydrogenase activity compared to adult human hepatocytes. Albumin synthesis and urea secretion level is also lower in fetal hepatic cells compared to adult ones [70,75,80].

Over the past decade, the liver biology community has tried different approaches to mature iPS/ES derived hepatocytes. In the following sections, we discuss the 2D and 3D differentiation strategies for removing the fetal obstacle for the use of iPS/ES derived hepatocyte cells as a renewable source of cells instead of human hepatocytes.

2.7.2 2D differentiation strategies to mature iPS/ES derived hepatocytes

It is clear that mouse iPS derived hepatocytes, unlike human iPS derived hepatocytes, are capable of forming mature, adult liver cells when provided with correct *in vivo* context and developmental cues. However, conducting the parallel experiment and similar conditioning of human iPS derived hepatocytes is not sufficient to promote complete maturation to a comparable, fully mature human hepatocyte. As a result, it is essential to know the network of signals from the ECM and nearby mesoderm during different stages of human liver development.

2D differentiation strategies are inspired by the information from the network of signals, growth factors, microRNA and transcription factors that play a role during human liver development. Therefore, it is mainly focused on adding growth factors at different stages of differentiation or induction of transcription factors by the viral infection. Most differentiation

protocols for the generation of hepatocyte-like cells from human pluripotent stem cells have 3 different phases. Phase I is definitive endoderm induction, phase II is the hepatic specification, and phase III is hepatocyte maturation [74,81–86]; different growth factors are necessary to induce each phase. To better understand the choice of growth factors used at each stage of differentiation, it is important to know the emergence and disappearance of growth factors at each stage of liver development.

During embryonic development, hepatic endoderm is formed when the medial and lateral domain of foregut endoderm are fused together [87,88]. Following this closure, the foregut endoderm is in close proximity of the developing heart and regions of the lateral plate mesoderm. As a result, it is shown that fibroblast growth factor (FGF)-1 and FGF-2 from the developing heart and bone morphogenic protein (BMP2 and BMP4) from the septum transversum mesenchyme are critical in hepatic endoderm induction [89–91]. Shortly after hepatic endoderm specification, laminin and collagen IV that surround the hepatic endoderm break down to allow hepatoblasts delaminate and migrate into the septum transversum mesenchyme to form the liver bud [88,92]. This process is controlled by different transcription factors. Delamination of hepatoblasts is controlled by transcription factors such as Prox1, Onecut-1 (OC-1 or HNF6) and Onecut-2 (OC-2) [93]. Following the hepatoblast migration into the septum transversum mesenchyme, the E-cadherin expression is downregulated. Also, ECM remodeling enzymes such as matrix metalloproteinases (MMP)-14 and MMP-2 start to become highly expressed in hepatic progenitors and surrounding mesenchyme, respectively [94]. Expansion of the liver bud happens by paracrine signals from the surrounding cells. HGF is needed in hepatoblast migration. FGF-8, BMP-4 [90,91,95–97] in conjunction with Wnt/ß-catenin [98–101], HGF [102,103] and TGFß [104,105] signaling are required for hepatoblast growth and proliferation. Hepatoblasts are bipotential cells

that can differentiate to both hepatocytes (AFP+/Albumin+) and cholangiocytes (CK-19+). A balance of signals between Activin and TGFß determines the fate of hepatoblast differentiation. Maturation of hepatocyte after differentiation is dependent on signals from hematopoietic cells such as cytokine Oncostatin M and HGF [99,106–108]. Oncostatin M is a member of the interleukin-6 (IL-6) family. It promotes the morphological maturation of fetal hepatocytes into polarized epithelium by binding to the gp130 receptor. It has been observed that continued supplementation of Oncostatin M beyond the first 20 days of differentiation promotes survival of the resulting hepatocyte-like cells but suppresses the late stages of hepatocyte maturation [109].

Different transcription factors such as CCAT-enhancer binding protein (C/EBPα), HNF1α, HNF3α-γ and HNF4α play important roles during hepatocyte maturation [110–113]. C/EBPα and HNF1α are also important for the metabolic function of hepatocytes like glycogen storage [114,115]. C/EBPα is induced by HGF and can inhibit hepatoblast proliferation by stabilizing the cycling dependent inhibitor kinase p21 (CDKN1A) and the S-phase specific E2F-p107 (RBL1) complex [116,117].

2.7.3 Small molecule screening strategies to mature iPS/ES derived hepatocytes

Small molecule screening to replace the costly growth factors and cytokines for stem cell differentiation protocols has gained momentum in the past few years. The use of small molecules instead of growth factors in differentiation protocols not only decreases the cost but also increases the reproducibility of differentiated cells. Small molecule screening for maturation of iPS/ES derived hepatocytes is determined based on the known signals during liver bud growth and hepatoblast specification. Recent studies have reported the use of small molecules to derive iPS/ES derived hepatocytes and showed the differentiated cells are as good as the established protocols

that use growth factors [118–120]. It has been shown that small molecules like FH1 and FPH1 promote maturation of iPS derived hepatocytes beyond what has been obtainable so far [109,120].

2.7.4 3D differentiation strategies to mature iPS/ES derived hepatocytes

As mentioned earlier, early attempts on hepatocyte maturation were focused on the 2D differentiation protocol and chemical and small molecule screening [81,82,86,109] until more evidence was provided that 3D culture better recapitulate the complex 3D interactions between cell-cell and cell-ECM in the liver. The focus of 3D strategies can be divided into two different groups: 1) cell-cell interaction and 2) cell-ECM interaction.

Takebe et al. showed that co-culture of hepatic endoderm, HUVECs, and mesenchymal stem cells results in the generation of 3D vascularized tissue that resembles the liver bud *in vivo* [45,46]. They also showed that the vascularized liver buds anastomose with the host vasculature within 48 hours after transplantation and the functional vasculature stimulated the maturity of liver buds to an adult looking liver tissue. Similarly, other groups showed that co-culture of iPS/ES derived hepatocytes with stromal cells mainly mouse 3TJ2 fibroblast cells in spheroid [121] or micro-patterned format [122] enhances the maturity of iPS derived hepatocytes. All of those studies showed the importance of cell-cell interactions in their co-culture systems.

On the other hand, Gieseck and colleagues were focused on both cell-cell and cell-ECM interaction and showed that culture of hepatocyte in the 3D collagen matrix improves functional maturation of iPS derived hepatocytes towards an adult phenotype [123]. Interestingly, the maturation was evident only if the pre-seeded hepatic cells were seeded to the 3D matrix in aggregates. When seeded to 3D collagen as single cells the ALB secretion was dropped, indicating the importance of cell-cell contact for mature hepatocytes.

In Section 2.8 we discuss the role of ECM on the maturation of iPS/ES derived hepatocytes and the evolution of liver ECM during liver development.

2.8 What is the role of extracellular matrix (ECM) on iPS/ ES derived hepatocytes maturation?

ECM is a dynamic structure that can regulate the biological response of the cells by its compositions and its stiffness. Mechanical signals from the ECM can regulate the differentiation of stem and progenitor cells. Thus, knowing the fetal and adult ECM components can help us to design an ECM that better mimics the liver microenvironment, and it may help us to overcome the maturity problem of the iPS/ ES derived hepatocytes. In the following sections, we first review the outside-in signaling as we looked at the components of ECM in adult and fetal liver, and then we review the inside-out signaling as we looked at the role of integrins during hepatogenesis.

2.8.1 Extracellular matrix composition of adult versus fetal liver

The liver ECM, like other tissues, consists of different types of collagens, adhesion proteins, glycosaminoglycans, and proteoglycans. In general, the main compositions of an adult human liver ECM are collagens (~61%), non-collagenous proteins (~28%), proteoglycans (~6%) and ECM associated proteins (~4%) [124].

As the hepatocyte properties vary from periportal (with more fetal phenotype) to the pericentral area (with more mature phenotype), the ECM compositions change as well [125]. Periportal (Zone 1) ECM is composed of laminin, collagen I, II, IV and V, fibronectin, hyaluranon, enactin, perlecan, chondroitin sulfate proteoglycans [125–128]. Pericentral (Zone 3) ECM is composed of collagen I, IV, VI and weak expression of collagen III, a high ratio of fibronectin compared to zone 1, syndecan, highly sulfated heparan proteoglycans, a large amount of tenascin

[125,127,129]. Unlike Zone 1, Zone 3 lacks laminin and enactin in its ECM composition. No fibronectin is detected around the bile duct, but a large amount of laminin 511 is detected around the bile duct [126]. Like Zone 3, sinusoids do not have laminin in their ECM composition, but it has elastin, which is expressed in the whole liver lobule. Space of Disse has a high level of fibronectin, collagen I, III, V, IV, VI, and perlecan [130,131].

In contrast, the fetal and neonatal livers ECM is mainly composed of laminin, type III and IV collagens, hyaluronans, and poorly sulfated proteoglycans [132]. Laminin and collagen IV were detected at the epithelial and vascular basement membrane. At 8, 9- and 10-weeks' gestation, laminin and collagen IV could be detected at the point of contact with the ductal plate. At 12 weeks' gestation, laminin and collagen IV were detected around the newly formed bile ducts and their tubular connections. Near birth, laminin and collagen IV were detectable around mature biliary structures, as in adult liver. Collagen I, III and VI were detected in the connective matrix of portal tracts from 8 week's gestation onward [133,134]. Laminin was detected at moderate amounts in the sinusoidal wall at early weeks' gestations, 5, 6 and 7, however, the expression level goes down at 8- and 9-weeks' gestation, and from 10 weeks' gestation onward it is completely undetectable in the sinusoidal area as it is in normal adult liver. Other ECM components, like collagen IV, I, II and VI existed along the sinusoidal area of the adult liver was detectable in the fetal hepatic sinusoidal area in early liver development (Fig. 2.2) [14,133]. At 8 week's gestation, tenascin is detectable around some branches of portal veins. Its expression level around the portal vein increased from 10 weeks' gestation. Tenascin expression faded away after 25 weeks' gestation onward and was not detectable in the portal tract any more as it is in the healthy adult liver. Tenascin expression along the sinusoids was detectable for the first time around 12 weeks'

gestation, and it progressively increases until 15 weeks' gestation. After this stage, its level of expression along the sinusoid is comparable to a normal adult human liver [133,134].

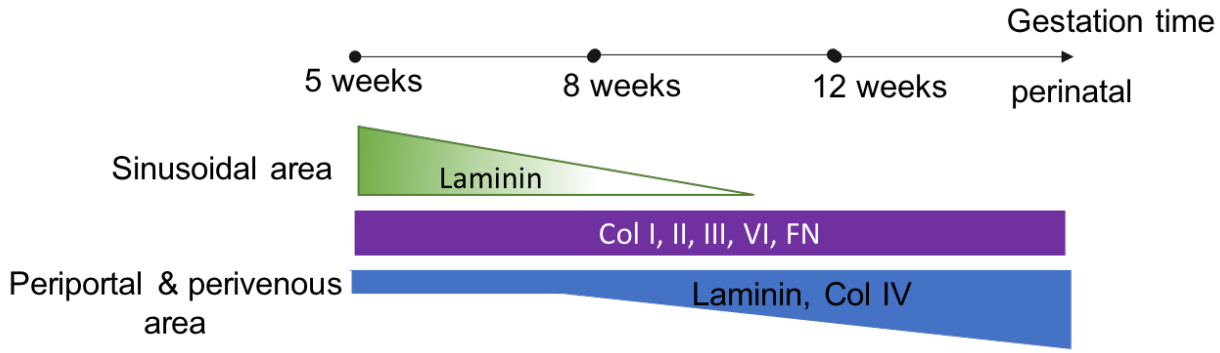

Figure 2.2 Evolving ECM composition of the human liver during development.

Different components of ECM along the liver lobule and during liver development would form complexes with growth factors and cytokines in the liver microenvironment. These complexes can provide signaling cues for the stepwise differentiation of cells to more adult fate [135]. In addition to ECM composition, the rigidity of ECM affects the biological response of the cells, including cell proliferation, motility, cell fate, and fibrotic liver diseases. Liver is soft tissue, and the mechanical measurement of the human bulk liver by rheometer shows a stiffness of 400–600 Pa for healthy liver and 1200–1600 Pa for the fibrotic liver [136,137]. The healthy liver is mechanically heterogeneous due to heterogeneity in its ECM composition, as the stiffness in the periportal zones is slightly higher with greater variability compared to the pericentral zones. As a result, hepatic cells can sense the mechanical signals presented in their microenvironment that can activate their downstream intracellular signaling pathways, involving integrin clustering and activation of focal adhesion kinases, Rho/Rho-associated protein kinase, or extracellular signal-regulated kinase [138].

2.8.2 Role of integrin binding peptides in the maturation of hepatocytes

Integrins are the dominant type of adhesion receptors that cells use to bind to the ECM components, and they play a pivotal role in structural and functional interactions between the cell and ECM. Integrins are heterodimeric molecules and composed of two subunits named α and a β. There are 18 α- and 8 β-subunits that assemble into 24 non-covalently associated heterodimers with distinct but overlapping specificities for ligands. Besides their role in cell anchorage via cell-cell and cell-matrix interactions, integrins control cell survival, proliferation, differentiation and migration in normal, injured and cancerous tissues [138,139]. Here, we review the evolution of integrins during liver development.

Integrin expression in hepatoblasts. At 5, 6- and 7-weeks' gestation, where hepatoblasts exist, only beta 1 chain of integrin was detectable. Among the alpha chain, only alpha 1, 5, 6 and 9 were detectable on the hepatoblast cell population. After 8 weeks' gestation where differentiation of hepatoblast starts, the same pattern of alpha and beta expression of integrin was detected on undifferentiated hepatoblasts that were located on the peripheral areas, where differentiation is delayed (Fig. 2.3) [133,134].

Integrin expression in hepatocytes. At 8 weeks' gestation where hepatoblasts start to differentiate into fetal hepatocyte and biliary epithelial cells, the same pattern of expression of alpha and beta integrin that was observed in hepatoblast was detected in fetal hepatocytes that exist in the hilar region of hepatic primordium. The combination of integrin expression of fetal hepatocyte remains unchanged from 8 to 30 weeks' gestation, however, there was an apparent decrease in levels of integrin in fetal hepatocytes compared to adjacent sinusoidal endothelial cells. Notably, alpha 5 and alpha 9 started to decrease at 8 weeks' gestation until 15 weeks' gestation, later on, alpha 1 and beta 1 decreases at 10 weeks' gestation until 15 weeks' gestation. Expression

of alpha 6 started to decrease at 15 weeks' gestation and continued until 30 weeks' gestation in which it was completely undetectable. From 30 weeks' gestation to the perinatal period, the pattern of expression of integrins remained unchanged on fetal hepatocytes. The fetal hepatocytes expressed faint expression of beta 1, alpha 1, 5 and 9 integrin chains, and lacks alpha 6. This is similar to human adult hepatocytes (Fig. 2.3) [133,134].

Integrin expression in biliary epithelial cells. At 8 weeks' gestation, primitive portal tracts are formed at the point of contact with the perihilar mesenchymal tissue. At this stage, the portal tract is a single-layered cylinder that is covered by fetal biliary epithelial cells. The formation of the ductal plate is accompanied by an increase in the expression of alpha 6 integrin chain. They also express beta 4 alpha 2 and 3 chains that are not detected on hepatoblasts and adjacent fetal hepatocytes. At 12 weeks' gestation, newly formed bile ducts express the following integrin combination: beta1 and 4, alpha 2, 3,5,6,9 and V. Expression of alpha 9 and V integrin were usually faint, and alpha 1 was not detectable at this point. This pattern of integrin combination on fetal biliary epithelial cells remained unchanged until the perinatal birth and was similar to what is seen in adult biliary epithelial cells (Fig. 2.3) [134]. The change in the combination of integrin expression that is observed at 8 weeks' gestation by emergence of biliary epithelial cell and fetal hepatocytes along with selective deposition of laminin at the point of contact with the ductal plate shows the critical role that integrin receptors and their extracellular ligands play in morphogenesis and differentiation of epithelial cells.

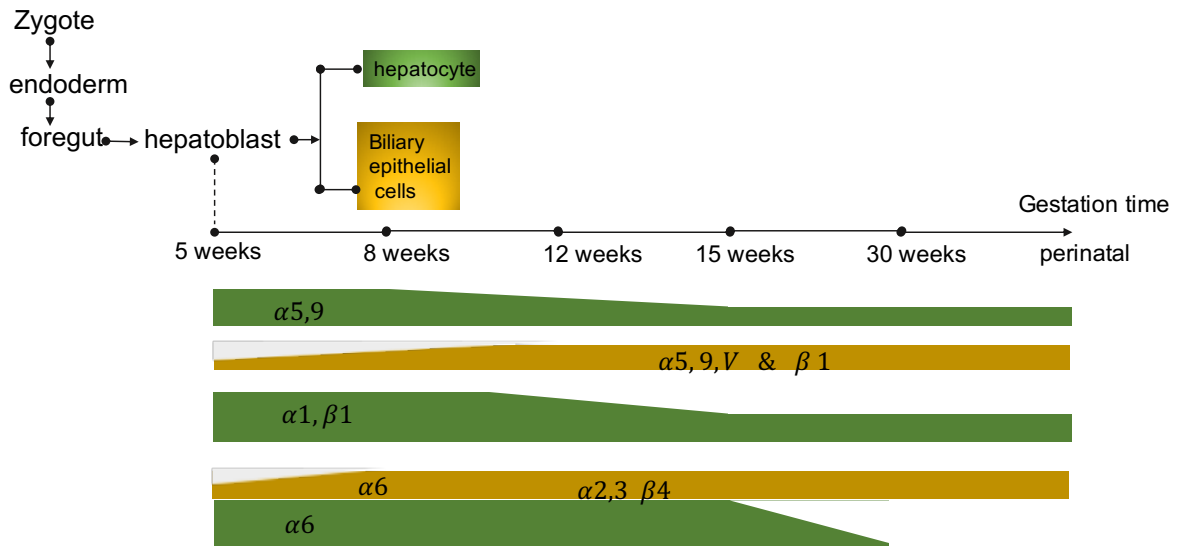

Figure 2.3 Integrins play an important role in differentiation of epithelial cells in the liver

Moreover, Apte and colleagues showed ablation of liver-specific integrin-linked kinase (ILK, β1- and β3-integrin-interacting cell-matrix adhesion protein) in mice results in an enlarged liver after partial hepatectomy (PH) [140]. Gkretsi and colleagues showed ILK ablation in mice results in histologic abnormalities characterized by disorderly hepatic plates, increased proliferation of hepatocytes and biliary cells, and increased deposition of extracellular matrix soon after birth [141]. After this transient proliferation of all epithelial components, proliferation subsides, and final liver to body weight ratio in livers with ILK deficient hepatocytes is two times that of wild type, similar to the observation of Apte et al. study. Speicher and colleagues showed that knock out and knockdown of β1-integrin in mice leads to severe liver necrosis and reduced hepatocyte proliferation after PH. This happens through inhibition of growth factor signaling. More specifically, loss of β1-integrin in hepatocytes, impairs ligand-induced phosphorylation of the epidermal growth factor and hepatocyte growth factor receptors, thereby attenuating downstream receptor signaling *in vitro* and *in vivo* [142]. Those results show the significance of ILK and hepatic ECM-signaling for the regulation of hepatocyte proliferation and differentiation.

2.9 Natural, synthetic and hybrid biomaterials used as extracellular matrix for human iPS/ES derived hepatocyte differentiation and maturation

Cell-ECM interactions are often neglected in differentiation protocols. iPS/ES derived cells are often cultured on the same matrix used initially for plating the pluripotent stem cells. However, ECM is a dynamic evolving entity that is changing during organ development. Hepatic differentiation of cells from hPSC is traditionally done on Matrigel [81,143,144]. Indeed, Matrigel is considered as a standard culture condition to which many new culture systems are being compared. Matrigel is a protein extract from Engelbreth–Holm-Swarm (EHS) mouse sarcoma cells. It mainly contains laminin-111 (~60%), collagen type IV (~30%), and entactin (~8%) together with numerous other proteins and several growth factors, like EGF, bFGF, IGF-1, TGF-β, PDGF, and NGF [145,146]. However, one of the drawbacks of Matrigel is undefined components in the product can lead to possible variations between independent cell culture experiments. Moreover, the use of animal origin matrices like Matrigel or mouse feeder cells can increase the risk of pathogen transmission that would cause immune rejection of transplanted cells later on. Martin MJ et al. demonstrated that hESCs cultured with animal or serum products retained non-human sialic acid, which was immunogenic when these cells were transplanted into humans [147].

Synthetic biomaterials can provide a more controlled and reproducible microenvironment for cultured cells compared to the naturally-derived biomaterials [148]. Biocompatible synthetic polymers are blank slates that should get functionalized with peptides or growth factors in order to increase their biochemical activity and to provide biological cues for cells.

Here, we introduce the natural, synthetic and hybrid biomaterials that have been used for differentiation and maturation of human pluripotent stem cell derived hepatocytes (Fig. 2.4).

In most of the methods, investigators took advantage of different types of ECM at the end stage of hepatocyte differentiation protocol, where fetal hepatocyte-like cells were produced. There are very few studies that the whole differentiation protocol was carried out on a substrate other than Matrigel.

Natural ECM: Due to the problems that Matrigel has and the difficulty of using the cells differentiated on Matrigel in clinical trials, other labs have tried to find a substitute for Matrigel. For example, Baharvand et al. (2006) examined the hepatic differentiation of hESCs in 2D and 3D using collagen type I. They noticed that the secretion of AFP and urea in 3D cultured cells was higher than those in 2D culture. However, there was no difference in ALB secretion in 2D and 3D cultures [149]. Gieseck *et al.* cultured hiPSC-derived hepatocytes at the end stage of differentiation in a 3D high-density collagen I systems called RAFT and showed that this method increases functional maturation of the iPS derived hepatocyte toward an adult phenotype compared to the conventional 2D system on Matrigel [123]. They observed more mature hepatocytes when cells were encapsulated as aggregates rather than single cells, evidenced by ALB secretion. This indicates the importance of cell-cell contact for mature hepatocytes.

Toivonen et al. used a well-defined plant derived system (Nanofibrillar cellulose hydrogel, Growdex) and demonstrated the enhancement in both phenotype and function compared to the 3D culture of cells in Matrigel [150]. They found higher hepatocyte-specific gene expression levels and enhanced cytochrome P450 functions compared to Matrigel.

Recombinant laminins LN-111 and LN-521 have been used for culturing hepatic cells [151–154]. All of the studies using laminin demonstrated higher CYP1A2 and CYP3A enzyme activity compared to cells cultured on Matrigel. Cameron et al. showed that hES derived hepatocytes on laminin 521 and the laminin 111 mix had very pronounced nuclei that were often

bi-nucleated [151]. They also showed the derived hepatocyte-like cells had functional efflux transport as evidenced by the uptake of 5(6)-carboxy-2′,7′-dichlorofluorescein diacetate (CDFDA). Takayama *et al.* tested four different laminins and showed that hepatoblast cells derived from ES cells attach to human laminin-111 (LN111) coated dish via integrin alpha 6 and beta 1 [153]. They also showed that hepatoblast cells have the potential to differentiate into both hepatic and biliary lineages and to integrate into the mouse liver parenchyma. Later, the same group differentiated human liver-derived iPSCs to hepatocyte-like cells in a similar culture setting with some modifications [155]. Interestingly, they observed that cells passaged at the hepatoblast stage showed higher expression of typical hepatocyte markers and secreted more ALB and urea compared to the cells without passaging.

Nagaoka et al. have shown that vitronectin, cell adhesion glycoprotein can support the hepatic differentiation of hPSCs [156]. They combined a fragment of vitronectin containing RGD (arginine-glycine-asparagine) peptide into the domain of immunoglobulin G (IgG) antibody, called as R-Fc and plated hPSCs on this matrix. The derived hepatic cells were positive for HNF4A and had a capacity for activity uptake of indocyanine green, a specific function of hepatic cells. However, the expression of AFP revealed that the cells were not fully mature. Moreover, the gene expression profile revealed that Matrigel-cultured cells expressed more mature hepatocyte markers compared to R-Fc-cultured cells.

Lozoya et al. showed that hepatic stem cells isolated from the human fetal liver could be differentiated towards hepatic progenitors and hepatocytes when cultured in 3D Hyaluronic acid hydrogel [157]. Hyaluronic acid is a non-sulfated glycosaminoglycan abundantly expressed in stem cell niches, and thus it is an attractive culture matrix for hepatic stem cells. Turner et al. noticed that the stiffness of the hydrogel plays a vital role in hepatic differentiation. The hydrogel

with shear modulus, a measure of gel stiffness, of 73-220 Pa resulted in best hepatic differentiation [158].

Cheng et al. have used chitosan matrices to differentiate human adipose-derived stem cells towards hepatocyte-like cells [159]. By culturing the adipose-derived stem cells on chitosan, cells formed spheroids. In proper induction media, they found that adipose-derived stem cell differentiation capabilities were significantly enhanced after spheroid formation, including increased trans-differentiation efficiency into the neuron and hepatocyte-like cells.

Collagen I, laminin, vitronectin, and hyaluronic acid are individual ECM proteins that can be extracted from animals or human or produced either in eukaryotic and prokaryotic expression systems or in transgenic organisms [160]. Unlike Matrigel, those proteins allow studying the specific effect of the protein on cell function.

Synthetic ECM: Though natural hydrogels have produced promising results for hepatocyte differentiation, there is still a need for a defined, xeno-free matrix that would not yield to the variable cell performance observed in natural matrices like Matrigel. However, there are very few publications that have studied the effect of synthetic hydrogels on iPS/ES derived hepatocyte differentiation and maturation.

Villarin *et al.* have shown that culturing hepatocytes derived from H9-ES cells on top of the optimized polyurethane (PU134) hydrogel yields to more stable hepatocyte cells compared to 2D culture on the Matrigel after 20 days. Compared to Matrigel culture, the cells cultured on polyurethane 134 produced more fibrinogen, transthyretin, and fibronectin, and their CYP1A2 activity was approximately six-times higher [161,162].

Lou et al. showed that culturing hiPS derived hepatoblasts in the nanofibrous hydrogel that is made from a self-assembled polypeptide, results in hepatocyte cells that express hepatocyte

markers and exhibit maturity and metabolic activity to a larger extent compared to the 2D traditional culture on Matrigel [163]. All in all, more studies need to be done with synthetic defined hydrogels to unravel the mechano-transduction signal that the ECM could send to hepatocyte and its role in maturation and differentiation of iPS/ES derived hepatocytes.

Hybrid ECM: Hybrid ECM refers to matrices that are a combination of synthetic and natural ECMs. Hybrid ECM offers more possibilities for creating the desired matrix, due to unlimited possibilities of combination of synthetic and natural polymers. Synthetic polymers can enhance the mechanical properties of natural ECM, and natural ECM can enhance the cell-matrix interaction of synthetic ECM.

Kazemnejad et al. combined biologically inert poly-ε- caprolactone (PCL) with collagen type I and polyethersulfone to achieve a porous nanofiber scaffold for differentiation of hMSCs towards hepatocyte-like cells [164]. Compared to standard 2D culture, the 3D cultured cells secreted approximately two-times more ALB indicating the improved status of hepatic differentiation.

Li et al. also used 3D scaffold made from polylactic-co-glycolic acid and collagen type I for hepatic differentiation of hMSCs [165]. Similar to Kazemnejad study, they showed that 3D scaffold better supported the hepatic differentiation compared to monolayer cultured as shown by ALB and urea synthesis.

Lozoya et al. performed an extensive screen of different ratios of HA and PEGDA to find the optimal matrix for human hepatic stem cells [157]. They noticed that the stiffness of the HA matrix controls the differentiation to hepatoblasts and committed progenitors in vitro. The secretion of AFP, ALB, and urea increased in hydrogels with the lower concentration of HA suggesting hepatic lineage maturation.

Wong et al. infused a poly-l-lactic acid (PLLA) scaffold with collagen I and showed the culture of iPS derived hepatocytes in their 3D hybrid ECM increased the function of the iPS derived hepatocytes. Cells had a significantly higher level of P450 (CYP2C9, CYP3A4, CYP1A2) mRNA levels and metabolic enzyme activity compared with iPS cells on Matrigel sandwich culture. Synthesis of albumin by iPS hepatocytes that were cultured within the ECM was significantly higher than that in the sandwich control group throughout the 14-day culture period [166].

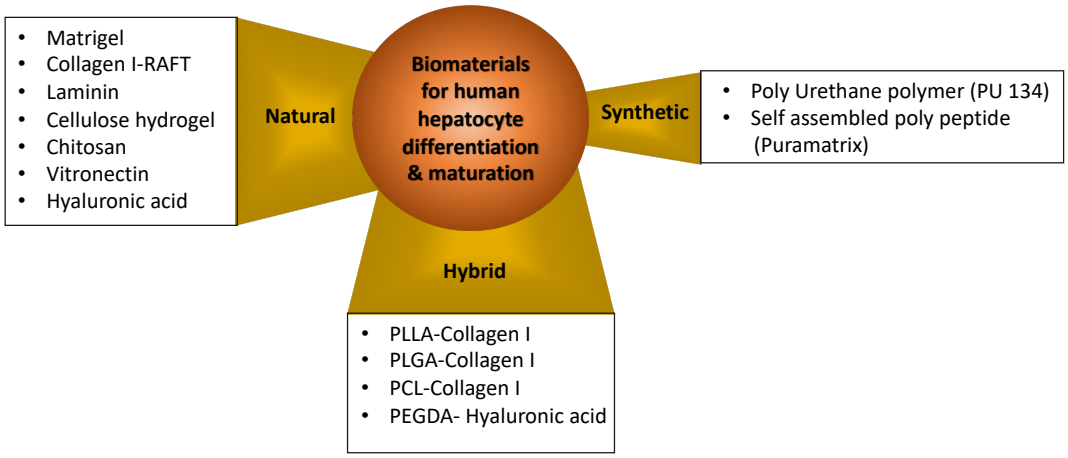

Figure 2.4 Biomaterials used for maturation and differentiation of pluripotent stem cell derived hepatocytes

2.10 Conclusion

Unfortunately, pluripotent stem cell-derived hepatocytes do not possess all functions of mature hepatocytes. This challenge, along with increasing demand for an exhaustible source of cells that is as good as primary human hepatocytes, limits the broader application of such cells. Liver maturation is a complex process that is stage specific, and many factors are involved in this

process. Understanding the factors involved in hepatocyte biology, from developmental point of view to mechanical point of view, along with all the new emerging technologies such as bio-fabrication and genetic programming would allow us to take more wholistic approaches to advance the development of human stem cell derived hepatocytes and make them suitable for *in vitro* studies and even bioartificial liver tissues.

2.11 References

[1] E. Crivellato, B. Nico, D. Ribatti, Contribution of endothelial cells to organogenesis: a modern reappraisal of an old Aristotelian concept, J. Anat. 211 (2007) 415–427. doi:10.1111/j.1469-7580.2007.00790.x.

[2] D.B. Azizoglu, O. Cleaver, Blood vessel crosstalk during organogenesis-focus on pancreas and endothelial cells: Vascular crosstalk during organogenesis, Wiley Interdiscip. Rev. Dev. Biol. 5 (2016) 598–617. doi:10.1002/wdev.240.

[3] H. Yoshitomi, Endothelial cell interactions initiate dorsal pancreas development by selectively inducing the transcription factor Ptf1a, Development. 131 (2004) 807–817. doi:10.1242/dev.00960.

[4] P. Jacquemin, H. Yoshitomi, Y. Kashima, G.G. Rousseau, F.P. Lemaigre, K.S. Zaret, An endothelial–mesenchymal relay pathway regulates early phases of pancreas development, Dev. Biol. 290 (2006) 189–199. doi:10.1016/j.ydbio.2005.11.023.

[5] O. Cleaver, D.A. Melton, Endothelial signaling during development, Nat. Med. 9 (2003) 661–668. doi:10.1038/nm0603-661.

[6] Y. Kitamoto, H. Tokunaga, K. Tomita, Vascular endothelial growth factor is an essential molecule for mouse kidney development: glomerulogenesis and nephrogenesis., J. Clin. Invest. 99 (1997) 2351–2357. doi:10.1172/JCI119416.

[7] H.P. Gerber, K.J. Hillan, A.M. Ryan, J. Kowalski, G.A. Keller, L. Rangell, B.D. Wright, F. Radtke, M. Aguet, N. Ferrara, VEGF is required for growth and survival in neonatal mice, Dev. Camb. Engl. 126 (1999) 1149–1159.

[8] X. Zeng, S.E. Wert, R. Federici, K.G. Peters, J.A. Whitsett, VEGF enhances pulmonary vasculogenesis and disrupts lung morphogenesis in vivo, Dev. Dyn. 211 (1998) 215–227. doi:10.1002/(SICI)1097-0177(199803)211:3<215::AID-AJA3>3.0.CO;2-K.

[9] G.K. Michalopoulos, Liver regeneration, J. Cell. Physiol. 213 (2007) 286–300. doi:10.1002/jcp.21172.

[10] K. Elvevold, B. Smedsrød, I. Martinez, The liver sinusoidal endothelial cell: a cell type of controversial and confusing identity, Am. J. Physiol. Gastrointest. Liver Physiol. 294 (2008) G391-400. doi:10.1152/ajpgi.00167.2007.

[11] S. Collardeau-Frachon, J.-Y. Scoazec, Vascular Development and Differentiation During Human Liver Organogenesis, Anat. Rec. Adv. Integr. Anat. Evol. Biol. 291 (2008) 614–627. doi:10.1002/ar.20679.

[12] J.M. Pérez-Pomares, R. Carmona, M. González-Iriarte, D. Macías, J.A. Guadix, R. Muñoz-Chápuli, Contribution of mesothelium-derived cells to liver sinusoids in avian

embryos, Dev. Dyn. Off. Publ. Am. Assoc. Anat. 229 (2004) 465–474. doi:10.1002/dvdy.10455.
[13] E. Wisse, R.B. De Zanger, K. Charels, P. Van Der Smissen, R.S. McCuskey, The liver sieve: considerations concerning the structure and function of endothelial fenestrae, the sinusoidal wall and the space of Disse, Hepatol. Baltim. Md. 5 (1985) 683–692.
[14] A. Couvelard, J.Y. Scoazec, M.C. Dauge, A.F. Bringuier, F. Potet, G. Feldmann, Structural and functional differentiation of sinusoidal endothelial cells during liver organogenesis in humans, Blood. 87 (1996) 4568–4580.
[15] J. Poisson, S. Lemoinne, C. Boulanger, F. Durand, R. Moreau, D. Valla, P.-E. Rautou, Liver sinusoidal endothelial cells: Physiology and role in liver diseases, J. Hepatol. 66 (2017) 212–227. doi:10.1016/j.jhep.2016.07.009.
[16] H. Enzan, H. Himeno, M. Hiroi, H. Kiyoku, T. Saibara, S. Onishi, Development of hepatic sinusoidal structure with special reference to the Ito cells, Microsc. Res. Tech. 39 (1997) 336–349. doi:10.1002/(SICI)1097-0029(19971115)39:4<336::AID-JEMT4>3.0.CO;2-F.
[17] M. Oda, H. Yokomori, J.-Y. Han, Regulatory mechanisms of hepatic microcirculation, Clin. Hemorheol. Microcirc. 29 (2003) 167–182.
[18] K. Matsumoto, Liver Organogenesis Promoted by Endothelial Cells Prior to Vascular Function, Science. 294 (2001) 559–563. doi:10.1126/science.1063889.
[19] M.A. Battle, G. Konopka, F. Parviz, A.L. Gaggl, C. Yang, F.M. Sladek, S.A. Duncan, Hepatocyte nuclear factor 4 orchestrates expression of cell adhesion proteins during the epithelial transformation of the developing liver, Proc. Natl. Acad. Sci. 103 (2006) 8419–8424. doi:10.1073/pnas.0600246103.
[20] P. Godoy, N.J. Hewitt, U. Albrecht, M.E. Andersen, N. Ansari, S. Bhattacharya, J.G. Bode, J. Bolleyn, C. Borner, J. Böttger, A. Braeuning, R.A. Budinsky, B. Burkhardt, N.R. Cameron, G. Camussi, C.-S. Cho, Y.-J. Choi, J. Craig Rowlands, U. Dahmen, G. Damm, O. Dirsch, M.T. Donato, J. Dong, S. Dooley, D. Drasdo, R. Eakins, K.S. Ferreira, V. Fonsato, J. Fraczek, R. Gebhardt, A. Gibson, M. Glanemann, C.E.P. Goldring, M.J. Gómez-Lechón, G.M.M. Groothuis, L. Gustavsson, C. Guyot, D. Hallifax, S. Hammad, A. Hayward, D. Häussinger, C. Hellerbrand, P. Hewitt, S. Hoehme, H.-G. Holzhütter, J.B. Houston, J. Hrach, K. Ito, H. Jaeschke, V. Keitel, J.M. Kelm, B. Kevin Park, C. Kordes, G.A. Kullak-Ublick, E.L. LeCluyse, P. Lu, J. Luebke-Wheeler, A. Lutz, D.J. Maltman, M. Matz-Soja, P. McMullen, I. Merfort, S. Messner, C. Meyer, J. Mwinyi, D.J. Naisbitt, A.K. Nussler, P. Olinga, F. Pampaloni, J. Pi, L. Pluta, S.A. Przyborski, A. Ramachandran, V. Rogiers, C. Rowe, C. Schelcher, K. Schmich, M. Schwarz, B. Singh, E.H.K. Stelzer, B. Stieger, R. Stöber, Y. Sugiyama, C. Tetta, W.E. Thasler, T. Vanhaecke, M. Vinken, T.S. Weiss, A. Widera, C.G. Woods, J.J. Xu, K.M. Yarborough, J.G. Hengstler, Recent advances in 2D and 3D in vitro systems using primary hepatocytes, alternative hepatocyte sources and non-parenchymal liver cells and their use in investigating mechanisms of hepatotoxicity, cell signaling and ADME, Arch. Toxicol. 87 (2013) 1315–1530. doi:10.1007/s00204-013-1078-5.
[21] F.T. Lee-Montiel, S.M. George, A.H. Gough, A.D. Sharma, J. Wu, R. DeBiasio, L.A. Vernetti, D.L. Taylor, Control of oxygen tension recapitulates zone-specific functions in human liver microphysiology systems, Exp. Biol. Med. 242 (2017) 1617–1632. doi:10.1177/1535370217703978.

[22] K. Jungermann, T. Keitzmann, Zonation of Parenchymal and Nonparenchymal Metabolism in Liver, Annu. Rev. Nutr. 16 (1996) 179–203. doi:10.1146/annurev.nu.16.070196.001143.
[23] K.H. Kaestner, In the Zone: How a Hepatocyte Knows Where It Is, Gastroenterology. 137 (2009) 425–427. doi:10.1053/j.gastro.2009.06.020.
[24] T. Kietzmann, Metabolic zonation of the liver: The oxygen gradient revisited, Redox Biol. 11 (2017) 622–630. doi:10.1016/j.redox.2017.01.012.
[25] T. Kietzmann, Y. Cornesse, K. Brechtel, S. Modaressi, K. Jungermann, Perivenous expression of the mRNA of the three hypoxia-inducible factor alpha-subunits, HIF1alpha, HIF2alpha and HIF3alpha, in rat liver, Biochem. J. 354 (2001) 531–537.
[26] M.A. Goldberg, T.J. Schneider, Similarities between the oxygen-sensing mechanisms regulating the expression of vascular endothelial growth factor and erythropoietin, J. Biol. Chem. 269 (1994) 4355–4359.
[27] T.J. Walter, A.E. Cast, K.A. Huppert, S.S. Huppert, Epithelial VEGF signaling is required in the mouse liver for proper sinusoid endothelial cell identity and hepatocyte zonation in vivo, Am. J. Physiol.-Gastrointest. Liver Physiol. 306 (2014) G849–G862. doi:10.1152/ajpgi.00426.2013.
[28] X.L. Wang, R. Suzuki, K. Lee, T. Tran, J.E. Gunton, A.K. Saha, M.-E. Patti, A. Goldfine, N.B. Ruderman, F.J. Gonzalez, C.R. Kahn, Ablation of ARNT/HIF1β in Liver Alters Gluconeogenesis, Lipogenic Gene Expression, and Serum Ketones, Cell Metab. 9 (2009) 565. doi:10.1016/j.cmet.2009.05.002.
[29] K. Tsukada, T. Tajima, S. Hori, T. Matsuura, R.S. Johnson, N. Goda, M. Suematsu, Hypoxia-Inducible Factor-1 Is a Determinant of Lobular Structure and Oxygen Consumption in the Liver, Microcirculation. 20 (2013) 385–393. doi:10.1111/micc.12033.
[30] A. Martinez-Hernandez, J. Martinez, The role of capillarization in hepatic failure: Studies in carbon tetrachloride-induced cirrhosis, Hepatology. 14 (1991) 864–874. doi:10.1002/hep.1840140519.
[31] B. Xu, U. Broome, M. Uzunel, S. Nava, X. Ge, M. Kumagai-Braesch, K. Hultenby, B. Christensson, B.-G. Ericzon, J. Holgersson, S. Sumitran-Holgersson, Capillarization of hepatic sinusoid by liver endothelial cell-reactive autoantibodies in patients with cirrhosis and chronic hepatitis, Am. J. Pathol. 163 (2003) 1275–1289. doi:10.1016/S0002-9440(10)63487-6.
[32] M. Fernández, D. Semela, J. Bruix, I. Colle, M. Pinzani, J. Bosch, Angiogenesis in liver disease, J. Hepatol. 50 (2009) 604–620. doi:10.1016/j.jhep.2008.12.011.
[33] B.-S. Ding, D.J. Nolan, J.M. Butler, D. James, A.O. Babazadeh, Z. Rosenwaks, V. Mittal, H. Kobayashi, K. Shido, D. Lyden, T.N. Sato, S.Y. Rabbany, S. Rafii, Inductive angiocrine signals from sinusoidal endothelium are required for liver regeneration, Nature. 468 (2010) 310–315. doi:10.1038/nature09493.
[34] G. Marrone, L. Russo, E. Rosado, D. Hide, G. García-Cardeña, J.C. García-Pagán, J. Bosch, J. Gracia-Sancho, The transcription factor KLF2 mediates hepatic endothelial protection and paracrine endothelial–stellate cell deactivation induced by statins, J. Hepatol. 58 (2013) 98–103. doi:10.1016/j.jhep.2012.08.026.
[35] P.F. Lalor, P. Shields, A. Grant, D.H. Adams, Recruitment of lymphocytes to the human liver, Immunol. Cell Biol. 80 (2002) 52–64. doi:10.1046/j.1440-1711.2002.01062.x.
[36] S. Shetty, C.J. Weston, Y.H. Oo, N. Westerlund, Z. Stamataki, J. Youster, S.G. Hubscher, M. Salmi, S. Jalkanen, P.F. Lalor, D.H. Adams, Common Lymphatic Endothelial and

Vascular Endothelial Receptor-1 Mediates the Transmigration of Regulatory T Cells across Human Hepatic Sinusoidal Endothelium, J. Immunol. 186 (2011) 4147–4155. doi:10.4049/jimmunol.1002961.

[37] A. Limmer, J. Ohl, C. Kurts, H.G. Ljunggren, Y. Reiss, M. Groettrup, F. Momburg, B. Arnold, P.A. Knolle, Efficient presentation of exogenous antigen by liver endothelial cells to CD8+ T cells results in antigen-specific T-cell tolerance, Nat. Med. 6 (2000) 1348–1354. doi:10.1038/82161.

[38] A. Carambia, B. Freund, D. Schwinge, M. Heine, A. Laschtowitz, S. Huber, D.C. Wraith, T. Korn, C. Schramm, A.W. Lohse, J. Heeren, J. Herkel, TGF-β-dependent induction of CD4+CD25+Foxp3+ Tregs by liver sinusoidal endothelial cells, J. Hepatol. 61 (2014) 594–599. doi:10.1016/j.jhep.2014.04.027.

[39] K. Neumann, C. Rudolph, C. Neumann, M. Janke, D. Amsen, A. Scheffold, Liver sinusoidal endothelial cells induce immunosuppressive IL-10-producing Th1 cells via the Notch pathway: Immunomodulation, Eur. J. Immunol. 45 (2015) 2008–2016. doi:10.1002/eji.201445346.

[40] B. Liu, M. Wang, X. Wang, D. Zhao, D. Liu, J. Liu, P.-J. Chen, D. Yang, F. He, L. Tang, Liver Sinusoidal Endothelial Cell Lectin Inhibits CTL-Dependent Virus Clearance in Mouse Models of Viral Hepatitis, J. Immunol. 190 (2013) 4185–4195. doi:10.4049/jimmunol.1203091.

[41] R.P. Visconti, V. Kasyanov, C. Gentile, J. Zhang, R.R. Markwald, V. Mironov, Towards organ printing: engineering an intra-organ branched vascular tree, Expert Opin. Biol. Ther. 10 (2010) 409–420. doi:10.1517/14712590903563352.

[42] J.W. Allen, In Vitro Zonation and Toxicity in a Hepatocyte Bioreactor, Toxicol. Sci. 84 (2005) 110–119. doi:10.1093/toxsci/kfi052.

[43] X. Li, S.M. George, L. Vernetti, A.H. Gough, D.L. Taylor, A glass-based, continuously zonated and vascularized human liver acinus microphysiological system (vLAMPS) designed for experimental modeling of diseases and ADME/TOX, Lab. Chip. 18 (2018) 2614–2631. doi:10.1039/C8LC00418H.

[44] S.D. Ramachandran, K. Schirmer, B. Münst, S. Heinz, S. Ghafoory, S. Wölfl, K. Simon-Keller, A. Marx, C.I. Øie, M.P. Ebert, H. Walles, J. Braspenning, K. Breitkopf-Heinlein, In Vitro Generation of Functional Liver Organoid-Like Structures Using Adult Human Cells, PLOS ONE. 10 (2015) e0139345. doi:10.1371/journal.pone.0139345.

[45] T. Takebe, K. Sekine, M. Enomura, H. Koike, M. Kimura, T. Ogaeri, R.-R. Zhang, Y. Ueno, Y.-W. Zheng, N. Koike, S. Aoyama, Y. Adachi, H. Taniguchi, Vascularized and functional human liver from an iPSC-derived organ bud transplant, Nature. 499 (2013) 481–484. doi:10.1038/nature12271.

[46] T. Takebe, R.-R. Zhang, H. Koike, M. Kimura, E. Yoshizawa, M. Enomura, N. Koike, K. Sekine, H. Taniguchi, Generation of a vascularized and functional human liver from an iPSC-derived organ bud transplant, Nat. Protoc. 9 (2014) 396–409. doi:10.1038/nprot.2014.020.

[47] S. Messner, I. Agarkova, W. Moritz, J.M. Kelm, Multi-cell type human liver microtissues for hepatotoxicity testing, Arch. Toxicol. 87 (2013) 209–213. doi:10.1007/s00204-012-0968-2.

[48] L.M. Norona, D.G. Nguyen, D.A. Gerber, S.C. Presnell, E.L. LeCluyse, Editor's Highlight: Modeling Compound-Induced Fibrogenesis *In Vitro* Using Three-Dimensional Bioprinted Human Liver Tissues, Toxicol. Sci. 154 (2016) 354–367. doi:10.1093/toxsci/kfw169.

[49] H. Lee, D.-W. Cho, One-step fabrication of an organ-on-a-chip with spatial heterogeneity using a 3D bioprinting technology, Lab. Chip. 16 (2016) 2618–2625. doi:10.1039/C6LC00450D.
[50] H. Kizawa, E. Nagao, M. Shimamura, G. Zhang, H. Torii, Scaffold-free 3D bio-printed human liver tissue stably maintains metabolic functions useful for drug discovery, Biochem. Biophys. Rep. 10 (2017) 186–191. doi:10.1016/j.bbrep.2017.04.004.
[51] K.R. Stevens, M.A. Scull, V. Ramanan, C.L. Fortin, R.R. Chaturvedi, K.A. Knouse, J.W. Xiao, C. Fung, T. Mirabella, A.X. Chen, M.G. McCue, M.T. Yang, H.E. Fleming, K. Chung, Y.P. de Jong, C.S. Chen, C.M. Rice, S.N. Bhatia, In situ expansion of engineered human liver tissue in a mouse model of chronic liver disease, Sci. Transl. Med. 9 (2017) eaah5505. doi:10.1126/scitranslmed.aah5505.
[52] Y. Du, N. Li, M. Long, Liver sinusoid on a chip, in: Methods Cell Biol., Elsevier, 2018: pp. 105–134. doi:10.1016/bs.mcb.2018.06.002.
[53] Y.-S. Weng, S.-F. Chang, M.-C. Shih, S.-H. Tseng, C.-H. Lai, Scaffold-Free Liver-On-A-Chip with Multiscale Organotypic Cultures, Adv. Mater. 29 (2017) 1701545. doi:10.1002/adma.201701545.
[54] K. Domansky, W. Inman, J. Serdy, A. Dash, M.H.M. Lim, L.G. Griffith, Perfused multiwell plate for 3D liver tissue engineering, Lab Chip. 10 (2010) 51–58. doi:10.1039/B913221J.
[55] K.R. Stevens, M.D. Ungrin, R.E. Schwartz, S. Ng, B. Carvalho, K.S. Christine, R.R. Chaturvedi, C.Y. Li, P.W. Zandstra, C.S. Chen, S.N. Bhatia, InVERT molding for scalable control of tissue microarchitecture, Nat. Commun. 4 (2013) 1847. doi:10.1038/ncomms2853.
[56] P.F. Lalor, W.K. Lai, S.M. Curbishley, S. Shetty, D.H. Adams, Human hepatic sinusoidal endothelial cells can be distinguished by expression of phenotypic markers related to their specialised functions in vivo, World J. Gastroenterol. 12 (2006) 5429–5439.
[57] S. March, E.E. Hui, G.H. Underhill, S. Khetani, S.N. Bhatia, Microenvironmental regulation of the sinusoidal endothelial cell phenotype in vitro, Hepatology. 50 (2009) 920–928. doi:10.1002/hep.23085.
[58] I. Martinez, G.I. Nedredal, C.I. Øie, A. Warren, O. Johansen, D.G. Le Couteur, B. Smedsrød, The influence of oxygen tension on the structure and function of isolated liver sinusoidal endothelial cells, Comp. Hepatol. 7 (2008) 4. doi:10.1186/1476-5926-7-4.
[59] T. Matsumura, M. Takesue, K.A. Westerman, T. Okitsu, M. Sakaguchi, T. Fukazawa, T. Totsugawa, H. Noguchi, S. Yamamoto, D.B. Stolz, N. Tanaka, P. Leboulch, N. Kobayashi, Establishment of an immortalized human-liver endothelial cell line with SV40T and hTERT, Transplantation. 77 (2004) 1357–1365.
[60] S. Hering, B.E. Griffin, M. Strauss, Immortalization of human fetal sinusoidal liver cells by polyoma virus large T antigen, Exp. Cell Res. 195 (1991) 1–7. doi:10.1016/0014-4827(91)90492-D.
[61] Y. Koui, T. Kido, T. Ito, H. Oyama, S.-W. Chen, Y. Katou, K. Shirahige, A. Miyajima, An In Vitro Human Liver Model by iPSC-Derived Parenchymal and Non-parenchymal Cells, Stem Cell Rep. 9 (2017) 490–498. doi:10.1016/j.stemcr.2017.06.010.
[62] M. Coll, L. Perea, R. Boon, S.B. Leite, J. Vallverdú, I. Mannaerts, A. Smout, A. El Taghdouini, D. Blaya, D. Rodrigo-Torres, I. Graupera, B. Aguilar-Bravo, C. Chesne, M. Najimi, E. Sokal, J.J. Lozano, L.A. van Grunsven, C.M. Verfaillie, P. Sancho-Bru, Generation of Hepatic Stellate Cells from Human Pluripotent Stem Cells Enables In Vitro Modeling of Liver Fibrosis, Cell Stem Cell. 23 (2018) 101-113.e7. doi:10.1016/j.stem.2018.05.027.

[63] J. Buchrieser, W. James, M.D. Moore, Human Induced Pluripotent Stem Cell-Derived Macrophages Share Ontogeny with MYB -Independent Tissue-Resident Macrophages, Stem Cell Rep. 8 (2017) 334–345. doi:10.1016/j.stemcr.2016.12.020.
[64] T.M. De Assuncao, Y. Sun, N. Jalan-Sakrikar, M.C. Drinane, B.Q. Huang, Y. Li, J.I. Davila, R. Wang, S.P. O'Hara, G.A. Lomberk, R.A. Urrutia, Y. Ikeda, R.C. Huebert, Development and characterization of human-induced pluripotent stem cell-derived cholangiocytes, Lab. Invest. 95 (2015) 684–696. doi:10.1038/labinvest.2015.51.
[65] N. Dianat, H. Dubois-Pot-Schneider, C. Steichen, C. Desterke, P. Leclerc, A. Raveux, L. Combettes, A. Weber, A. Corlu, A. Dubart-Kupperschmitt, Generation of functional cholangiocyte-like cells from human pluripotent stem cells and HepaRG cells, Hepatology. 60 (2014) 700–714. doi:10.1002/hep.27165.
[66] F. Sampaziotis, M. Cardoso de Brito, P. Madrigal, A. Bertero, K. Saeb-Parsy, F.A.C. Soares, E. Schrumpf, E. Melum, T.H. Karlsen, J.A. Bradley, W.T.H. Gelson, S. Davies, A. Baker, A. Kaser, G.J. Alexander, N.R.F. Hannan, L. Vallier, Cholangiocytes derived from human induced pluripotent stem cells for disease modeling and drug validation, Nat. Biotechnol. 33 (2015) 845–852. doi:10.1038/nbt.3275.
[67] S. Wilkening, F. Stahl, A. Bader, Comparison of primary human hepatocytes and hepatoma cell line Hepg2 with regard to their biotransformation properties, Drug Metab. Dispos. Biol. Fate Chem. 31 (2003) 1035–1042. doi:10.1124/dmd.31.8.1035.
[68] S. Anthérieu, C. Chesné, R. Li, C. Guguen-Guillouzo, A. Guillouzo, Optimization of the HepaRG cell model for drug metabolism and toxicity studies, Toxicol. In Vitro. 26 (2012) 1278–1285. doi:10.1016/j.tiv.2012.05.008.
[69] J.V. Castell, R. Jover, C.P. Martnez-Jimnez, M.J. Gmez-Lechn, Hepatocyte cell lines: their use, scope and limitations in drug metabolism studies, Expert Opin. Drug Metab. Toxicol. 2 (2006) 183–212. doi:10.1517/17425255.2.2.183.
[70] N. Dianat, C. Steichen, L. Vallier, A. Weber, A. Dubart-Kupperschmitt, Human Pluripotent Stem Cells for Modelling Human Liver Diseases and Cell Therapy, Curr. Gene Ther. 13 (2013) 120–132. doi:10.2174/1566523211313020006.
[71] J.A. Thomson, J. Itskovitz-Eldor, S.S. Shapiro, M.A. Waknitz, J.J. Swiergiel, V.S. Marshall, J.M. Jones, Embryonic stem cell lines derived from human blastocysts, Science. 282 (1998) 1145–1147.
[72] K. Takahashi, K. Tanabe, M. Ohnuki, M. Narita, T. Ichisaka, K. Tomoda, S. Yamanaka, Induction of Pluripotent Stem Cells from Adult Human Fibroblasts by Defined Factors, Cell. 131 (2007) 861–872. doi:10.1016/j.cell.2007.11.019.
[73] J. Yu, M.A. Vodyanik, K. Smuga-Otto, J. Antosiewicz-Bourget, J.L. Frane, S. Tian, J. Nie, G.A. Jonsdottir, V. Ruotti, R. Stewart, I.I. Slukvin, J.A. Thomson, Induced Pluripotent Stem Cell Lines Derived from Human Somatic Cells, Science. 318 (2007) 1917–1920. doi:10.1126/science.1151526.
[74] J.A. Heslop, S.A. Duncan, The use of human pluripotent stem cells for modelling liver development and disease, Hepatology. (2018). doi:10.1002/hep.30288.
[75] M. Baxter, S. Withey, S. Harrison, C.-P. Segeritz, F. Zhang, R. Atkinson-Dell, C. Rowe, D.T. Gerrard, R. Sison-Young, R. Jenkins, J. Henry, A.A. Berry, L. Mohamet, M. Best, S.W. Fenwick, H. Malik, N.R. Kitteringham, C.E. Goldring, K. Piper Hanley, L. Vallier, N.A. Hanley, Phenotypic and functional analyses show stem cell-derived hepatocyte-like cells better mimic fetal rather than adult hepatocytes, J. Hepatol. 62 (2015) 581–589. doi:10.1016/j.jhep.2014.10.016.

[76] C. Chen, A. Soto-Gutierrez, P.M. Baptista, B. Spee, Biotechnology Challenges to In Vitro Maturation of Hepatic Stem Cells, Gastroenterology. 154 (2018) 1258–1272. doi:10.1053/j.gastro.2018.01.066.
[77] S. Celton-Morizur, C. Desdouets, Polyploidization of liver cells, Adv. Exp. Med. Biol. 676 (2010) 123–135.
[78] G. Gentric, S. Celton-Morizur, C. Desdouets, Polyploidy and liver proliferation, Clin. Res. Hepatol. Gastroenterol. 36 (2012) 29–34. doi:10.1016/j.clinre.2011.05.011.
[79] G. Gentric, C. Desdouets, Polyploidization in Liver Tissue, Am. J. Pathol. 184 (2014) 322–331. doi:10.1016/j.ajpath.2013.06.035.
[80] C. Rowe, D.T. Gerrard, R. Jenkins, A. Berry, K. Durkin, L. Sundstrom, C.E. Goldring, B.K. Park, N.R. Kitteringham, K.P. Hanley, N.A. Hanley, Proteome-wide analyses of human hepatocytes during differentiation and dedifferentiation, Hepatology. 58 (2013) 799–809. doi:10.1002/hep.26414.
[81] K. Si-Tayeb, F.K. Noto, M. Nagaoka, J. Li, M.A. Battle, C. Duris, P.E. North, S. Dalton, S.A. Duncan, Highly efficient generation of human hepatocyte-like cells from induced pluripotent stem cells, Hepatology. 51 (2010) 297–305. doi:10.1002/hep.23354.
[82] Z. Song, J. Cai, Y. Liu, D. Zhao, J. Yong, S. Duo, X. Song, Y. Guo, Y. Zhao, H. Qin, X. Yin, C. Wu, J. Che, S. Lu, M. Ding, H. Deng, Efficient generation of hepatocyte-like cells from human induced pluripotent stem cells, Cell Res. 19 (2009) 1233–1242. doi:10.1038/cr.2009.107.
[83] Y. Duan, A. Catana, Y. Meng, N. Yamamoto, S. He, S. Gupta, S.S. Gambhir, M.A. Zern, Differentiation and Enrichment of Hepatocyte-Like Cells from Human Embryonic Stem Cells In Vitro and In Vivo, Stem Cells. 25 (2007) 3058–3068. doi:10.1634/stemcells.2007-0291.
[84] G. Brolén, L. Sivertsson, P. Björquist, G. Eriksson, M. Ek, H. Semb, I. Johansson, T.B. Andersson, M. Ingelman-Sundberg, N. Heins, Hepatocyte-like cells derived from human embryonic stem cells specifically via definitive endoderm and a progenitor stage, J. Biotechnol. 145 (2010) 284–294. doi:10.1016/j.jbiotec.2009.11.007.
[85] D.C. Hay, D. Zhao, A. Ross, R. Mandalam, J. Lebkowski, W. Cui, Direct Differentiation of Human Embryonic Stem Cells to Hepatocyte-like Cells Exhibiting Functional Activities, Cloning Stem Cells. 9 (2007) 51–62. doi:10.1089/clo.2006.0045.
[86] T. Touboul, N.R.F. Hannan, S. Corbineau, A. Martinez, C. Martinet, S. Branchereau, S. Mainot, H. Strick-Marchand, R. Pedersen, J. Di Santo, A. Weber, L. Vallier, Generation of functional hepatocytes from human embryonic stem cells under chemically defined conditions that recapitulate liver development, Hepatology. 51 (2010) 1754–1765. doi:10.1002/hep.23506.
[87] K.S. Zaret, Genetic programming of liver and pancreas progenitors: lessons for stem-cell differentiation, Nat. Rev. Genet. 9 (2008) 329–340. doi:10.1038/nrg2318.
[88] K.S. Zaret, Regulatory phases of early liver development: paradigms of organogenesis, Nat. Rev. Genet. 3 (2002) 499–512. doi:10.1038/nrg837.
[89] J. Jung, M. Zheng, M. Goldfarb, K.S. Zaret, Initiation of mammalian liver development from endoderm by fibroblast growth factors, Science. 284 (1999) 1998–2003.
[90] J.M. Rossi, N.R. Dunn, B.L. Hogan, K.S. Zaret, Distinct mesodermal signals, including BMPs from the septum transversum mesenchyme, are required in combination for hepatogenesis from the endoderm, Genes Dev. 15 (2001) 1998–2009. doi:10.1101/gad.904601.

[91] A. Calmont, E. Wandzioch, K.D. Tremblay, G. Minowada, K.H. Kaestner, G.R. Martin, K.S. Zaret, An FGF response pathway that mediates hepatic gene induction in embryonic endoderm cells, Dev. Cell. 11 (2006) 339–348. doi:10.1016/j.devcel.2006.06.015.
[92] R. Zhao, S.A. Duncan, Embryonic development of the liver, Hepatol. Baltim. Md. 41 (2005) 956–967. doi:10.1002/hep.20691.
[93] S. Margagliotti, F. Clotman, C.E. Pierreux, J.-B. Beaudry, P. Jacquemin, G.G. Rousseau, F.P. Lemaigre, The Onecut transcription factors HNF-6/OC-1 and OC-2 regulate early liver expansion by controlling hepatoblast migration, Dev. Biol. 311 (2007) 579–589. doi:10.1016/j.ydbio.2007.09.013.
[94] S. Margagliotti, F. Clotman, C.E. Pierreux, P. Lemoine, G.G. Rousseau, P. Henriet, F.P. Lemaigre, Role of metalloproteinases at the onset of liver development, Dev. Growth Differ. 50 (2008) 331–338. doi:10.1111/j.1440-169X.2008.01031.x.
[95] M. Yanai, N. Tatsumi, N. Hasunuma, K. Katsu, F. Endo, Y. Yokouchi, FGF signaling segregates biliary cell-lineage from chick hepatoblasts cooperatively with BMP4 and ECM components in vitro, Dev. Dyn. Off. Publ. Am. Assoc. Anat. 237 (2008) 1268–1283. doi:10.1002/dvdy.21520.
[96] D. Shin, C.H. Shin, J. Tucker, E.A. Ober, F. Rentzsch, K.D. Poss, M. Hammerschmidt, M.C. Mullins, D.Y.R. Stainier, Bmp and Fgf signaling are essential for liver specification in zebrafish, Dev. Camb. Engl. 134 (2007) 2041–2050. doi:10.1242/dev.000281.
[97] S.S. Sekhon, X. Tan, A. Micsenyi, W.C. Bowen, S.P.S. Monga, Fibroblast growth factor enriches the embryonic liver cultures for hepatic progenitors, Am. J. Pathol. 164 (2004) 2229–2240. doi:10.1016/S0002-9440(10)63779-0.
[98] T. Berg, C.B. Rountree, L. Lee, J. Estrada, F.G. Sala, A. Choe, J.M. Veltmaat, S. De Langhe, R. Lee, H. Tsukamoto, G.M. Crooks, S. Bellusci, K.S. Wang, Fibroblast growth factor 10 is critical for liver growth during embryogenesis and controls hepatoblast survival via beta-catenin activation, Hepatol. Baltim. Md. 46 (2007) 1187–1197. doi:10.1002/hep.21814.
[99] X. Tan, Y. Yuan, G. Zeng, U. Apte, M.D. Thompson, B. Cieply, D.B. Stolz, G.K. Michalopoulos, K.H. Kaestner, S.P.S. Monga, Beta-catenin deletion in hepatoblasts disrupts hepatic morphogenesis and survival during mouse development, Hepatol. Baltim. Md. 47 (2008) 1667–1679. doi:10.1002/hep.22225.
[100] V.A. McLin, S.A. Rankin, A.M. Zorn, Repression of Wnt/beta-catenin signaling in the anterior endoderm is essential for liver and pancreas development, Dev. Camb. Engl. 134 (2007) 2207–2217. doi:10.1242/dev.001230.
[101] S.P.S. Monga, W.M. Mars, P. Pediaditakis, A. Bell, K. Mulé, W.C. Bowen, X. Wang, R. Zarnegar, G.K. Michalopoulos, Hepatocyte growth factor induces Wnt-independent nuclear translocation of beta-catenin after Met-beta-catenin dissociation in hepatocytes, Cancer Res. 62 (2002) 2064–2071.
[102] G.K. Michalopoulos, W. Bowen, A.K. Nussler, M.J. Becich, T.A. Howard, Comparative analysis of mitogenic and morphogenic effects of HGF and EGF on rat and human hepatocytes maintained in collagen gels, J. Cell. Physiol. 156 (1993) 443–452. doi:10.1002/jcp.1041560303.
[103] C. Schmidt, F. Bladt, S. Goedecke, V. Brinkmann, W. Zschiesche, M. Sharpe, E. Gherardi, C. Birchmeier, Scatter factor/hepatocyte growth factor is essential for liver development, Nature. 373 (1995) 699–702. doi:10.1038/373699a0.

[104] D.C. Weinstein, A. Ruiz i Altaba, W.S. Chen, P. Hoodless, V.R. Prezioso, T.M. Jessell, J.E. Darnell, The winged-helix transcription factor HNF-3 beta is required for notochord development in the mouse embryo, Cell. 78 (1994) 575–588.
[105] A. Moumen, A. Ieraci, S. Patané, C. Solé, J.X. Comella, R. Dono, F. Maina, Met signals hepatocyte survival by preventing Fas-triggered FLIP degradation in a PI3k-Akt-dependent manner, Hepatol. Baltim. Md. 45 (2007) 1210–1217. doi:10.1002/hep.21604.
[106] G.K. Michalopoulos, W.C. Bowen, K. Mulè, J. Luo, HGF-, EGF-, and dexamethasone-induced gene expression patterns during formation of tissue in hepatic organoid cultures, Gene Expr. 11 (2003) 55–75.
[107] Y. Ito, T. Matsui, A. Kamiya, T. Kinoshita, A. Miyajima, Retroviral gene transfer of signaling molecules into murine fetal hepatocytes defines distinct roles for the STAT3 and ras pathways during hepatic development, Hepatol. Baltim. Md. 32 (2000) 1370–1376. doi:10.1053/jhep.2000.19815.
[108] A. Suzuki, A. Iwama, H. Miyashita, H. Nakauchi, H. Taniguchi, Role for growth factors and extracellular matrix in controlling differentiation of prospectively isolated hepatic stem cells, Dev. Camb. Engl. 130 (2003) 2513–2524.
[109] J. Shan, R.E. Schwartz, N.T. Ross, D.J. Logan, D. Thomas, S.A. Duncan, T.E. North, W. Goessling, A.E. Carpenter, S.N. Bhatia, Identification of small molecules for human hepatocyte expansion and iPS differentiation, Nat. Chem. Biol. 9 (2013) 514–520. doi:10.1038/nchembio.1270.
[110] D.T. Odom, N. Zizlsperger, D.B. Gordon, G.W. Bell, N.J. Rinaldi, H.L. Murray, T.L. Volkert, J. Schreiber, P.A. Rolfe, D.K. Gifford, E. Fraenkel, G.I. Bell, R.A. Young, Control of pancreas and liver gene expression by HNF transcription factors, Science. 303 (2004) 1378–1381. doi:10.1126/science.1089769.
[111] W. Cheng, L. Guo, Z. Zhang, H.M. Soo, C. Wen, W. Wu, J. Peng, HNF factors form a network to regulate liver-enriched genes in zebrafish, Dev. Biol. 294 (2006) 482–496. doi:10.1016/j.ydbio.2006.03.018.
[112] I. Kyrmizi, P. Hatzis, N. Katrakili, F. Tronche, F.J. Gonzalez, I. Talianidis, Plasticity and expanding complexity of the hepatic transcription factor network during liver development, Genes Dev. 20 (2006) 2293–2305. doi:10.1101/gad.390906.
[113] C. Gérard, J. Tys, F.P. Lemaigre, Gene regulatory networks in differentiation and direct reprogramming of hepatic cells, Semin. Cell Dev. Biol. 66 (2017) 43–50. doi:10.1016/j.semcdb.2016.12.003.
[114] N.D. Wang, M.J. Finegold, A. Bradley, C.N. Ou, S.V. Abdelsayed, M.D. Wilde, L.R. Taylor, D.R. Wilson, G.J. Darlington, Impaired energy homeostasis in C/EBP alpha knockout mice, Science. 269 (1995) 1108–1112.
[115] M. Pontoglio, J. Barra, M. Hadchouel, A. Doyen, C. Kress, J.P. Bach, C. Babinet, M. Yaniv, Hepatocyte nuclear factor 1 inactivation results in hepatic dysfunction, phenylketonuria, and renal Fanconi syndrome, Cell. 84 (1996) 575–585.
[116] H. Yamasaki, A. Sada, T. Iwata, T. Niwa, M. Tomizawa, K.G. Xanthopoulos, T. Koike, N. Shiojiri, Suppression of C/EBPalpha expression in periportal hepatoblasts may stimulate biliary cell differentiation through increased Hnf6 and Hnf1b expression, Dev. Camb. Engl. 133 (2006) 4233–4243. doi:10.1242/dev.02591.
[117] M. Rastegar, G.G. Rousseau, F.P. Lemaigre, CCAAT/enhancer-binding protein-alpha is a component of the growth hormone-regulated network of liver transcription factors, Endocrinology. 141 (2000) 1686–1692. doi:10.1210/endo.141.5.7478.

[118] S. Mathapati, R. Siller, A.A.R. Impellizzeri, M. Lycke, K. Vegheim, R. Almaas, G.J. Sullivan, Small-Molecule-Directed Hepatocyte-Like Cell Differentiation of Human Pluripotent Stem Cells: hPSC-Derived Hepatocytes Using Small Molecules, in: M. Bhatia, A.G. Elefanty, S.J. Fisher, R. Patient, T. Schlaeger, E.Y. Snyder (Eds.), Curr. Protoc. Stem Cell Biol., John Wiley & Sons, Inc., Hoboken, NJ, USA, 2016: pp. 1G.6.1-1G.6.18. doi:10.1002/cpsc.13.

[119] R. Siller, S. Greenhough, E. Naumovska, G.J. Sullivan, Small-Molecule-Driven Hepatocyte Differentiation of Human Pluripotent Stem Cells, Stem Cell Rep. 4 (2015) 939–952. doi:10.1016/j.stemcr.2015.04.001.

[120] C. Du, Y. Feng, D. Qiu, Y. Xu, M. Pang, N. Cai, A.P. Xiang, Q. Zhang, Highly efficient and expedited hepatic differentiation from human pluripotent stem cells by pure small-molecule cocktails, Stem Cell Res. Ther. 9 (2018). doi:10.1186/s13287-018-0794-4.

[121] W. Song, Y.-C. Lu, A.S. Frankel, D. An, R.E. Schwartz, M. Ma, Engraftment of human induced pluripotent stem cell-derived hepatocytes in immunocompetent mice via 3D co-aggregation and encapsulation, Sci. Rep. 5 (2015). doi:10.1038/srep16884.

[122] D.R. Berger, B.R. Ware, M.D. Davidson, S.R. Allsup, S.R. Khetani, Enhancing the functional maturity of induced pluripotent stem cell-derived human hepatocytes by controlled presentation of cell-cell interactions in vitro, Hepatol. Baltim. Md. 61 (2015) 1370–1381. doi:10.1002/hep.27621.

[123] R.L. Gieseck III, N.R.F. Hannan, R. Bort, N.A. Hanley, R.A.L. Drake, G.W.W. Cameron, T.A. Wynn, L. Vallier, Maturation of Induced Pluripotent Stem Cell Derived Hepatocytes by 3D-Culture, PLoS ONE. 9 (2014) e86372. doi:10.1371/journal.pone.0086372.

[124] A. Baiocchini, C. Montaldo, A. Conigliaro, A. Grimaldi, V. Correani, F. Mura, F. Ciccosanti, N. Rotiroti, A. Brenna, M. Montalbano, G. D'Offizi, M.R. Capobianchi, R. Alessandro, M. Piacentini, M.E. Schininà, B. Maras, F. Del Nonno, M. Tripodi, C. Mancone, Extracellular Matrix Molecular Remodeling in Human Liver Fibrosis Evolution, PLOS ONE. 11 (2016) e0151736. doi:10.1371/journal.pone.0151736.

[125] R. McClelland, E. Wauthier, J. Uronis, L. Reid, Gradients in the Liver's Extracellular Matrix Chemistry from Periportal to Pericentral Zones: Influence on Human Hepatic Progenitors, Tissue Eng. Part A. 14 (2008) 59–70. doi:10.1089/ten.a.2007.0058.

[126] Y. Kikkawa, R. Sudo, J. Kon, T. Mizuguchi, M. Nomizu, K. Hirata, T. Mitaka, Laminin α5 mediates ectopic adhesion of hepatocellular carcinoma through integrins and/or Lutheran/basal cell adhesion molecule, Exp. Cell Res. 314 (2008) 2579–2590. doi:10.1016/j.yexcr.2008.05.021.

[127] Y. Wang, C.-B. Cui, M. Yamauchi, P. Miguez, M. Roach, R. Malavarca, M.J. Costello, V. Cardinale, E. Wauthier, C. Barbier, D.A. Gerber, D. Alvaro, L.M. Reid, Lineage restriction of human hepatic stem cells to mature fates is made efficient by tissue-specific biomatrix scaffolds, Hepatology. 53 (2011) 293–305. doi:10.1002/hep.24012.

[128] Liisa Kanninen, Bioinspired matrices for in vitro hepatic differentiation, University of Helsinki, 2016. https://helda.helsinki.fi/bitstream/handle/10138/161533/bioinspi.pdf?sequence=1.

[129] G. Mazza, K. Rombouts, A. Rennie Hall, L. Urbani, T. Vinh Luong, W. Al-Akkad, L. Longato, D. Brown, P. Maghsoudlou, A.P. Dhillon, B. Fuller, B. Davidson, K. Moore, D. Dhar, P. De Coppi, M. Malago, M. Pinzani, Decellularized human liver as a natural 3D-scaffold for liver bioengineering and transplantation, Sci. Rep. 5 (2015). doi:10.1038/srep13079.

[130] A. Martinez-Hernandez, P.S. Amenta, The extracellular matrix in hepatic regeneration, FASEB J. Off. Publ. Fed. Am. Soc. Exp. Biol. 9 (1995) 1401–1410.
[131] A. Martinez-Hernandez, P.S. Amenta, The hepatic extracellular matrix. I. Components and distribution in normal liver, Virchows Arch. A Pathol. Anat. Histopathol. 423 (1993) 1–11.
[132] A.P. Kourouklis, K.B. Kaylan, G.H. Underhill, Substrate stiffness and matrix composition coordinately control the differentiation of liver progenitor cells, Biomaterials. 99 (2016) 82–94. doi:10.1016/j.biomaterials.2016.05.016.
[133] P.R. Sudhakaran, Hepatocyte-matrix interaction, Proc. Indian Acad. Sci. - Chem. Sci. 111 (1999) 331. doi:10.1007/BF02871913.
[134] A. Couvelard, A.-F. Bringuier, M.-C. Dauge, M. Nejjari, E. Darai, J.-L. Benifla, G. Feldmann, D. Henin, J.-Y. Scoazec, Expression of integrins during liver organogenesis in humans, Hepatology. 27 (1998) 839–847. doi:10.1002/hep.510270328.
[135] R. Turner, O. Lozoya, Y. Wang, V. Cardinale, E. Gaudio, G. Alpini, G. Mendel, E. Wauthier, C. Barbier, D. Alvaro, L.M. Reid, Human hepatic stem cell and maturational liver lineage biology, Hepatology. 53 (2011) 1035–1045. doi:10.1002/hep.24157.
[136] W.-C. Yeh, P.-C. Li, Y.-M. Jeng, H.-C. Hsu, P.-L. Kuo, M.-L. Li, P.-M. Yang, P.-H. Lee, Elastic modulus measurements of human liver and correlation with pathology, Ultrasound Med. Biol. 28 (2002) 467–474.
[137] S.S. Desai, J.C. Tung, V.X. Zhou, J.P. Grenert, Y. Malato, M. Rezvani, R. Español-Suñer, H. Willenbring, V.M. Weaver, T.T. Chang, Physiological ranges of matrix rigidity modulate primary mouse hepatocyte function in part through hepatocyte nuclear factor 4 alpha: Matrix rigidity modulates hepatocyte function, Hepatology. 64 (2016) 261–275. doi:10.1002/hep.28450.
[138] J.D. Humphrey, E.R. Dufresne, M.A. Schwartz, Mechanotransduction and extracellular matrix homeostasis, Nat. Rev. Mol. Cell Biol. 15 (2014) 802–812. doi:10.1038/nrm3896.
[139] R.O. Hynes, Integrins: bidirectional, allosteric signaling machines, Cell. 110 (2002) 673–687.
[140] U. Apte, V. Gkretsi, W.C. Bowen, W.M. Mars, J.-H. Luo, S. Donthamsetty, A. Orr, S.P.S. Monga, C. Wu, G.K. Michalopoulos, Enhanced liver regeneration following changes induced by hepatocyte-specific genetic ablation of integrin-linked kinase, Hepatology. 50 (2009) 844–851. doi:10.1002/hep.23059.
[141] V. Gkretsi, U. Apte, W.M. Mars, W.C. Bowen, J.-H. Luo, Y. Yang, Y.P. Yu, A. Orr, R. St.-Arnaud, S. Dedhar, K.H. Kaestner, C. Wu, G.K. Michalopoulos, Liver-specific ablation of integrin-linked kinase in mice results in abnormal histology, enhanced cell proliferation, and hepatomegaly, Hepatology. 48 (2008) 1932–1941. doi:10.1002/hep.22537.
[142] T. Speicher, B. Siegenthaler, R.L. Bogorad, R. Ruppert, T. Petzold, S. Padrissa-Altes, M. Bachofner, D.G. Anderson, V. Koteliansky, R. Fässler, S. Werner, Knockdown and knockout of β1-integrin in hepatocytes impairs liver regeneration through inhibition of growth factor signalling, Nat. Commun. 5 (2014). doi:10.1038/ncomms4862.
[143] D.C. Hay, J. Fletcher, C. Payne, J.D. Terrace, R.C.J. Gallagher, J. Snoeys, J.R. Black, D. Wojtacha, K. Samuel, Z. Hannoun, A. Pryde, C. Filippi, I.S. Currie, S.J. Forbes, J.A. Ross, P.N. Newsome, J.P. Iredale, Highly efficient differentiation of hESCs to functional hepatic endoderm requires ActivinA and Wnt3a signaling, Proc. Natl. Acad. Sci. 105 (2008) 12301–12306. doi:10.1073/pnas.0806522105.

[144] N.R.F. Hannan, C.-P. Segeritz, T. Touboul, L. Vallier, Production of hepatocyte-like cells from human pluripotent stem cells, Nat. Protoc. 8 (2013) 430–437. doi:10.1038/nprot.2012.153.
[145] C.S. Hughes, L.M. Postovit, G.A. Lajoie, Matrigel: A complex protein mixture required for optimal growth of cell culture, PROTEOMICS. 10 (2010) 1886–1890. doi:10.1002/pmic.200900758.
[146] BD Matrigel Matrix, (n.d.). http://fscimage.fishersci.com/cmsassets/downloads/segment/Scientific/pdf/BD/bd_cellculture_matrigel_faq.pdf.
[147] M.J. Martin, A. Muotri, F. Gage, A. Varki, Human embryonic stem cells express an immunogenic nonhuman sialic acid, Nat. Med. 11 (2005) 228–232. doi:10.1038/nm1181.
[148] M.P. Lutolf, Synthetic matrix metalloproteinase-sensitive hydrogels for the conduction of tissue regeneration: Engineering cell-invasion characteristics, Proc. Natl. Acad. Sci. 100 (2003) 5413–5418. doi:10.1073/pnas.0737381100.
[149] H. Baharvand, S.M. Hashemi, S. Kazemi Ashtiani, A. Farrokhi, Differentiation of human embryonic stem cells into hepatocytes in 2D and 3D culture systems in vitro, Int. J. Dev. Biol. 50 (2006) 645–652. doi:10.1387/ijdb.052072hb.
[150] S. Toivonen, M.M. Malinen, J. Küblbeck, A. Petsalo, A. Urtti, P. Honkakoski, T. Otonkoski, Regulation of Human Pluripotent Stem Cell-Derived Hepatic Cell Phenotype by Three-Dimensional Hydrogel Models, Tissue Eng. Part A. 22 (2016) 971–984. doi:10.1089/ten.tea.2016.0127.
[151] K. Cameron, R. Tan, W. Schmidt-Heck, G. Campos, M.J. Lyall, Y. Wang, B. Lucendo-Villarin, D. Szkolnicka, N. Bates, S.J. Kimber, J.G. Hengstler, P. Godoy, S.J. Forbes, D.C. Hay, Recombinant Laminins Drive the Differentiation and Self-Organization of hESC-Derived Hepatocytes, Stem Cell Rep. 5 (2015) 1250–1262. doi:10.1016/j.stemcr.2015.10.016.
[152] L.K. Kanninen, R. Harjumäki, P. Peltoniemi, M.S. Bogacheva, T. Salmi, P. Porola, J. Niklander, T. Smutný, A. Urtti, M.L. Yliperttula, Y.-R. Lou, Laminin-511 and laminin-521-based matrices for efficient hepatic specification of human pluripotent stem cells, Biomaterials. 103 (2016) 86–100. doi:10.1016/j.biomaterials.2016.06.054.
[153] K. Takayama, Y. Nagamoto, N. Mimura, K. Tashiro, F. Sakurai, M. Tachibana, T. Hayakawa, K. Kawabata, H. Mizuguchi, Long-Term Self-Renewal of Human ES/iPS-Derived Hepatoblast-like Cells on Human Laminin 111-Coated Dishes, Stem Cell Rep. 1 (2013) 322–335. doi:10.1016/j.stemcr.2013.08.006.
[154] Y. Wang, S. Alhaque, K. Cameron, J. Meseguer-Ripolles, B. Lucendo-Villarin, H. Rashidi, D.C. Hay, Defined and Scalable Generation of Hepatocyte-like Cells from Human Pluripotent Stem Cells, J. Vis. Exp. (2017). doi:10.3791/55355.
[155] K. Takayama, Y. Morisaki, S. Kuno, Y. Nagamoto, K. Harada, N. Furukawa, M. Ohtaka, K. Nishimura, K. Imagawa, F. Sakurai, M. Tachibana, R. Sumazaki, E. Noguchi, M. Nakanishi, K. Hirata, K. Kawabata, H. Mizuguchi, Prediction of interindividual differences in hepatic functions and drug sensitivity by using human iPS-derived hepatocytes, Proc. Natl. Acad. Sci. 111 (2014) 16772–16777. doi:10.1073/pnas.1413481111.
[156] M. Nagaoka, M. Kobayashi, C. Kawai, S.K. Mallanna, S.A. Duncan, Design of a Vitronectin-Based Recombinant Protein as a Defined Substrate for Differentiation of Human Pluripotent Stem Cells into Hepatocyte-Like Cells, PLOS ONE. 10 (2015) e0136350. doi:10.1371/journal.pone.0136350.

[157] O.A. Lozoya, E. Wauthier, R.A. Turner, C. Barbier, G.D. Prestwich, F. Guilak, R. Superfine, S.R. Lubkin, L.M. Reid, Regulation of hepatic stem/progenitor phenotype by microenvironment stiffness in hydrogel models of the human liver stem cell niche, Biomaterials. 32 (2011) 7389–7402. doi:10.1016/j.biomaterials.2011.06.042.

[158] R.A. Turner, E. Wauthier, O. Lozoya, R. McClelland, J.E. Bowsher, C. Barbier, G. Prestwich, E. Hsu, D.A. Gerber, L.M. Reid, Successful transplantation of human hepatic stem cells with restricted localization to liver using hyaluronan grafts†, Hepatology. 57 (2013) 775–784. doi:10.1002/hep.26065.

[159] N.-C. Cheng, S. Wang, T.-H. Young, The influence of spheroid formation of human adipose-derived stem cells on chitosan films on stemness and differentiation capabilities, Biomaterials. 33 (2012) 1748–1758. doi:10.1016/j.biomaterials.2011.11.049.

[160] F. Ruggiero, M. Koch, Making recombinant extracellular matrix proteins, Methods. 45 (2008) 75–85. doi:10.1016/j.ymeth.2008.01.003.

[161] B.L. Villarin, K. Cameron, D. Szkolnicka, H. Rashidi, N. Bates, S.J. Kimber, O. Flint, S.J. Forbes, J.P. Iredale, M. Bradley, D.C. Hay, Polymer Supported Directed Differentiation Reveals a Unique Gene Signature Predicting Stable Hepatocyte Performance, Adv. Healthc. Mater. 4 (2015) 1820–1825. doi:10.1002/adhm.201500391.

[162] B. Lucendo-Villarin, K. Cameron, D. Szkolnicka, P. Travers, F. Khan, J.G. Walton, J. Iredale, M. Bradley, D.C. Hay, Stabilizing Hepatocellular Phenotype Using Optimized Synthetic Surfaces, J. Vis. Exp. (2014). doi:10.3791/51723.

[163] Y. Luo, C. Lou, S. Zhang, Z. Zhu, Q. Xing, P. Wang, T. Liu, H. Liu, C. Li, W. Shi, Z. Du, Y. Gao, Three-dimensional hydrogel culture conditions promote the differentiation of human induced pluripotent stem cells into hepatocytes, Cytotherapy. 20 (2018) 95–107. doi:10.1016/j.jcyt.2017.08.008.

[164] S. Kazemnejad, A. Allameh, M. Soleimani, A. Gharehbaghian, Y. Mohammadi, N. Amirizadeh, M. Jazayery, Biochemical and molecular characterization of hepatocyte-like cells derived from human bone marrow mesenchymal stem cells on a novel three-dimensional biocompatible nanofibrous scaffold, J. Gastroenterol. Hepatol. 24 (2009) 278–287. doi:10.1111/j.1440-1746.2008.05530.x.

[165] J. Li, R. Tao, W. Wu, H. Cao, J. Xin, J. Li, J. Guo, L. Jiang, C. Gao, A.A. Demetriou, D.L. Farkas, L. Li, 3D PLGA Scaffolds Improve Differentiation and Function of Bone Marrow Mesenchymal Stem Cell–Derived Hepatocytes, Stem Cells Dev. 19 (2010) 1427–1436. doi:10.1089/scd.2009.0415.

[166] B. Wang, A.E. Jakus, P.M. Baptista, S. Soker, A. Soto-Gutierrez, M.M. Abecassis, R.N. Shah, J.A. Wertheim, Functional Maturation of Induced Pluripotent Stem Cell Hepatocytes in Extracellular Matrix-A Comparative Analysis of Bioartificial Liver Microenvironments, Stem Cells Transl. Med. 5 (2016) 1257–1267. doi:10.5966/sctm.2015-0235.

Chapter 3: Structure, Function and development of blood vessels: Lessons for Tissue Engineering

Elements of this chapter have been published as:

Hamisha Ardalani, Amir H. Assadi, William L. Murphy (2014). "Structure, Function, and Development of Blood Vessels: Lessons for Tissue Engineering." In Engineering in Translational Medicine (pp. 155-182). Springer London.

DOI: https://doi.org/10.1007/978-1-4471-4372-7_6

3.1 Preface

In chapter 2, we provided an overview of factors affecting maturation of hepatocytes during different stages of liver development, from the effect of sinusoidal endothelial cells (sECs) to extracellular matrix (ECM) and integrin-binding ligands on hepatocyte maturation, and how this information can be used to produce more mature induced pluripotent stem (iPS) or embryonic stem (ES) derived cells. Endothelial cells and vascular development play an essential role in organ development and particularly liver development; however, its role is often underscored in developed in vitro liver models. Here, we provide an overview of the structure of blood vessels and key signaling molecules, which play a significant role in vasculogenesis, angiogenesis, and maturation of nascent blood, the role of ECM and recent advances in making tissue-engineered blood vessels (both macro- and micro-vessels) *ex vivo*.

3.2 Introduction

The establishment of blood-vessel networks is a matter of life and death for tissues and organisms. Failure to form a functional vascular network causes early death of embryos, and also

dysfunction of endothelial cells contributes to many diseases, including stroke, thrombosis and atherosclerosis. Furthermore, there is a considerable clinical need for alternatives to the autologous vein and artery tissues used for vascular reconstructive surgeries such as lower limb bypass, arteriovenous shunts and repairs of congenital defects to the pulmonary outflow tract. So far, synthetic materials, particularly in small diameter applications have not matched the efficacy of native tissues. Therefore, substantial resources are being directed towards research into the cellular, molecular and physical factors that regulate the formation, stability and functional responses of the vasculature. While academic research in the field of tissue engineering in general has been active, yet there has been no clear example of clinical and commercial success. The recent transition of cell-based therapies from experimental to clinical use, however, is a breakthrough in the field of cardiovascular tissue engineering.

Here, we discuss the structure of blood vessels and key signaling molecules, which play significant role in vasculogenesis, angiogenesis and maturation of nascent blood vessels in section 3.1 and 3.2, respectively. The discussion is followed by a description of promising approaches specific to tissue-engineered blood vessels and a brief introduction to some clinical results in section 3.4. But before we explain about tissue engineering approaches finding the appropriate sources of endothelial cells is of utmost importance, which is discussed in section 3.3. The unique regulatory, reimbursement and production challenges facing personalized medicine are also discussed in the last section 3.5.

3.3 Structure of blood vessels

Delivery of nutrients and other molecules as well as blood and immune cells to all tissues in our body is done by blood vessels. Nascent vessels consist of a tube of ECs that mature into four

specialized structures: *capillaries*, *arteries*, *veins and lymphatics*. Endothelial cells and mural cells that are surrounded by extracellular matrix (ECM) comprise the walls of vessels.

To form mature blood vessels, immature blood vessels formed by vasculogenesis and angiogenesis must mature at two levels: the *level of vessel wall* as well as *network level*. *Vessel wall* maturation is the result of mural cell recruitment, development of surrounding matrix and elastic laminae, and organ specific specialization of ECs, mural cells and matrix. Optimal patterning of network by branching, expanding and pruning to meet local demands leads to *network level* maturation [1,2].

3.3.1 Capillaries

The most abundant vessels in our body are capillaries. Capillaries consist of ECs covered with a sparse layer of pericytes that is surrounded by basement membrane. Because of their wall structure and large surface-area-to-volume ratio, these vessels form the main site of exchange of nutrients between blood and tissue. Depending upon the organ or tissue, the capillary endothelial layer could be continuous (as in muscle), fenestrated (as in kidney or endocrine glands) or discontinuous (as in liver sinusoids). The endothelia of the blood-brain barrier or blood-retina barrier are further specialized to include tight junctions, and are thus impermeable to various molecules [1].

3.3.2 Arterioles and Venules

Arterioles and venules are small diameter blood vessels in the microcirculation that extend and branch out from an artery and vein respectively, which lead to capillaries [1]. These vessels have an increased coverage of mural cells compared with capillaries. Pre-capillary arterioles are completely invested with vascular SMCs that form their own basement membrane and are

circumferentially arranged, closely packed and tightly associated with the endothelium. Extravasation of macromolecules and cells from the blood stream typically occurs from post-capillary venules [2, 3].

3.3.3 Arteries and Veins

Arteries are blood vessels that carry blood away from the heart. This blood is normally oxygenated, with the exception of the pulmonary and umbilical arteries. Veins are blood vessels that carry blood towards the heart. Most veins carry deoxygenated blood from the tissues back to the heart; exceptions are the pulmonary and umbilical veins, both of which carry oxygenated blood to the heart. Larger vessels, arteries and veins, consist of three specialized layers as shown in Figure 3.1: tunica intima, the tunica media, and the tunica adventitia. The tunica intima is made of a monolayer of ECs with an underlying basement membrane. The tunica media is generally composed of a dense population of concentrically organized SMCs and is separated from the tunica intima by an internal elastic lamina. The tunica adventitia forms the external layer and contains fibroblast cells, collagenous ECM, nerves, and vasa vasorum [4]. The vascular wall ECM, composed of structural proteins like collagen and elastin and adhesion proteins like fibronectin and laminin, as well as glycosaminoglycans, proteoglycans, growth factors, cytokines, and matrix-degrading enzymes and their inhibitors [5,6].

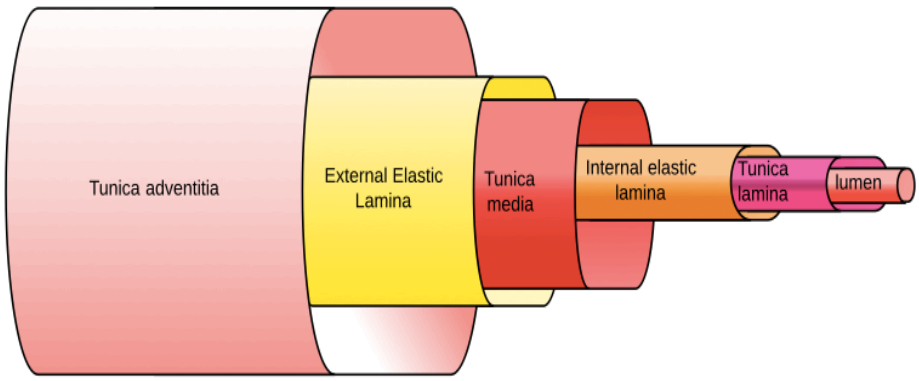

Figure 3.1 Schematic representation of various layers in blood vessels

3.4 Important signaling molecules in vasculogenesis and angiogenesis

Understanding important signaling molecules at each level of development of arteries, veins and capillaries and their maturation could help us to engineer blood vessels that are a more faithful mimic of the natural system. Here we review briefly the important molecules and pathways in vasculogenesis, angiogenesis and maturation. Tissue-engineering strategies may benefit from generating materials that can guide these biological events in the formation of vascular networks. How scientists and researchers use this information to engineer the blood vessels is discussed in section 3.4.

3.4.1 Formation of immature vasculature by vasculogenesis and angiogenesis

During embryonic development, angioblasts migrate to various regions of the developing embryo and differentiate into endothelial cells in response to local cues such as growth factors and extracellular matrix (ECM) components. The endothelial cells then form a vascular plexus, which is a network built by connections (anastomoses) between blood vessels. This process is called vasculogenesis and it is not limited to the embryonic period, as a similar process can also occur in adults through the recruitment and participation of bone marrow derived endothelial progenitor

cells [3,7,8].

Angiogenesis is another mechanism of blood vessel formation that occurs through the sprouting of existing blood vessels. Angiogenesis is a sequential, multistep process that begins with activation of a quiescent endothelium by proangiogenic factors such as vascular endothelial growth factor (VEGF), fibroblast growth factor (FGF), and angiopoietin-2 (Ang2) that are often produced by hypoxic or tumorigenic tissues[3,8]. Hypoxia up-regulates expression of a number of genes involved in vessel formation, patterning and maturation, including nitric oxide synthase, *VEGF*, and Ang2. Nitric oxide, which is a product of nitric oxide synthase, dilates vessels and make them more responsive to VEGF because they become leakier. Ang2 also facilitates sprout formation in the presence of VEGF. The sprouts anastomose to form vascular loops and networks[3].

Angiogenesis is also dependent on degradation of the basement membrane (BM), a thin layer of ECM between the epithelial cell layer and the endothelial cell lining of blood vessels. Degradation of BM is due to up-regulation of matrix metalloproteinases (MMPs) such as MMP2, MMP3 and MMP9, and suppression of protease inhibitors such as tissue inhibitor of metalloproteinase-2 (TIMP2). BM degradation is followed by migration of an endothelial tip cell from the leading edge of a vascular sprout; this leading edge defines the direction of the newly growing sprout [2,6,7].

3.4.2 Endothelial cell branching and proliferation

High levels of proangiogenic factors (such as VEGFA and VEGFC) and of VEGF receptor 2 (VEGFR2) or VEGFR3 signaling select ‘tip cells’ (TCs) for sprouting during angiogenesis. By contrast, Delta-like 4-Notch signaling laterally inhibits TC fate in adjacent ECs. TC sprouting behavior is facilitated by the vascular endothelial cadherin-mediated loosening of EC–EC junctions, matrix metalloproteinase-mediated degradation of extracellular matrix (ECM) and the

detachment of pericytes. Guidance of TC sprouting is due to the gradients of proangiogenic growth factors and various environmental guidance cues, such as semaphorins and ephrins. During sprout elongation, TCs are trailed by endothelial 'stalk cells' (SCs), which maintain connectivity with parental vessels and initiate partitioning-defective3 (PAR3)-mediated vascular lumen morphogenesis. Expression of VEGFR1 and activation of Notch, Roundabout homologue 4 and WNT signaling in SCs repress TC behavior to maintain the hierarchical organization of sprouting ECs. However, TCs and SCs may also shuffle and exchange positions during angiogenic sprouting. Upon contact with other vessels, TC behavior is repressed, and vessels fuse by the process of anastomosis, which is assisted by associated myeloid cells. The endothelial cells adjacent to the tip cells begin to proliferate and elongate to form capillary sprouts, which then assemble to form a vessel lumen. After the activation and proliferation stages, a nascent blood vessel must mature to become functional [6–11].

3.4.3 Stabilization of immature vasculature

After the activation and proliferation stages, a nascent blood vessel must mature to become functional. The nascent vessels are stabilized by recruiting mural cells and by deposition of an ECM, in a process known as arteriogenesis. There are at least four molecular pathways that regulate this process, including:

1) Platelet-derived growth factor PDGFB and PDGF receptor (PDGFR)-β
2) Sphingosine-1-phosphate-1 (S1P) - endothelial differentiation sphingolipid G-protein-coupled receptor-1 (EDG1)
3) Ang1-Tie2
4) Transforming growth factor TGF-β1

Recruitment of mural cells such as pericytes and smooth muscle cells (SMCs) to the developing immature vasculature by platelet-derived growth factor B (PDGFB) and transforming growth factor-β1 (TGFβ1) stabilize the vessel wall [2,7,12,13]. The contact between ECs and mural cells is strengthened by bioactive lipid spingosine1 phosphate (S1P) through activating the guanine nucleotide binding coupled receptor, and S1P receptor 1(S1PR1 or EDG1) signaling [7,14]. Tie receptors (Tie1 and Tie2) and their ligands Ang1 and Ang2 are also critical for vessel formation and stabilization. Main sources of Ang1 and Ang2 are the mural cells and ECs, respectively. Ang1 stabilizes nascent vessels by facilitating communication between ECs and mural cells. Ang2 acts as an antagonist of Ang1 in the absence of VEGF, and destabilizes vessels in the presence of VEGF [15].

TGF-β1 is a multifunctional growth factor that promotes vessel maturation by stimulating ECM production and by inducing differentiation of mesenchymal cells to mural cells. It is expressed in a number of cell types, including ECs and mural cells, and depending on the context and concentration, could be pro or anti-angiogenic. Recent *in vitro* studies indicate that the TGF-β1−ALK1 pathway is a positive regulator of endothelial cell migration and proliferation by inducing ECs and fibroblasts to express Id1, a protein required for proliferation and migration. On the other hand, the TGF-β1−ALK5 pathway is a positive regulator of vessel maturation by inducing the plasminogen activator inhibitor (PAI1) in endothelial cells. PAI1 promotes vessel maturation by preventing degradation of the provisional matrix around the nascent vessel. Thus, the degree to which TGF-β signals through ALK1 versus ALK5 can determine the pro or anti-angiogenic effect of TGF-β[2,10]. Figure 3.2 shows important signaling molecules that are involved in vasculogenesis, maturation of blood vessels and angiogenesis.

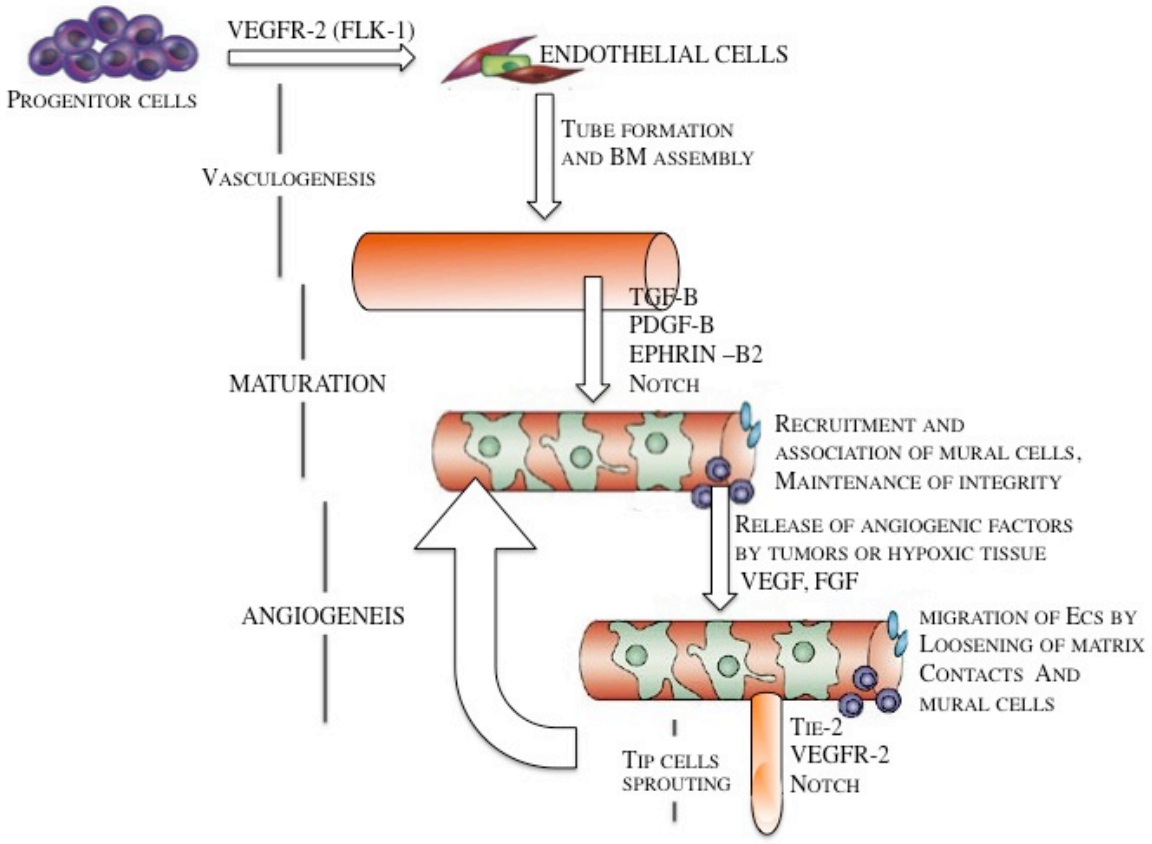

Figure 3.2 Schematic of important signaling molecules that are involved in vasculogenesis, maturation of blood vessels and angiogenesis, modified from reference [6]

3.4.3.1 Role of basement membrane in stabilization of immature blood vessels

As mentioned earlier BM degradation happens during the complicated multistep angiogenesis process. Direct contact between the basement membrane and the EC layer provides important signals that control the stability of EC layer and facilitate EC tube stabilization. Vascular basement membrane matrices are largely composed of structural components, including laminin (particularly laminin IV), collagen IV and fibronectin. Other proteins provide bridging functions such as nidogens 1 and 2, and the heparan sulfate proteoglycan perlecan, which facilitate the co-assembly of basement membrane components [16–18]. It has long been known that

endothelial cells have the capacity to synthesize most if not all of these proteins, so it was generally assumed that basement membrane assembly occurred through ECs alone. However, in a variety of tissues, most notably the skin, it is clear that basement membrane assembly requires more than keratinocytes and was strongly stimulated by the presence of fibroblasts in collagenous matrices underlying the keratinocyte layer. Thus, by analogy with these findings, it is likely that vascular basement membrane assembly may require heterotypic cell-cell contacts, which was originally suggested by Davis and Senger [19]. A recent study by Stratman et al. demonstrates that pericyte recruitment to EC-lined tubes *in vitro* and *in vivo* is necessary to stimulate vascular basement membrane matrix assembly, a key step in vascular maturation and stabilization [20].

Collectively, the matrix serves as a store for various growth factors and pro-enzymes involved in vessel development. The balance between proteases (such as MMP2, MMP3, MMP9, and urokinase plasminogen activator) and their inhibitors (such as tissue inhibitors of metalloproteinases and PAI1) controls basement membrane and ECM degradation and could influence EC and mural-cell migration [7,20,21]. These proteases also lead to the release of various pro-angiogenic growth factors, such as VEGF and basic fibroblast growth factor (bFGF), which are sequestered in the matrix. Protease activity can also generate anti-angiogenic molecules by cleaving plasma proteins (such as angiostatin from plasminogen), matrix molecules (such as tumstatin from collagen type IV), or the proteases themselves (such as PEX from MMP2). Thus, branching patterns of vessels are tightly regulated by spatial and temporal concentration profiles of growth factors and protein fragments that transport and bind to the matrix [2,4]

3.5 Sources of Endothelial cells and their progenitors

One potential source of endothelial cells are embryonic stem cells, which are pluripotent and thus capable of differentiating into all cell types of the endoderm, ectoderm, and mesoderm.

Although ESCs have the advantages of greater proliferative capacity and pluripotential when compared to other endothelial cell precursors, these properties also raise a concern. Specifically, the inadvertent administration of an undifferentiated (and thus pluripotent) ESC to a patient would risk teratoma formation. Accordingly, the clinical development of this cell therapy will require robust differentiation and purification protocols, supported by data showing the safety of these cells. The therapeutic use of these cells is further complicated because they are allogeneic and therapeutic engraftment may require immunosuppression, which carries additional risk. Finally, the clinical use of these cells may be influenced by the ethical debate surrounding the isolation of cells from human embryos. Accordingly, there is great interest in a new form of pluripotential cell that can obviate some of these concerns. Induced pluripotent stem cells (iPSCs) can be "reprogrammed" from adult somatic cells using a variety of methods, established primarily by Yamanaka and Thomson. iPSCs have the potential to generate patient-specific tissues for disease modeling and regenerative medicine applications. However, before iPSC technology can progress to the translational phase, several obstacles must be overcome. These include uncertainty regarding the ideal somatic cell type for reprogramming, the low kinetics and efficiency of reprogramming, and karyotype discrepancies between iPSCs and their somatic precursors. In this section, we describe different sources of endothelial cells and common endothelial cell markers that have been investigated so far by researchers, from embryonic and induced pluripotent stem cells to adult cells.

3.5.1 Embryonic Stem cell derived Endothelial cells

- *From Embryoid Bodies (EB)*

Mouse embryonic stem cells (mESCs) can differentiate into hemangioblasts after forming

embryoid bodies (EBs). Hemangioblasts that form blood islands, contain endothelial and haematopoietic progenitors [22]. Formation of a vessel like network are the result of further differentiation of the EBs [23]. Moreover, it's been shown that endothelial cell markers differentiated from EBs are expressed in the same order that is expressed in endothelial differentiation during embryonic development [24].

During human EB differentiation, endothelial cell markers such as CD31, CD34, VE-cad and GATA-2 show increasing trends in their expression [25,26]. CD31, CD34, and VE-cad reach a maximum at days 13-15 and GATA-2 around day 18. Other endothelial markers such as VCAM1, FLT-1, 2; vasculogenic growth factors such as VEGF, Ang-1, 2 and PDGF and transcription factors such as GATA1, 3 are up regulated as well [27]. Like mouse ESCs, human ESCs (hESCs) can spontaneously differentiate and organize within EBs into three-dimensional vessel-like structures, in a pattern that resembles embryonic vascularization. The capillary area in the human EBs increases during subsequent maturation steps, starting from cell clusters that later sprout into capillary-like structures and eventually organize in a network-like arrangement. These isolated $CD31^+$ cells from human EBs (days 13–15), express endothelial markers and can form vascular tubes in vitro and in vivo [28].

- *On feeder layer and ECM*

Seeding ES cells on feeder cells or within an ECM can also induce differentiation into haematopoietic and endothelial lineages. For example, mouse endothelial progenitors ($Flk\text{-}1^+$ cells) were isolated following the differentiation of ESCs on collagen. The isolated $Flk\text{-}1^+$ cells in mouse systems are precursors for haematopoietic, endothelial and smooth muscle cells and can also give rise to contracting cardiac cells, thus acting as cardiohemangioblasts [29,30]. Culturing

of human embryonic stem cells (hESC) on collagen IV resulted in two types of cell population that differ by size. The smaller cell population showed an upregulation of specific endothelial markers, such as CD31, CD34, Tei2 and GATA2. Cord-like organization of the cells (20% endothelial cells) was observed by re-plating the smaller population of cells on collagen IV with VEGF supplementation. Moreover, addition of PDGFB induced differentiation into smooth muscle cells [31]. Seeding hESCs on stromal feeder cells (bone marrow and yolk sac) could lead to differentiation into $CD34^+$ cells (1–2%). Interestingly, about 50% of the $CD34^+$ cells also express CD31. The $CD34^+$ cells were isolated and differentiated into haematopoietic cells [32].

3.5.2 Adult derived Endothelial cells

Human umbilical vein endothelial cells (HUVECs) show relatively higher proliferative potential among the isolated $CD31^+$ endothelial cells that originate from veins and arteries of different tissues [28]. Isolation of $CD34^+$ and Flk-1^+ cells from peripheral blood using magnetic beads is another source of adult endothelial cells [16]. These isolated progenitor cells could differentiate into endothelial cells and incorporate into neovascularization sites in mouse and rabbit hind-limb ischaemic models [34]. $CD34^+$ cells, mobilized from the bone marrow following treatment with granulocyte macrophage colony stimulating factor, improved ventricular function and neoangiogenesis in ischaemic nude rat myocardium [35]. $CD133^+$ cells purified from bone marrow were also shown to enhance human myocardial perfusion and global function [36]. Another important source of adult endothelial cells is the umbilical cord blood, which contains more $CD133^+$ and $CD34^+$ cells than adult peripheral blood and has higher proliferation capacity [37].

3.5.3 Induced Pluripotent Stem cell derived endothelial cells

Yamanaka et al. have shown systematic differentiation of cardiovascular cells from mouse induced pluripotent stem cells. Induced pluripotent stem (iPS) cells were generated from mouse skin fibroblasts by introducing 4 transcription factors (Oct3/4, Sox2, Klf4, c-myc) and then the same approach was applied on ES cells to induce cardiovascular differentiation. They showed that $Flk1^{+}$ cells could differentiate into artery, vein and mural cells . [38]. Rufaihah et al. have differentiated human iPSCs (hiPSCs) into endothelial cells (hiPSC-ECs) to assess their ability to improve perfusion in a murine model of peripheral arterial disease [39,40]. In brief, endothelial differentiation was initiated by culturing hiPSCs for 14 days in differentiation media supplemented with bone morphogenetic protein 4 and vascular endothelial growth factor. They purified the heterogenous mixture of cells by FACS using an antibody directed against CD31. The purified hiPSC- ECs generated capillary-like structures when grown in matrigel and incorporated acetylated-LDL cholesterol. These cells expressed Endothelial markers such as FLK-1 (KDR), CD31, CD144, and eNOS. When exposed to hypoxia the hiPSC-ECs produced angiogenic cytokines and growth factors. Subsequently, they transduced the cells with a double fusion construct comprising firefly luciferase for BLI and green fluorescence protein for histochemistry. The hiPSC-ECs were administered at day 0 and day 7 after femoral artery ligation into the ischemic hindlimb of immunodeficient mice. Over a two-week period, BLI revealed reduction of cells, but some hiPSC-ECs survived in the ischemic limb for at least 2 weeks. At that time, and for up to 4 weeks, perfusion was improved by over 30% by comparison to the vehicle treated group, as assessed by laser Doppler imaging. This effect was associated with a 60% increase in the total number of capillaries in the ischemic limb of mice receiving hiPSC-EC injections by comparison to the vehicle-treated group. This preclinical work provided proof-of-concept for the use of hiPSC-EC in peripheral arterial disease [41].

Figure 3.3 shows development of therapeutic cells from human induced pluripotent cells. Readily accessible somatic cells (e.g. skin fibroblasts) are harvested from a patient and expanded in culture. Cells are exposed to reprogramming transcriptional factors, in the form of cell permeant peptides and modified mRNA. The resulting iPSC colonies are differentiated into vascular progenitor cells, that are administered directly to patients with vascular disease, or which are incorporated into matrices as a biological conduit such as cylindrical bioengineered matrix or decellularized cadaveric vessels for surgical implantation. These bioengineered conduits would serve to replace autologous saphenous vein in patients that have insufficient or diseased veins [41].

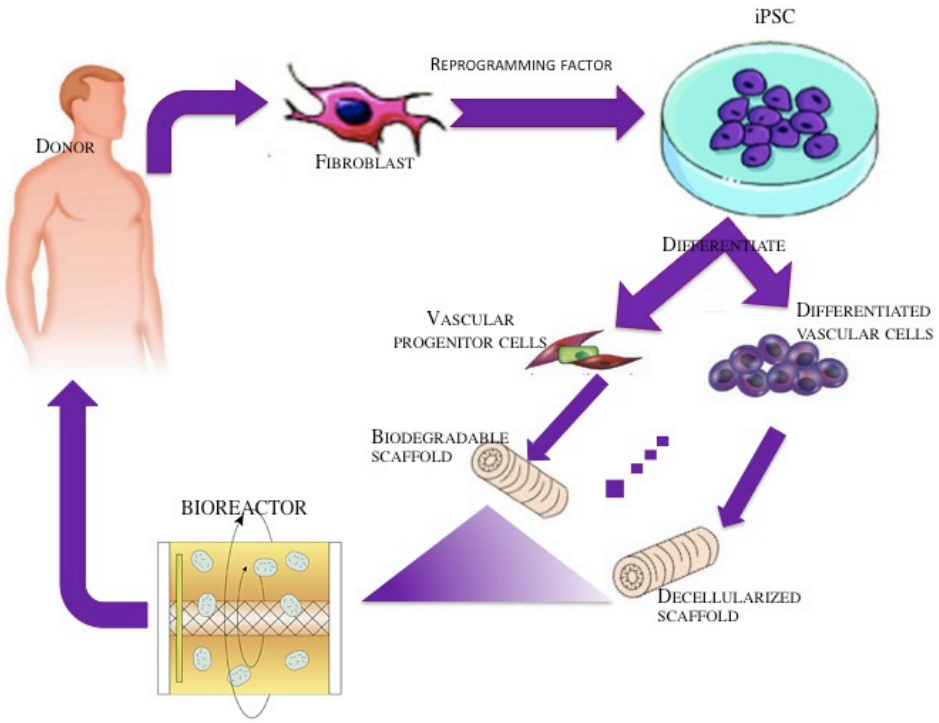

Figure 3.3 Development of therapeutic cells from human induced pluripotent cells

3.6 Engineering blood vessels from stem cell derived endothelial cells: recent advances and applications

In the last three sections we introduced the structure of blood vessels, important cell signaling molecules in vasculogenesis/angiogenesis and different cell sources for ECs. Now we will describe the tissue engineering approaches are available for making macrovessels and microvessels.

3.6.1 Approaches to macrovessel tissue engineering (e.g. heart valve)

The approaches to engineer macrovessels can be divided into several distinct categories, although there may be some overlapping features. Successful application of these approaches, either individually or in combination, is expected to enhance therapeutic opportunities by building functional tissue and organ systems for regenerative medicine.

1. Formation of a tissue in vitro by seeding cells on a biodegradable scaffold and maturing a tissue (to be implanted in vivo) in a bioreactor
2. Cell-seeded natural biodegradable scaffolds
3. Guided tissue regeneration via implanted degradable tissue that is remodeled by endogenous cells
4. Implantation of decellularized valvular material
5. Other approaches such as microfabrication techniques and scaffold free approaches

In all of the mentioned approaches, choosing the right cell among the spectrum of stem cells to differentiated cells and also the right scaffold is of utmost importance [42]. The scaffold should provide the initial requisite mechanical strength to withstand in vivo hemodynamic forces until vascular smooth muscle cells and fibroblasts reinforce the extracellular matrix of the vessel wall. Hence, the choice of scaffold is crucial for providing guidance cues to the cells to behave in the required manner to produce tissues and organs of the desired shape and size. Several types of

scaffolds have been used for the reconstruction of blood vessels. They can be broadly classified as biological scaffolds, decellularized matrices, and polymeric biodegradable scaffolds. A review written by Pankajakhshan et al. focuses on the different types of scaffolds that have been designed, developed and tested for tissue engineering of blood vessels [43].

3.4.1.1 Bioreactor approach

The bioreactor approach should provide a desirable physiological, metabolic and mechanical environment for blood vessel formation in vitro. To develop well developed and effective construct for implantation and remodeling one approach would be to optimize the cellular component, the scaffolds and the in vitro process conditions. Novel scaffolds are also under investigation. Multiple studies have emphasized that dynamic conditioning using bioreactors that provide a flow regime that mimics that of the intended application enhances construct tissue properties [44,45]. Oxygen tension might be a key parameter for the achievement of sufficient tissue quality and mechanical integrity in tissue-engineered heart valves [46,47]. A mesenchymal stem cell-seeded, valve-shaped construct has been assembled from layered collagenous scaffolds. Autologous fibrin-based engineered heart valves showed favorable results both in vitro and in vivo [48,49]. Culturing vascular cells on polymer scaffolds and subjecting the scaffold to pulsating flow is another approach that is studied by Niklason et al. [50]. In fact, they seeded bovine aortic smooth muscle cells into hollow tubular polyglycolic acid (PGA) scaffolds, and then injected bovine aortic endothelial cells into the lumen. Compared with native arteries, the engineered arteries demonstrate similarities in wall thickness and collagen content after eight weeks of culture in a bioreactor. A key issue moving forward will be the real-time noninvasive and nondestructive assessment of mechanical properties of engineered heart valves both in vitro and utilization of such techniques in vivo to ensure quality.

3.4.1.2 Decellularized vascular material

Removal of all viable cells while preserving the extracellular matrix integrity is the goal in producing decellularized xenogeneic tissue. This method provides valuable material for heart valve tissue engineering. Decellularized materials have the advantage of preserving ECM components that may support cell adhesion and molecular sequestering, as well as desirable mechanical properties. However, ECM disruption by the decellularization process and immunogenicity are concerns inherent in the use of decellularized ECMs. For instance, decellularization resulted in substantial microscopic disruption of the ECM, which may negatively impact the durability of heart valve leaflets[51]. Moreover, evaluation of the relative immune responses of different valve components of decellularized porcine aortic valve compared with native and glutaraldehyde fixed valves showed that collagen I elicited a strong response but elastin induced a minimal response [52]. Recellularization of these valves has been reported in an aortic valve replacement model in juvenile pigs [53]. Another study investigated the function, histological changes, potential of in vivo reendothelialization of decellularized aortic valve allografts in orthotopic position in sheep. The valves exhibited trivial regurgitation and normal morphology with no signs of graft dilatation, degeneration or rejection [54]. Toxicity that is introduced to scaffold by the chemicals used in the decellularization process is another concern in decellularized natural ECMss. A clinical study investigated the safety and effectiveness of the Ross procedure (pulmonary to aortic valve autograft) using a decellularized, fibronectin-coated pulmonary valve allograft or xenograft seeded with autologous vascular endothelial cells from a forearm or saphenous vein to reconstruct the right ventricular outflow tract. These valves showed excellent hemodynamic performance during midterm follow-up [55]. In contrast, recurrent right-sided heart failure after the Ross procedure was reported in a study done by Hiemann et al [56].

3.4.1.3 Cell seeded natural biodegradable scaffold

The cell seeded natural biodegradable scaffold approach involves isolating and growing endothelial cells on polymer scaffolds in vitro, followed by in vivo implantation. This method has been tested in an ovine model, where expanded pulmonary arterial cells were grown on polyglactin/poly (lactic-co-glycolic acid) tubular scaffolds for one week before transplantation into pulmonary arteries of lamb. Over a period of 24 weeks, the vascular grafts showed growth and development of endothelial lining and the production of extracellular matrix components, such as collagen and elastin fibers[57].

3.4.1.4 Microfabrication technique

Another approach for the in vitro induction of endothelial networks in engineered tissue constructs is to prefabricate scaffolds to include channels that later could be lined with endothelial cells. Microfabrication techniques are currently under way to engineer such network structures that will mimic the capillary network, expanding from a main vessel (like arteries) and merging back to a single vessel (like veins). In such systems, endothelial cells are seeded into the channel network and their attachment and behavior under flow are analyzed. Ink-jet printing can be used to pattern cells into tubular structures. This technique, as well as other cell-printing techniques such as laser-guided direct writing, could be used in the future for the assembly of complex vascularized tissues. In one such approach, Tien and coworkers developed a method to prefabricate hollow channels within collagen gels. Endothelial cells were then seeded along the interior of the channel such that they formed a vessel-like structure that permitted flow of solution through the tube lumen. The authors demonstrated endothelial barrier function and appropriate barrier breakdown upon exposure to inflammatory cytokines [58].

3.4.1.5 Cell-synthesized ECM- scaffold free approach

Although biomaterials-based solutions are promising, there are challenges that need to be solved. Some of the key issues that may affect the long term behavior of the engineered tissue construct, and directly interfere with its primary biological function, are scaffold choice, immunogenicity, degradation rate, toxicity of degradation products, host inflammatory responses, fibrous tissue formation due to scaffold degradation and mechanical mismatch with the surrounding tissue. To address these problems, fabrication techniques for production of scaffold-free engineered tissue constructs have recently emerged. Norotte et al. reported a fully biological self-assembly approach, which was implemented through a rapid prototyping bioprinting method for scaffold-free small diameter vascular reconstruction. Various vascular cell types, including smooth muscle cells and fibroblasts, were aggregated into discrete units, either multicellular spheroids or cylinders of controllable diameter (300–500 mm). These were printed layer-by-layer concomitantly with agarose rods, used as a molding template. A unique aspect of the method is the ability to engineer vessels of distinct shapes and hierarchical trees that combine tubes of distinct diameters. The technique is rapid and scalable [59].

In another study done by L'Heureux et al. the SMCs and fibroblasts were cultured in medium containing sodium ascorbate for increased ECM deposition. After 1 month of in vitro culture, the sheet of SMCs in their own ECM was wrapped around a tube, covered with a sheet of fibroblasts in their own ECM, and then the luminal surface was seeded with ECs. This construct reportedly had burst strength of over 2 000 mm Hg. In addition, the SMCs expressed desmin, and the ECs strongly inhibited platelet adhesion in vitro. However, when these grafts were implanted in dogs as a canine femoral arterial interposition graft, they had a patency rate of approximately 50%. In addition, the grafts required 3 months for production. This approach has been further

tested in 3 patients undergoing hemodialysis. The vessels constructed from autologous dermal fibroblasts and ECs were implanted as arteriovenous fistulas for dialysis access and were allowed to mature in vivo before use. During 5 months of implantation, no failures were observed, and the grafts functioned well. Although the results are encouraging, this approach requires long culture and maturation periods that would limit the application of these vessels in urgent cases [60,61].

3.6.2 Approaches to microvessel tissue engineering (e.g., capillaries)

Incorporation of a microcirculation into engineered tissues presents multiple challenges, including the formation of microscale vascular conduits for blood flow, a functional endothelium that regulates vascular activity, and specialized cell types that perform the physiological function of the tissue of interest. Several approaches have been developed to address these challenges, including:

1. Incorporation of biomolecular cues within the material
2. Seeding of vascular or vascular-inducing cells in the scaffold
3. Use of microfabrication technologies to engineer branched microfluidic channels within biocompatible materials.

Here we discuss each of the above-mentioned approaches in more detail.

3.6.2.1 Incorporation of biomolecular cues within the material

Growth factor incorporation in three-dimensional (3D) engineered tissues is crucial for angiogenesis and vascularization. In order to establish a functional microvascular network, coordinated delivery of several key factors such as VEGF, FGFs, PDGFs, TGFs, angiopoietins, ephrins, placental growth factors and various chemokines are beneficial. Presentation of a single factor such as VEGF is not typically sufficient to form functional conduits and can, in contrast,

lead to induction of tortuous and leaky vessels. Thus, spatial and temporal regulation of growth factor signaling may help ensure accurate vessel growth and remodeling [62,63].

The need for materials that could be chemically and mechanically tailored to incorporate and release bioactive molecule, while meeting biocompatibility and biodegradability standards, has led to further use of hydrogels as scaffolds for engineered tissue constructs. Hydrogels are hydrated materials made from a cross-linked network of hydrophilic polymers. The integration of factors that induce rapid endothelial cell ingrowth and that stabilize the vascular network as it forms could support the success of these hydrogels [6]. We discuss growth factor releasing hydrogels and protease sensitive hydrogels in Section 3.4.2.1.1 and 3.4.2.1.2, respectively. ECM peptides that induce vasculogenesis/angiogenesis in hydrogels are discussed in Section 3.4.2.1.3. These discussions are followed by the effect of hydrogel stiffness and porosity on angiogenesis/vasculogenesis (Section 3.4.2.1.4).

3.4.2.1.1 Tissue Engineering approaches to deliver Growth Factors

Strategies for biomaterial presentation of growth factors in tissue engineering can be conceptually divided into two areas:

1. Chemical immobilization (covalent or non-covalent) of the growth factor into or onto the matrix; and
2. Physical encapsulation of growth factors in the delivery system.

The first approach typically involves chemical binding or affinity interaction between the growth factor-containing polymer and a cell or a tissue. The second approach is achieved by the encapsulation, diffusion and pre-programmed release of growth factor from substrate into the surrounding tissue. There are several methods for each approach that are described in detail in a

review by Mooney and coworkers [64].

Investigators have developed a wide range of ECM-mimicking biomaterials to immobilize growth factors or growth factor mimics, including hydrogels containing ligands from fibronectin, laminin, collagen, elastin or the glycosaminoglycans (GAGs) heparin sulphate, chondroitin sulphate, hyaluronic acid or a variety of synthetic hydrogels [64].In a study by Hubble and coworkers, a rationally designed combinatorial approach was used to discover a sulfated tetra-peptide that binds to vascular endothelial growth factor (VEGF). SY(SO3)DY(SO3) was identified as the top binder to VEGF, which mimics heparin binding to VEGF as a potential improvement over natural heparin [65]. Koch *et al.* similarly used a synthetic homo-bifunctional polymer cross-linker, disuccinimidyl disuccinate poly (ethylene glycol), to attach VEGF to collagen matrices [66]. PEG-ephrinA1 immoblized to hydrogel surfaces induced endothelial cell tubulogenesis with luminal diameters in the range of 5-30 μm, creating structures resembling early stage capillaries [67]. In another study, PEG-VEGF not only increased endothelial cell tubulogenesis, but also increased endothelial cell motility 14-fold and cell-cell connections 3- fold in a three-dimensional, biodegradable hydrogel [68].

Saik et al. developed MMP-sensitive PEGDA hydrogels immobilized with ephrin A1 ligands, which stimulate a wide range of receptors that induce vascularization. The efficacy of ephrin A1 ligand conjugation was demonstrated 14 days after implantation, by comparing vascular network parameters such as vessel density, branch points of MMP-sensitive, PDGF-BB–containing PEGDA hydrogels with or without immobilized ligand. The biodegradable, bioactive hydrogels immobilized with ephrin A1 ligand produced a denser vasculature in the mouse cornea pocket relative to the non–ligand-containing scaffold [69].

Transfecting cells to overexpress angiogenic growth factor genes is another way to promote prolonged, local growth factor delivery [70,71]. In one example, mononuclear cells, which give rise to endothelial progenitor cells, were transfected to overexpress VEGF. Transfection with a VEGF-encoding gene stimulated their differentiation into endothelial cells for vasculogenesis, while also enhancing local angiogenesis [70]. Myoblasts have also been transfected to express VEGF and bFGF to improve vascularity in engineered muscle tissue [72].

3.4.2.1.2 Protease sensitive hydrogels

Cell- induced proteolysis is often required for 3-D cell migration and invasion, because the porosity of the ECM may lead to barrier function and thus inhibit migration [73]. Whereas many synthetic biomaterials have been designed to degrade by ester hydrolysis, such non-enzymatic hydrolysis of matrices is not cell mediated, and is less directly responsive to cell-mediated remodeling and tissue morphogenesis. Cell induced proteolysis is a reciprocal interaction between ECM and the cells, as the ECM stimulates the cells and the cellular proteases remodel the ECM and release associated bioactive components from it. For example, Phelps et al. seeded NIH3T3 fibroblasts in poly (ethylene glycol) diacrylate (PEGDA)–based degradable scaffold and incorporated some responsive elements, such as protease-labile cross-links, cell adhesive peptides, and conjugated VEGF. They demonstrated that both adhesive ligands and MMP-degradable sites were necessary for cells to spread. Furthermore, implantation of VEGF-conjugated scaffolds into a mouse model of hind-limb ischemia, resulted in rapid vascularization of the biomaterial that remained stable for at least 4 weeks [74].

Exciting progress has been made in mimicking the proteolytic recognition of natural ECMs in synthetic polymer gels. Protease-sensitive peptides can be categorized in two main general groups: Plasmin sensitive peptides and MMP sensitive peptides. For example, a fibrinogen derived

(R chain, residues $L^{94}I^{119}$) peptide sequence that is combined with RGD cell adhesion site is a plasmin sensitive peptide. (LR*GD*FSSANNR↓DNTYNR↓VSEDLRSRI, ↓ indicating the plasmin cleavage site) [75]. Alison *et al.* evaluated plasmin substrate sites reported in fibrinogen as potential substrate sites in the crosslinker peptide. After considering solubility and hydrophobicity and some other practical parameters they came up with the engineered peptide sequence CYKNRDC. Because of a negative influence of the aspartate (D) residue on the reactivity of the cysteine © thiol toward vinyl-sulfone, this residue was eliminated from the final crosslinking peptide design [71].

Sequence (GGGPQG↓IWGQGK) is an MMP-sensitive peptide that can be incorporated in the backbone of the PEG block polymers with acrylate terminal groups, which allows crosslinking of precursors into networks. GGGPQG↓IWGQGK is a mutated version of α1(I) collagen chain for increased degradation kinetics with various MMPs [76]. Anseth and coworkers incorporated a cysteine-containing bifunctional peptide, CPE↓NFFRGD into PEG hydrogels by thiol-acrylate photopolymerization. This peptide has the RGD motif for cell adhesion and the sequence of PENFF for MMP-13-sensitive cleavage [77]. The resulting hydrogels provided a platform that mimics the native upregulation and downregulation of cell adhesive proteins by the cell-secreted enzymes in the ECM for differentiating human mesenchymal stem cells (hMSCs). A review written by Zhu provides more information about other enzyme sensitive peptides that have been used in the proteolytically degradable PEG hydrogel [78].

3.4.2.1.3 ECM peptides used in the hydrogel backbone to induce angiogenesis and vasculogenesis

Cell adhesion to traditional biomaterials, such as polyethylene, polytetrafluoroethylene or silicone rubber, is based upon nonspecific adsorption of proteins from the body fluids to the

material surface. A subset of these adsorbed proteins, including fibronectin, fibrinogen, and vitronectin, promote cell adhesion by interacting with the corresponding adhesion receptors on the cell surface. To achieve similar cell adhesion in a more well-defined synthetic context, several investigators have tested ECM protein-derived cell adhesive peptides as a component of biomaterials. These peptides are based on the primary amino acid sequence or structure of the receptor-binding domains of proteins such as fibronectin and laminin. Early work demonstrated an important possible advantage of working with short adhesion peptides, rather than the complete parent protein, as the peptides could be displayed in a manner that enhanced peptide availability to cell-surface receptors [63]. Cell adhesive peptides are mainly derived from four ECM proteins, including fibronectin (FN) (e.g., RGD, KQAGDV, REDV and PHSRN), laminin (LN) (e.g., YIGSR, LGTIPG, IKVAV, PDGSR, LRE, LRGDN and IKLLI), collagen (e.g., DGEA and GFOGER) and elastin (e.g., VAPG). RGD is the most commonly used cell adhesive peptide, perhaps due to its long history of use and its effectiveness in promoting cell adhesion. RGD peptides are typically used in either linear (RGD) or cyclic (cRGD) form. Research has demonstrated that cRGD peptides have the advantage of increasing the affinity to integrin $\alpha_v\beta_3$ and enhancing biological activity up to 240 times in comparison with linear RGD analogues [79]. This enhanced effectiveness of cRGD is biomimetic, as the RGD sequence in the cell-binding domain of FN is exposed at the tip of a loop with a spatial constraint that results in increased affinity for cell binding. Thus, incorporation of cRGD peptides into PEGDA hydrogels can better mimic the native RGD loop structure and benefit cell adhesion [80].

In another study, Hubble et al. showed that within the adhesion protein fibronectin, the tetra-peptide REDV is a more specific ligand for integrin receptor $\alpha_4\beta_1$, which is present on the endothelial cell but not the blood platelet. It would be beneficial to use this specificity to develop

vascular grafts that support endothelial cell adhesion and migration, while rejecting the adhesion of blood platelets [63].

3.4.2.1.4 Hydrogel stiffness and porosity

The physical properties of hydrogels can be regulated by the chemistry of the polymeric backbone, its hydrophilicity, polymer concentration, and crosslinking density. Increasing the crosslinking density and/or monomer concentration generally results in increased stiffness and reduced degradation rates because of a larger number of bonds that need to be cleaved during degradation of the material. The stiffness of hydrogels can be adjusted by varying the percentage of polymer used in the solution before the crosslinking procedure and can be controlled by adjusting the crosslinking agent and the crosslinking density during hydrogel formation. Increasing the number of bonds in the polymer also limits the ability of water molecules to diffuse in and out of the material. Thus, the degree of crosslinking of polymer networks can be used to tailor both the structural stability and the porosity of the material [81]. As a result, the degree of crosslinking is an important aspect in regulating the transport of solutes through hydrogel structures [82]. A recent study by West and colleagues showed that hydrogel stiffness affects the degree of endothelial tubule formation. In stiffer hydrogels tubule formation was reduced and cell clusters remained short and rudimentary, as cells failed to migrate as much as they do in softer matrices [62]. Ghajar et al. studied the effect of matrix density on the regulation of 3-D capillary morphogenesis and demonstrated a key role for both matrix stiffness and ligand density [83].

3.6.2.2 Seeding of vascular or vascular-inducing cells in the scaffold

Encapsulation of endothelial cells and supporting cells within biomaterials are common strategies that have attracted a great deal of attention. This encapsulation strategy benefits from

cell signaling, differentiation, and migration as well as the dynamic interactions between cells that provide the biochemical environment beneficial for the ensuing tissue remodeling. For example, to mimic skin tissue vascularization, Black et al. co-cultured human umbilical vein endothelial cells (HUVECs), human-derived fibroblasts and keratinocytes (skin cells) housed within a collagen-based scaffold [84]. Biochemical coordination between the ECM generated by the fibroblasts and growth factors such as VEGF and TGF-β secreted by neighboring cells in the presence of HUVECs promoted the development of a vascular network both in vitro and in a mouse model [85,86]. Furthermore, recent studies highlight the benefits gained from the addition of epithelial cells—those that line the body cavities such the gut and lungs—to stabilize and regulate the size and formation of capillaries within the vascularized model. Thus, various cell types can play complementary roles in tailoring vascularization.

The idea of implanting a co-culture of endothelial cells with ECM-forming fibroblasts or bone-forming osteoblasts in vivo was validated by Alajati et al. HUVECs and osteoblasts were encapsulated within a scaffolding material composed of VEGF and FGF-2 in Matrigel (a murine tumor–derived ECM), fibrin, and thrombin, and the biomaterial was implanted subcutaneously in a severe combined immunodeficiency (SCID) mouse model for up to 20 days. The result was a durable perfused vascular network in vivo [87]. In another study, HUVECs were used to promote the human MSC differentiation into an endothelial lineage, promoting the formation of 3D vascular structures for up to 2 weeks in a Matrigel-based ECM [88]. A mature vascular network was also formed by combining HUVECs and human MSCs in a polymeric scaffold in vivo 4 to 7 days after implantation, thus accelerating the functional remodeling of the implant when used as a bone graft [89].

All in all, the scaffold is a crucial component that regulates the dynamic vascularization process. Scaffolds used in this area are either natural biodegradable materials, such as collagen and Matrigel, or synthetic biodegradable scaffolds, such as poly-L-lactic acid (PLLA) or poly-D,L-lactic-co-glycolic acid (PLGA). However, because of shortcomings seen in their mechanical strength, durability, immunogenicity, and other application-specific requirements, researchers continue to develop more suitable scaffolds for endothelial cell–based vascularization for specific applications.

3.6.2.3 Use of microfabrication technologies to engineer branched microfluidic channels within biocompatible materials

Micro-engineered scaffolds containing channels can be used to seed endothelial cells to form a confluent endothelium on the walls of the vascular channels [90]. Micro-engineering techniques can be categorized into two different groups based on the dimensionality of the produced structures: *1) techniques that produce planar structure* such as photolithography and molding; and *2) techniques that produce 3D structure* such as direct ink writing and omnidirectional printing. Photolithography is a process that uses light illumination through a mask to generate structures from light-sensitive materials, while molding is a process that uses a hollowed-out pattern to which a deposited material conforms. Photolithography and molding are both planar. A 3D structure can result from stacked 2D structures that comprise channels with rectangular cross sections instead of channels with circular cross sections [6]. Raghavan et al. developed a novel approach to control endothelial tubulogenesis by spatially patterning cells within micro-molded collagen gels. Endothelial cells cultured within microscale channels that were filled with collagen hydrogel organized into tubes with lumens within 24–48 h of seeding. These tubes extended up to 1 cm in length, and exhibited cell–cell junction formation characteristic

of early stage capillary vessels [91]. In another study, a 3D tissue construct composed of endothelialized hollow vascular structures was produced using a self-assembled monolayer (SAM)–based cell deposition technique and a hydrogel photocrosslinking method to provide a robust hydrogel-based scaffold for endothelial cell attachment [92].

Direct ink writing and omnidirectional printing within a gel reservoir can create 3D vascular structures in vitro. In a recent study by Chen et al., a printing approach was used to generate a micropatterned sugar-based sacrificial layer around which cell-laden hydrogels could be built. The sugar-based layer was then dissolved, creating a 3D microarchitecture consisting of microvascular networks. Moreover, Chrobak et al. validated the hypothesis that the existent flow and shear conditions within such microscale channels are favorable for endothelium sustainability [58].

Zheng and co-workers created microvessels that replicated some aspects of angiogenesis using silicone molds together with casting gels made out of collagen. The researchers report that the microvessels were lined with continuous endothelium and did not leak. Moreover, when activated with appropriate biochemical signals the vessels produced new branches and recruited mural cells, which normally associate with blood vessels and affect their functions. As such, the device not only allowing the researchers to shape the network, but also permits the biological elements (cells and their products) to reshape or remodel the system dynamically [90]. Despite these substantial advances, new technologies are required to more accurately recreate the complexity of native tissues and enable formation of robust, functional micro-capillary networks [93].

3.6.3 Mechanisms for connecting Micro-vessels to Macro-vessels

The in vitro formation of mature vessel networks ready to anastomose with the host vasculature shortly after implantation has the potential to dramatically improve the rate of oxygen and nutrient delivery and waste product removal, and thus increases the viability of larger implanted tissues. Rapid (~1 day) anastomosis of engineered vessels with host vasculature is likely necessary for the survival and function of tissue specific cells, especially for oxygen-sensitive cells such as cardiomyocytes, hepatocytes, and various stem cells, all of which are of tremendous interest in the field of regenerative medicine [94]. Limited studies suggest that during embryonic vasculogenesis and angiogenesis, anastomosis is accomplished via connection of extended cellular processes followed by lumen propagation through intracellular and intercellular vacuole fusion, with macrophages playing an accessory role. However, it is not known whether this is the only mechanism for connecting vessels. Without a basic understanding of the cellular mechanisms of anastomosis, it is difficult to develop strategies for accelerating this critical step for perfusing engrafted tissues [95]. This section will describe the different mechanisms that are involved in anastomosis, based on a limited range of insights published to date in this area.

3.6.3.1 Engineered blood vessel networks connect to host vasculature via wrapping-and-tapping anastomosis

Cheng et al. showed that implanted vascular networks anastomose with host vessels through a previously unidentified process of “wrapping and tapping” between the engrafted endothelial cells (ECs) and the host vasculature. At the host-implant interface, implanted ECs first wrap around nearby host vessels and then cause basement membrane and pericyte reorganization and localized displacement of the underlying host endothelium. In this way, the implanted ECs replace segments of host vessels to divert blood flow to the developing implanted vascular network. The process is facilitated by high levels of matrix metalloproteinase-14 and matrix

metalloproteinase-9 expressed by the wrapping ECs. These findings open the door to new strategies for improving perfusion of tissue grafts and may have implications for other physiologic and pathologic processes involving postnatal vasculogenesis. They found that tip cell connections and vacuole fusion were not integrally involved in host-implant vascular anastomosis, but instead the engrafted endothelial networks wrapped around host vessels at the host-implant interface and then replaced sections of the underlying vessel wall to tap into the host blood supply [95].

3.6.3.2 Tensional forces in the collagen matrix control directional capillary sprouting and anastomosis

Formation of capillary anastomoses is associated with tensional remodeling of the collagen matrix and directional sprouting of outgrowing capillaries towards each other. To analyze whether directional sprouting is dependent on cytokine gradients or on endothelial cell-derived traction forces transduced through the extracellular matrix, Korff and Augustin designed a matrix tension generator that enables the application of defined tensional forces on the extracellular matrix. Using this matrix tension generator, causal evidence is presented that tensional forces on a fibrillar extracellular matrix such as type I collagen, but not fibrin, were sufficient to guide directional outgrowth of endothelial cells [96].

3.6.3.3 High density of co-transplanted fibroblasts promotes rapid anastomosis of endothelial progenitor cell derived vessels with host vasculature

Chen et al. have shown that both endothelial progenitor cell-derived endothelial cells (EPC–ECs) and a high density of fibroblasts significantly accelerate the rate of functional anastomosis, and that pre-vascularizing an engineered tissue may be an effective strategy to enhance transport of nutrients in vivo. In this study, Chen et al. developed three-dimensional engineered vessel

networks in vitro by co-culture of endothelial cells (ECs) and fibroblasts in a fibrin gel for 7 days. Vessels formed by cord blood endothelial progenitor cell–derived ECs (EPC-ECs) in the presence of a high density of fibroblasts created an interconnected tubular network within 4 days, compared with 5–7 days in the presence of a low density of fibroblasts. Vessels derived from human umbilical vein ECs (HUVECs) in vitro showed similar kinetics. Implantation of the pre-vascularized tissues into immune-compromised mice, however, revealed a dramatic difference in the ability of EPC-ECs and HUVECs to form anastomoses with the host vasculature. Vascular beds derived from EPC-ECs were perfused within 1 day of implantation, whereas no HUVEC vessels were perfused at day 1. Further, while almost 90% of EPC-EC–derived vascular beds were perfused at day 3, only one-third of HUVEC-derived vascular beds were perfused. In both cases, a high density of fibroblasts accelerated anastomosis by 2–3 days [94]. This study and others described above emphasizes the critical need to select suitable cell types and engineer surrounding microenvironments that optimize vascular network formation and anastomosis with the host in vivo.

3.7 Challenges for future translation of engineered tissue vessels to the clinic

Balloon angioplasty, stent placement, graft bypass surgery, and use of pharmacological agents are current treatment options for vascular diseases. Vascular grafts that are being used in patients can be divided into three categories, in order of decreasing diameter. Large and medium caliber synthetic grafts are used in the thoracic and abdominal cavities with good long-term outcomes. Almost 1,200,000 small-caliber grafts (<6 mm) are used every year for vascular access, to relieve lower limb ischemia and for coronary bypass surgery. Autologous veins or arteries are being used to replace small caliber arteries, but in 30–40% of patients these are not available due to prior harvesting or preexisting conditions. Using synthetic grafts, which provide poor outcomes

is often the only option left for those patients. It is reported that ~50% of these synthetic grafts will occlude within 5 years, potentially leading to amputation [97].

Considering the need for vascular graft that is been estimated to be about 1.4 million in the US alone [98], there is a need for engineered blood vessels that are non-thrombogenic, withstand adequate burst pressure, show appropriate remodeling responses and are vasoactive [99]. Thus, for successful clinical translation of biomaterials that we discussed in Section 3.4, it is essential that researchers identify parameters that can be controlled to promote and regulate angiogenesis and vasculogenesis. The long-term in vivo function of various engineered vascular networks and tissue-engineered vessels still need to be further investigated.

Moreover, it is important that the engineered tissue vessels elicit the least inflammatory response. Ideally, a tissue-engineered vessel should not be immunogenic, nor should it induce thromboembolic complications or excessive and prolonged inflammation. Unfortunately, few biomaterials exist which can be considered biologically inert. For example, Teflon® (expanded polytetrafluoroethylene; ePTFE) and Dacron (polyethylene terephthalate; PET) vascular grafts function well in large diameter graft applications without endothelial cell coverage but when used in peripheral applications, one half of these grafts occlude within the first five years of implantation [52,97]. Moreover, preexisting pathology or existing risk factors could affect the long-term success of the implants. For example, implantation of a vascular graft in an atherosclerosis-prone patient results in decreased patency. So designing new approaches that account for the pathological status of the tissue, organ or patient on the engineered tissue vessel could increase the rate of translational success of tissue engineered vessels [97,100].

It is also important to keep in mind efforts to link in vivo with in vitro research successfully in tissue engineering. *In vitro* culture of tissues and vascular cells provides the basis for our

understanding of endothelial cell biology, cell-shape regulation and blood vessel responses to physical forces. However, most *in vitro* models lack the three-dimensional complexity, blood flow, cell–cell interactions and proper extracellular (matrix) environment that are typical of living tissues [101]. In vitro systems that more faithfully mimic the "context" of the native vasculature may lead to more informative in vitro studies.

After an initial period of hype and hope, we are now closer to clinical application. The prospects of using scaffolds, cells, and biochemical or biomechanical stimuli to create functional tissues such as valves and arteries are a power previously unimaginable. However, critical challenges remain for translation of blood vessel tissue engineering strategies. While the field continues to address these challenges, and to further understand the intricate biology of the endothelium, novel biomaterials and cell sources will be critical. In view of emerging advances in biomaterials synthesis/design and stem cell biology, tissue engineered blood vessels at both the macro-scale and the micro-scale may soon impact thousands of patients in need of tissue regeneration and repair.

3.8 References

[1] P. Carmeliet, Mechanisms of angiogenesis and arteriogenesis, Nat. Med. 6 (2000) 389–395. doi:10.1038/74651.

[2] R.K. Jain, Molecular regulation of vessel maturation, Nature Medicine. 9 (2003) 685–693. doi:10.1038/nm0603-685.

[3] A. Maton, inc Prentice-Hall, Human biology and health, Prentice Hall, Englewood Cliffs, N.J., 1994.

[4] D. Pankajakshan, D.K. Agrawal, Scaffolds in tissue engineering of blood vessels, Canadian Journal of Physiology and Pharmacology. 88 (2010) 855–873. doi:10.1139/Y10-073.

[5] E. Ruoslahti, E. Engvall, Integrins and vascular extracellular matrix assembly, J. Clin. Invest. 100 (1997) S53-56.

[6] H. Bae, A.S. Puranik, R. Gauvin, F. Edalat, B. Carrillo-Conde, N.A. Peppas, A. Khademhosseini, Building Vascular Networks, Sci Transl Med. 4 (2012) 160ps23-160ps23. doi:10.1126/scitranslmed.3003688.

[7] S.P. Herbert, D.Y.R. Stainier, Molecular control of endothelial cell behaviour during blood vessel morphogenesis, Nature Reviews Molecular Cell Biology. 12 (2011) 551–564. doi:10.1038/nrm3176.
[8] M.T. Holderfield, C.C.W. Hughes, Crosstalk between vascular endothelial growth factor, notch, and transforming growth factor-β in vascular morphogenesis, Circulation Research. 102 (2008) 637–652.
[9] R.C.A. Sainson, Cell-autonomous notch signaling regulates endothelial cell branching and proliferation during vascular tubulogenesis, The FASEB Journal. (2005). doi:10.1096/fj.04-3172fje.
[10] L. Cao, P.R. Arany, Y.-S. Wang, D.J. Mooney, Promoting angiogenesis via manipulation of VEGF responsiveness with notch signaling, Biomaterials. 30 (2009) 4085–4093. doi:10.1016/j.biomaterials.2009.04.051.
[11] P. Carmeliet, R.K. Jain, Molecular mechanisms and clinical applications of angiogenesis, Nature. 473 (2011) 298–307. doi:10.1038/nature10144.
[12] R.H. Adams, K. Alitalo, Molecular regulation of angiogenesis and lymphangiogenesis, Nat. Rev. Mol. Cell Biol. 8 (2007) 464–478. doi:10.1038/nrm2183.
[13] K. Gaengel, G. Genové, A. Armulik, C. Betsholtz, Endothelial-mural cell signaling in vascular development and angiogenesis, Arterioscler. Thromb. Vasc. Biol. 29 (2009) 630–638. doi:10.1161/ATVBAHA.107.161521.
[14] M.L. Allende, T. Yamashita, R.L. Proia, G-protein-coupled receptor S1P1 acts within endothelial cells to regulate vascular maturation, Blood. 102 (2003) 3665–3667. doi:10.1182/blood-2003-02-0460.
[15] H.G. Augustin, G.Y. Koh, G. Thurston, K. Alitalo, Control of vascular morphogenesis and homeostasis through the angiopoietin-Tie system, Nat. Rev. Mol. Cell Biol. 10 (2009) 165–177. doi:10.1038/nrm2639.
[16] G. Bix, R.V. Iozzo, Novel interactions of perlecan: Unraveling perlecan's role in angiogenesis, Microscopy Research and Technique. 71 (2008) 339–348. doi:10.1002/jemt.20562.
[17] R. Hallmann, N. Horn, M. Selg, O. Wendler, F. Pausch, L.M. Sorokin, Expression and function of laminins in the embryonic and mature vasculature, Physiol. Rev. 85 (2005) 979–1000. doi:10.1152/physrev.00014.2004.
[18] K. Hayashi, Endothelial cells interact with the core protein of basement membrane perlecan through beta 1 and beta 3 integrins: an adhesion modulated by glycosaminoglycan, The Journal of Cell Biology. 119 (1992) 945–959. doi:10.1083/jcb.119.4.945.
[19] G.E. Davis, Endothelial Extracellular Matrix: Biosynthesis, Remodeling, and Functions During Vascular Morphogenesis and Neovessel Stabilization, Circulation Research. 97 (2005) 1093–1107. doi:10.1161/01.RES.0000191547.64391.e3.
[20] A.N. Stratman, G.E. Davis, Endothelial Cell-Pericyte Interactions Stimulate Basement Membrane Matrix Assembly: Influence on Vascular Tube Remodeling, Maturation, and Stabilization, Microscopy and Microanalysis. 18 (2011) 68–80. doi:10.1017/S1431927611012402.
[21] W.B. Saunders, B.L. Bohnsack, J.B. Faske, N.J. Anthis, K.J. Bayless, K.K. Hirschi, G.E. Davis, Coregulation of vascular tube stabilization by endothelial cell TIMP-2 and pericyte TIMP-3, J. Cell Biol. 175 (2006) 179–191. doi:10.1083/jcb.200603176.

[22] W. Risau, H. Sariola, H.G. Zerwes, J. Sasse, P. Ekblom, R. Kemler, T. Doetschman, Vasculogenesis and angiogenesis in embryonic-stem-cell-derived embryoid bodies, Development. 102 (1988) 471–478.
[23] D. Vittet, M.H. Prandini, R. Berthier, A. Schweitzer, H. Martin-Sisteron, G. Uzan, E. Dejana, Embryonic stem cells differentiate in vitro to endothelial cells through successive maturation steps, Blood. 88 (1996) 3424–3431.
[24] K. Choi, Y.S. Chung, W.J. Zhang, Hematopoietic and endothelial development of mouse embryonic stem cells in culture, Methods Mol. Med. 105 (2005) 359–368.
[25] S. Levenberg, Endothelial cells derived from human embryonic stem cells, Proceedings of the National Academy of Sciences. 99 (2002) 4391–4396. doi:10.1073/pnas.032074999.
[26] S. Levenberg, Engineering blood vessels from stem cells: recent advances and applications, Current Opinion in Biotechnology. 16 (2005) 516–523.
[27] S. Gerecht-Nir, J.-E. Dazard, M. Golan-Mashiach, S. Osenberg, A. Botvinnik, N. Amariglio, E. Domany, G. Rechavi, D. Givol, J. Itskovitz-Eldor, Vascular gene expression and phenotypic correlation during differentiation of human embryonic stem cells, Dev. Dyn. 232 (2005) 487–497. doi:10.1002/dvdy.20247.
[28] S. Rafii, D. Lyden, Therapeutic stem and progenitor cell transplantation for organ vascularization and regeneration, Nat. Med. 9 (2003) 702–712. doi:10.1038/nm0603-702.
[29] J. Yamashita, H. Itoh, M. Hirashima, M. Ogawa, S. Nishikawa, T. Yurugi, M. Naito, K. Nakao, S. Nishikawa, Flk1-positive cells derived from embryonic stem cells serve as vascular progenitors, Nature. 408 (2000) 92–96. doi:10.1038/35040568.
[30] M. Iida, T. Heike, M. Yoshimoto, S. Baba, H. Doi, T. Nakahata, Identification of cardiac stem cells with FLK1, CD31, and VE-cadherin expression during embryonic stem cell differentiation, FASEB J. 19 (2005) 371–378. doi:10.1096/fj.04-1998com.
[31] S. Gerecht-Nir, A. Ziskind, S. Cohen, J. Itskovitz-Eldor, Human embryonic stem cells as an in vitro model for human vascular development and the induction of vascular differentiation, Lab. Invest. 83 (2003) 1811–1820.
[32] D.S. Kaufman, Hematopoietic colony-forming cells derived from human embryonic stem cells, Proceedings of the National Academy of Sciences. 98 (2001) 10716–10721. doi:10.1073/pnas.191362598.
[33] T. Asahara, Isolation of Putative Progenitor Endothelial Cells for Angiogenesis, Science. 275 (1997) 964–966. doi:10.1126/science.275.5302.964.
[34] A. Kawamoto, H.-C. Gwon, H. Iwaguro, J.-I. Yamaguchi, S. Uchida, H. Masuda, M. Silver, H. Ma, M. Kearney, J.M. Isner, T. Asahara, Therapeutic Potential of Ex Vivo Expanded Endothelial Progenitor Cells for Myocardial Ischemia, Circulation. 103 (2001) 634–637. doi:10.1161/01.CIR.103.5.634.
[35] A.A. Kocher, M.D. Schuster, M.J. Szabolcs, S. Takuma, D. Burkhoff, J. Wang, S. Homma, N.M. Edwards, S. Itescu, Neovascularization of ischemic myocardium by human bone-marrow-derived angioblasts prevents cardiomyocyte apoptosis, reduces remodeling and improves cardiac function, Nat. Med. 7 (2001) 430–436. doi:10.1038/86498.
[36] C. Stamm, B. Westphal, H.-D. Kleine, M. Petzsch, C. Kittner, H. Klinge, C. Schümichen, C.A. Nienaber, M. Freund, G. Steinhoff, Autologous bone-marrow stem-cell transplantation for myocardial regeneration, Lancet. 361 (2003) 45–46. doi:10.1016/S0140-6736(03)12110-1.
[37] D.A. Ingram, L.E. Mead, H. Tanaka, V. Meade, A. Fenoglio, K. Mortell, K. Pollok, M.J. Ferkowicz, D. Gilley, M.C. Yoder, Identification of a novel hierarchy of endothelial

progenitor cells using human peripheral and umbilical cord blood, Blood. 104 (2004) 2752–2760. doi:10.1182/blood-2004-04-1396.

[38] G. Narazaki, H. Uosaki, M. Teranishi, K. Okita, B. Kim, S. Matsuoka, S. Yamanaka, J.K. Yamashita, Directed and Systematic Differentiation of Cardiovascular Cells From Mouse Induced Pluripotent Stem Cells, Circulation. 118 (2008) 498–506. doi:10.1161/CIRCULATIONAHA.108.769562.

[39] A.J. Rufaihah, N.F. Huang, S. Jamé, J.C. Lee, H.N. Nguyen, B. Byers, A. De, J. Okogbaa, M. Rollins, R. Reijo-Pera, S.S. Gambhir, J.P. Cooke, Endothelial cells derived from human iPSCS increase capillary density and improve perfusion in a mouse model of peripheral arterial disease, Arterioscler. Thromb. Vasc. Biol. 31 (2011) e72-79. doi:10.1161/ATVBAHA.111.230938.

[40] A.J. Rufaihah, N.F. Huang, J. Kim, J. Herold, K.S. Volz, T.S. Park, J.C. Lee, E.T. Zambidis, R. Reijo-Pera, J.P. Cooke, Human induced pluripotent stem cell-derived endothelial cells exhibit functional heterogeneity, Am J Transl Res. 5 (2013) 21–35.

[41] K.S. Volz, E. Miljan, A. Khoo, J.P. Cooke, Development of pluripotent stem cells for vascular therapy, Vascul. Pharmacol. 56 (2012) 288–296. doi:10.1016/j.vph.2012.02.010.

[42] F.J. Schoen, Heart valve tissue engineering: quo vadis?, Current Opinion in Biotechnology. 22 (2011) 698–705. doi:10.1016/j.copbio.2011.01.004.

[43] D. Pankajakshan, D.K. Agrawal, Scaffolds in tissue engineering of blood vessels, Canadian Journal of Physiology and Pharmacology. 88 (2010) 855–873. doi:10.1139/Y10-073.

[44] R. Vismara, M. Soncini, G. Talò, L. Dainese, A. Guarino, A. Redaelli, G.B. Fiore, A bioreactor with compliance monitoring for heart valve grafts, Ann Biomed Eng. 38 (2010) 100–108. doi:10.1007/s10439-009-9803-1.

[45] M.P. Rubbens, A. Driessen-Mol, R.A. Boerboom, M.M.J. Koppert, H.C. Assen, B.M. TerHaar Romeny, F.P.T. Baaijens, C.V.C. Bouten, Quantification of the Temporal Evolution of Collagen Orientation in Mechanically Conditioned Engineered Cardiovascular Tissues, Annals of Biomedical Engineering. 37 (2009) 1263–1272. doi:10.1007/s10439-009-9698-x.

[46] A. Balguid, A. Mol, M.A.A. van Vlimmeren, F.P.T. Baaijens, C.V.C. Bouten, Hypoxia induces near-native mechanical properties in engineered heart valve tissue, Circulation. 119 (2009) 290–297. doi:10.1161/CIRCULATIONAHA.107.749853.

[47] L. Wang, S.-P. Wilshaw, S. Korossis, J. Fisher, Z. Jin, E. Ingham, Factors influencing the oxygen consumption rate of aortic valve interstitial cells: application to tissue engineering, Tissue Eng Part C Methods. 15 (2009) 355–363. doi:10.1089/ten.tec.2008.0415.

[48] P.S. Robinson, S.L. Johnson, M.C. Evans, V.H. Barocas, R.T. Tranquillo, Functional tissue-engineered valves from cell-remodeled fibrin with commissural alignment of cell-produced collagen, Tissue Eng Part A. 14 (2008) 83–95. doi:10.1089/ten.a.2007.0148.

[49] T.C. Flanagan, J.S. Sachweh, J. Frese, H. Schnöring, N. Gronloh, S. Koch, R.H. Tolba, T. Schmitz-Rode, S. Jockenhoevel, In vivo remodeling and structural characterization of fibrin-based tissue-engineered heart valves in the adult sheep model, Tissue Eng Part A. 15 (2009) 2965–2976. doi:10.1089/ten.TEA.2009.0018.

[50] L.E. Niklason, Functional Arteries Grown in Vitro, Science. 284 (1999) 489–493. doi:10.1126/science.284.5413.489.

[51] J. Liao, E.M. Joyce, M.S. Sacks, Effects of decellularization on the mechanical and structural properties of the porcine aortic valve leaflet, Biomaterials. 29 (2008) 1065–1074. doi:10.1016/j.biomaterials.2007.11.007.

[52] A. Bayrak, M. Tyralla, J. Ladhoff, M. Schleicher, U.A. Stock, H.-D. Volk, M. Seifert, Human immune responses to porcine xenogeneic matrices and their extracellular matrix constituents in vitro, Biomaterials. 31 (2010) 3793–3803. doi:10.1016/j.biomaterials.2010.01.120.

[53] J.L. Honge, J. Funder, E. Hansen, P.M. Dohmen, W. Konertz, J.M. Hasenkam, Recellularization of aortic valves in pigs, Eur J Cardiothorac Surg. 39 (2011) 829–834. doi:10.1016/j.ejcts.2010.08.054.

[54] H. Baraki, I. Tudorache, M. Braun, K. Höffler, A. Görler, A. Lichtenberg, C. Bara, A. Calistru, G. Brandes, M. Hewicker-Trautwein, A. Hilfiker, A. Haverich, S. Cebotari, Orthotopic replacement of the aortic valve with decellularized allograft in a sheep model, Biomaterials. 30 (2009) 6240–6246. doi:10.1016/j.biomaterials.2009.07.068.

[55] P.M. Dohmen, A. Lembcke, S. Holinski, D. Kivelitz, J.P. Braun, A. Pruss, W. Konertz, Mid-term clinical results using a tissue-engineered pulmonary valve to reconstruct the right ventricular outflow tract during the Ross procedure, Ann. Thorac. Surg. 84 (2007) 729–736. doi:10.1016/j.athoracsur.2007.04.072.

[56] N.E. Hiemann, M. Mani, M. Huebler, R. Meyer, R. Hetzer, R. Thieme, C. Bethge, Complete destruction of a tissue-engineered porcine xenograft in pulmonary valve position after the Ross procedure, J. Thorac. Cardiovasc. Surg. 139 (2010) e67-68. doi:10.1016/j.jtcvs.2008.12.033.

[57] T. Shinoka, D. Shum-Tim, P.X. Ma, R.E. Tanel, N. Isogai, R. Langer, J.P. Vacanti, J.E. Mayer Jr, Creation of viable pulmonary artery autografts through tissue engineering, J. Thorac. Cardiovasc. Surg. 115 (1998) 536–545; discussion 545-546.

[58] K.M. Chrobak, D.R. Potter, J. Tien, Formation of perfused, functional microvascular tubes in vitro, Microvasc. Res. 71 (2006) 185–196. doi:10.1016/j.mvr.2006.02.005.

[59] C. Norotte, F.S. Marga, L.E. Niklason, G. Forgacs, Scaffold-free vascular tissue engineering using bioprinting, Biomaterials. 30 (2009) 5910–5917. doi:10.1016/j.biomaterials.2009.06.034.

[60] N. L'heureux, S. Pâquet, R. Labbé, L. Germain, F.A. Auger, A completely biological tissue-engineered human blood vessel, FASEB J. 12 (1998) 47–56.

[61] N. L'Heureux, N. Dusserre, A. Marini, S. Garrido, L. de la Fuente, T. McAllister, Technology Insight: the evolution of tissue-engineered vascular grafts—from research to clinical practice, Nature Clinical Practice Cardiovascular Medicine. 4 (2007) 389–395. doi:10.1038/ncpcardio0930.

[62] J.E. Saik, M.K. McHale, J.L. West, Biofunctional materials for directing vascular development, Curr Vasc Pharmacol. 10 (2012) 331–341.

[63] J.A. Hubbell, Bioactive biomaterials, Curr. Opin. Biotechnol. 10 (1999) 123–129.

[64] K. Lee, E.A. Silva, D.J. Mooney, Growth factor delivery-based tissue engineering: general approaches and a review of recent developments, J R Soc Interface. 8 (2011) 153–170. doi:10.1098/rsif.2010.0223.

[65] H.D. Maynard, J.A. Hubbell, Discovery of a sulfated tetrapeptide that binds to vascular endothelial growth factor, Acta Biomater. 1 (2005) 451–459. doi:10.1016/j.actbio.2005.04.004.

[66] S. Koch, C. Yao, G. Grieb, P. Prével, E.M. Noah, G.C.M. Steffens, Enhancing angiogenesis in collagen matrices by covalent incorporation of VEGF, J Mater Sci Mater Med. 17 (2006) 735–741. doi:10.1007/s10856-006-9684-x.

[67] J.J. Moon, S.-H. Lee, J.L. West, Synthetic biomimetic hydrogels incorporated with ephrin-A1 for therapeutic angiogenesis, Biomacromolecules. 8 (2007) 42–49. doi:10.1021/bm060452p.
[68] J.E. Leslie-Barbick, J.J. Moon, J.L. West, Covalently-immobilized vascular endothelial growth factor promotes endothelial cell tubulogenesis in poly(ethylene glycol) diacrylate hydrogels, J Biomater Sci Polym Ed. 20 (2009) 1763–1779. doi:10.1163/156856208X386381.
[69] J.E. Saik, D.J. Gould, A.H. Keswani, M.E. Dickinson, J.L. West, Biomimetic hydrogels with immobilized ephrinA1 for therapeutic angiogenesis, Biomacromolecules. 12 (2011) 2715–2722. doi:10.1021/bm200492h.
[70] Y. Ikeda, N. Fukuda, M. Wada, T. Matsumoto, A. Satomi, S.-I. Yokoyama, S. Saito, K. Matsumoto, K. Kanmatsuse, H. Mugishima, Development of angiogenic cell and gene therapy by transplantation of umbilical cord blood with vascular endothelial growth factor gene, Hypertens. Res. 27 (2004) 119–128.
[71] A.B. Pratt, F.E. Weber, H.G. Schmoekel, R. Müller, J.A. Hubbell, Synthetic extracellular matrices for in situ tissue engineering, Biotechnol. Bioeng. 86 (2004) 27–36. doi:10.1002/bit.10897.
[72] C. Rinsch, P. Quinodoz, B. Pittet, N. Alizadeh, D. Baetens, D. Montandon, P. Aebischer, M.S. Pepper, Delivery of FGF-2 but not VEGF by encapsulated genetically engineered myoblasts improves survival and vascularization in a model of acute skin flap ischemia, Gene Ther. 8 (2001) 523–533. doi:10.1038/sj.gt.3301436.
[73] M.P. Lutolf, J.A. Hubbell, Synthetic biomaterials as instructive extracellular microenvironments for morphogenesis in tissue engineering, Nature Biotechnology. 23 (2005) 47–55. doi:10.1038/nbt1055.
[74] E.A. Phelps, N. Landázuri, P.M. Thulé, W.R. Taylor, A.J. García, Bioartificial matrices for therapeutic vascularization, Proc. Natl. Acad. Sci. U.S.A. 107 (2010) 3323–3328. doi:10.1073/pnas.0905447107.
[75] S. Halstenberg, A. Panitch, S. Rizzi, H. Hall, J.A. Hubbell, Biologically engineered protein-graft-poly(ethylene glycol) hydrogels: a cell adhesive and plasmin-degradable biosynthetic material for tissue repair, Biomacromolecules. 3 (2002) 710–723.
[76] J.J. Moon, J.E. Saik, R.A. Poché, J.E. Leslie-Barbick, S.-H. Lee, A.A. Smith, M.E. Dickinson, J.L. West, Biomimetic hydrogels with pro-angiogenic properties, Biomaterials. 31 (2010) 3840–3847. doi:10.1016/j.biomaterials.2010.01.104.
[77] C.N. Salinas, K.S. Anseth, The enhancement of chondrogenic differentiation of human mesenchymal stem cells by enzymatically regulated RGD functionalities, Biomaterials. 29 (2008) 2370–2377. doi:10.1016/j.biomaterials.2008.01.035.
[78] J. Zhu, Bioactive modification of poly(ethylene glycol) hydrogels for tissue engineering, Biomaterials. 31 (2010) 4639–4656. doi:10.1016/j.biomaterials.2010.02.044.
[79] Y. Xiao, G.A. Truskey, Effect of receptor-ligand affinity on the strength of endothelial cell adhesion, Biophysical Journal. 71 (1996) 2869–2884. doi:10.1016/S0006-3495(96)79484-5.
[80] B.K. Wacker, S.K. Alford, E.A. Scott, M. Das Thakur, G.D. Longmore, D.L. Elbert, Endothelial Cell Migration on RGD-Peptide-Containing PEG Hydrogels in the Presence of Sphingosine 1-Phosphate, Biophysical Journal. 94 (2008) 273–285. doi:10.1529/biophysj.107.109074.
[81] G. Papavasiliou, S. Sokic, M. Turturro, Synthetic PEG Hydrogels as Extracellular Matrix Mimics for Tissue Engineering Applications, in: R. Sammour (Ed.), Biotechnology -

Molecular Studies and Novel Applications for Improved Quality of Human Life, InTech, 2012. http://www.intechopen.com/books/biotechnology-molecular-studies-and-novel-applications-for-improved-quality-of-human-life/synthetic-peg-hydrogels-as-extracellular-matrix-mimics-for-tissue-engineering-applications (accessed April 15, 2013).

[82] R. Gauvin, R. Parenteau-Bareil, M.R. Dokmeci, W.D. Merryman, A. Khademhosseini, Hydrogels and microtechnologies for engineering the cellular microenvironment, Wiley Interdiscip Rev Nanomed Nanobiotechnol. 4 (2012) 235–246. doi:10.1002/wnan.171.

[83] C.M. Ghajar, X. Chen, J.W. Harris, V. Suresh, C.C.W. Hughes, N.L. Jeon, A.J. Putnam, S.C. George, The effect of matrix density on the regulation of 3-D capillary morphogenesis, Biophys. J. 94 (2008) 1930–1941. doi:10.1529/biophysj.107.120774.

[84] A.F. Black, F. Berthod, N. L'heureux, L. Germain, F.A. Auger, In vitro reconstruction of a human capillary-like network in a tissue-engineered skin equivalent, FASEB J. 12 (1998) 1331–1340.

[85] V. Hudon, F. Berthod, A.F. Black, O. Damour, L. Germain, F.A. Auger, A tissue-engineered endothelialized dermis to study the modulation of angiogenic and angiostatic molecules on capillary-like tube formation in vitro, Br. J. Dermatol. 148 (2003) 1094–1104.

[86] P.-L. Tremblay, V. Hudon, F. Berthod, L. Germain, F.A. Auger, Inosculation of tissue-engineered capillaries with the host's vasculature in a reconstructed skin transplanted on mice, Am. J. Transplant. 5 (2005) 1002–1010. doi:10.1111/j.1600-6143.2005.00790.x.

[87] A. Alajati, A.M. Laib, H. Weber, A.M. Boos, A. Bartol, K. Ikenberg, T. Korff, H. Zentgraf, C. Obodozie, R. Graeser, S. Christian, G. Finkenzeller, G.B. Stark, M. Héroult, H.G. Augustin, Spheroid-based engineering of a human vasculature in mice, Nat. Methods. 5 (2008) 439–445. doi:10.1038/nmeth.1198.

[88] J.M. Sorrell, M.A. Baber, A.I. Caplan, Influence of adult mesenchymal stem cells on in vitro vascular formation, Tissue Eng Part A. 15 (2009) 1751–1761. doi:10.1089/ten.tea.2008.0254.

[89] O. Tsigkou, I. Pomerantseva, J.A. Spencer, P.A. Redondo, A.R. Hart, E. O'Doherty, Y. Lin, C.C. Friedrich, L. Daheron, C.P. Lin, C.A. Sundback, J.P. Vacanti, C. Neville, Engineered vascularized bone grafts, Proc. Natl. Acad. Sci. U.S.A. 107 (2010) 3311–3316. doi:10.1073/pnas.0905445107.

[90] Y. Zheng, J. Chen, M. Craven, N.W. Choi, S. Totorica, A. Diaz-Santana, P. Kermani, B. Hempstead, C. Fischbach-Teschl, J.A. López, In vitro microvessels for the study of angiogenesis and thrombosis, Proceedings of the National Academy of Sciences. 109 (2012) 9342–9347.

[91] S. Raghavan, C.M. Nelson, J.D. Baranski, E. Lim, C.S. Chen, Geometrically Controlled Endothelial Tubulogenesis in Micropatterned Gels, Tissue Engineering Part A. 16 (2010) 2255–2263. doi:10.1089/ten.tea.2009.0584.

[92] N. Sadr, M. Zhu, T. Osaki, T. Kakegawa, Y. Yang, M. Moretti, J. Fukuda, A. Khademhosseini, SAM-based cell transfer to photopatterned hydrogels for microengineering vascular-like structures, Biomaterials. 32 (2011) 7479–7490. doi:10.1016/j.biomaterials.2011.06.034.

[93] J.S. Miller, K.R. Stevens, M.T. Yang, B.M. Baker, D.-H.T. Nguyen, D.M. Cohen, E. Toro, A.A. Chen, P.A. Galie, X. Yu, R. Chaturvedi, S.N. Bhatia, C.S. Chen, Rapid casting of patterned vascular networks for perfusable engineered three-dimensional tissues, Nature Materials. 11 (2012) 768–774. doi:10.1038/nmat3357.

[94] X. Chen, A.S. Aledia, S.A. Popson, L. Him, C.C.W. Hughes, S.C. George, Rapid anastomosis of endothelial progenitor cell–derived vessels with host vasculature is promoted by a high density of cotransplanted fibroblasts, Tissue Engineering Part A. 16 (2009) 585–594.

[95] G. Cheng, S. Liao, H.K. Wong, D.A. Lacorre, E. di Tomaso, P. Au, D. Fukumura, R.K. Jain, L.L. Munn, Engineered blood vessel networks connect to host vasculature via wrapping-and-tapping anastomosis, Blood. 118 (2011) 4740–4749.

[96] T. Korff, H.G. Augustin, Tensional forces in fibrillar extracellular matrices control directional capillary sprouting, Journal of Cell Science. 112 (1999) 3249–3258.

[97] A. Simionescu, J.B. Schulte, G. Fercana, D.T. Simionescu, Inflammation in Cardiovascular Tissue Engineering: The Challenge to a Promise: A Minireview, International Journal of Inflammation. 2011 (2011) 1–11. doi:10.4061/2011/958247.

[98] L.E. Niklason, R.S. Langer, Advances in tissue engineering of blood vessels and other tissues, Transpl. Immunol. 5 (1997) 303–306.

[99] A. Patel, B. Fine, M. Sandig, K. Mequanint, Elastin biosynthesis: The missing link in tissue-engineered blood vessels, Cardiovasc. Res. 71 (2006) 40–49. doi:10.1016/j.cardiores.2006.02.021.

[100] S.K. Singh, N.D. Desai, S.D. Petroff, S. Deb, E.A. Cohen, S. Radhakrishnan, L. Schwartz, J. Dubbin, S.E. Fremes, The impact of diabetic status on coronary artery bypass graft patency: insights from the radial artery patency study, Circulation. 118 (2008) S222-225. doi:10.1161/CIRCULATIONAHA.107.757161.

[101] C. Franco, H. Gerhardt, Tissue engineering: Blood vessels on a chip, Nature. 488 (2012) 465–466. doi:10.1038/488465a.

Chapter 4: 3-D Culture and Endothelial Cells Improve Maturity of Human Pluripotent Stem Cell-Derived Hepatocytes

Elements of this chapter have been published as:

Hamisha Ardalani, Srikumar Sengupta, Victoria Harms, Vernella Vickerman, James A.Thomson, William L. Murphy (2019). "3-D Culture and Endothelial Cells Improve Maturity of Human Pluripotent Stem Cell-Derived Hepatocytes." In Acta Biomaterialia

https://doi.org/10.1016/j.actbio.2019.07.047

4.1 Preface

In Chapter 2, we provided an overview of the current state of the art in approaches to mature iPS-ES-derived hepatocytes. While so much progress has been made to improve the 2D differentiation protocols by chemical and small molecule screening, the hepatocyte-like cells are still far from the primary human hepatocytes. In this chapter, we describe a 3D co-culture strategy for improving the metabolic function and CYP450 enzyme activity of human iPS-derived hepatocytes. This work demonstrates the value of 3D culture and heterotypic cell-cell interactions on improving the maturity of human iPS-derived hepatocyte.

4.2 Abstract

Human-induced pluripotent stem cell (hiPSC)-derived hepatocytes (iHEP) offer an attractive alternative to primary human hepatocytes (PHH) for drug toxicity studies, as PHHs are limited in supply, vary in their metabolic activity between donors, and rapidly lose their functionality *in vitro*. However, one of the major drawbacks with iHEP cells in drug safety studies is their decreased phenotypic maturity, with lower liver specific enzyme activity compared with that of PHH. Here we evaluated the effects of 3D culture and non-parenchymal cells on the

maturation of iHEPs. We describe a serum-free, chemically defined 3D in vitro model using iHEP cells, which is compatible with automation and conventional assay plates. The iHEP cells cultured in this model form polarized aggregates with functional bile canaliculi and strongly increased expression of albumin, urea and genes encoding phase I and II drug metabolism enzymes and bile transporters. Cytochrome P450-mediated metabolism is significantly higher in 3D iHEP aggregates compared to 2D iHEP culture. Furthermore, addition of human liver sinusoidal endothelial cells (sECs) and iPS-derived endothelial cells (iECs) improved mature hepatocyte function and CYP450 enzyme activity. Also, ECs formed endothelial networks within the hepatic 3D cultures, mimicking aspects of an *in vivo* architecture. Collectively, these results suggest that the iHEP/EC aggregates described here may have the potential to be used for many applications, including as an in vitro model to study liver diseases associated with sinusoidal endothelial cells.

4.3 Introduction

Pluripotent stem cell-derived liver cells are a promising cell source for *in vitro* liver models and tissue-engineering applications. However, these cells do not replicate the function of primary human hepatocytes (PHH). Hepatocyte-like cells differentiated from pluripotent stem cells have lower synthetic ability and metabolic enzyme activity compared to primary hepatocytes, and unlike primary hepatocytes they consistently express immature hepatic markers such as α-fetoprotein (AFP). On the other hand, the use of PHH in applications such as drug toxicity screening [1] is limited due to donor to donor variability, limited supply, tendency to de-differentiate and rapid loss of hepatocyte-specific functions in conventional 2D monolayer cultures [2–4]. Therefore, there is a need for new approaches to mature induced pluripotent stem cell (iPS)-derived or embryonic stem cell (ES)-derived hepatocytes [5–7] as a substitute for PHH.

Early attempts to mature iPS/ES-derived hepatocytes were focused on two-dimensional (2D) differentiation protocols and use of chemical and small molecules [5–8]. More recent studies have demonstrated that three-dimensional (3D) culture better recapitulated the complex 3D interactions between cell-cell and cell-extracellular matrix (ECM) in the liver [9,10]. 3D cell culture systems, such as collagen matrices [11], micropatterned formats [12] or spheroid culture [13–15], have been used to recreate cell-cell junctions and mimic liver architecture more effectively than traditional sandwich cultures, leading to enhanced iPS-derived hepatocyte function. Limitations of these previous cell cultures include limited scalability, drug absorption/adsorption to the ECM, and batch-to-batch differences in 3D ECMs [16]. 3D spheroids may circumvent these limitations. However, 3D spheroid cultures that include non-parenchymal cells (NPCs) have typically been conducted with mouse primary cells [15], which do not recapitulate human liver physiology.

In this work, we evaluated the effect of heterotypic co-cultures on hiPS-derived hepatocyte (iHEP) function in a 3D culture format, in which all cells were of human origin. We describe a serum-free, chemically defined 3D *in vitro* model using iHEP cells, which is compatible with automation and conventional assay plates. iHEP cells cultured in this model form polarized aggregates with functional bile canaliculi and strongly increased expression of albumin, urea and genes encoding phase I and II drug metabolism enzymes and bile transporters. Cytochrome P450-mediated metabolism was significantly higher in 3D iHEP aggregates compared to 2D culture. Furthermore, we found that the addition of human liver sinusoidal endothelial cells (sECs) or iPS-derived endothelial cells (iECs) improved mature hepatocyte function and CYP450 enzyme activity of iHEPs. Also, we observed that each of the EC types formed endothelial networks within the hepatic 3D cultures, mimicking aspects of an *in vivo* architecture. Collectively, these results suggest that the iHEP/EC aggregates that described here may have potential to be used for many

applications, including as in-vitro model to study liver diseases associated with sinusoidal endothelial cells.

4.4 Materials and Methods

4.4.1 Hepatocyte cell culture

iCell Hepatocyte 2.0 (from Cellular Dynamics International) was thawed and plated into collagen I-coated 24 and 96-well plates at a $3x10^5$ cells/cm^2. Plating volumes for 24 and 96-well plates were 0.57 ml and 0.1 ml, respectively. Maintenance medium used for 2D culture of hepatocytes was DEME/F12 medium, no phenol red supplemented with B27 supplement (1x), Dexamethasone (0.1 μM) and Oncostatin M (20 ng/ml). On day 1 through day 4 post-plating, spent medium is replaced daily. On day 5, medium is replaced with Maintenance medium minus Oncostatin and spent medium is replaced every two days thereafter.

4.4.2 Non-parenchymal cell culture

Human hepatic stellate cells were from ScienCell Research laboratories (Cat# 5300). Cells were thawed and cultured on poly-L-lysine coated plates and recommended media based on the manufacturer's protocol. Human cholangiocyte primary cells were from CELPROGEN stem cell research and therapeutics. Cells were thawed and cultured on the proprietary coated plates and medium recommended by the company. Human liver sinusoidal endothelial cells were from Cell Systems. The cells were cultured and expanded on plates coated with proprietary cell attachment factor coated plates and the recommended medium.

Human induced pluripotent stem cell-derived endothelial cells (iEC) (from Cellular Dynamics International) were cultured according to the manufacturer's protocol on fibronectin-coated plates in VascuLife Medium (Lifeline Cell Technologies).

4.4.3 Aggregate formation and maintenance

iHEP spheroid culture. On day 5-7 post iHEP 2D culture Accutase was used to dissociate iHEPs. Cells were seeded into ultra-low attachment (ULA) 96-well plates (Corning) at 1500 viable cells per well and subsequently centrifuged at 100 ×g for 2 min. Cells were seeded in iHEP Maintenance medium (Section 4.4.1) minus Oncostatin M. Aggregates were maintained in serum-free medium with 50% medium change every 48-72 h. The cells formed spheroids within 24-48 hours after transfer to the ULA plates (Fig. 4.1a).

Co-culture spheroids. When used, co-culture of iHEP and non-parenchymal cells originating from human were seeded at a ratio of 1:0.7:0.2:0.1 (iHEP:EC:hSC:CC) and 1500:1050:300:150 viable cells per well into ultra-low attachment plates. The ratios are adapted from a well-cited published study demonstrating formation of liver bud from human induced pluripotent stem cells [17]. Aggregates that were co-cultured with ECs were maintained in a medium supplemented with 40 ng/ml VEGF.

4.4.4 RNA isolation and RT-qPCR analysis

Cells were lysed with ice-cold RLT plus buffer supplemented with β-Mercaptoethanol and total RNA was extracted using the RNeasy Micro plus Kit (Qiagen). The total RNA concentration was quantified using Nanodrop spectrophotometer. Conversion of total RNA to cDNA was carried out using the SuperScript™ IV Vilo™ Master Mix (Invitrogen). qPCR was performed on the Applied Biosystems instruments in 384-well format using TaqMan universal master mix II

(Applied Biosystems). The data were analyzed using the $2^{-\Delta\Delta Ct\ methods}$. All genes were normalized to the geometric mean of GAPDH and ACTB using the ΔCt method and were normalized to the expression of fresh iHEP using the ΔΔCt method unless stated otherwise. Fresh iHEP refers to freshly thawed hepatocytes that were not cultured in 2D or 3D format. Pre-designed TaqMan primers were purchased from ThermoFisher Scientific. Taqman primers used in this study can be found in Table S4.1.

4.4.5 Immuno-staining and imaging

Aggregates were fixed for 30 minutes with 4% paraformaldehyde and washed 3 times with DPBS. Samples were permeabilized and blocked with 0.1% Triton X-100 and 10% donkey serum for 30 minutes, respectively. The samples were then incubated with the following primary antibodies diluted in 1% donkey serum overnight at 4^0C: ALB (1:100; SC69873, Santa Cruz and NBP1-32458, Novus Biologics), Desmin (1:100; SC-7559, Santa Cruz), Vimentin (1:100; NB300-223SS, Novus Biologics), S1004A (1:100; NBP1-89402, Novus Biologics), MRP2 (1:100; MAB4150, MDS-Millipore Sigma), CYP3A4 (1:100; AB1254, MDS-Millipore Sigma), and PECAM (1:100; M082301-2, DAKO), and Alexa Fluor™ 568 Phalloidin (1:100; A12380, R&D Systems) for F-actin staining. Cells were washed three times with PBS for 30 minutes each. Cells were incubated for 2 hours at room temperature with appropriate secondary antibodies diluted in 1% donkey serum: Alexa Fluor 488 series (1:500; Life Science), and Alexa Fluor 568 series (1:500; Life Science). Nuclei were stained using 4,6-diamidino-2-phenylindole (DAPI) or Hoechst 3342 (1:10000 in DPBS; Sigma) for 30 minutes. Cells were then washed three times with PBS for 30 minutes each and then imaged using a Nikon A1R laser scanning confocal microscope with Plan Apo 10×, Plan Fluor 20×Ph1 DLL, or Plan Apo 20×DIC M objectives (0.95–3.35 µm z-steps).

4.4.5.1 Bile canaliculi staining

Aggregates were washed three times with PBS and incubated with 5(6)-carboxy-2',7'-dichlrofluoroscin diacetate (CFDA) at a final concentration of 10 μg/ml for 30 minutes at 37°C. Cultures were subsequently rinsed several times with ice-cold PBS containing calcium and magnesium and imaging was performed with confocal microscopy (Nikon). Images were acquired at excitation/emission λ: 495/520 nm.

4.4.7 Biochemical Assays

4.4.7.1 ALB and Urea Secretion

Albumin and urea secretion were analyzed by measuring the concentration of albumin and urea in culture medium. Culture supernatants were assayed for albumin levels using an enzyme-linked immunosorbent assay (ELISA) kit (E88-129, Bethyl Laboratories). Urea concentration was measured using a calorimetric assay kit from Bioassay Systems (DIUR-100).

4.4.7.2 Cytochrome P450

Luminescence-based assays (Promega, Madison, WI) for CYP2C9 (luciferin-H), CYP3A4 (luciferin-IPA) and CYP1A2 (luciferin-1A2) were used to measure CYP450 activity. Briefly, cultures were rinsed in phenol red-free culture medium and incubated with luminescent substrates, diluted in same medium, for 1 hour (3μM luciferin-IPA) or 3 hours (100μM luciferin-H) at 37°C. For CYP1A2 cultures were rinsed with PBS and incubated with luminescent substrate diluted in PBS for 1 hour (6μM luciferin-1A2). Following incubation, supernatant was processed according to manufacturer instructions and luminescence was measured using luminometer (Promega GloMax plate reader).

Drug dosing. For CYP450 induction studies, cultures were treated in serum-free culture medium with rifampicin (25 μM) or 0.1% vol/vol DMSO control dissolved in culture medium for 3 days, followed by quantitation of CYP3A4 and CYP2C9 activities using the luminescent assays described above. Analogously, cultures were treated with omeprazole (100 μM) and dexamethasone (50 μM) for 3 days, followed by quantitation of CYP1A2 activity and CYP3A4 activity, respectively. Since dexamethasone is a known inducer of cytochrome P450 3A4, dexamethasone was extracted from the medium to lower CYP3A4 basal activity.

4.4.7.3 ATP viability and Toxicity assays and DNA Quantification

Cell viability was assessed by determining the ATP content of aggregates with CellTiter-Glo 3D Cell Viability Assay (Promega). DNA within the resulting lysates was measured by reading fluorescein at 485/535 nm using Quant-it^{TM} PicoGreen dsDNA kit (Invitrogen). Known concentration of iHEP mono/co-cultured aggregates was used to construct a standard curve and correlate DNA concentration to cell number. Estimated DNA content was used to normalize the readout data for assays mentioned earlier.

At the same time-points, cell culture medium was collected to assess the cytotoxicity effect of drugs on aggregates. Cytotoxicity was measured using the Cytotox 96 Non-Radioactive Cytotoxicity Assay (Promega).

4.4.8 Statistical analysis

Experiments were repeated 2-3 times with 4-6 replicate samples for each condition. Data from representative experiments are presented, whereas similar trends were seen in multiple repeats. Statistical significance was determined using Unpaired Two-tailed *t*-test with Welch's correction

(GraphPad Prism version 8.0C for Mac, GraphPad Software, La Jolla California USA). All error bars represent standard deviation. P-values below 0.05 were considered significant for this study.

4.5 Results

4.5.1 Mature hepatocyte markers were enhanced in 3D-cultured iHEP aggregates

Real time PCR analysis showed that expression of genes representing the liver maturation factors ALB (albumin), AAT (alpha-1 antitrypsin deficiency, also known as SERPINA1) and HNF4α (hepatocyte nuclear factor 4 alpha) was higher in 3D iHEP aggregates when compared to 2D iHEP cultures. mRNA transcript levels of these genes decreased after 11 days in 2D culture, while they were significantly higher in 3D aggregates (Fig. 4.1b (I, III, IV)). Alpha-fetoprotein (AFP) was still detected in 3D iHEP aggregates, but 3D iHEP aggregates showed greater decrease in AFP expression during cell culture when compared to 2D iHEP cultures (Fig. 4.1b (II)). 3D iHEP aggregates had a higher ALB/AFP ratio compared with cells grown in 2D on day 11 (Fig. 4.1b (V)), suggesting an improvement in maturation. In addition, albumin protein levels were 3000-fold higher in 3D iHEP cultures compared to 2D cultures (Fig. 4.1b (VI)). Albumin protein levels was stable from day 7 to day 11 in 3D iHEP aggregates unlike 2D iHEP cultures. Similarly, immunostaining of 3D iHEP aggregates showed presence of albumin both in 2D and 3D (Fig. 4.1b (VII)). Urea production was higher in 3D aggregates compared to 2D culture (Fig. 4.1b (VIII)). Taken together, these data suggest that iHEP cultured in 3D are more mature than iHEPs cultured in 2D.

4.5.2 Metabolic competence was enhanced in 3D-cultured iHEP aggregates

Real time PCR analysis showed higher expression of various phase I and II metabolic enzymes and bile transporters in 3D iHEP aggregates compared to 2D cultures (Fig. 4.2a (I-III)). mRNA transcript levels of phase I xenobiotic metabolizing enzymes CYP3A4, CYP1A2 and CYP2C9 were analyzed over a period of 11 days. Expression level of CYP3A4 decreased after 11 days in 2D iHEP cultures. Notably, CYP1A2 and CYP2C9 were nearly undetectable in iHEP cells cultured in 2D. However, the expression levels of those genes, which represent major phase I metabolizing enzymes, were increased in 3D aggregates compared to 2D cultures (Fig. 4.2a (I, II and III)). Similarly, the mRNA levels of phase II xenobiotic metabolizing enzymes UGT1A1 and UGT1A6 also increased in 3D iHEP cultures (Fig. 4.3a (I-II)).

To evaluate whether increased mRNA levels of metabolic enzymes correlated with increased functional metabolism, we compared the basal activity of CYP450 enzymes in iHEPs cultured in 2D and 3D. Basal activity of phase I metabolizing enzymes measured after 11 days was higher in 3D versus 2D cultures (Fig. 4.2a (IV)). Immunostaining of 3D iHEP aggregates showed presence of CYP3A4 both in 2D and 3D (Fig. 4.2b). Together, these data showed that the increased expression of numerous Phase I, II and III enzymes and increased xenobiotic metabolic competence were associated with 3D aggregate culture.

4.5.3 Functional bile canaliculi were formed in 3D iHEP aggregates

The gene expression levels of bile canaliculi transporters (MRP2 and BSEP) were increased in 3D iHEP cultures compared with 2D iHEP cultures (Fig. 4.3b (I, II)). Bile salts are transported by hepatocytes into the bile canaliculi, and perturbation of this process is often associated with drug-induced liver injury. Immunofluorescence staining for F-Actin as a cytoskeleton marker confirmed the presence of polarized epithelial structures in the 3D iHEP aggregates (Fig. 4.3c (II)). Intracellular localization of F-actin indicated a polarized cellular organization. In particular, F-

actin enrichment at cellular junctions resembled biliary-like structures, which mimicked the interconnectivity between bile canaliculi.

CFDA (5-(and-6)-carboxy-2',7'-dichlorofluorescein diacetate) accumulated in canaliculi structures of 3D iHEP aggregates, suggesting that 3D iHEP aggregates formed rudimentary canaliculi (Fig. 4.3d (I)). In contrast, there was less accumulation of CFDA in 2D iHEP cultures (Fig. 4.3d (II)). Uptake of non-fluorogenic CFDA into hepatocytes in human liver is mediated by phase II esterases into fluorogenic carboxy fluorescein (CF) and excreted into canaliculi via phase III transporters including MRP2 [18]. Immunostaining clearly showed MRP2 on iHEP aggregates in the apical regions (Fig. 4.3c (I)). The mRNA level of MRP2 was also found to be 130-fold higher in 3D iHEP aggregates compared to 2D iHEP cultures after 11 days (Fig. 4.3b (I)). These results suggest that 3D iHEP aggregates were able to take up bile salts actively and transport them into canalicular structures.

4.5.4 Endothelial cells improved the maturity of 3D iHEP aggregates

iHEP/EC aggregate co-cultures showed increased hepatocyte function when compared to iHEP aggregate monocultures. Albumin and urea secretions in iHEP/EC aggregate co-cultures were greater ($2X$-$50X$) than in iHEP aggregate monocultures (Figs. 4.4a, 4.4b). Without the support of ECs, albumin secretion from iHEP aggregates remained at 604 $\pm$116 pg and in case of CC quickly decreased to 69$\pm$26 pg after 7 days of culture in 3D. However, addition of hSC and ECs significantly improved albumin secretion of iHEP/hSC, iHEP/sEC, iHEP/iECs and iHEP/hSC/sEC aggregates, which increased during 7 days of culture and was stable until 11 days (Fig. 4.4a). Although, albumin secretion of iHEP/sEC aggregates declined after 11 days it was still 2.7-fold higher than that of iHEP aggregate on day 11. All cell aggregates positively stained with Albumin (Fig. 4.5a, b). The addition of sECs also led to a significant increase in urea secretion

across the time course of experiment (Fig. 4.4b). Although iECs did not increase the urea levels compared to iHEP monoculture on day 7, iEC support maintained the urea levels until day 11. Although, iHEP/sECs showed decrease in urea secretion on day 11, it was still higher than iHEP monoculture on day 11 (Fig. 4.4b). Addition of hSCs led to a significant decrease in urea secretion compared to iHEP monoculture aggregates. Similarly, addition of CCs, led to significant decrease in both albumin and urea production of iHEP aggregates.

4.5.5 CYP450 basal activity and induction were enhanced in 3D iHEP aggregates co-cultured with ECs

Basal activity of CYP450 enzyme in iHEP/EC aggregates were higher compared to iHEP aggregates (Fig. 4.4c-e). Activity of CYP3A4, CYP1A2 and CYP2C9 in iHEP/sEC aggregates were 1.7-fold, 1.7-fold and 2.2-fold higher than that in iHEP monoculture, respectively, and activity of each enzyme was 1.5-fold higher than that in iHEP/hSC aggregates. Similarly, activity of CYP3A4, CYP1A2 and CYP2C9 in iHEP/iEC aggregates were 1.7-fold, 3.1-fold and 1.6-fold higher than that in iHEP aggregates, and 1.5-fold, 2.9-fold and 1.2-fold higher than that in iHEP/hSC aggregates.

Rifampicin and dexamethasone induced CYP3A4 activity by at least 2-fold in all the conditions, with slightly more induction of CYP3A4 in iHEP/sEC aggregates than in iHEP aggregates on day 11. CYP3A4 activity was 2-fold higher with rifampicin induction in iHEP/sEC/hSC aggregates when compared to dexamethasone induction (Fig. 4.4c). However, induction of CYP2C9 by rifampicin was modest compared with CYP3A4 in iHEP, iHEP/sEC, iHEP/hSC and iHEP/sEC/hSC (Fig. 4.4d). CYP2C9 activity was not induced for iHEP/sEC/hSC aggregates or iHEP/CC aggregates (Fig. 4.4d). Omeprazole increased basal activity of CYP1A2 by 2.3-fold in iHEP aggregates and iHEP/sEC aggregates, and by 1.4-fold in iHEP/iEC aggregates.

CYP1A2 activity in iHEP/hSC aggregates did not change after induction with omeprazole (Fig. 4e). CYP2C9, 3A4 and 1A2 levels in iHEP/CC aggregates were each significantly lower than that in iHEP aggregates. This may be attributed to increased growth of CCs and their dominance in the 3D co-culture with iHEP cells. Drugs at chosen concentration did not have any cytotoxic effects on 3D iHEP co-cultures (Fig. S4.3). Taken together, activity of CYP1A2, CYP2C9 and CYP3A4 in iHEP aggregates tended to increase more with the support of sECs and iECs.

4.5.6 Morphology of 3D iHEP aggregates co-cultured with ECs, hSCs and CCs

Nonparenchymal cells were clearly detectable after aggregate formation (Figs. 4.5a, 4.5b). Endothelial cells were detected within the iHEP/sECs and iHEP/iECs aggregates and instead of randomly distributed within the aggregates they were organized in capillary like structures evidenced by CD31 staining after 11 days (Fig. 4.5a). Co-staining with desmin (hSC marker) and CD31 (EC marker) in iHEP/sEC/hSC aggregates showed hSCs are located where sECs existed. A z-stack series from iHEP/sEC aggregates on day 8 showed a lack of sEC organization into capillary-like structures (Movie S4.1), suggesting organization of ECs in iHEP/ECs aggregates happened between 8 and 11 days of culture. Moreover, mesh-like structures observed in scanning electron micrographs of 3D co-cultures was an indicative of extracellular matrix deposition within the aggregates (Fig. S4.1a).

Phase contrast images taken from the co-culture conditions that included CCs showed large aggregates and loss of clear, defined boundaries, unlike co-culture with ECs and hSCs (Fig. S4.1b). Co-staining against S1004A and vimentin as activated CC markers and ALB as iHEP marker in iHEP/CC showed presence of both iHEP and CCs, however there were more CCs than iHEPs contrary to the starting cell numbers, where the number of CCs were $1/10^{th}$ of the iHEPs (Fig. 4.5b). Moreover, the expression of transcription factors and genes attributed to activated CCs were

significantly higher in iHEP/CC aggregates compared to other 3D co-cultured aggregates (Fig. S4.2). Therefore, overgrowth of iHEP/CC aggregates could be due to the CC activation.

Similar to 3D iHEP aggregates, uptake and transformation of non-fluorogenic CFDA to fluorogenic CF in iHEP/sECs, iHEP/hSCs and iHEP/sECs/hSCs indicated that phase II esterases existed in those aggregates. However, localization of fluorogenic CF dye in cell-cell junctions was only observed in iHEP/sECs (Fig. 4.5c), suggesting of phase III transporters and rudimentary bile canaliculi in iHEP/sEC and their lack in iHEP/hSCs and iHEP/sECs/hSCs aggregates (Fig. 4.5c).

4.6 Discussion

One of the major drawbacks with human pluripotent stem cell derivatives, including hepatocyte-like cells, is their decreased phenotypic maturity with lower liver-specific enzyme activities compared with PHH. This limited maturity has limited their utility in drug safety evaluation studies. Thus, *in vitro* culture protocols need to be improved to further mature iHEPs towards the adult PHH phenotype. Here, we studied the effect of heterotypic cell interactions (iHEP and liver non-parenchymal cells) and 3D culture on the maturation of iHEPs. Unlike previous studies, all the cells used in this study are of human origin, and this is important due to differences in drug metabolism and toxicity pathways between rodents and humans [19–22]. 3D aggregates presented here were also maintained in chemically-defined, serum-free conditions (Fig. 4.1a). This is important for studies in which binding of drugs or drug metabolites to serum proteins may confound the interpretation of data. In addition, the compatibility with standard assay plates and automation equipment in our current study makes the approach potentially suitable for high-throughput toxicity screening.

The iHEP aggregates described here outperformed iHEPs cultured in 2D, as expected. In particular, the levels of hepatocyte functions, such as ALB secretion, urea secretion, hepatocyte

related gene expression (Fig. 4.1b) and CYP450 basal activity (Fig. 2) of 3D iHEP aggregates were higher than those of iHEP 2D cultures. This performance improvement can perhaps be attributed to the preserved structural and functional polarity of 3D iHEP cultures (Fig. 4.3c). Previous studies have also shown that a 3D culture conditions could maintain the hepatic characteristics of differentiated hepatocytes [9–11,14]. When we analyzed key proteins for bile transport in iHEP aggregates, we found that the bile acid pump BSEP and bile exporter pump MRP2 are expressed at higher levels after 11 days (Fig. 4.3b) when compared to 2D iHEP cultures, suggesting that molecular machinery involved in bile acid circulation was functional in 3D iHEP aggregates. Thus, 3D iHEP aggregates have the potential to be used as in vitro systems for evaluation of cholestasis and steatosis, understanding the underlying disease mechanism or the pharmacological action of new drugs.

Next, we created cocultures of iHEP, primary human stellate cell and endothelial cells. We evaluated both primary human liver sinusoidal endothelial cells and human iPS- derived endothelial cells. The source of cells used in *in vitro* liver models has a significant impact on observed biological responses, as well as the relevancy of those models to human liver physiology. As shown in Fig. 4.4c-d, cell aggregates of iHEP/ECs have increased CYP450 activities. We found that sECs improved maturation of iHEP cells, as evidenced by increased secreted albumin and urea (Fig. 4.4a, b). Our observations with iHEP/EC co-cultures are generally consistent with previously published data on self-assembled spheroid/organoids models [10,23,24]. However, the endothelial cells used in previous studies were either immortalized human liver endothelial cells (TMNK) or human umbilical vein endothelial cells (HUVEC) instead of primary human liver sinusoidal endothelial cells [25,26]. The immortality of the produced cell lines makes them susceptible to react differently than primary sECs. Ware et al. [27] has shown that TMNK cells cause severe

decline in PHH morphology and functionality, likely because of overgrowth. Our observations are also consistent with previously published data in co-culture of rat hepatocyte and endothelial cells, which has shown relatively stable hepatocyte function for several weeks [28,29].

3D aggregates containing sECs also displayed endothelial organization into a network of capillary-like structures, reminiscent of liver sinusoids (Fig. 4.5a). To the best of our knowledge, this is the first demonstration of self-assembly of endothelial networks within 3D iHEP aggregates. Our aggregates can potentially be integrated with perfusable vascularized networks using microfluidic platforms, which may further improve the nutrient and oxygen delivery to the core of the aggregates and create larger-sized aggregates. The perfusion in such a system would expose endothelial cells to shear stress while protecting the iHEP cells from shear stress, much like an in vivo environment. Furthermore, the aggregate co-cultures described here may be used to evaluate the reciprocal interactions between endothelial cells and iHEPs in physiological and pathophysiological conditions. For example, some drugs like azathioprine are known to be more toxic to sECs, which can lead to downstream effects in PHH cells due to release of apoptotic factors from sECs [30–32]. Our co-cultures have the potential to study such cellular cross-talk during and after drug exposure.

Contrary to ECs, addition of cholangiocytes to iHEPs resulted in a diminished metabolic activity, urea and albumin secretion, likely because of CC overgrowth (Figs. 4.4, 4.5b and S4.1b). CC activation has been reported in cholestatic liver diseases, such as inherited diseases (Agile syndrome and cystic fibrosis), autoimmune cholangitis, and primary biliary cirrhosis [33–35]. Activated cells typically lose their cell-cell contact and acquire a motile phenotype, similar to what we observed in iHEP/CC aggregates (Figs. 4.5b and S4.1b). Real time PCR analysis showed higher expression of known activated CC markers (vimentin and S1004A (also known as FSP-1)) [33,36–

42] and activated transcription factors (ZEB and TWIST) [39–42] in iHEP/CC aggregates compared to other conditions (Fig. S4.2). Immunostaining for vimentin and S1004A also confirmed the presence of those activated markers at protein level (Fig. 4.5b). Our results suggest that CC-containing aggregates may be adopting a liver disease relevant phenotype. However, more experiments are necessary to decipher the mechanism of CC activation for use in liver disease modeling.

4.7 Conclusions

In summary, we presented a 3D hepatic co-culture model, in which we showed that hiPSC-derived hepatocytes co-cultured with ECs improve hepatic functionality. In 3D co-cultures, the hepatocytes demonstrated a polarized phenotype, formed bile canaliculi, and the ECs formed capillary-like structures reminiscent of liver sinusoids. Heterotypic 3D co-cultures with ECs also showed an improved metabolic and enzyme activity. Although iHEPs in 3D co-cultured with ECs were significantly more mature than iHEPs in monoculture, they still express fetal markers and do not approach the maturity of adult PHHs. To further promote iHEP differentiation towards the adult PHH phenotype, alternative approaches should be explored, such as stimulation with small molecules or culturing iHEP cells in ECMs derived from the liver.

4.8 Disclosure of Potential Conflicts of Interest

The authors declare no competing financial interests.

4.9 Acknowledgments

This research was funded by the Environmental Protection Agency, USA (STAR Grant no. 83573701) and the National Institutes of Health, USA (1U01TR002383-01).

Supplementary movie to this article can be found online at

https://doi.org/10.1016/j.actbio.2019.070.047.

4.10 References

[1] I.M. Arias, ed., The liver: biology and pathobiology, 5. ed., 1. impr, Wiley-Blackwell, Chichester, 2009.
[2] G. Elaut, T. Henkens, P. Papeleu, S. Snykers, M. Vinken, T. Vanhaecke, V. Rogiers, Molecular mechanisms underlying the dedifferentiation process of isolated hepatocytes and their cultures, Curr. Drug Metab. 7 (2006) 629–660.
[3] J. Fraczek, J. Bolleyn, T. Vanhaecke, V. Rogiers, M. Vinken, Primary hepatocyte cultures for pharmaco-toxicological studies: at the busy crossroad of various anti-dedifferentiation strategies, Arch. Toxicol. 87 (2013) 577–610. doi:10.1007/s00204-012-0983-3.
[4] T.D. Boyer, M.P. Manns, A.J. Sanyal, D. Zakim, eds., Zakim and Boyer's hepatology: a textbook of liver disease, 6th ed, Saunders/Elsevier, Philadelphia, PA, 2012.
[6] K. Si-Tayeb, F.K. Noto, M. Nagaoka, J. Li, M.A. Battle, C. Duris, P.E. et al., Highly efficient generation of human hepatocyte-like cells from induced pluripotent stem cells, Hepatology. 51 (2010) 297–305. doi:10.1002/hep.23354.
[7] Z. Song, J. Cai, Y. Liu, D. Zhao, J. Yong, S. Duo, et al., Efficient generation of hepatocyte-like cells from human induced pluripotent stem cells, Cell Res. 19 (2009) 1233–1242. doi:10.1038/cr.2009.107.
[7] T. Touboul, N.R.F. Hannan, S. Corbineau, A. Martinez, C. Martinet, S. Branchereau, S. Mainot, H. Strick-Marchand, R. Pedersen, J. Di Santo, A. Weber, L. Vallier, Generation of functional hepatocytes from human embryonic stem cells under chemically defined conditions that recapitulate liver development, Hepatology. 51 (2010) 1754–1765. doi:10.1002/hep.23506.
[8] J. Shan, R.E. Schwartz, N.T. Ross, D.J. Logan, D. Thomas, S.A. Duncan, T.E. North, W. Goessling, A.E. Carpenter, S.N. Bhatia, Identification of small molecules for human hepatocyte expansion and iPS differentiation, Nat. Chem. Biol. 9 (2013) 514–520. doi:10.1038/nchembio.1270.
[9] T. Takebe, K. Sekine, M. Enomura, H. Koike, M. Kimura, T. Ogaeri, R.-R. Zhang, Y. Ueno, Y.-W. Zheng, N. Koike, S. Aoyama, Y. Adachi, H. Taniguchi, Vascularized and functional human liver from an iPSC-derived organ bud transplant, Nature. 499 (2013) 481–484. doi:10.1038/nature12271.
[10] T. Takebe, R.-R. Zhang, H. Koike, M. Kimura, E. Yoshizawa, M. Enomura, N. Koike, K. Sekine, H. Taniguchi, Generation of a vascularized and functional human liver from an iPSC-derived organ bud transplant, Nat. Protoc. 9 (2014) 396–409. doi:10.1038/nprot.2014.020.
[11] R.L. Gieseck III, N.R.F. Hannan, R. Bort, N.A. Hanley, R.A.L. Drake, G.W.W. Cameron, T.A. Wynn, L. Vallier, Maturation of Induced Pluripotent Stem Cell Derived Hepatocytes by 3D-Culture, PLoS ONE. 9 (2014) e86372. doi:10.1371/journal.pone.0086372.
[12] D.R. Berger, B.R. Ware, M.D. Davidson, S.R. Allsup, S.R. Khetani, Enhancing the functional maturity of induced pluripotent stem cell-derived human hepatocytes by controlled presentation of cell-cell interactions in vitro, Hepatol. Baltim. Md. 61 (2015) 1370–1381. doi:10.1002/hep.27621.
[13] K. Takayama, K. Kawabata, Y. Nagamoto, K. Kishimoto, K. Tashiro, F. Sakurai, M. Tachibana, K. Kanda, T. Hayakawa, M.K. Furue, H. Mizuguchi, 3D spheroid culture of

hESC/hiPSC-derived hepatocyte-like cells for drug toxicity testing, Biomaterials. 34 (2013) 1781–1789. doi:10.1016/j.biomaterials.2012.11.029.
[14] S. Sengupta, B.P. Johnson, S.A. Swanson, R. Stewart, C.A. Bradfield, J.A. Thomson, Aggregate Culture of Human Embryonic Stem Cell-Derived Hepatocytes in Suspension Are an Improved In Vitro Model for Drug Metabolism and Toxicity Testing, Toxicol. Sci. 140 (2014) 236–245. doi:10.1093/toxsci/kfu069.
[15] W. Song, Y.-C. Lu, A.S. Frankel, D. An, R.E. Schwartz, M. Ma, Engraftment of human induced pluripotent stem cell-derived hepatocytes in immunocompetent mice via 3D co-aggregation and encapsulation, Sci. Rep. 5 (2015). doi:10.1038/srep16884.
[16] P. Godoy, N.J. Hewitt, U. Albrecht, M.E. Andersen, N. Ansari, S. Bhattacharya, J.G. Bode, J. Bolleyn, C. Borner, J. Böttger, A. Braeuning, R.A. Budinsky, B. Burkhardt, N.R. Cameron, G. Camussi, C.-S. Cho, Y.-J. Choi, J. Craig Rowlands, U. Dahmen, G. Damm, O. Dirsch, M.T. Donato, J. Dong, S. Dooley, D. Drasdo, R. Eakins, K.S. Ferreira, V. Fonsato, J. Fraczek, R. Gebhardt, A. Gibson, M. Glanemann, C.E.P. Goldring, M.J. Gómez-Lechón, G.M.M. Groothuis, L. Gustavsson, C. Guyot, D. Hallifax, S. Hammad, A. Hayward, D. Häussinger, C. Hellerbrand, P. Hewitt, S. Hoehme, H.-G. Holzhütter, J.B. Houston, J. Hrach, K. Ito, H. Jaeschke, V. Keitel, J.M. Kelm, B. Kevin Park, C. Kordes, G.A. Kullak-Ublick, E.L. LeCluyse, P. Lu, J. Luebke-Wheeler, A. Lutz, D.J. Maltman, M. Matz-Soja, P. McMullen, I. Merfort, S. Messner, C. Meyer, J. Mwinyi, D.J. Naisbitt, A.K. Nussler, P. Olinga, F. Pampaloni, J. Pi, L. Pluta, S.A. Przyborski, A. Ramachandran, V. Rogiers, C. Rowe, C. Schelcher, K. Schmich, M. Schwarz, B. Singh, E.H.K. Stelzer, B. Stieger, R. Stöber, Y. Sugiyama, C. Tetta, W.E. Thasler, T. Vanhaecke, M. Vinken, T.S. Weiss, A. Widera, C.G. Woods, J.J. Xu, K.M. Yarborough, J.G. Hengstler, Recent advances in 2D and 3D in vitro systems using primary hepatocytes, alternative hepatocyte sources and non-parenchymal liver cells and their use in investigating mechanisms of hepatotoxicity, cell signaling and ADME, Arch. Toxicol. 87 (2013) 1315–1530. doi:10.1007/s00204-013-1078-5.
[17] T. Takebe, K. Sekine, M. Kimura, E. Yoshizawa, S. Ayano, M. Koido, S. Funayama, N. Nakanishi, T. Hisai, T. Kobayashi, T. Kasai, R. Kitada, A. Mori, H. Ayabe, Y. Ejiri, N. Amimoto, Y. Yamazaki, S. Ogawa, M. Ishikawa, Y. Kiyota, Y. Sato, K. Nozawa, S. Okamoto, Y. Ueno, H. Taniguchi, Massive and Reproducible Production of Liver Buds Entirely from Human Pluripotent Stem Cells, Cell Rep. 21 (2017) 2661–2670. doi:10.1016/j.celrep.2017.11.005.
[18] M.J. Zamek-Gliszczynski, Pharmacokinetics of 5 (and 6)-Carboxy-2',7'-Dichlorofluorescein and Its Diacetate Promoiety in the Liver, J. Pharmacol. Exp. Ther. 304 (2003) 801–809. doi:10.1124/jpet.102.044107.
[19] C. Lu, A.P. Li, Species comparison in P450 induction: effects of dexamethasone, omeprazole, and rifampin on P450 isoforms 1A and 3A in primary cultured hepatocytes from man, Sprague-Dawley rat, minipig, and beagle dog, Chem. Biol. Interact. 134 (2001) 271–281.
[20] H. Shih, G.V. Pickwell, D.K. Guenette, B. Bilir, L.C. Quattrochi, Species differences in hepatocyte induction of CYP1A1 and CYP1A2 by omeprazole, Hum. Exp. Toxicol. 18 (1999) 95–105. doi:10.1177/096032719901800206.
[21] D.R. Nelson, Cytochrome P450 and the individuality of species, Arch. Biochem. Biophys. 369 (1999) 1–10. doi:10.1006/abbi.1999.1352.
[22] H. Olson, G. Betton, D. Robinson, K. Thomas, A. Monro, G. Kolaja, P. Lilly, J. Sanders, G. Sipes, W. Bracken, M. Dorato, K. Van Deun, P. Smith, B. Berger, A. Heller, Concordance of

the Toxicity of Pharmaceuticals in Humans and in Animals, Regul. Toxicol. Pharmacol. 32 (2000) 56–67. doi:10.1006/rtph.2000.1399.
[23] L.M. Norona, D.G. Nguyen, D.A. Gerber, S.C. Presnell, E.L. LeCluyse, Editor's Highlight: Modeling Compound-Induced Fibrogenesis *In Vitro* Using Three-Dimensional Bioprinted Human Liver Tissues, Toxicol. Sci. 154 (2016) 354–367. doi:10.1093/toxsci/kfw169.
[24] S.D. Ramachandran, K. Schirmer, B. Münst, S. Heinz, S. Ghafoory, S. Wölfl, K. Simon-Keller, A. Marx, C.I. Øie, M.P. Ebert, H. Walles, J. Braspenning, K. Breitkopf-Heinlein, In Vitro Generation of Functional Liver Organoid-Like Structures Using Adult Human Cells, PLOS ONE. 10 (2015) e0139345. doi:10.1371/journal.pone.0139345.
[25] T. Matsumura, M. Takesue, K.A. Westerman, T. Okitsu, M. Sakaguchi, T. Fukazawa, T. Totsugawa, H. Noguchi, S. Yamamoto, D.B. Stolz, N. Tanaka, P. Leboulch, N. Kobayashi, Establishment of an immortalized human-liver endothelial cell line with SV40T and hTERT, Transplantation. 77 (2004) 1357–1365.
[26] S. Hering, B.E. Griffin, M. Strauss, Immortalization of human fetal sinusoidal liver cells by polyoma virus large T antigen, Exp. Cell Res. 195 (1991) 1–7. doi:10.1016/0014-4827(91)90492-D.
[27] B.R. Ware, M.J. Durham, C.P. Monckton, S.R. Khetani, A Cell Culture Platform to Maintain Long-term Phenotype of Primary Human Hepatocytes and Endothelial Cells, Cell. Mol. Gastroenterol. Hepatol. 5 (2018) 187–207. doi:10.1016/j.jcmgh.2017.11.007.
[28] Y.B. (Abraham) Kang, S. Rawat, J. Cirillo, M. Bouchard, H. (Moses) Noh, Layered long-term co-culture of hepatocytes and endothelial cells on a transwell membrane: toward engineering the liver sinusoid, Biofabrication. 5 (2013) 045008. doi:10.1088/1758-5082/5/4/045008.
[29] Y.B.A. Kang, T.R. Sodunke, J. Lamontagne, J. Cirillo, C. Rajiv, M.J. Bouchard, M. Noh, Liver sinusoid on a chip: Long-term layered co-culture of primary rat hepatocytes and endothelial cells in microfluidic platforms: Liver Sinusoid on a Chip, Biotechnol. Bioeng. 112 (2015) 2571–2582. doi:10.1002/bit.25659.
[30] Z. Kmieć, Cooperation of liver cells in health and disease, Adv. Anat. Embryol. Cell Biol. 161 (2001) III–XIII, 1–151.
[31] L.D. Deleve, Dacarbazine toxicity in murine liver cells: a model of hepatic endothelial injury and glutathione defense, J. Pharmacol. Exp. Ther. 268 (1994) 1261–1270.
[32] L.D. DeLeve, X. Wang, J.F. Kuhlenkamp, N. Kaplowitz, Toxicity of azathioprine and monocrotaline in murine sinusoidal endothelial cells and hepatocytes: The role of glutathione and relevance to hepatic venoocclusive disease, Hepatology. 23 (1996) 589–599. doi:10.1002/hep.510230326.
[33] S. Priester, Involvement of cholangiocyte proliferation in biliary fibrosis, World J. Gastrointest. Pathophysiol. 1 (2010) 30. doi:10.4291/wjgp.v1.i2.30.
[34] C. Yin, K.J. Evason, K. Asahina, D.Y.R. Stainier, Hepatic stellate cells in liver development, regeneration, and cancer, J. Clin. Invest. 123 (2013) 1902–1910. doi:10.1172/JCI66369.
[35] G. Xie, A.M. Diehl, Evidence for and against epithelial-to-mesenchymal transition in the liver, AJP Gastrointest. Liver Physiol. 305 (2013) G881–G890. doi:10.1152/ajpgi.00289.2013.
[36] M. Scarpa, A.R. Grillo, P. Brun, V. Macchi, A. Stefani, S. Signori, A. Buda, P. Fabris, M.T. Giordani, R. De Caro, G. Palu, I. Castagliuolo, D. Martines, Snail1 transcription factor is a critical mediator of hepatic stellate cell activation following hepatic injury, AJP Gastrointest. Liver Physiol. 300 (2011) G316–G326. doi:10.1152/ajpgi.00141.2010.

[37] J. Pritchett, V.S. Athwal, E. Harvey, K. Martin, J. Llewellyn, P. Ireland, A. Nicolaides, M.J. Humphries, N. Bobola, N.A. Hanley, K. Piper Hanley, Epimorphin Alters the Inhibitory Effects of SOX9 on Mmp13 in Activated Hepatic Stellate Cells, PLoS ONE. 9 (2014) e100091. doi:10.1371/journal.pone.0100091.
[38] Yamagiwa Y, Patel T., Cytokine Regulation of Cholangiocyte Growth., in: Madame Curie Biosci. Database Internet Austin TX Landes Biosci. 2000-2013 Available, n.d. https://www.ncbi.nlm.nih.gov/books/NBK6579/.
[39] Y. Xiao, Y. Zhou, Y. Chen, K. Zhou, J. Wen, Y. Wang, J. Wang, W. Cai, The expression of epithelial–mesenchymal transition–related proteins in biliary epithelial cells is associated with liver fibrosis in biliary atresia, Pediatr. Res. 77 (2015) 310–315. doi:10.1038/pr.2014.181.
[40] K. Taura, K. Iwaisako, E. Hatano, S. Uemoto, Controversies over the Epithelial-to-Mesenchymal Transition in Liver Fibrosis, J. Clin. Med. 5 (2016) 9. doi:10.3390/jcm5010009.
[41] S. Lamouille, J. Xu, R. Derynck, Molecular mechanisms of epithelial–mesenchymal transition, Nat. Rev. Mol. Cell Biol. 15 (2014) 178–196. doi:10.1038/nrm3758.
[42] M. Pinzani, Epithelial–mesenchymal transition in chronic liver disease: Fibrogenesis or escape from death?, J. Hepatol. 55 (2011) 459–465. doi:10.1016/j.jhep.2011.02.001.

4.11 Figures

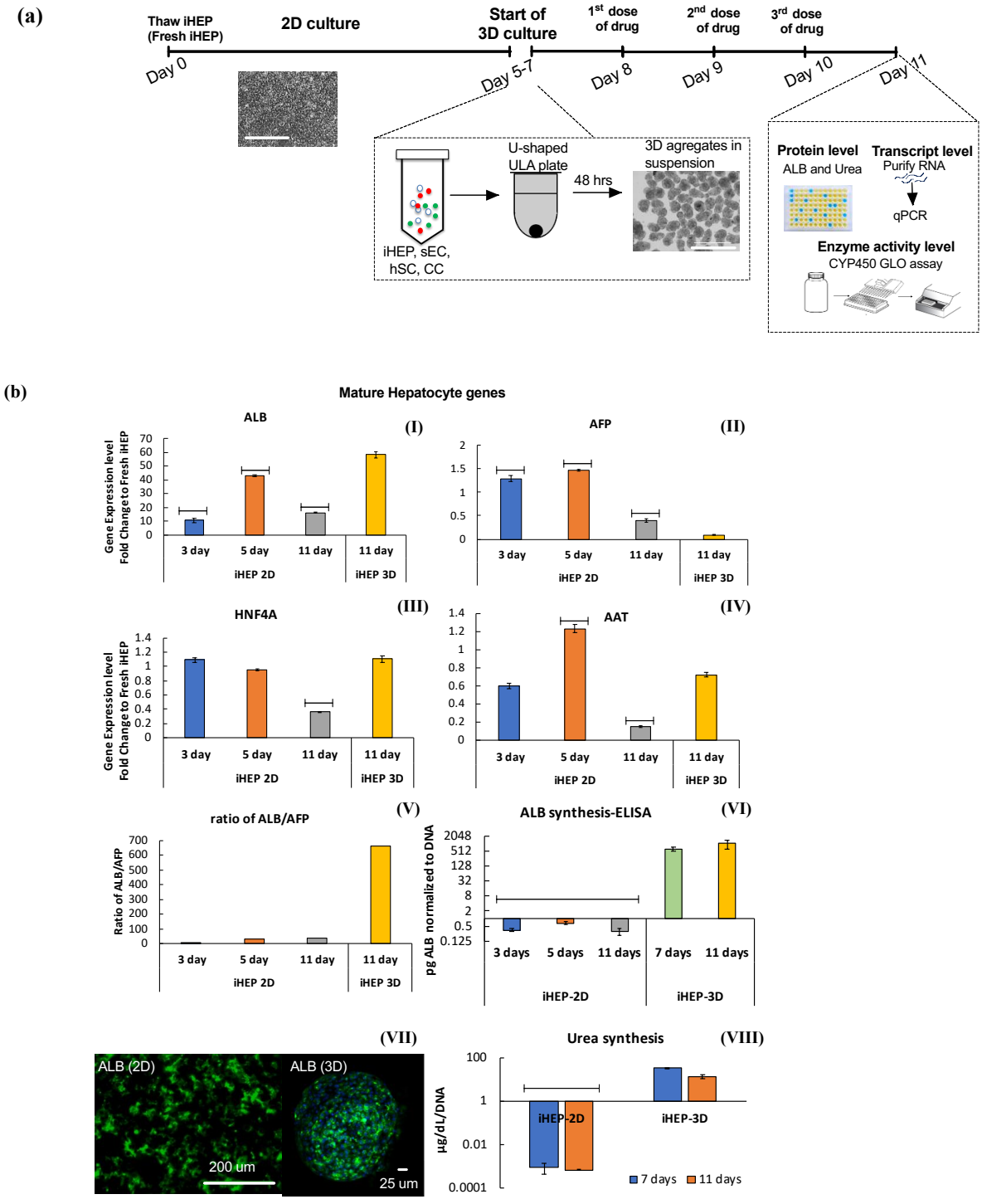

Figure 4.1 Functionality of iPS-derived hepatocyte is enhanced in a 3D aggregate format. (a) Schematic depicting the experimental procedure for iHEP culture and 3D aggregate formation. **(b(I-V))**

Comparison of mature hepatic markers in 2D versus 3D at transcript level. Relative mRNA expression of noted genes was quantitated by qPCR. Fold change is relative to values obtained for fresh iHEP. **(b(VI and VIII))** Comparison of albumin and urea secretion in 2D versus 3D. **(b(VII))** Immunofluorescence staining of iHEP cells after 11 days with epithelial cell marker albumin in 3D and 2D culture, counterstained with Hoechst dye for nuclei; * = $p < 0.05$, ** = $p < 0.01$ compared to iHEP (3D) at 7 days and 11 days.

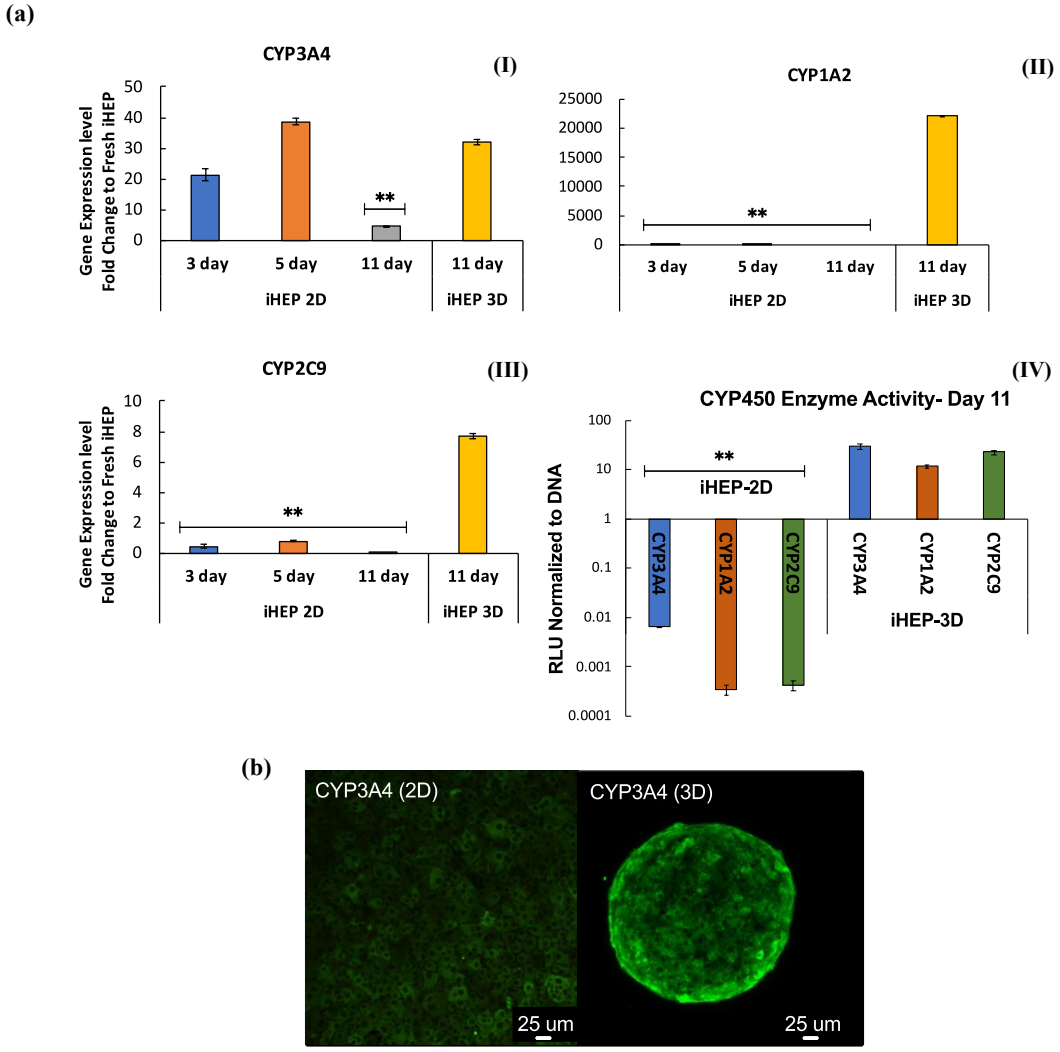

Figure 4.2 Metabolic competence is enhanced in 3D-cultured iHEP aggregates (a(I-III)) Comparison of CYP450 enzymes in 2D versus 3D at transcript level; * = $p < 0.05$, ** = $p < 0.01$ compared to iHEP (3D) at 11 days **(a(IV))** Comparison of basal level of CYP450 activities in 3D versus 2D after 11 days; * = $p < 0.05$, ** = $p < 0.01$ compared to CYP450 enzyme activity of iHEP (3D)

(b) Immunofluorescence staining of iHEP cells after 11 days with CYP3A4 antibody in 3D and 2D culture.

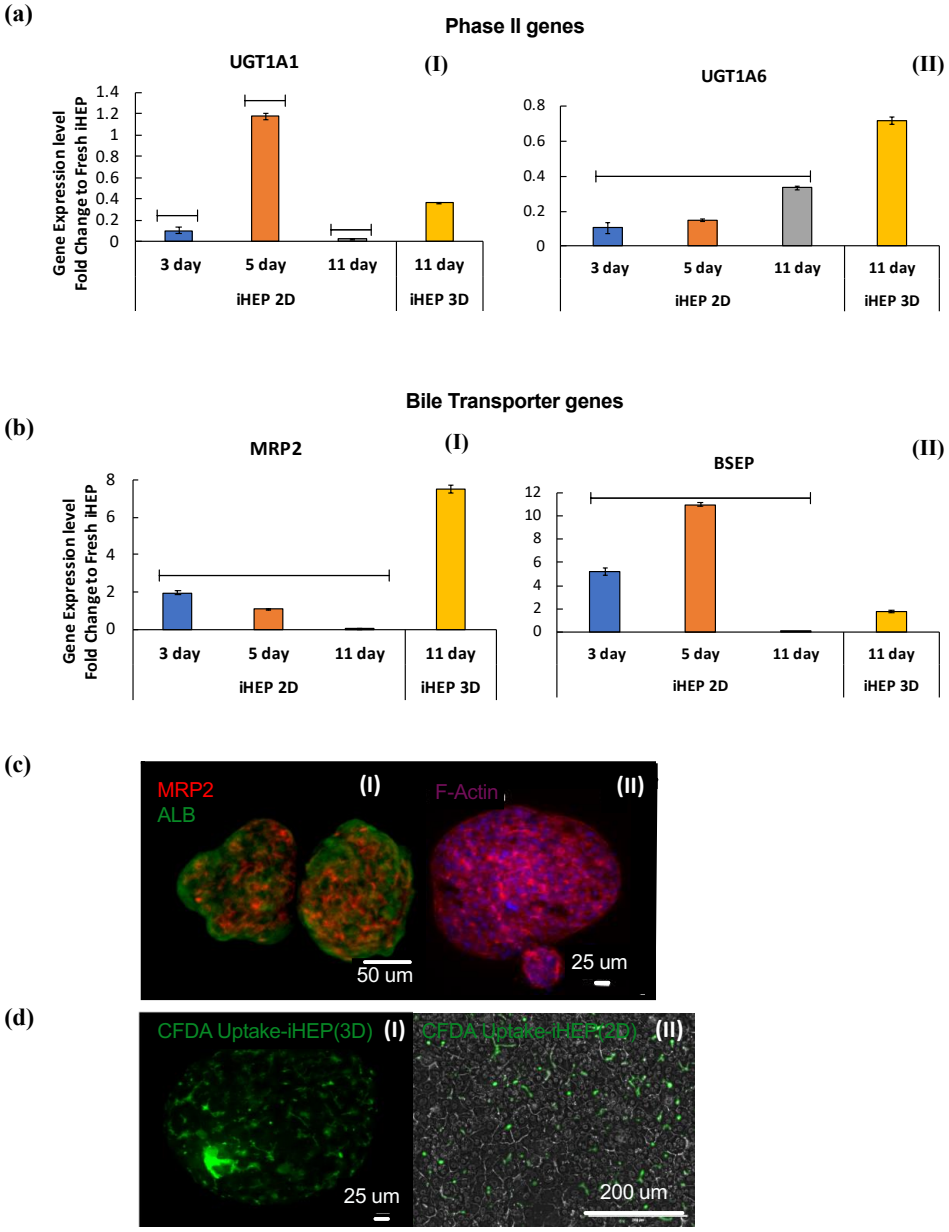

Figure 4.3 Functional bile canaliculi are formed in 3D iHEP aggregates (a & b) Comparison of Phase II metabolic genes and bile transporter genes in 2D versus 3D at transcript level. **(c)** Immunofluorescence staining of iHEP cells after 11 days with MRP2 (red), albumin (green) and phalloidin for F-actin and Hoechst for nuclei **(d)** Functional bile canaliculi (green stain, assessed by CFDA excretion) in 3D iHEP culture as described in the methods; * = $p < 0.05$, ** = $p < 0.01$ compared to iHEP (3D) at 11 days.

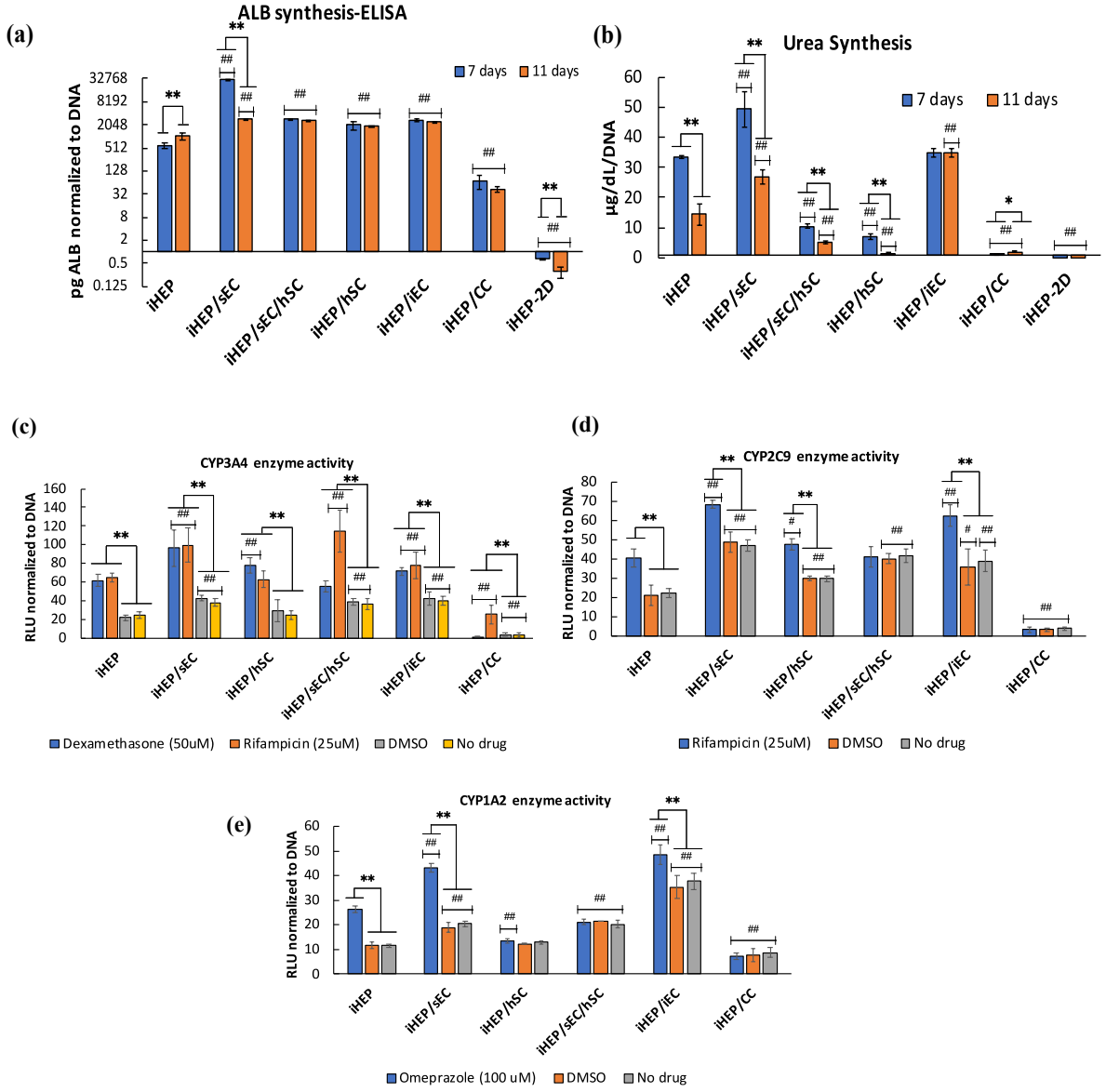

Figure 4.4 Endothelial cells improved the maturity of 3D iHEP aggregates (a) Albumin secretion in iHEP co-cultures **(b)** Urea secretion in iHEP co-cultures; * = $p < 0.05$, ** = $p < 0.01$ compared to 11 days; $^{\#}$ = $p < 0.05$, $^{\#\#}$ = $p < 0.01$ compared to the corresponding day of iHEP (3D) **(c)** Evaluation of CYP3A4 basal activity and induction by dexamethasone and rifampicin in iHEP co-cultures after 11 days **(d)** Evaluation of CYP2C9 basal activity and induction by rifampicin in iHEP co-cultures after 11 days **(e)** Evaluation of CYP1A2 basal activity and induction by omeprazole in iHEP co-cultures after 11 days; * = $p < 0.05$, ** = $p < 0.01$ compared to DMSO and No drug condition within each group; $^{\#}$ = $p < 0.05$, $^{\#\#}$ = $p < 0.01$ compared to the corresponding condition of iHEP (3D).

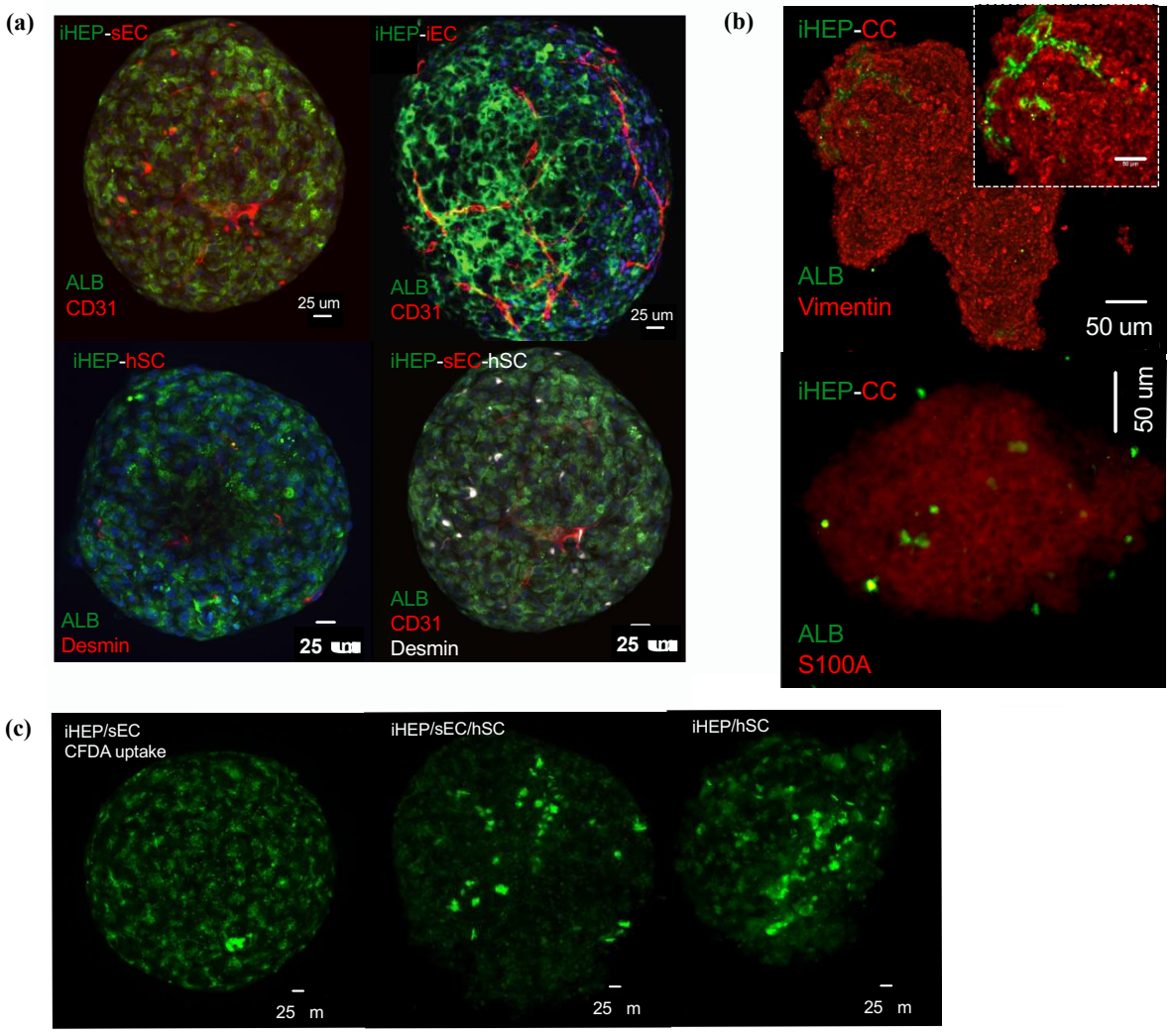

Figure 4.5 Morphology of 3D iHEP aggregates co-cultured with ECs, hSCs and CCs (a) Immunostaining of iHEP aggregates co-cultured with ECs and hSCs with anti-CD31 (ECs), anti-albumin (iHEP) and anti-desmin (hSC) and Hoechst (nuclei) after 11 days **(b)** Immunostaining of iHEP/CC aggregates with anti-vimentin and anti S1004A (activated CC) and anti-albumin (iHEP) after 11 days **(c)** Assessment of bile canaliculi formation (green stain, assessed by CFDA excretion) in 3D iHEP co-cultures.

4.12 Supplementary Figures and Table

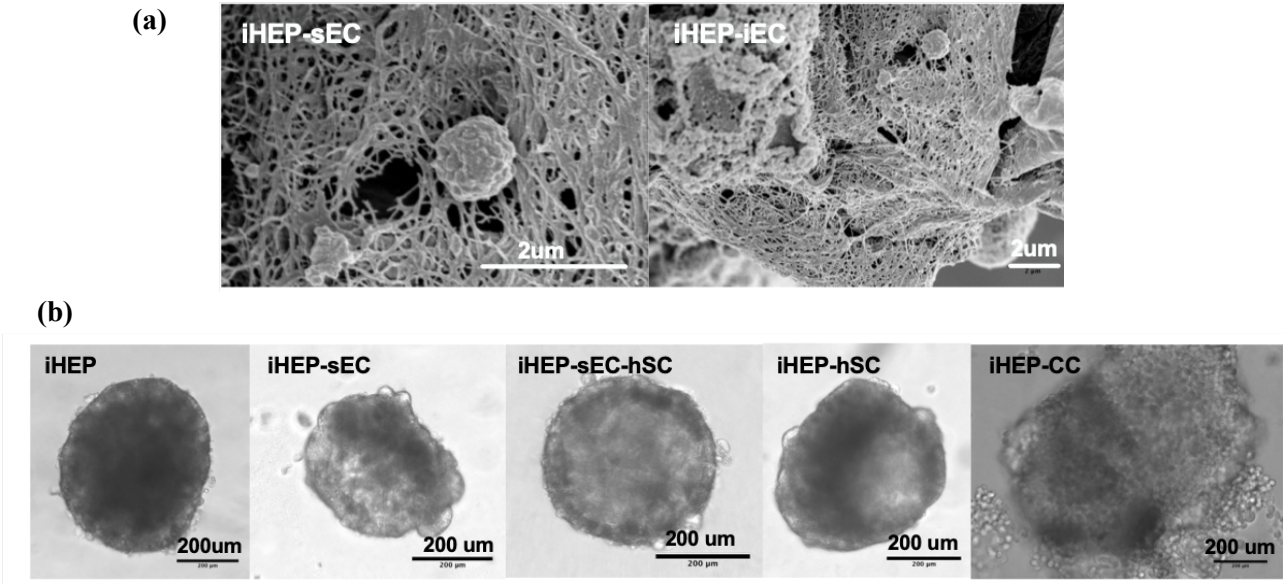

Figure S4.1 Phenotypic characterization of 3D iHEPs cultured with nonparenchymal cells (a) Scanning electron micrograph of iHEP aggregates co-cultured with ECs at higher magnification after 11 days illustrating extracellular matrix deposition. Scale bar is 2 μm. **(b)** Phase contrast image of iHEP aggregates cocultured with ECs, hSCs and CC.

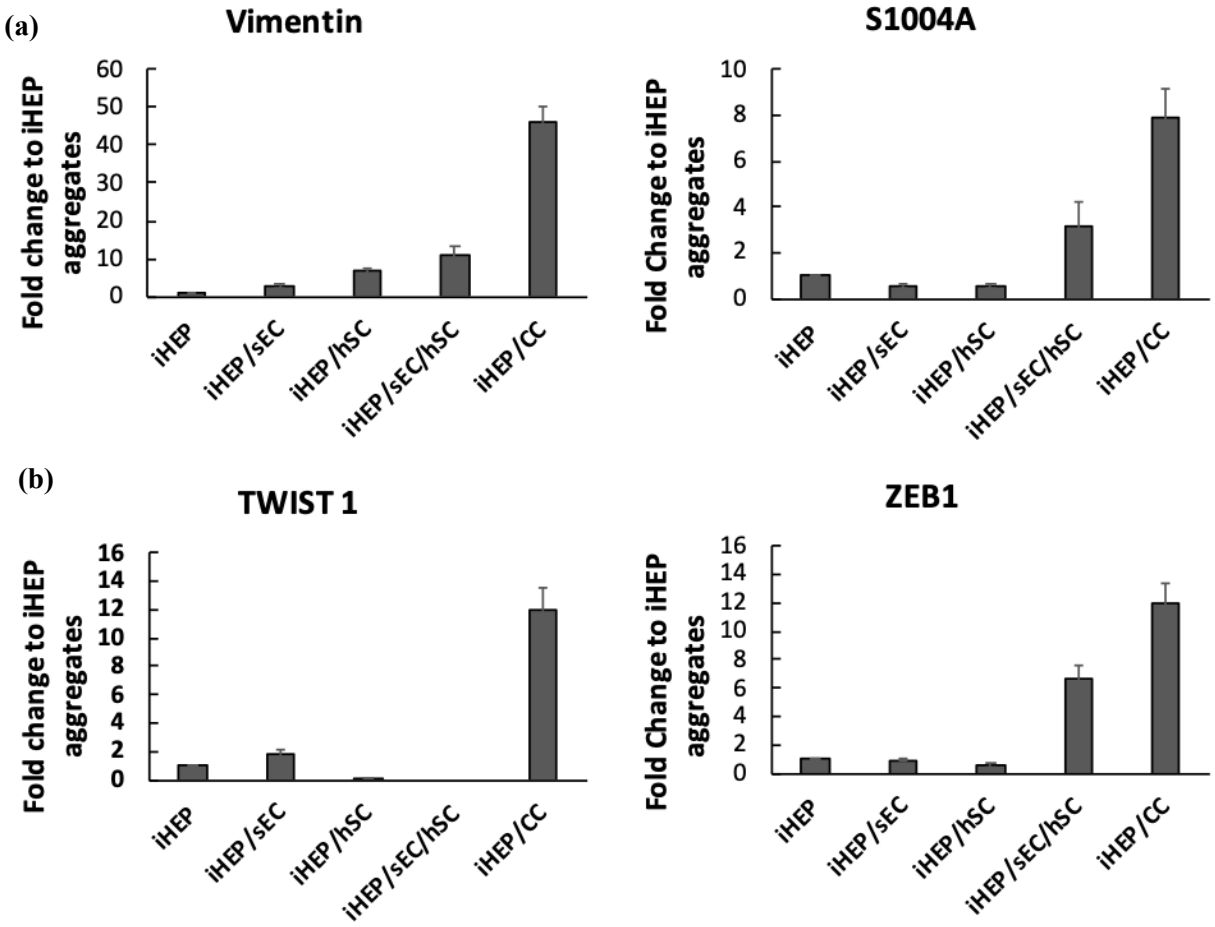

Figure S4.2 The irregular proliferation of iHEP aggregates with CC might be due to activated CC **(a)** Expression levels of the genes associated with activated CCs in the co-cultured aggregates after 11 days **(b)** Transcription factors associated with activated CC and EMT after 11 days. Relative mRNA expression of noted genes was quantitated by qPCR. GAPDH is used as the housekeeping gene.

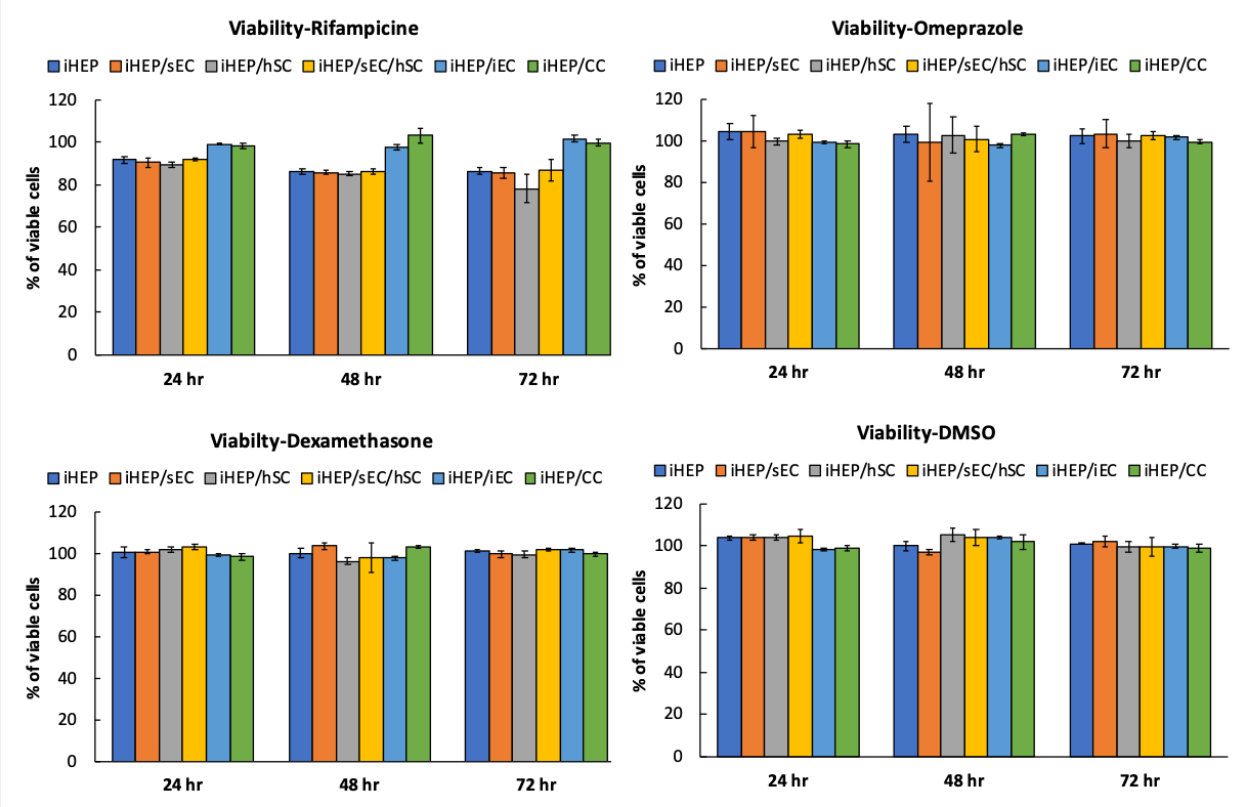

Figure S4.3 Assessment of cytotoxicity of drugs on iHEP cocultures over three days

(a) iHEP/sEC (8 days)

(b) iHEP/sEC (11 days)

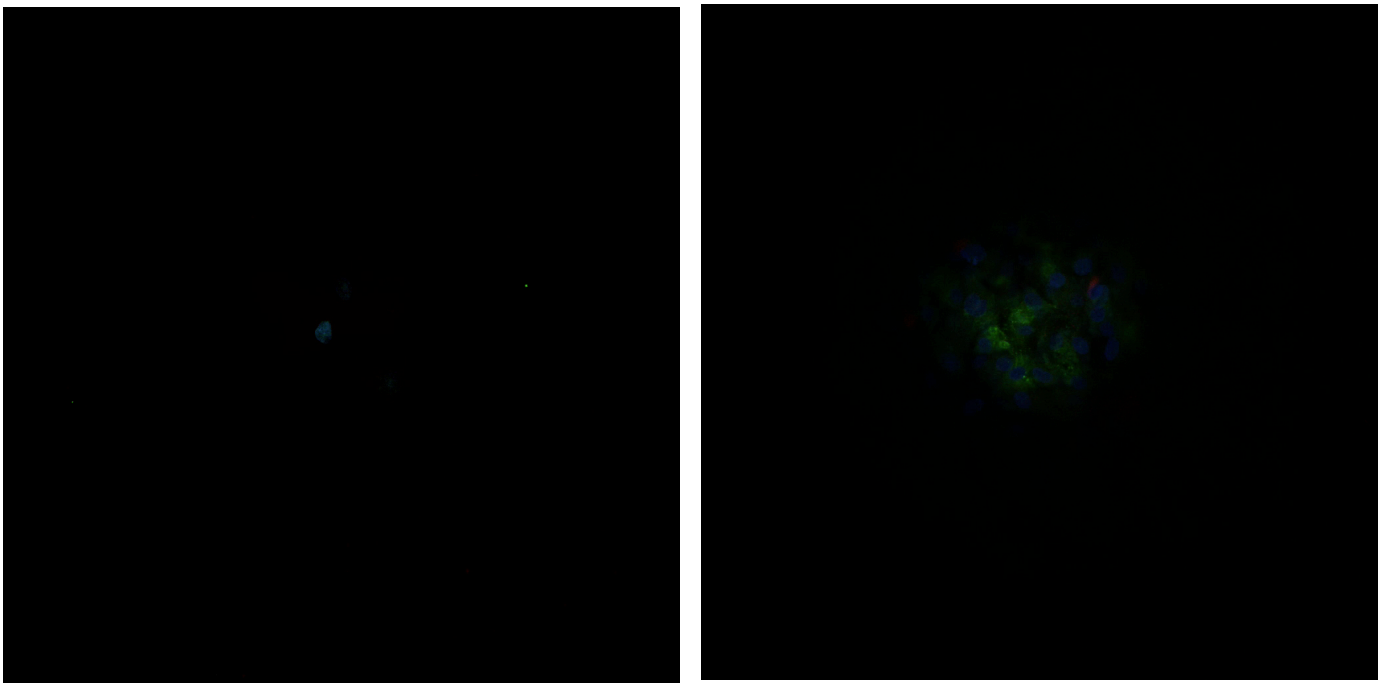

Movie S4.1 Formation of capillary-like structures by sECs (a) Movie of z-stack series from iHEP/sEC aggregates after 8 days illustrating PECAM (red) and ALB (green). **(b)** Movie of z-stack series from iHEP/sEC aggregates after 11 days illustrating PECAM (red) and ALB (green).

Supplementary movie S4.1 can be found online at https://doi.org/10.1016/j.actbio.2019.070.047.

Table S4.1 List of TaqMan primers from ThermoFisher Scientific

Gene Name	Taqman Assay ID- Thermofisher Scientific
AAT(SERPINA1)	Hs00165475_m1
ACTB	Hs01060665_g1
ALB	Hs00910225_m1
AFP	Hs00173490_m1
BSEP(ABCB11)	Hs02513517-s1
CYP3A4	Hs00604506_m1
CYP1A1	Hs01054794_m1
CYP1A2	Hs00167927_m1
CYP2C9	Hs00426397_m1
FOXA2	Hs00232764_m1
GADPH	Hs02758991_g1
HNF4α	Hs00230853_m1
MRP2 (ABCC2)	Hs02510929_s1
PECAM	Hs01065279_m1
TTR	Hs00174914_m1
UGT1A6	Hs01592477_m1
UGT1A1	Hs02511055_s1

Chapter 5: Synthetic Hydrogel that Is Permissive for Vascular Morphogenesis

Elements of this chapter have been published as:

Hamisha Ardalani*, Matthew R. Zanotelli*, Jue Zhang, Zhonggang Hou, Eric H. Nguyen, Scott Swanson, Bao Kim Nguyen, Jennifer Bolin, Angela Elwell, Lauren L. Bischel, Angela W. Xie, Ron Stewart, David J. Beebe, James A. Thomson, Michael P. Schwartz, William L. Murphy (2016). " Stable engineered vascular networks from human induced pluripotent stem cell-derived endothelial cells cultured in synthetic hydrogels" In Acta Biomaterialia

*Equal Contribution.

5.1 Preface

In Chapter 3, we describe an overview of the current state of the art in the design and development of synthetic biomaterial for modeling angiogenesis and vasculogenesis in vitro. While so much has been done, most of the previous studies relied on the help of mural cells (pericyte) to be able to create a vascular model that is stable for long term culture. Here, we combined the advantages that microfluidic platforms offered with synthetic biomaterials and showed that we could create a stable capillary network from iPS-derived endothelial cells that is stable for over 14 days. We did not use any mural cells in this study and showed that providing additional mechanical support to iPS-derived ECs encapsulated in synthetic PEG hydrogels outside of the microfluidic platforms, can stabilize the capillary networks for over 14 days. This work demonstrates the value of synthetic biomaterials, microfluidics, and novel technologies like RNA-seq to deconstruct the complex role of ECM on stem cell fate. The work described here is an essential building block towards developing vascularized in vitro liver models, discussed further in chapter 7.

5.2 Abstract

Here, we describe an *in vitro* strategy to model vascular morphogenesis where human induced pluripotent stem cell-derived endothelial cells (iPSC-ECs) are encapsulated in peptide-functionalized poly (ethylene glycol) (PEG) hydrogels, either on standard well plates or within a passive pumping polydimethylsiloxane (PDMS) tri-channel microfluidic device. PEG hydrogels permissive towards cellular remodeling were fabricated using thiol-ene photopolymerization to incorporate matrix metalloproteinase (MMP)-degradable crosslinks and CRGDS cell adhesion peptide. Time lapse microscopy, immunofluorescence imaging, and RNA sequencing (RNA-Seq) demonstrated that iPSC-ECs formed vascular networks through mechanisms that were consistent with *in vivo* vasculogenesis and angiogenesis when cultured in PEG hydrogels. Migrating iPSC-ECs condensed into clusters, elongated into tubules, and formed polygonal networks through sprouting. Genes upregulated for iPSC-ECs cultured in PEG hydrogels relative to control cells on tissue culture polystyrene (TCP) surfaces included adhesion, matrix remodeling, and Notch signaling pathway genes relevant to *in vivo* vascular development. Vascular networks with lumens were stable for at least 14 days when iPSC-ECs were encapsulated in PEG hydrogels that were polymerized within the central channel of the microfluidic device. Therefore, iPSC-ECs cultured in peptide-functionalized PEG hydrogels offer a defined platform for investigating vascular morphogenesis *in vitro* using both standard and microfluidic formats.

5.3 Introduction

The lack of a functional vasculature and pathological disruption of circulation are unresolved challenges that have limited the success for many tissue engineering and wound healing approaches [1-3]. Furthermore, the incorporation of a vascular component is expected to improve human cellular models by recapitulating cell-cell interactions during tissue formation [4, 5] and by supporting the function of model organ systems [6, 7]. Finally, while target organs such as the heart, liver or central nervous system have been the focus for many *in vitro* toxicity screening strategies [8], vascular models have also been identified as a promising tool for predictive toxicology [9, 10]. Therefore, several emerging applications would benefit from *in vitro* assays that enable systematic investigation of factors that promote blood vessel formation and stabilization [1-3].

Endothelial cells cultured *in vitro* will spontaneously "self-assemble" into organized networks [11-17], and several studies have demonstrated that capillary tubules can be perfused when subjected to flow [18-23]. While extracellular matrix (ECM) components such as collagen or Matrigel are often used as culture substrates when modeling vascular morphogenesis *in vitro* [12-14, 16, 17], these materials can be limiting for screening approaches due to batch variability, properties that are sensitive to reaction conditions, and poorly-defined compositions [24-26]. To address these limitations, synthetic strategies have increasingly been applied to investigate factors that instruct endothelial phenotypes [27-35]. Hydrogels formed via thiol-ene photopolymerization represent an emerging class of cell culture materials [36, 37] that are formed through a radical-initiated step-growth mechanism that couples thiols and alkenes with high specificity [38]. A growing body of literature has demonstrated the versatility of thiol-ene photochemistry for incorporating biomolecules such as peptides, growth factors, gelatin, and hyaluronic acid into synthetic hydrogels [4, 35-37, 39-47]. Hydrogels formed via thiol-ene photopolymerization enable

spatial patterning of biochemical and mechanical properties [35, 39-41], sequestering and controlled release of growth factors [45], rapid photopolymerization for 3D bioprinting of encapsulated cells [44], and protein-free backgrounds for identifying ECM components deposited in the matrix during cellular remodeling [47]. Thus, thiol-ene chemistry offers a potentially powerful tool for modeling vascular morphogenesis by providing control over a wide range of matrix properties relevant to blood vessel formation [4, 35].

While engineering platforms provide control over the 3D microenvironment when modeling vascular morphogenesis [1-3], the heterogeneity and donor-to-donor variability of primary human endothelial cells may be limiting for applications that require standardization or scale-up [1, 48]. Human umbilical vein endothelial cells (HUVECs) can be used for standardized screening of angiogenesis inhibitors *in vitro*, but require processing and pre-validation to identify donor sources with similar function [10]. Human pluripotent stem cells [49-51] offer promise for predictive toxicology [8], and have been used to derive endothelial cells that form vascular networks *in vitro* and functional blood vessels *in vivo* [23, 30, 52, 53]. Importantly, human induced pluripotent stem cell-derived endothelial cells (iPSC-ECs) can be produced with high batch uniformity [23], which may be beneficial for vascular disease models or screening approaches that require standardization or scale-up [9, 54].

The strategy reported here combines a uniform endothelial cell source [23], a tunable synthetic ECM [36], and a tri-channel microfluidic device [55] to model vascular morphogenesis *in vitro*. Thiol-ene photopolymerization was used to fabricate peptide functionalized PEG hydrogels permissive towards cellular remodeling [36] and the iPSC-ECs were previously characterized by high lot-to-lot purity to at least 6 passages [23]. The passive flow concept that is the essence of the microfluidic device described here uses standard culture techniques for loading

cells and exchanging media [55], and therefore provides an accessible format that takes advantage of microscale features such as decreased requirements for reagents and cells [56]. Our combined results provide evidence that iPSC-ECs self-assemble into vascular networks through physiologically-relevant mechanisms when cultured in PEG hydrogels, and capillary tubules with lumens were stable for at least two weeks when the hydrogels were polymerized within the microfluidic device.

5.4 Materials and Methods

5.4.1 Cell culture.

Human induced pluripotent stem cell-derived endothelial cells ("iPSC-ECs", Cellular Dynamics, iCell® Endothelial Cells) were cultured according to the manufacturer's protocol. Briefly, iPSC-ECs were expanded to passage 3 and cryopreserved for additional use. Passage 3 iPSC-ECs were thawed and plated at 10,000-15,000 iPSC-ECs/cm^2 onto tissue culture plates treated with 3 μg/cm^2 fibronectin (Invitrogen) and passaged every 3 to 4 days with TrypLE (Invitrogen). The manufacturer's recommenced growth medium was used for culturing iPSC-ECs, which consists of VascuLife VEGF Medium (Lifeline Cell Technologies) that was modified as follows: 10 mL glutamine supplement was added to 500 mL medium (rather than the 25 mL provided) and the FBS supplement was replaced with iCell® Endothelial Cells Medium Supplement (Cellular Dynamics). Cells were incubated at 37°C and 5% CO_2 for all experiments. ***Microfluidic channels.*** Microfluidic experiments were conducted using iPSC-ECs cultured in the growth medium described above ("Control"), or in growth medium supplemented within 100-1000 ng/mL VEGF-165 (Catalog # 293-VE, Lot 114714051, 97% purity from R&D), as described in

Results and Discussion. The iPSC-ECs were encapsulated in PEG hydrogels that were polymerized within the central channel of the tri-channel device (see details below). All fluid was removed from both outer channels daily and replaced with a total of 10 μL of fresh medium.

5.4.2 Microfluidic Device Fabrication.

The tri-channel microfluidic device was fabricated as previously described without modification [55]. Briefly, polydimethylsiloxane (PDMS, Sylgard 184 Silicone Elastomer Kit, Dow Corning) elastomer base and curing agent were mixed at a 10:1 ratio and degassed under vacuum for 45 min (room temperature). The degassed PDMS was poured over SU-8 master molds, which were generated using standard soft lithography methods [57]. The PDMS was cured for 4 hr (80°C), allowed to cool to room temperature, and removed from the master mold. The PDMS device was autoclaved for 20 min at 120° C. Six hours before loading the cell/monomer solution, devices were oxygen-plasma-treated to bond the PDMS channels to the inside of a glass-bottom Petri dish (MatTek).

5.4.3 Poly (ethylene glycol) (PEG) hydrogel preparation.

Poly(ethylene glycol) (PEG) hydrogels were formed using thiol-ene photopolymerization chemistry (Fig. 1A) [36]. For most experiments, 8-arm PEG-norbornene was purchased from a commercial source (JenKem USA: 20,000 MW, 8ARM (TP)-NB-20K). For some experiments, 8-arm PEG-NB monomer was synthesized as previously described [35]. Stock PEG solutions were prepared by adding 0.8 mL 1X PBS to 300 mg lyophilized 8-arm PEG-NB powder (final volume = 1 mL) and filtered through a 0.2 μm nylon syringe filter (Fisher) for a final concentration of 300 mg/mL sterile monomer. Monomer solutions for cell encapsulation were prepared in 1X PBS with 40 mg/mL 8-arm PEG-NB in which 40-60% of the available norbornene arms were cross-linked

with a matrix metalloproteinase (MMP)-degradable peptide with cysteines flanking the active sequence (KCG**GPQG*IWGQ**GCK, GenScript; active sequence in bold; * = cleavage site) [58, 59]. To promote cell adhesion [60], 2 mM C**RGDS** (GenScript, active sequence in bold) was incorporated as a pendant group through the terminal cysteine.

5.4.4 Quantification of Shear Modulus.

To measure the shear modulus of PEG hydrogels, 72 μL precursor solutions were pipetted into 8.0 mm diameter, 1.2 mm depth Teflon wells and cured for 8 sec using 365 nm UV light at a dose rate of 90 mW/cm^2. The resulting hydrogels were swollen to equilibrium in 1X PBS for 24 hr. The samples were tested using an Ares-LS2 rheometer (TA Instruments). A 20 g force was applied to the samples via parallel plate crossheads and a strain sweep test at 1 Hz fixed frequency was performed from 0.1 to 20% strain. If the sample was not robust enough to withstand a 20 g force the gap between the parallel plates of the rheometer was set to 1.0 mm distance. Measurements for complex shear modulus for each hydrogel formulation were taken at 1 Hz, 2–20% strain.

5.4.5 Cell encapsulation and polymerization of PEG hydrogels.

Cells pellets were re-suspended in a 2X photoinitiator solution (0.1 % wt./wt. Irgacure 2959) and mixed 1:1 with a 2X PEG monomer solution. For experiments using standard plates, 5 μL of the cell/monomer solution was pipetted onto tissue culture treated surfaces and polymerized for 2 min using ~5-10 mW/cm^2 UV light centered at ~365 nm (multiwell plates were placed on the top shelf of the exposure stand for a UVP XX-15L series UV lamp, Fisher). ***Microfluidic device***. For microfluidic experiments, 2.5 μl of the cell/monomer solution was polymerized in the middle channel of the tri-channel device.

5.4.6 Microscopy.

Immunofluorescence images were collected using a Nikon A1R laser scanning confocal microscope with Plan Apo 10x, Plan Fluor 20x Ph1 DLL, or Plan Apo 20x DIC M objectives (0.95-3.35 μm z-steps) unless otherwise noted. Some confocal z-stacks were drift corrected before creating maximum projection images using the "Align Current ND Document" command in NIS Elements. Time-lapse and viability images were collected using a Nikon TI Eclipse fluorescence microscope (20 μm z-steps). For time-lapse imaging, cells were housed in a Nikon environmental chamber with external heater (in vivo Scientific) and CO_2 regulator (in vivo Scientific) to control temperature and CO_2 levels. Some time-lapse images were drift corrected using the StackReg plugin [61] for ImageJ [62, 63].

5.4.7 Quantification of cell viability.

Cell viability was quantified for iPSC-ECs encapsulated in PEG hydrogels using the LIVE/DEAD® Viability/Cytotoxicity kit (Life Technologies). Cells were rinsed with 1X PBS and stained with calcein AM and ethidium homodimer-1 for 30 min using the manufacturer's recommended dilutions. Samples were then washed with 1X PBS and fixed in 10% buffered formalin (4% formaldehyde, Fischer) for 30 min. Following fixation, cell nuclei were stained with 1:500 DAPI (Sigma-Aldrich) for 30 min. The fraction of dead cells was quantified by determining the ratio of ethidium homodimer$^+$ nuclei to total nuclei.

5.4.8 Immunofluorescence (IF) imaging.

***Standard well plates*.** Antibody dilutions were 1:200 mouse anti-CD31 (MAB2148, R&D Systems or M082301-2, DAKO), 1:100 goat anti-VE cadherin (AF938, R&D Systems), and 1:200 secondary antibodies (Alexa fluor 488 donkey anti-mouse, A-21202 or Alexa fluor 568 donkey

anti-goat, A-11057, Life Technologies). Cells encapsulated in PEG hydrogels were fixed in 10% buffered formalin (4% formaldehyde, Fischer) for 30-60 min. Following fixing, samples were rinsed 2 x 15 minutes with wash buffer (0.05% Triton-X 100 in PBS). Cells were then permeabilized and blocked for at least 60 min using 0.25% Triton X-100 and 1% (wt/wt) bovine serum albumin (BSA, Fisher Scientific) in PBS, followed by an additional two rinses with wash buffer. Samples were then incubated with primary antibody in incubation buffer (0.05% Triton X100 and 1% BSA in PBS) for 4 hr at room temperature or overnight at 4°C. After rinsing 2 x 15 min and once for at least 30 min in wash buffer, samples were incubated with secondary antibody and 1:500 DAPI (Sigma-Aldrich) in incubation buffer for 4 hr at room temperature or overnight at 4°C. Samples were rinsed 2 x 15 min in wash buffer and stored in PBS at 4°C until imaging (at least overnight). ***Microfluidics device.*** Cells encapsulated within microfluidic devices were fixed with 4% paraformaldehyde (PFA) for 30 min. Samples for immunofluorescence imaging of CD31 and VE-Cadherin were prepared as described above. For experiments that illustrate f-actin only, samples were rinsed with PBS and then incubated with 1:1000 DAPI and 1:50 phalloidin in PBS (added to the side channels) for 1 hr at room temperature, followed by at least 2x15 min incubation in PBS. All samples were stored in PBS until imaging.

5.4.9 RNA sequencing.

Total RNA was isolated using the RNeasy Kit (Qiagen) and included lysing in 350 μL RLT lysis buffer and the optional DNase treatment. cDNA libraries were prepared from 50 nanograms of total RNA and indexed with Illumina's TruSeq RNA Sample Preparation Kit v2 (RS-122-2001 and RS-122-2002). Final indexed cDNA libraries were pooled with 12 uniquely indexed TruSeq cDNA libraries for a total of 6 samples per lane. Multiplexed samples were sequenced on an Illumina HiSeq 2500 with a single 51 bp read and a 7 bp index read. Base-calling and

demultiplexing were performed using Casava (v1.8.2). Sequences were filtered and trimmed to remove low quality reads, adapters, and other sequencing artifacts. The remaining reads were aligned to 19084 Refseq genes extracted from the Illumina iGenomes reference, selecting only those with 'NM_' annotations. Bowtie (v 0.12.9) was used for alignment, allowing two mismatches in a 28 bp seed [64]. Reads with more than 200 alignments were excluded from further analysis. RSEM (v1.2.3) was used to estimate isoform and relative gene expression levels (transcripts per million or "TPM") [65]. LOG-fold changes are calculated as LOG2[(iPSC-EC TPM+1)/ (iPSC TPM +1)] to avoid calculation errors associated with samples that have zero expression. ***Differential gene expression***. Differentially expressed genes between individual samples were calculated from RSEM expected read counts (EC) using EBSeq (v1.5.3)[66], with median quantile normalization of EC and a maximum False Discovery Rate of 0.005. Differentially expressed genes between individual samples were calculated in EBSeq using expected read counts and the False Discovery Rate cutoff was set at FDR ≤ 0.005. ***Gene Ontology analysis***. The DAVID Bioinformatics Database Functional Annotation Tool (v6.7) was used to identify Gene Ontology terms [67-70] from differentially expressed genes. DAVID analysis was done using the following settings: Gene Ontology category GOTERM_BP_FAT; Threshold options: Counts = 10, EASE = 0.001. GO lists presented in Tables S5.2-S5.3 were limited to the Top 25 GO terms and Benjamini corrected p-value ≤ 0.05 (thus, some lists included fewer than 25 terms). ***Code availability (EBSeq)***. Details about the EBSeq algorithm were previously described in detail [66]. EBSeq download and documentation is available at:

http://www.bioconductor.org/packages/devel/bioc/html/EBSeq.html

Additional files and instructions for downloading the user interface and instructions for installing the EBSeq toolshed for Galaxy are available at:

https://www.biostat.wisc.edu/~kendzior/EBSEQ/

5.4.10 Statistical analysis

Statistical significance for data in Fig. S5.5 was calculated using a one-way ANOVA with a post hoc Tukey-Kramer test for individual comparisons ($\alpha = 0.05$).

5.5 Results and Discussion

Induced pluripotent stem cell-derived endothelial cells (iPSC-ECs) were encapsulated in peptide-functionalized PEG hydrogels to establish an *in vitro* vascular model using a uniform cell source [23] and a synthetic extracellular matrix (ECM) [36]. Thiol-ene photopolymerization was used to incorporate protease-degradable peptide crosslinks [58] and cell adhesion peptides [60] into PEG hydrogels to provide a synthetic ECM permissive towards cellular remodeling (Fig. 5.1A) [36]. The iPSC-ECs were previously characterized by uniform purity between lots and functional characteristics that included thrombin-dependent barrier function, TNF-α responsiveness, and shear stress-induced alignment [23]. Here, calcein/ethidium homodimer staining (Fig. 5.1B-C) and time-lapse microscopy (Suppl. Fig. S5.1, Suppl. Movie S5.1) demonstrated that iPSC-ECs were viable and self-assembled into interconnected vascular networks during the first three days of culture in peptide-functionalized PEG hydrogels. After encapsulation, iPSC-ECs condensed into clusters, elongated, and extended protrusions to establish connections (Suppl. Fig. S5.1A, Suppl. Movie S5.2), which resembled vasculogenic sprouting *in vivo* [71, 72]. Sprouting from existing tubules played a dynamic role during iPSC-EC assembly (Suppl. Fig. S5.1B, Suppl. Movie S5.1), as sprouts often retracted before establishing new connections or formed tubules that later disassembled (Suppl. Movie S5.3). Vacuoles also appeared to play a role in tubule formation by iPSC-ECs (Suppl. Movie S5.4), such as previously

observed *in vitro* and *in vivo* [73]. By day 3, capillary networks with polygonal organization were evident throughout the hydrogel spot (Suppl. Fig. S5.1C), which resembled mechanisms described for endothelial cells in naturally-derived matrices *in vitro* [15-17] and blood vessel development *in vivo* [71, 72].

RNA-Seq was used to analyze global gene expression for iPSC-ECs during vascular network formation in PEG hydrogels (Suppl. Table S5.1). Immunofluorescence imaging demonstrated that iPSC-EC networks in PEG hydrogels were $CD31^+$ and VE-$Cadherin^+$ by immunofluorescence (Fig. 5.2A-C), and both genes were highly expressed by RNA-Seq for 2D and 3D culture (Fig. 5.2D-E). Normalized gene expression was ranked for iPSC-ECs within the Gene Ontology (GO) categories vasculature development (GO:0001944) and biological adhesion (GO:0022610) (Suppl. Fig. S5.2), which are functional terms from the Gene Ontology Consortium [69, 70] chosen for their relevance to mechanisms that guide vascular morphogenesis [17, 74, 75]. Genes that were highly expressed by iPSC-ECs included many regulators of vascular function, such as cell-matrix and cell-cell adhesion genes (e.g., KDR/VEGFR-2, CD99, MCAM/CD146, CLDN5/claudin-5, integrins, etc.) and genes relevant to matrix remodeling (e.g., laminins, collagens, TIMPs, and MMPs; Suppl. Fig. S5.2) [17, 74]. Thus, iPSC-ECs were characterized by gene expression profiles and cell-cell adhesions that are characteristic of an endothelial phenotype, which agrees with previous results using the same cell line [23].

EBseq [66] was then used to identify differentially expressed genes for iPSC-ECs compared to undifferentiated iPS cells (Suppl. Table S5.2) or iPSC-ECs in 3D (PEG hydrogels) relative to 2D (TCP) culture (Suppl. Table S5.3). Differentially expressed genes were further analyzed for functional properties by identifying GO terms using the DAVID Functional Annotation Tool [67-70]. Genes upregulated by iPSC-ECs relative to iPS cells were enriched

within GO categories that included vasculature development (Fig. 5.3), biological adhesion, cell motion (GO:0006928), and others that were relevant to vascular morphogenesis (see Suppl. Table S5.2 for full lists). EBSeq identified 23 upregulated and 16 downregulated vasculature development genes for iPSC-ECs in 3D relative to 2D culture (Fig. 5.4A; at least one time point). Genes that were upregulated by iPSC-ECs in 3D culture also included 20 regulation of locomotion genes (GO:0040012) and 19 responses to hypoxia genes (GO:0001666), whereas genes upregulated in 2D culture were predominantly enriched within GO categories related to proliferation (e.g., 127 cell cycle genes) (Suppl. Table S5.3). Upregulated genes in 3D culture also included Notch signaling genes, adhesion genes, and others that regulate mechanisms such as tip and stalk cell specification and branching during angiogenesis (Fig. 5.4B; NOTCH4, GJA4, GJA5, CLDN5, UNC5B, etc.) [74, 76], which is consistent with observations by time-lapse microscopy.

Vascular morphogenesis is dependent on coordinated interactions between endothelial cells and the ECM, which includes proteolytic matrix remodeling, a balance of cell-cell and cell-matrix adhesions, and deposition of matrix components such as collagens and laminins (e.g., for basement membrane assembly) [16, 17, 74]. Genes that were upregulated by iPSC-ECs in 3D relative to 2D culture included COL1A1, COL1A2, COL6A3, and ITGA1, which encode the α1 and α2 subunits of type I collagen, the α3 subunit of type VI collagen, and integrin α_1, respectively (Fig. 5.4, Suppl. Table S5.3). Integrin α_1 is a cell adhesion receptor for interstitial collagens, as well as ECM components of the basement membrane (collagen IV and laminin-1 [77, 78]) and vascular subendothelium (collagen VI [79, 80]) [81]. Further, endothelial cells have been characterized by increased expression of collagen I during tube formation *in vitro* [82-85] and α_1 integrin during angiogenesis *in vivo* [86, 87] and vascular morphogenesis *in vitro* [88]. Additional genes that have been implicated in ECM remodeling during vascular morphogenesis and were

upregulated for iPSC-ECs in 3D culture included MMP9 (matrix metalloproteinase 9), TIMP3 (tissue inhibitor of metalloproteinase-3) and NID2 (nidogen-2) [17] (Suppl. Table S5.3), while other related matrix remodeling and cell adhesion genes were highly expressed in both 2D and 3D culture (Suppl. Fig. S5.2). Our combined results demonstrate that iPSC-ECs self-assemble in PEG hydrogels through mechanisms that are consistent with *in vitro* and *in vivo* vascular morphogenesis [16, 17, 71, 74].

Finally, vascular network formation was investigated for iPSC-ECs encapsulated in PEG hydrogels that were polymerized within a tri-channel microfluidic device (Figs. 5.5A) [55]. The passive flow microfluidic format uses standard pipetting to introduce cells and exchange media [55], and such "tubeless" designs can be arrayed and interfaced with automated liquid handlers for enhanced-throughput applications [89]. Vascular network formation was investigated within PEG hydrogels with shear moduli ranging from 183 ± 10 – 1612 ± 95 Pa, which were fabricated by maintaining a constant concentration for the PEG-NB backbone (2 mM 8-arm PEG-NB, 16 mM available norbornene groups) while varying the fraction of MMP-degradable peptide crosslinks (40-60% molar ratio thiol:norbornene) (Fig. 5.5B). Only limited tubule formation was evident after eight days when $1x10^7$ iPSC-ECs per mL were encapsulated in 40-60% crosslinked hydrogels and cultured in basal medium ("Control", includes 5 ng/mL VEGF, Fig. 5.5C,E,G). Vascular network formation was improved for each PEG formulation when iPSC-ECs were cultured in basal medium supplemented with 200 ng/mL VEGF ("200 VEGF", Fig. 5.5D,F,H), and further optimization for iPSC-ECs encapsulated in 50% crosslinked PEG hydrogels demonstrated that vascular networks were most pronounced at intermediate VEGF concentrations (Suppl. Fig. S5.3). The optimal VEGF dose qualitatively increased when iPSC-ECs were encapsulated in PEG hydrogels at higher cell density ($8.5x10^7$ iPSC-ECs per mL), and vascular network formation was completely

disrupted at the highest VEGF concentration (1000 ng/mL) (Suppl. Fig. S5.4). Importantly, capillary tubules with lumens were stable to at least 14 days in the microfluidic device when $1x10^7$ iPSC-ECs per mL were encapsulated in 50% crosslinked PEG hydrogels and cultured in medium that was supplemented with 100 ng/mL VEGF (Fig. 5.6). Thus, vascular network formation by iPSC-ECs depended on an optimal VEGF concentration that was cell density-dependent, which is consistent with the role for VEGF during vascular morphogenesis *in vitro* [17, 90] and *in vivo* [74, 91].

Previous studies have demonstrated that endothelial cells will self-assemble into vascular networks within engineered matrices under static conditions, but these networks often regress within a few days in the absence of mural cells such as fibroblasts, mesenchymal stem cells, or pericytes [29-34]. The absence of pericytes in PDGF-B and PDGFR-β knockout mouse models leads to hyperplasia and other blood vessel abnormalities, but microvessel density, length, and branching are similar to wild type mice and the mutant animals survive into adulthood [92]. Thus, *in vivo* capillaries retain some level of function even in the absence of pericytes [92], which suggests that a lack of mural cells does not entirely account for regression of vascular networks *in vitro*. HUVECs form *in vitro* networks that are stable for at least five days in collagen when soluble factors are optimized [15], and up to 10 days in starPEG-heparin hydrogels that sequester VEGF, bFGF, and SDF1α during encapsulation [34]. Here, iPSC-ECs in PEG hydrogels formed capillary tubules with lumens that were stable for at least 14 days in microfluidic channels when VEGF concentration was optimized (Fig. 5.6). Vascular network stability could also be improved for iPSC-ECs in PEG hydrogels in standard well plates by adding a second cell-free hydrogel layer to provide mechanical support after initial cellular self-assembly (Suppl. Fig. S5.5). These combined

results demonstrate the value of engineering approaches for extending the stability of *in vitro* vascular networks using endothelial cell monocultures.

5.6 Conclusions

The aim of the present study was to develop a vascular model by encapsulating human iPSC-ECs [23] in a synthetic extracellular matrix (ECM) formed via thiol-ene photopolymerization [36]. Time-lapse microscopy, immunofluorescence imaging, and RNA-sequencing (RNA-Seq) demonstrated that iPSC-ECs encapsulated in PEG hydrogels self-assembled into capillary networks through mechanisms that are consistent with *in vitro* and *in vivo* vascular morphogenesis. Capillary tubules with lumens were stable for at least 14 days when iPSC-ECs were encapsulated in PEG hydrogels that were polymerized within a passive flow microfluidic device. Thus, the *in vitro* model described here mimics important aspects of vascular morphogenesis by incorporating iPSC-ECs into chemically-defined PEG hydrogels using standard and microfluidic formats.

5.7 Acknowledgments

The authors would like to acknowledge funding from the National Institutes of Health (NIH R01HL093282-01A1, R21EB016381-01, 1UH2TR000506-01, 3UH2TR000506-02S1, T32HL007889, T32HL07936, R01EB10039, and the Biotechnology Training Program NIGMS5T32GM08349), the Environmental Protection Agency (83573701), and the UW-Madison Graduate Engineering Research Scholars program. Mechanical testing data was obtained using the Ares LS2 rheometer at the UW-Madison Soft Materials Laboratory.

5.8 Competing Financial Interest

J.A.T. was a founder and stockholder for Cellular Dynamics, Inc at the time of manuscript submission. D.J.B. holds equity in Bellbrook Labs, LLC, Tasso, Inc., Stacks for the Future, LLC and Salus Discovery, LLC. W.L.M. is a founder and stockholder for Stem Pharm, Inc., and Tissue Regeneration Systems, Inc.

Supplementary movies and tables to this article can be found online at:

doi: 10.1016/j.actbio.2016.03.001

5.9 References

[1] Novosel EC, Kleinhans C, Kluger PJ. Vascularization is the key challenge in tissue engineering. Adv Drug Deliv Rev. 2011;63:300-11.
[2] Phelps EA, García AJ. Engineering more than a cell: vascularization strategies in tissue engineering. Curr Opin Biotechnol. 2010;21:704-9.
[3] Hasan A, Paul A, Vrana NE, Zhao X, Memic A, Hwang Y-S, et al. Microfluidic techniques for development of 3D vascularized tissue. Biomaterials. 2014;35:7308-25.
[4] Schwartz MP, Hou Z, Propson NE, Zhang J, Engstrom CJ, Costa VS, et al. Human pluripotent stem cell-derived neural constructs for predicting neural toxicity. Proc Natl Acad Sci U S A. 2015;112:12516-21.
[5] Martins-Green M, Li Q-J, Yao M. A new generation organ culture arising from cross-talk between multiple primary human cell types. The FASEB Journal. 2005;19:222-4.
[6] Takebe T, Sekine K, Enomura M, Koike H, Kimura M, Ogaeri T, et al. Vascularized and functional human liver from an iPSC-derived organ bud transplant. Nature. 2013;499:481-+.
[7] Sekine H, Shimizu T, Sakaguchi K, Dobashi I, Wada M, Yamato M, et al. In vitro fabrication of functional three-dimensional tissues with perfusable blood vessels. Nat Commun. 2013;4.
[8] Scott CW, Peters MF, Dragan YP. Human induced pluripotent stem cells and their use in drug discovery for toxicity testing. Toxicol Lett. 2013;219:49-58.
[9] Kleinstreuer NC, Yang J, Berg EL, Knudsen TB, Richard AM, Martin MT, et al. Phenotypic screening of the ToxCast chemical library to classify toxic and therapeutic mechanisms. Nat Biotechnol. 2014;32:583-+.
[10] Sarkanen J-R, Mannerstrom M, Vuorenpaa H, Uotila J, Ylikomi T, Heinonen T. Intra-laboratory validation of a human cell based in vitro angiogenesis assay for testing angiogenesis modulators. Frontiers in Pharmacology. 2011;1.
[11] Folkman J, Haudenschild C. Angiogenesis in vitro. Nature. 1980;288:551-6.
[12] Maciag T, Kadish J, Wilkins L, Stemerman MB, Weinstein R. Organizational behavior of human umbilical vein endothelial cells. The Journal of Cell Biology. 1982;94:511-20.
[13] Montesano R, Orci L, Vassalli P. In vitro rapid organization of endothelial cells into capillary-like networks is promoted by collagen matrices. J Cell Biol. 1983;97:1648-52.
[14] Kubota Y, Kleinman HK, Martin GR, Lawley TJ. Role of laminin and basement membrane in the morphological differentiation of human endothelial cells into capillary-like structures. J Cell Biol. 1988;107:1589-98.
[15] Davis GE, Camarillo CW. An alpha 2 beta 1 integrin-dependent pinocytic mechanism involving intracellular vacuole formation and coalescence regulates capillary lumen and tube formation in three-dimensional collagen matrix. Exp Cell Res. 1996;224:39-51.
[16] Vernon RB, Sage EH. Between molecules and morphology - Extracellular matrix and creation of vascular form. Am J Pathol. 1995;147:873-83.
[17] Davis GE, Senger DR. Endothelial extracellular matrix - Biosynthesis, remodeling, and functions during vascular morphogenesis and neovessel stabilization. CircRes. 2005;97:1093-107.
[18] Vickerman V, Blundo J, Chung S, Kamm R. Design, fabrication and implementation of a novel multi-parameter control microfluidic platform for three-dimensional cell culture and real-time imaging. Lab Chip. 2008;8:1468-77.
[19] Whisler JA, Chen MB, Kamm RD. Control of perfusable microvascular network morphology using a multiculture microfluidic system. Tissue Eng Part C-Methods. 2014;20:543-52.
[20] Tourovskaia A, Fauver M, Kramer G, Simonson S, Neumann T. Tissue-engineered microenvironment systems for modeling human vasculature. Exp Biol Med. 2014;239:1264-71.

[21] Moya ML, Hsu Y, Lee AP, Hughes CCW, George SC. In vitro perfused human capillary networks. Tiss Eng C: Methods. 2013;doi:10.1089/ten.tec.2012.0430.
[22] Kim S, Lee H, Chung M, Jeon NL. Engineering of functional, perfusable 3D microvascular networks on a chip. Lab Chip. 2013;13:1489-500.
[23] Belair D, Whisler J, Valdez J, Velazquez J, Molenda J, Vickerman V, et al. Human vascular tissue models formed from human induced pluripotent stem cell derived endothelial cells. Stem Cell Rev Rep. 2014:1-15.
[24] Yang YL, Leone LM, Kaufman LJ. Elastic moduli of collagen gels can be predicted from two-dimensional confocal microscopy. Biophys J. 2009;97:2051-60.
[25] Hughes CS, Postovit LM, Lajoie GA. Matrigel: A complex protein mixture required for optimal growth of cell culture. Proteomics. 2010;10:1886-90.
[26] Vukicevic S, Kleinman HK, Luyten FP, Roberts AB, Roche NS, Reddi AH. Identification of multiple active growth factors in basement membrane Matrigel suggests caution in interpretation of cellular activity related to extracellular matrix components. Exp Cell Res. 1992;202:1-8.
[27] Zisch AH, Lutolf MP, Ehrbar M, Raeber GP, Rizzi SC, Davies N, et al. Cell-demanded release of VEGF from synthetic, biointeractive cell-ingrowth matrices for vascularized tissue growth. The FASEB Journal. 2003.
[28] Leslie-Barbick JE, Moon JJ, West JL. Covalently immobilized vascular endothelial growth factor promotes endothelial cell tubulogenesis in poly(ethylene glycol) diacrylate hydrogels. J Biomater Sci-Polym Ed. 2009;20:1763-79.
[29] Moon JJ, Saik JE, Poche RA, Leslie-Barbick JE, Lee SH, Smith AA, et al. Biomimetic hydrogels with pro-angiogenic properties. Biomaterials. 2010;31:3840-7.
[30] Kusuma S, Shen Y-I, Hanjaya-Putra D, Mali P, Cheng L, Gerecht S. Self-organized vascular networks from human pluripotent stem cells in a synthetic matrix. Proceedings of the National Academy of Sciences. 2013;110:12601-6.
[31] Chen YC, Lin RZ, Qi H, Yang YZ, Bae HJ, Melero-Martin JM, et al. Functional human vascular network generated in photocrosslinkable gelatin methacrylate hydrogels. Adv Funct Mater. 2012;22:2027-39.
[32] Culver JC, Hoffmann JC, Poché RA, Slater JH, West JL, Dickinson ME. Three-dimensional biomimetic patterning in hydrogels to guide cellular organization. Adv Mater. 2012;24:2344-8.
[33] Turturro MV, Christenson MC, Larson JC, Young DA, Brey EM, Papavasiliou G. MMP-sensitive PEG diacrylate hydrogels with spatial variations in matrix properties stimulate directional vascular sprout formation. PLoS One. 2013;8:e58897.
[34] Chwalek K, Tsurkan MV, Freudenberg U, Werner C. Glycosaminoglycan-based hydrogels to modulate heterocellular communication in in vitro angiogenesis models. Sci Rep. 2014;4.
[35] Nguyen EH, Zanotelli MR, Schwartz MP, Murphy WL. Differential effects of cell adhesion, modulus and VEGFR-2 inhibition on capillary network formation in synthetic hydrogel arrays. Biomaterials. 2014;35:2149-61.
[36] Fairbanks BD, Schwartz MP, Halevi AE, Nuttelman CR, Bowman CN, Anseth KS. A versatile synthetic extracellular matrix mimic via thiol-norbornene photopolymerization. Adv Mater. 2009;21:5005-10.
[37] Lin C-C, Ki CS, Shih H. Thiol–norbornene photoclick hydrogels for tissue engineering applications. J Appl Polym Sci. 2015;132:41563.
[38] Hoyle CE, Bowman CN. Thiol-ene click chemistry. Angew Chem-Int Edit. 2010;49:1540-73.

[39] Singh SP, Schwartz MP, Lee JY, Fairbanks BD, Anseth KS. A peptide functionalized poly(ethylene glycol) (PEG) hydrogel for investigating the influence of biochemical and biophysical matrix properties on tumor cell migration. Biomaterials Science. 2014;2:1024-34.
[40] Gramlich WM, Kim IL, Burdick JA. Synthesis and orthogonal photopatterning of hyaluronic acid hydrogels with thiol-norbornene chemistry. Biomaterials. 2013;34:9803-11.
[41] Munoz Z, Shih H, Lin CC. Gelatin hydrogels formed by orthogonal thiol-norbornene photochemistry for cell encapsulation. Biomaterials Science. 2014;2:1063-72.
[42] Van Hove AH, Beltejar M-JG, Benoit DSW. Development and in vitro assessment of enzymatically-responsive poly(ethylene glycol) hydrogels for the delivery of therapeutic peptides. Biomaterials. 2014;35:9719-30.
[43] Wang C, Tong XM, Yang F. Bioengineered 3D brain tumor model to elucidate the effects of matrix stiffness on glioblastoma cell behavior using PEG-based hydrogels. Mol Pharm. 2014;11:2115-25.
[44] Hynes WF, Doty NJ, Zarembinski TI, Schwartz MP, Toepke MW, Murphy WL, et al. Micropatterning of 3D microenvironments for living biosensor applications. Biosensors. 2014;4:28-44.
[45] Belair DG, Murphy WL. Specific VEGF sequestering to biomaterials: Influence of serum stability. Acta Biomater. 2013;9:8823-31.
[46] Lin C-C, Raza A, Shih H. PEG hydrogels formed by thiol-ene photo-click chemistry and their effect on the formation and recovery of insulin-secreting cell spheroids. Biomaterials. 2011;32:9685-95.
[47] Anderson SB, Lin CC, Kuntzler DV, Anseth KS. The performance of human mesenchymal stem cells encapsulated in cell-degradable polymer-peptide hydrogels. Biomaterials. 2011;32:3564-74.
[48] Chi J-T, Chang HY, Haraldsen G, Jahnsen FL, Troyanskaya OG, Chang DS, et al. Endothelial cell diversity revealed by global expression profiling. Proceedings of the National Academy of Sciences. 2003;100:10623-8.
[49] Yu JY, Vodyanik MA, Smuga-Otto K, Antosiewicz-Bourget J, Frane JL, Tian S, et al. Induced pluripotent stem cell lines derived from human somatic cells. Science. 2007;318:1917-20.
[50] Takahashi K, Tanabe K, Ohnuki M, Narita M, Ichisaka T, Tomoda K, et al. Induction of pluripotent stem cells from adult human fibroblasts by defined factors. Cell. 2007;131:861-72.
[51] Thomson JA, Itskovitz-Eldor J, Shapiro SS, Waknitz MA, Swiergiel JJ, Marshall VS, et al. Embryonic stem cell lines derived from human blastocysts. Science. 1998;282:1145-7.
[52] Samuel R, Daheron L, Liao S, Vardam T, Kamoun WS, Batista A, et al. Generation of functionally competent and durable engineered blood vessels from human induced pluripotent stem cells. Proc Natl Acad Sci U S A. 2013;110:12774-9.
[53] Levenberg S, Golub JS, Amit M, Itskovitz-Eldor J, Langer R. Endothelial cells derived from human embryonic stem cells. Proc Natl Acad Sci U S A. 2002;99:4391-6.
[54] Pitrez PR, Rosa SC, Praça C, Ferreira L. Vascular disease modeling using induced pluripotent stem cells: Focus in Hutchinson-Gilford Progeria Syndrome. Biochem Biophys Res Commun. 2015.
[55] Bischel LL, Young EWK, Mader BR, Beebe DJ. Tubeless microfluidic angiogenesis assay with three-dimensional endothelial-lined microvessels. Biomaterials. 2013;34:1471-7.
[56] Beebe DJ, Mensing GA, Walker GM. Physics and applications of microfluidics in biology. Annu Rev Biomed Eng. 2002;4:261-86.

[57] Jo BH, Van Lerberghe LM, Motsegood KM, Beebe DJ. Three-dimensional micro-channel fabrication in polydimethylsiloxane (PDMS) elastomer. J Microelectromech Syst. 2000;9:76-81.
[58] Nagase H, Fields GB. Human matrix metalloproteinase specificity studies using collagen sequence-based synthetic peptides. Biopolymers. 1996;40:399-416.
[59] Netzel-Arnett S, Sang QX, Moore WGI, Navre M, Birkedal-Hansen H, Van Wart HE. Comparative sequence specificities of human 72- and 92-kDa gelatinases (type IV collagenases) and PUMP (matrilysin). Biochemistry. 1993;32:6427-32.
[60] Pierschbacher MD, Ruoslahti E. Cell attachment activity of fibronectin can be duplicated by small synthetic fragments of the molecule. Nature. 1984;309:30-3.
[61] Thevenaz P, Ruttimann UE, Unser M. A pyramid approach to subpixel registration based on intensity. IEEE Trans Image Process. 1998;7:27-41.
[62] Rasband WS. Image J, U.S. National Institutes of Health, Bethesda, Maryland, USA, http://imagej.nih.gov/ij/ 1997-2012.
[63] Schneider CA, Rasband WS, Eliceiri KW. NIH Image to ImageJ: 25 years of image analysis. Nat Meth. 2012;9:671-5.
[64] Langmead B, Trapnell C, Pop M, Salzberg S. Ultrafast and memory-efficient alignment of short DNA sequences to the human genome. Genome Biol. 2009;10:R25.
[65] Li B, Dewey CN. RSEM: accurate transcript quantification from RNA-Seq data with or without a reference genome. BMC Bioinformatics. 2011;12:323.
[66] Leng N, Dawson JA, Thomson JA, Ruotti V, Rissman AI, Smits BMG, et al. EBSeq: an empirical Bayes hierarchical model for inference in RNA-seq experiments. Bioinformatics. 2013;29:1035-43.
[67] Huang DW, Sherman BT, Lempicki RA. Bioinformatics enrichment tools: paths toward the comprehensive functional analysis of large gene lists. Nucleic Acids Research. 2009;37:1-13.
[68] Huang DW, Sherman BT, Lempicki RA. Systematic and integrative analysis of large gene lists using DAVID bioinformatics resources. Nat Protocols. 2008;4:44-57.
[69] Consortium TGO. Gene Ontology Consortium: going forward. Nucleic Acids Research. 2015;43:D1049-D56.
[70] Ashburner M, Ball CA, Blake JA, Botstein D, Butler H, Cherry JM, et al. Gene Ontology: tool for the unification of biology. Nature Genet. 2000;25:25-9.
[71] Czirok A, Zamir EA, Szabo A, Little CD. Multicellular sprouting during vasculogenesis. In: Santiago Schnell PKMSAN, Timothy JN, editors. Current Topics in Developmental Biology: Academic Press; 2008. p. 269-89.
[72] Rupp PA, Czirók A, Little CD. αvβ3 integrin-dependent endothelial cell dynamics in vivo. Development. 2004;131:2887-97.
[73] Kamei M, Saunders WB, Bayless KJ, Dye L, Davis GE, Weinstein BM. Endothelial tubes assemble from intracellular vacuoles in vivo. Nature. 2006;442:453-6.
[74] Herbert SP, Stainier DYR. Molecular control of endothelial cell behaviour during blood vessel morphogenesis. Nat Rev Mol Cell Biol. 2011;12:551-64.
[75] Ramjaun AR, Hodivala-Dilke K. The role of cell adhesion pathways in angiogenesis. The International Journal of Biochemistry & Cell Biology. 2009;41:521-30.
[76] Roca C, Adams RH. Regulation of vascular morphogenesis by Notch signaling. Genes Dev. 2007;21:2511-24.
[77] Kleinman HK, McGarvey ML, Liotta LA, Robey PG, Tryggvason K, Martin GR. Isolation and characterization of Type IV procollagen, laminin, and heparin sulfate proteoglycan from the EHS sarcoma. Biochemistry. 1982;21:6188-93.

[78] Timpl R, Rohde H, Robey PG, Rennard SI, Foidart JM, Martin GR. Laminin - Glycoprotein from basement membranes. J Biol Chem. 1979;254:9933-7.
[79] Rand JH, Wu XX, Potter BJ, Uson RR, Gordon RE. Colocalization of von Willebrand factor and Type VI collagen in human vascular subendothelium. Am J Pathol. 1993;142:843-50.
[80] Rand JH, Patel ND, Schwartz E, Zhou SL, Potter BJ. 150 kD von Willebrand factor binding protein extracted from human vascular subendothelium is Type VI collagen. J Clin Invest. 1991;88:253-9.
[81] Tulla M, Pentikäinen OT, Viitasalo T, Käpylä J, Impola U, Nykvist P, et al. Selective Binding of Collagen Subtypes by Integrin α1I, α2I, and α10I Domains. J Biol Chem. 2001;276:48206-12.
[82] Iruela-Arispe ML, Hasselaar P, Sage H. Differential expression of extracellular proteins is correlated with angiogenesis in vitro. Lab Invest. 1991;64:174-86.
[83] Iruela-Arispe ML, Diglio CA, Sage EH. Modulation of extracellular matrix proteins by endothelial cells undergoing angiogenesis in vitro. Arteriosclerosis and Thrombosis. 1991;11:805-15.
[84] Fouser L, Iruelaarispe L, Bornstein P, Sage EH. Transcriptional activity of the alpha1(I) collagen promoter is correlated with the formation of capillary-like structures by endothelial cells in vitro. J Biol Chem. 1991;266:18345-51.
[85] Myers JC. Differential expression of type I collagen and cellular fibronectin isoforms in endothelial cell variants. Kidney Int. 1993;43:45-52.
[86] Senger DR, Perruzzi CA, Streit M, Koteliansky VE, de Fougerolles AR, Detmar M. The alpha(1)beta(1) and alpha(2)beta(1) Integrins provide critical support for vascular endothelial growth factor signaling, endothelial cell migration, and tumor angiogenesis. Am J Pathol. 2002;160:195-204.
[87] Senger DR, Claffey KP, Benes JE, Perruzzi CA, Sergiou AP, Detmar M. Angiogenesis promoted by vascular endothelial growth factor: Regulation through alpha(1)beta(1) and alpha(2)beta(1) integrins. Proc Natl Acad Sci U S A. 1997;94:13612-7.
[88] Bell SE, Mavila A, Salazar R, Bayless KJ, Kanagala S, Maxwell SA, et al. Differential gene expression during capillary morphogenesis in 3D collagen matrices: regulated expression of genes involved in basement membrane matrix assembly, cell cycle progression, cellular differentiation and G-protein signaling. J Cell Sci. 2001;114:2755-73.
[89] Meyvantsson I, Warrick JW, Hayes S, Skoien A, Beebe DJ. Automated cell culture in high density tubeless microfluidic device arrays. Lab Chip. 2008;8:717-24.
[90] Pepper MS, Ferrara N, Orci L, Montesano R. Potent synergism between vascular endothelial growth factor and basic fibroblast growth factor in the induction of angiogenesis in vitro Biochem Biophys Res Commun. 1992;189:824-31.
[91] Connolly DT, Heuvelman DM, Nelson R, Olander JV, Eppley BL, Delfino JJ, et al. Tumor vascular permeability factor stimulates endothelial cell growth and angiogenesis J Clin Invest. 1989;84:1470-8.
[92] Hellström M, Gerhardt H, Kalén M, Li X, Eriksson U, Wolburg H, et al. Lack of pericytes leads to endothelial hyperplasia and abnormal vascular morphogenesis. The Journal of Cell Biology. 2001;153:543-54.

5.10 Figures

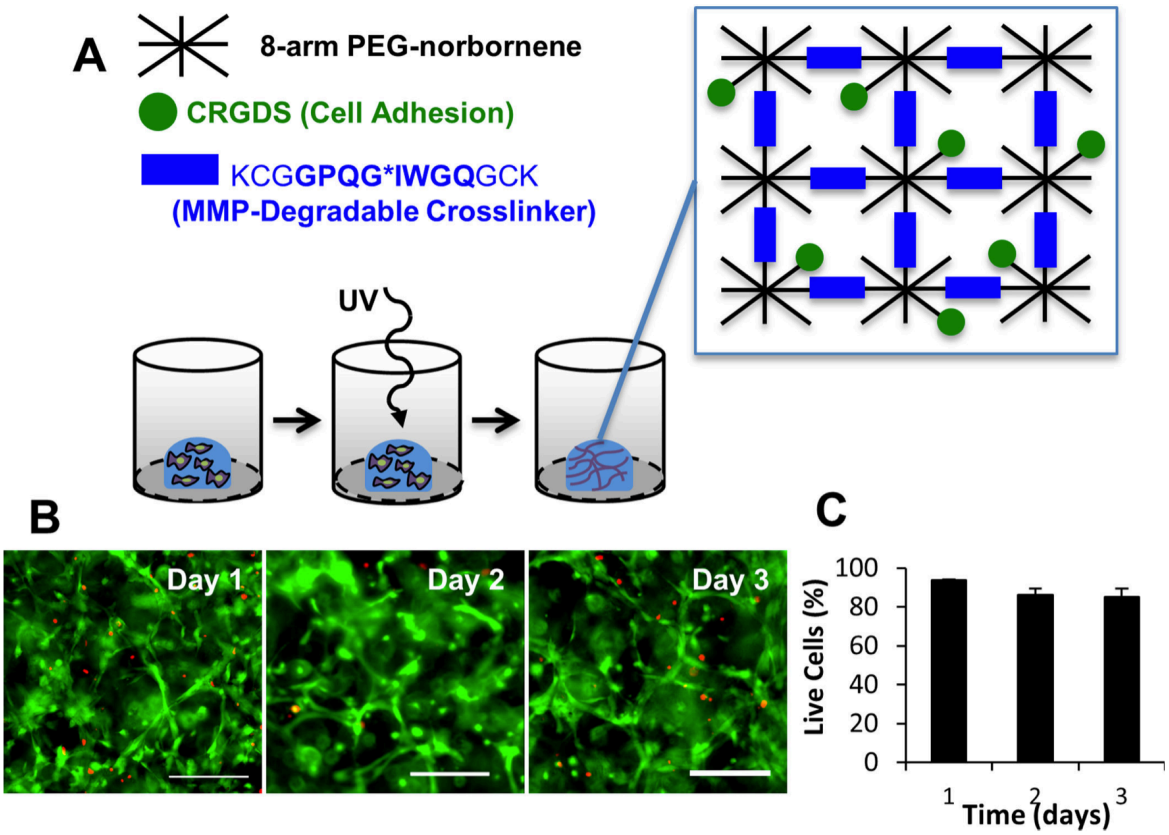

Figure 5.1 Synthetic extracellular matrix (ECM) formulations for culturing iPSC-ECs. (A) Peptide-functionalized poly (ethylene glycol) (PEG) hydrogels were fabricated as a synthetic extracellular matrix (ECM) permissive towards cellular remodeling. Thiol-ene photopolymerization chemistry was used to crosslink 8-arm poly PEG-norbornene molecules with cysteine flanked matrix metalloproteinase (MMP)-degradable peptide (active sequence in bold, cleavage site denoted by *) and to incorporate CRGDS cell adhesion peptide through the terminal cysteine. **(B)** Calcein (live cells, green) and ethidium homodimer (dead cells, red) staining (**Scale bars:** 200 μm) and **(C)** the fraction of live cells (Mean ± S.D., 3 replicate experiments) for iPSC-ECs during the first three days of culture in 50% crosslinked PEG hydrogels.

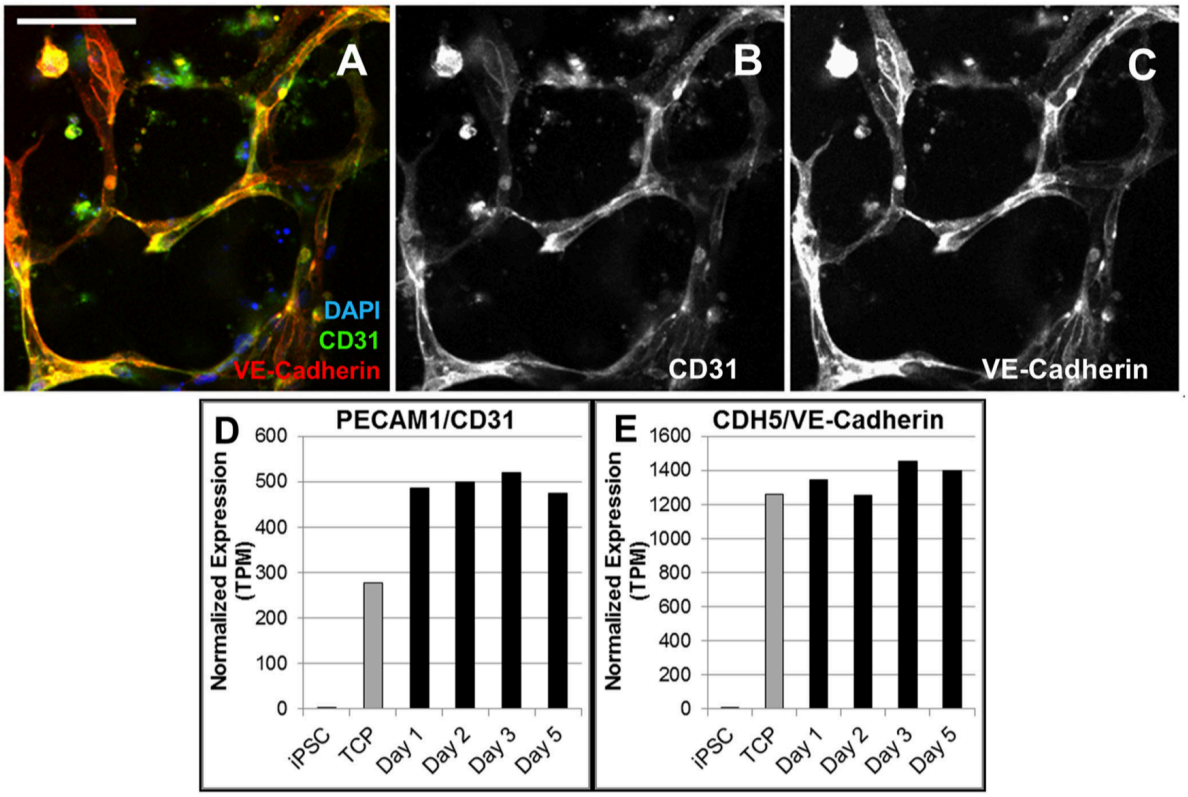

Figure 5.2 Expression of characteristic adhesion components by iPSC-ECs cultured in PEG hydrogels. Maximum intensity z-projection images for iPSC-ECs after three days of culture in 50% crosslinked synthetic ECM illustrating **(A)** CD31 (green), VE-Cadherin (red), and DAPI (nuclei, blue) expression and single channels for **(B)** CD31 and **(C)** VE-Cadherin. **Scale bar**: 100 μm. **(D-E)** Normalized gene expression ("transcripts per million" or "TPM") for undifferentiated iPS cells (iPSC), iPSC-ECs in 2D culture on tissue culture polystyrene (TCP), or 3D culture in PEG hydrogels at different time points (Days 1, 2, 3, and 5): **(G)** PECAM/CD31 and **(H)** CDH5/VE-Cadherin.

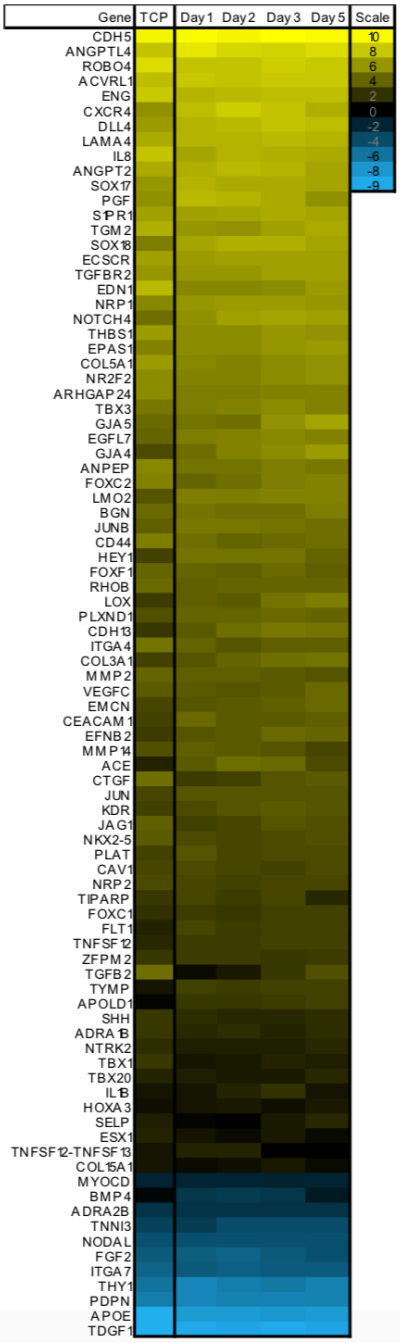

Figure 5.3 Differentially expressed vasculature development genes for iPSC-ECs relative to undifferentiated iPS cells. LOG2-fold changes in gene expression for iPSC-ECs relative to undifferentiated iPS cells. All differentially expressed genes from the GO category "vasculature development" (GO:0001944) with an EBseq FDR ≤ 0.005 for at least one time point were included. The iPSC-ECs were cultured on tissue culture polystyrene (TCP) or in PEG hydrogels at different time points (Days 1, 2, 3, and 5).

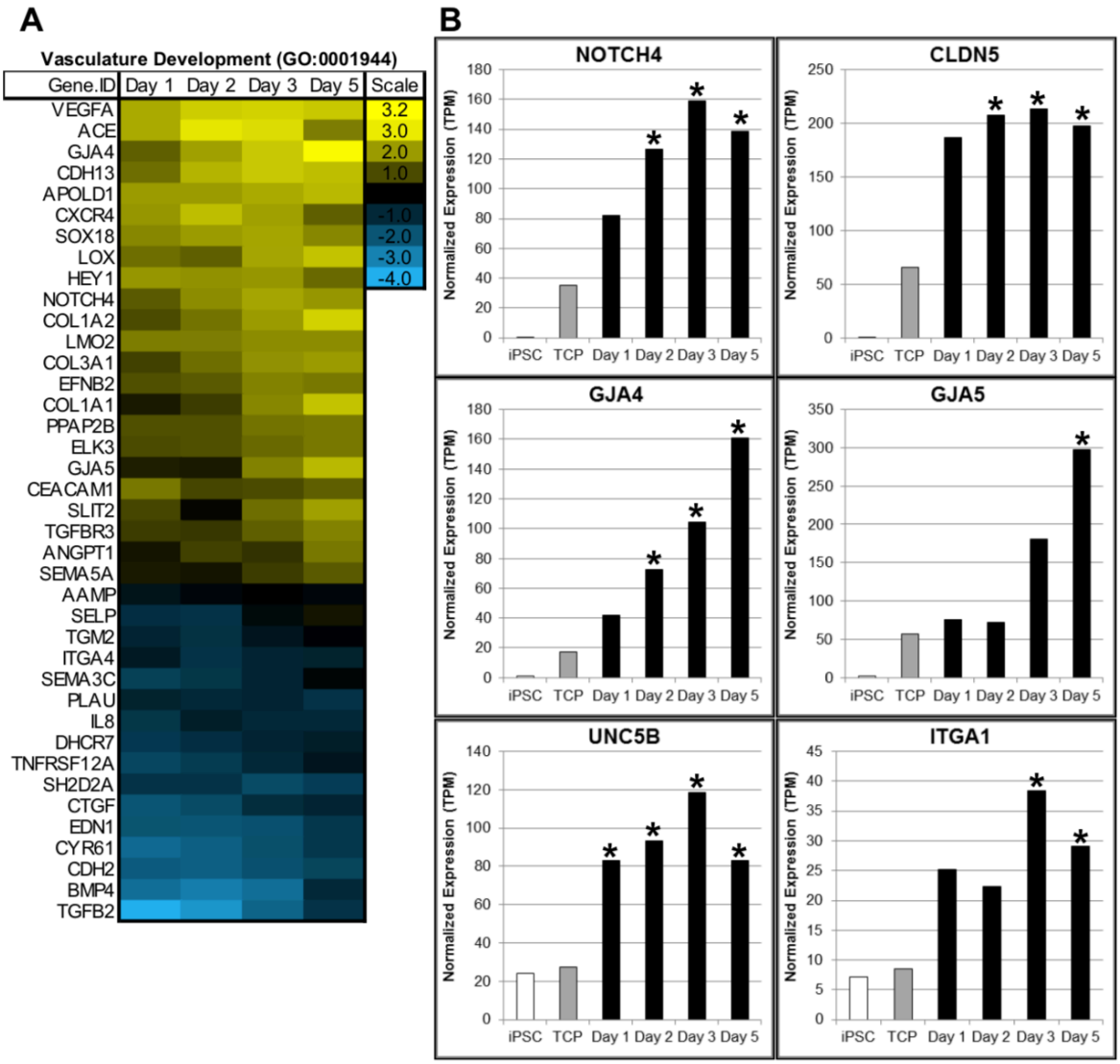

Figure 5.4 Differentially expressed vasculature development genes for iPSC-ECs in 2D and 3D culture. (A) Heatmap illustrating LOG2-fold changes in normalized expression for iPSC-ECs in synthetic ECM (3D) relative to cells cultured on TCP (2D). All differentially expressed genes from the GO category "vasculature development" (GO:0001944) with an EBseq FDR ≤ 0.005 for at least one time point were included. **(B)** Normalized gene expression ("transcripts per million" or TPM) for undifferentiated iPS cells (iPSC), iPSC-ECs in 2D culture on tissue culture polystyrene (TCP), or 3D culture in PEG hydrogels at different time points (Days 1, 2, 3, and 5). Select genes relevant to vascular morphogenesis that were upregulated by iPSC-ECs in 3D culture are shown (* = FDR ≤ 0.005 relative to 2D culture on TCP).

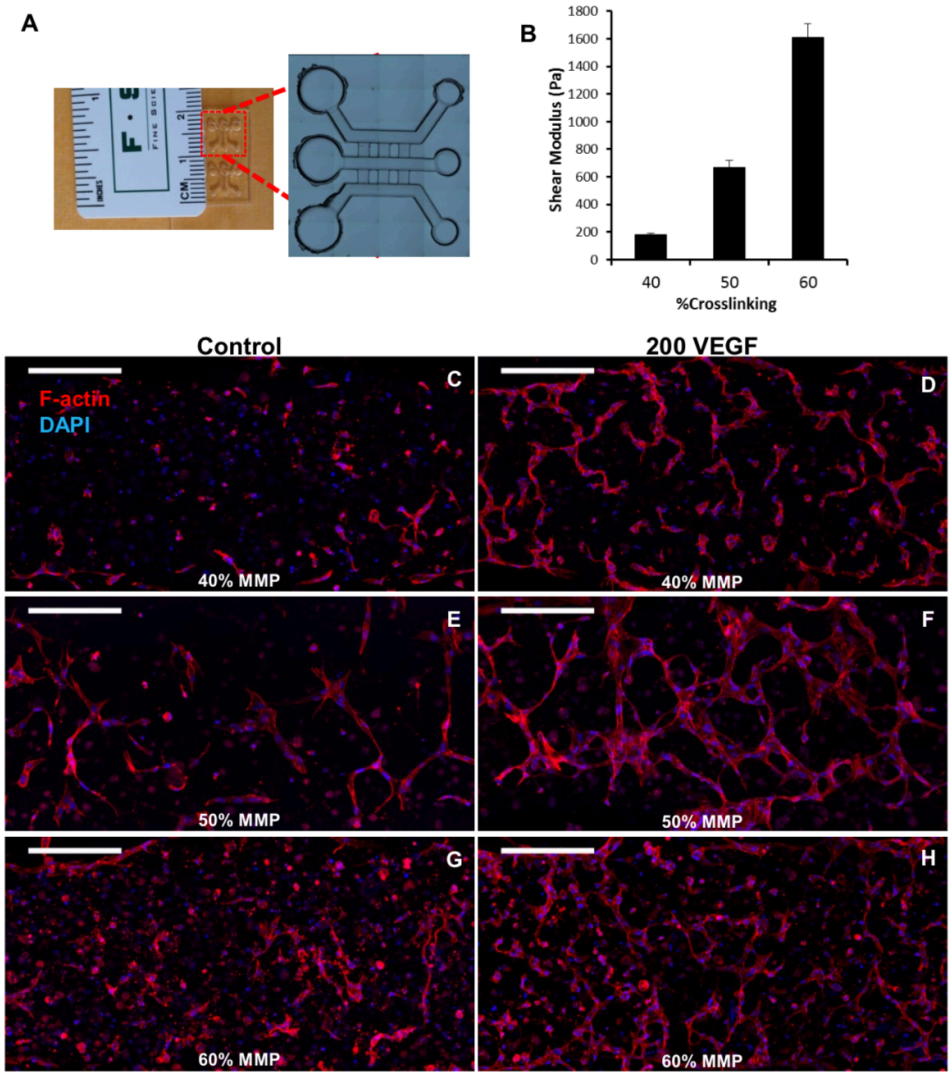

Figure 5.5 Vascular network formation as a function of crosslinking density for iPSC-ECs cultured in PEG hydrogels that were polymerized within a microfluidic device. (A) A passive pumping tri-channel microfluidic device was fabricated in polydimethylsiloxane (PDMS) (see Bischel et al, *Biomaterials* 34(5):1471-1477). $1x10^7$ iPSC-ECs / mL were suspended in a PEG monomer and polymerized within the central channel of the device. **(B)** The PEG hydrogel shear modulus was tuned from 183±10 Pa-1612±95 Pa by maintaining a constant PEG-norbornene concentration while varying the crosslinking density from 40-60% molar ratio thiol:norbornene. **(C-H)** Maximum intensity projection confocal z-stacks illustrating phalloidin (F-actin, red) and DAPI (nuclei, blue) staining for iPSC-ECs encapsulated in **(C, D)** 40%, **(C, D)** 50%, or **(C, D)** 60% crosslinked PEG hydrogels. Encapsualted iPSC-ECs were cultured in **(C, E, G)** basal medium (Control, includes 5 ng/mL VEGF) or **(D, F, H)** basal medium supplemented with 200 ng/mL VEGF (200 VEGF). **Scale bars**: 250 μm.

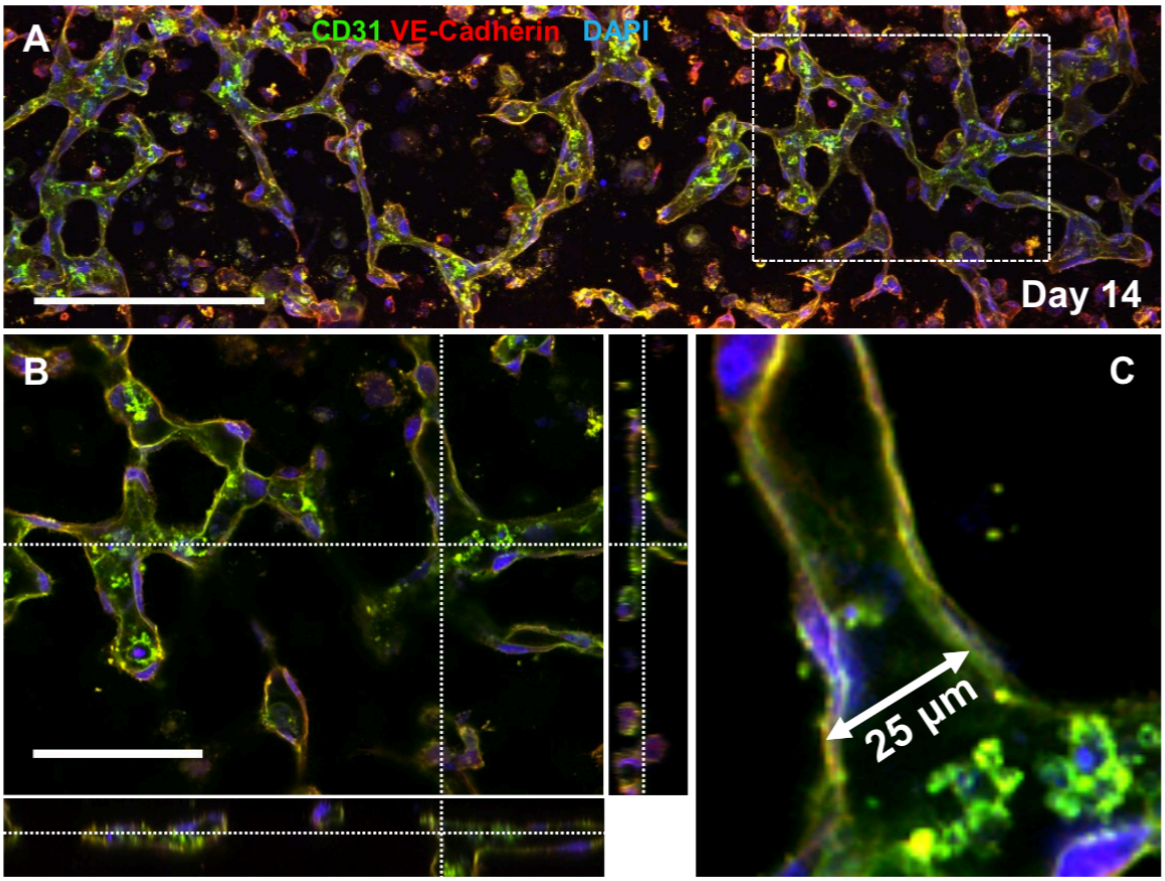

Figure 5.6 Capillary networks with lumens for iPSC-ECs after 14 days of culture in PEG hydrogels that were polymerized within a microfluidic device. CD31 (green), VE-Cadherin (red) and DAPI (nuclei, blue) expression for $1x10^7$ iPSC-ECs/mL that were suspended in a 50% crosslinked PEG hydrogel and polymerized in the central channel of a tri-channel microfluidic device. Cells were cultured for 14 days in basal medium supplemented with 100 ng/mL VEGF. **(A)** A maximum intensity z-projection (45 µm thickness) in the central region of a microfluidic channel. **(B)** A 1 µm thick z-slice within the boxed region shown in **A**. Slice View images through the XZ and YZ planes along the dashed lines are shown to illustrate the organization through the thickness of the channel (45 µm thickness shown). **(C)** Zoomed image from region where dashed lines intersect in **B** illustrating lumen diameter for a larger capillary tubule. **Scale bars**: **(A)** 250 µm; **(B)** 100 µm.

5.11 Supplementary Figures, tables and movies

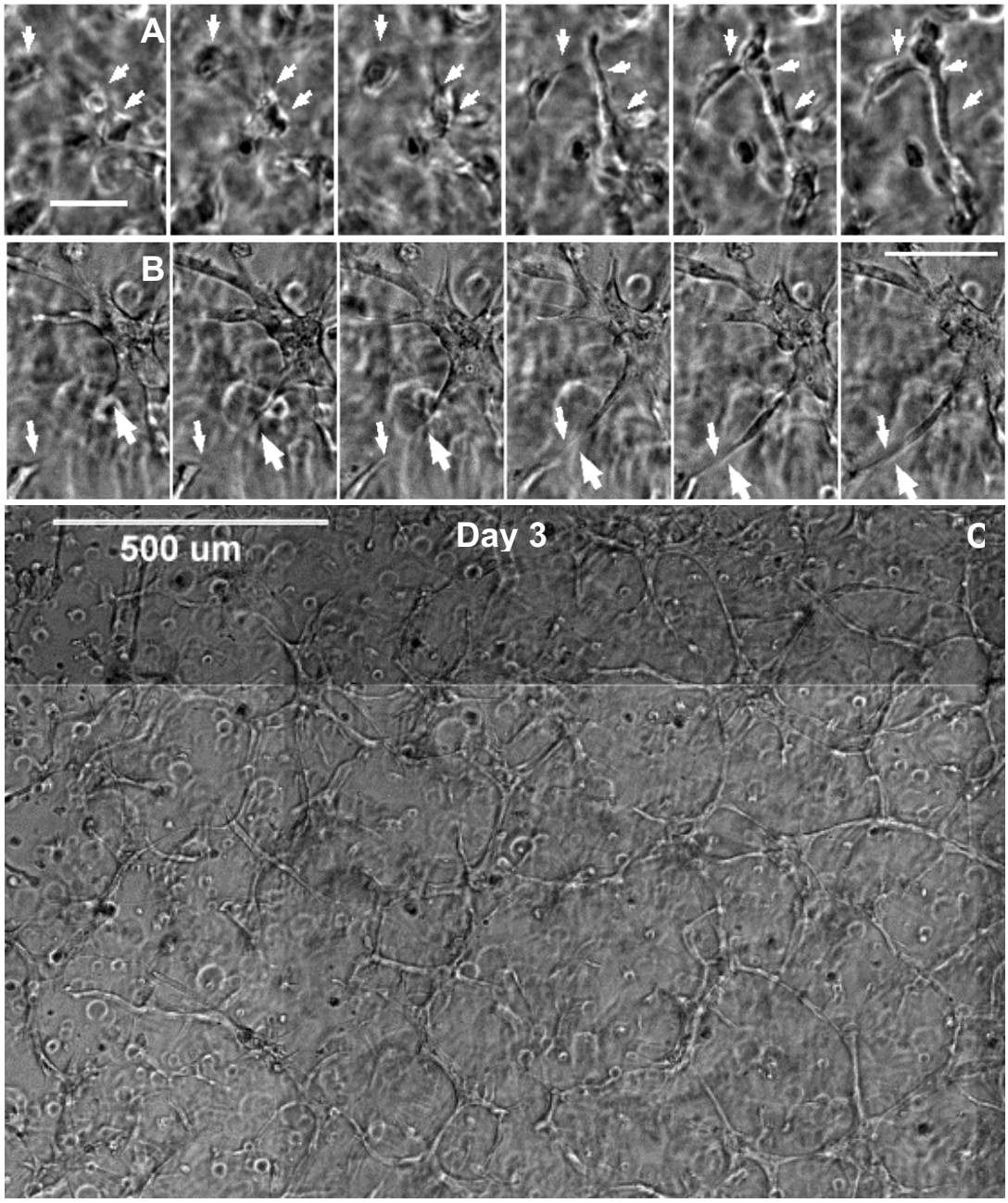

Figure S5.1 Vascular network formation by endothelial cells cultured in synthetic ECM. **(A)** Tubule formation from condensing clusters, **(B)** sprouting, and **(C)** macroscopic interconnectivity after 3 days for iPSC-ECs cultured in 50% crosslinked PEG hydrogels. Also see Supplemental Movies 1-3. **Scale bars**: **(A)** 50 μm; **(B)** 100 μm; **(C)** 500 μm.

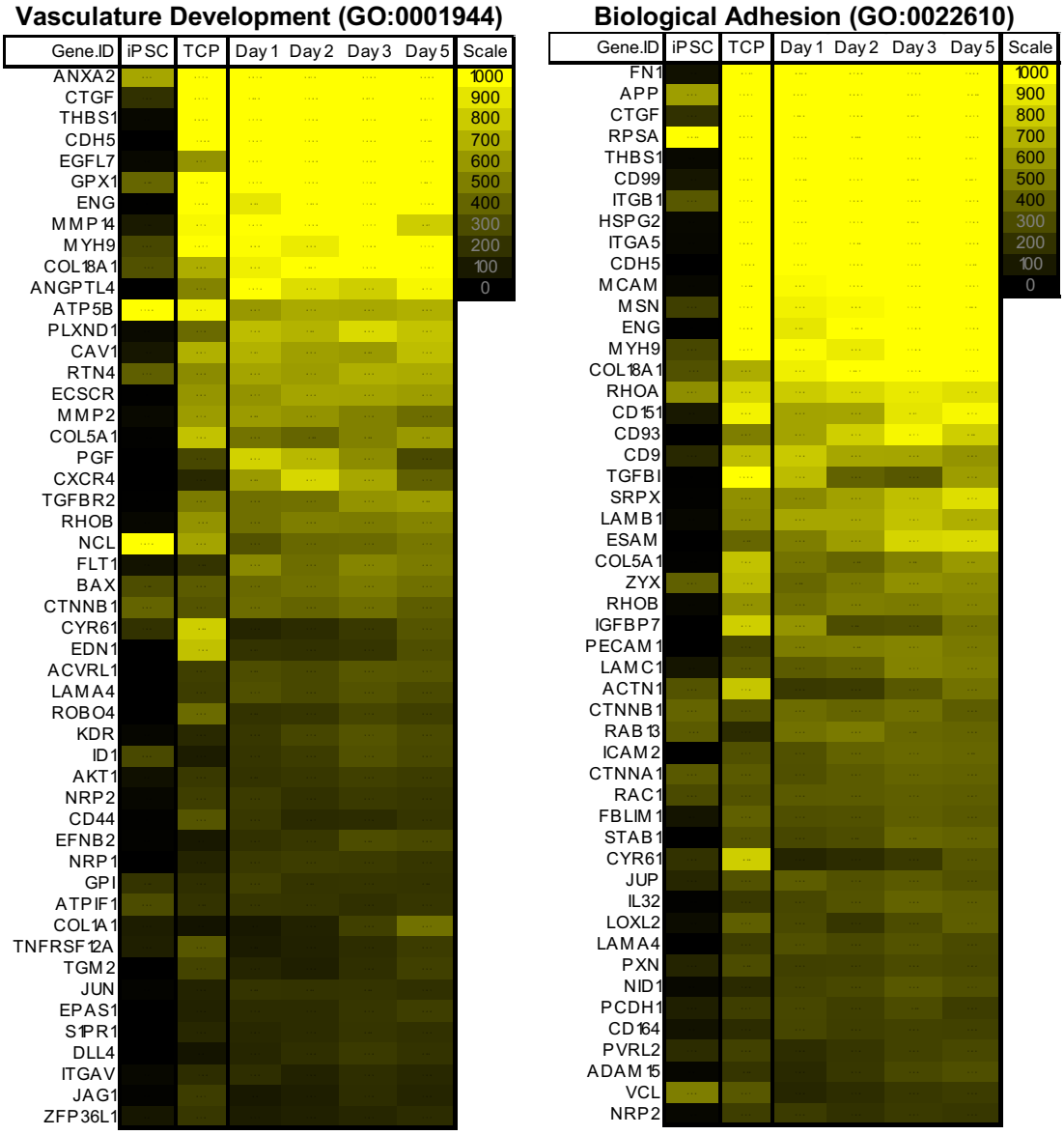

Figure S5.2 The top 50 ranked vasculature development and biological adhesion genes for iPSC-ECs in 2D and 3D culture. The top 50 expressed genes within the Gene Ontology (GO) categories "vasculature development" (GO:0001944) and "biological adhesion" (GO:0022610) ranked by mean normalized expression (TPM) for iPSC-ECs cultured on tissue culture polystyrene (2D) and in synthetic ECM (3D, Days 1, 2, 3, and 5). Normalized gene expression is reported as "transcripts per million" (TPM), where the value for each gene is scaled such that the sum of expression for all 19,084 genes equals one million (see Suppl. Table 1 for full list). Gene expression is also shown for undifferentiated iPS cells (iPSC) in normal culture (the TPM values were not included when ranking the top 50 expressed genes).

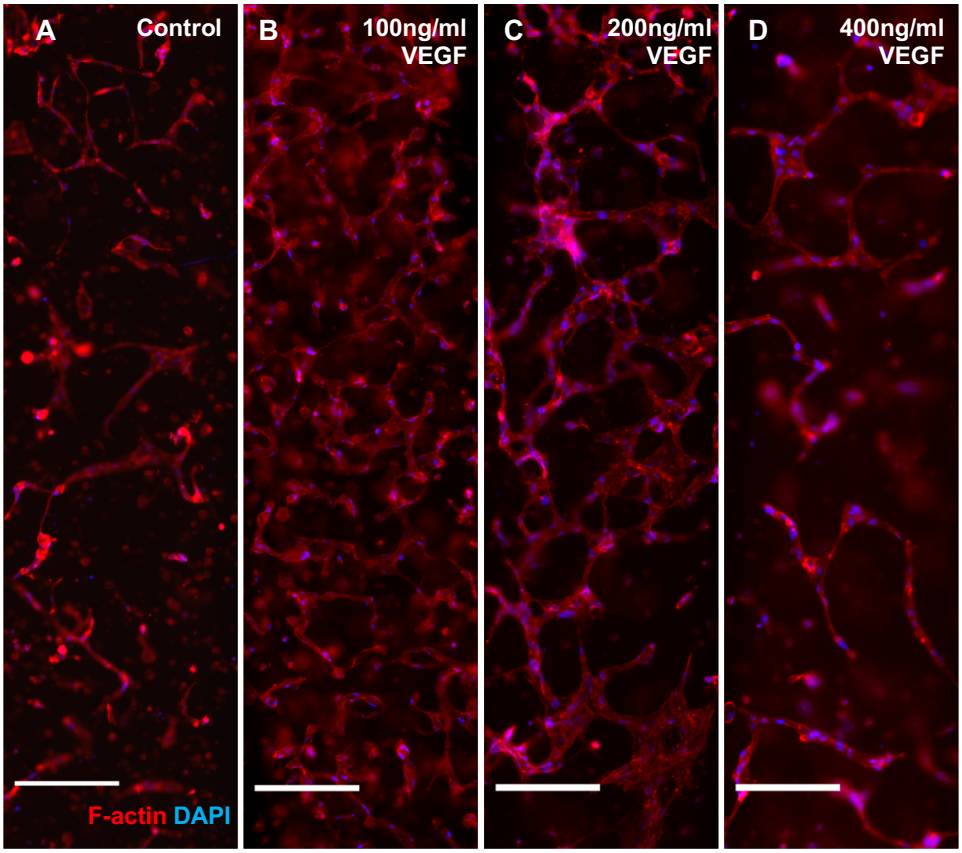

Figure S5.3 Vascular network formation by iPSC-ECs within a microfluidic channel is most pronounced at intermediate VEGF concentration. Phalloidin (F-actin, red) and DAPI (nuclei, blue) staining for iPSC-ECs cultured in in 50% crosslinked PEG hydrogels. $1x10^7$ iPSC-ECs per mL were cultured for 8 days in **(A)** basal medium ("Control", contains 5 ng/mL VEGF) or medium that was supplemented with **(B)** 100 ng/mL VEGF, **(C)** 200 ng/mL VEGF, or **(D)** 400 ng/mL VEGF. Images were collected using an EVOS FL fluorescence microscope. **Scale bars**: 250 μm.

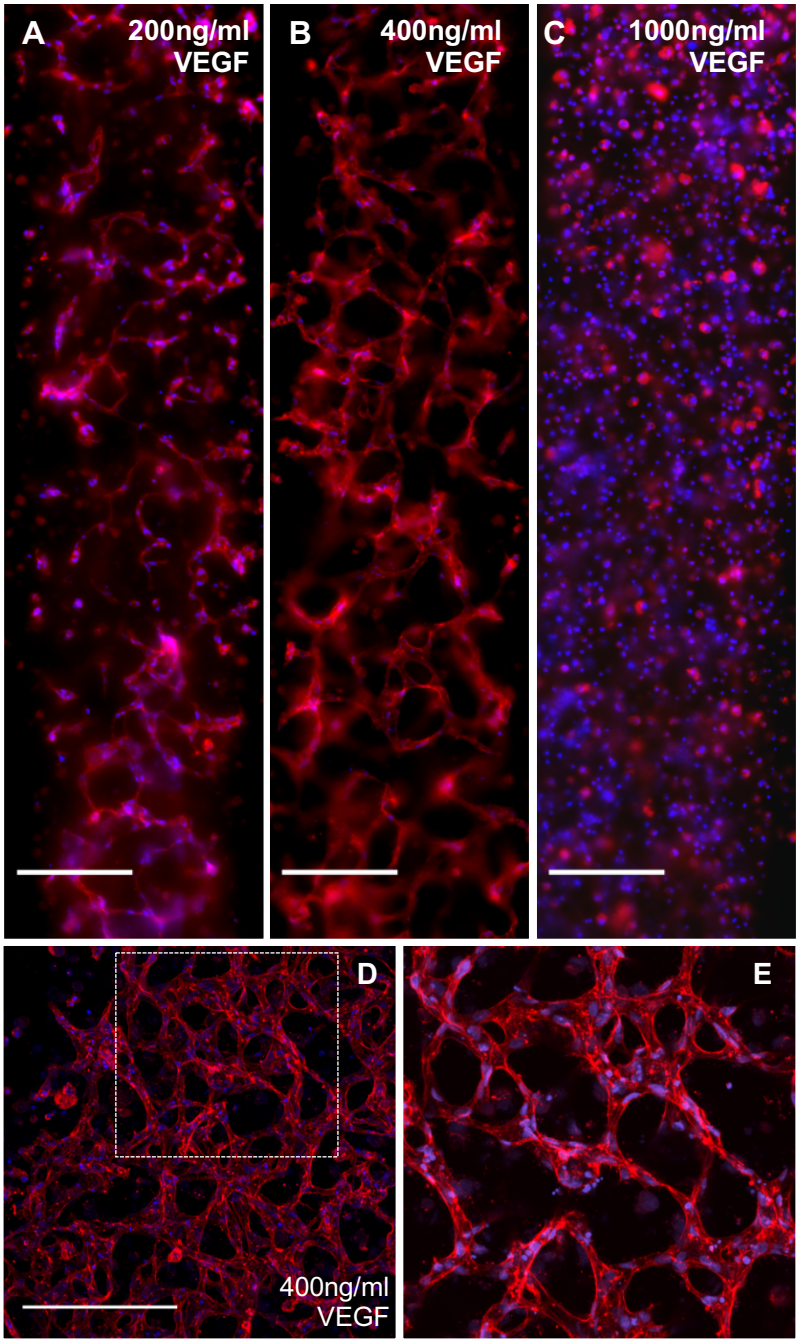

Figure S5.4 Vascular network formation by iPSC-ECs seeded at high density shifts the optimal VEGF dose to higher concentration. Phalloidin (F-actin, red) and DAPI (nuclei, blue) staining for $8.5x10^7$ iPSC-ECs per mL in 50% crosslinked PEG hydrogels. Cells were cultured for 9 days in basal medium (contains 5 ng/mL VEGF) that was supplemented with **(A)** 200 ng/mL VEGF, **(B)** 400 ng/mL VEGF, or **(C)** 1000 ng/mL VEGF. Images in **A-C** were collected using an EVOS FL fluorescence microscope. **(D, E)** Higher resolution confocal images for the 200 ng/mL VEGF condition for a (D) 75 μm and (E) 25 μm thick z-stack. The boxed region in **D** is shown in **E**. **Scale bars**: 250 μm.

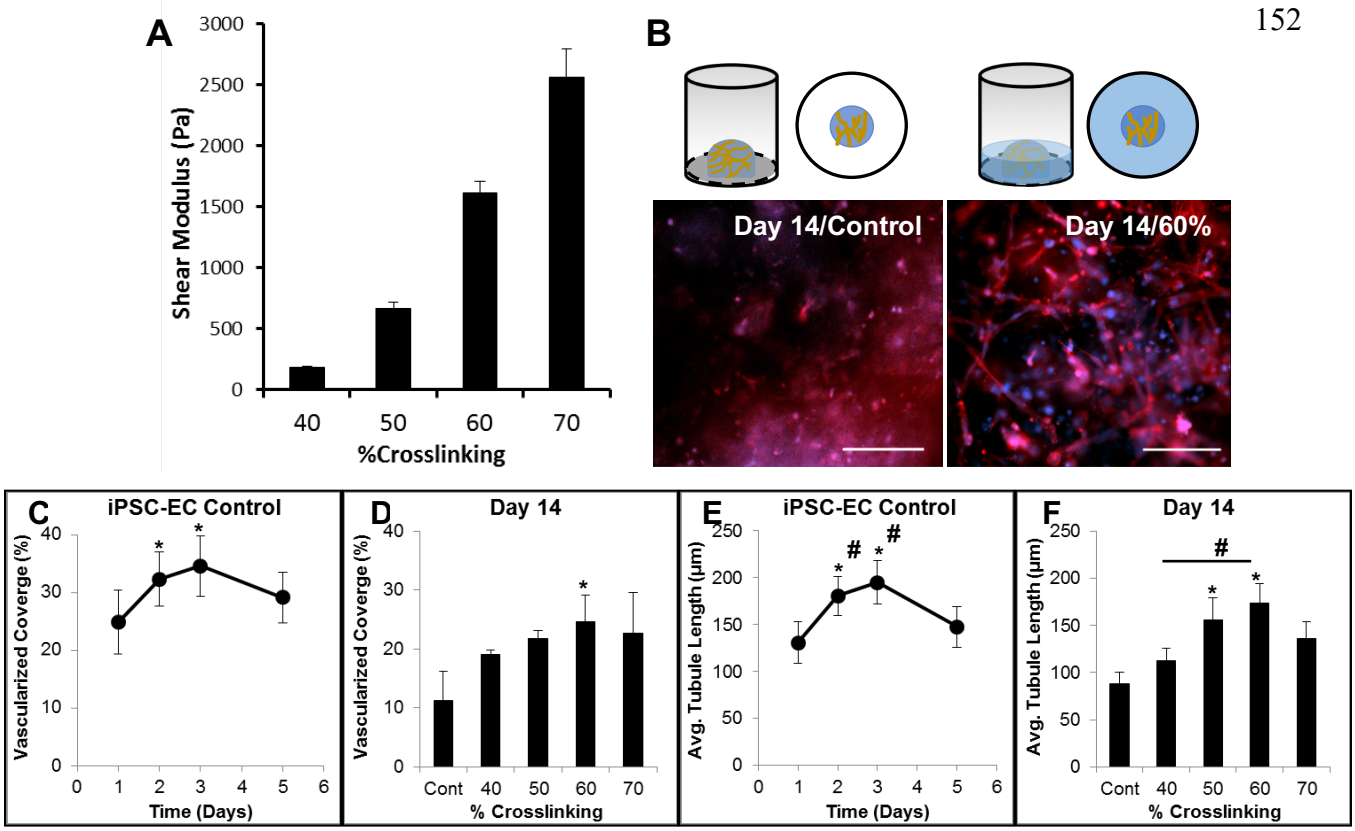

Figure S5.5 Vascular network stability is improved by adding a supporting PEG layer. (A) Shear modulus (Mean±S.D.; n = 3 hydrogels) for PEG hydrogels with 40-70% MMP-degradable peptide crosslinks (molar ratio Thiol:Norbornene groups). **(B)** Phalloidin (F-actin, red) and DAPI (nuclei, blue) staining for iPSC-ECs encapsulated in PEG hydrogels and spotted on the bottom of a tissue culture polystyrene plate and cultured for 14 days without (Control) or with a supporting PEG hydrogel layer (60% crosslinked supporting layer shown). A PEG hydrogel supporting layer (100 μL) was added two days after iPSC-ECs were encapsulated in 50% crosslinked PEG hydrogels to permit initial vascular network formation. The PEG hydrogel supporting layer was prepared without CRGDS adhesion peptide to minimize sprouting. **Scale bars**: 100 μm. **(C-F)** Vascular network structure was quantified using CD31 immunofluorescence images. A Nikon TI Eclipse fluorescence microscope was used to image each hydrogel with a z-stack depth of 900 μm (20 μm slices). NIS-Elements (Nikon) software was used to generate a maximum intensity projection image from the z-stack with fluorescent peaks detected (matrix level = 3, count = 12). Each image was then thresholded (threshold lower limit = 180-260, cutoff length = 20 μm), and all detected vascular structures were skeletonized and pruned (pruning = 10). Average structure length and area was automatically calculated for a 3700 x 1900-pixel (3367 x 1729 μm) region of interest (ROI) using the "Automated Measurement" feature. **(C,D)** Vascular coverage (Mean ± S.D.; ≥ 4 replicate samples) **(C)** during the first 5 days of culture without a supporting layer (* = significance vs. Day 1) and **(D)** after 14 days of culture without ("Cont") or with a supporting layer (40-70% crosslinking; * = significance vs. Cont). **(E,F)** Average tubule length (Mean ± S.D.; ≥ 4 replicate samples) **(E)** during the first 5 days of culture without a supporting layer (* = significance vs. Day 1; # = significance vs. Day 5) and **(F)** after 14 days of culture without ("Cont") or with a supporting layer (40-70% crosslinking; * = significance vs. Cont ; # = significance 40 vs 60% crosslinking). Statistical significance was calculated using a one-way ANOVA with a post hoc Tukey-Kramer test for individual comparisons (α = 0.05).

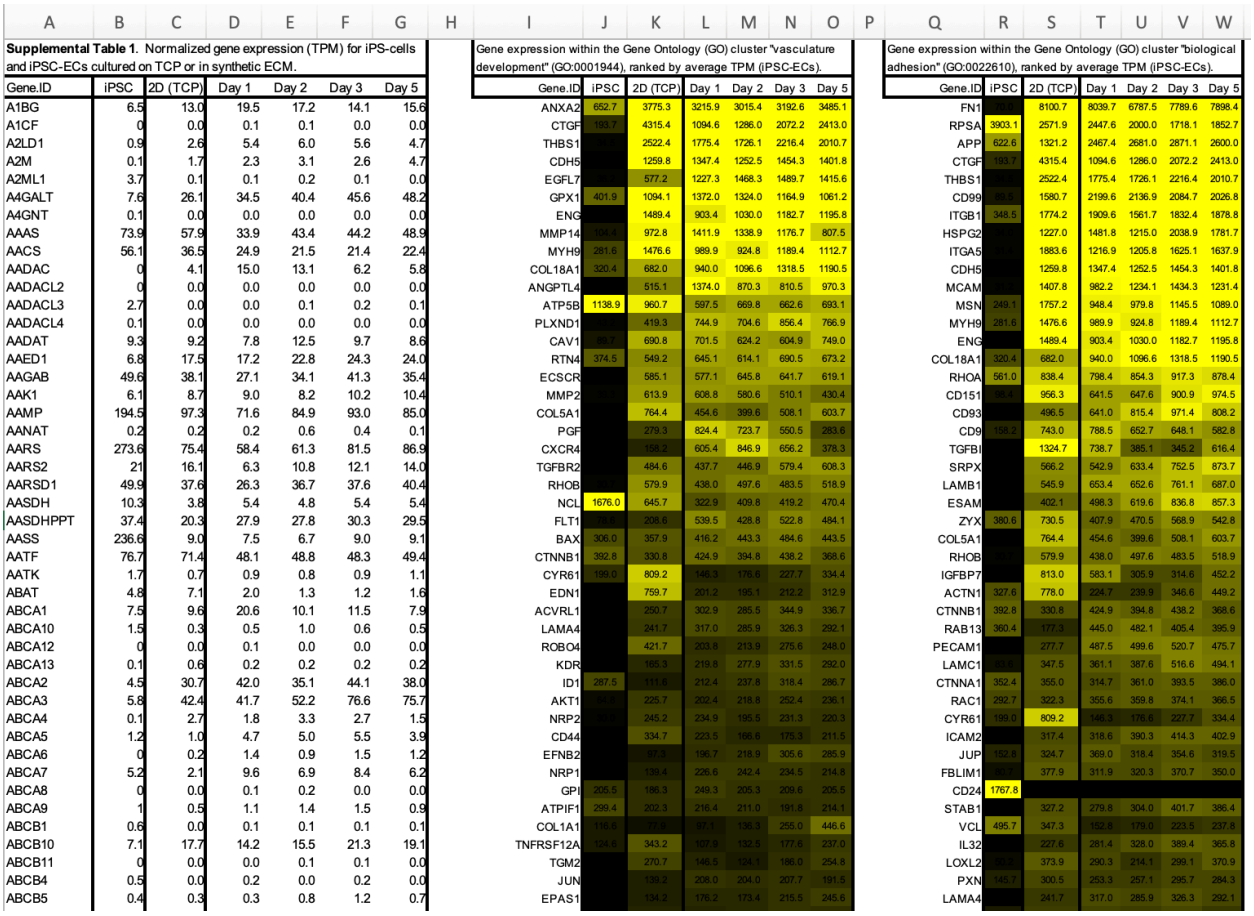

Supplemental Table 1. Normalized gene expression (TPM) for iPS-cells and iPSC-ECs cultured on TCP or in synthetic ECM.

Gene.ID	iPSC	2D (TCP)	Day 1	Day 2	Day 3	Day 5
A1BG	6.5	13.0	19.5	17.2	14.1	15.6
A1CF	0	0.0	0.1	0.1	0.0	0.0
A2LD1	0.9	2.6	5.4	6.0	5.6	4.7
A2M	0.1	1.7	2.3	3.1	2.6	4.7
A2ML1	3.7	0.1	0.1	0.2	0.1	0.0
A4GALT	7.6	26.1	34.5	40.4	45.6	48.2
A4GNT	0.1	0.0	0.0	0.0	0.0	0.0
AAAS	73.9	57.9	33.9	43.4	44.2	48.9
AACS	56.1	36.5	24.9	21.5	21.4	22.4
AADAC	0	4.1	15.0	13.1	6.2	5.8
AADACL2	0	0.0	0.0	0.0	0.0	0.0
AADACL3	2.7	0.0	0.0	0.1	0.2	0.1
AADACL4	0.1	0.0	0.0	0.0	0.0	0.0
AADAT	9.3	9.2	7.8	12.5	9.7	8.6
AAED1	6.8	17.5	17.2	22.8	24.3	24.0
AAGAB	49.6	38.1	27.1	34.1	41.3	35.4
AAK1	6.1	8.7	9.0	8.2	10.2	10.4
AAMP	194.5	97.3	71.6	84.9	93.0	85.0
AANAT	0.2	0.2	0.2	0.6	0.4	0.1
AARS	273.6	75.4	58.4	61.3	81.5	86.9
AARS2	21	16.1	6.3	10.8	12.1	14.0
AARSD1	49.9	37.6	26.3	36.7	37.6	40.4
AASDH	10.3	3.8	5.4	4.8	5.4	5.4
AASDHPPT	37.4	20.3	27.9	27.8	30.3	29.5
AASS	236.6	9.0	7.5	6.7	9.0	9.1
AATF	76.7	71.4	48.1	48.8	48.3	49.4
AATK	1.7	0.7	0.9	0.8	0.9	1.1
ABAT	4.8	7.1	2.0	1.3	1.2	1.6
ABCA1	7.5	9.6	20.6	10.1	11.5	7.9
ABCA10	1.5	0.3	0.5	1.0	0.6	0.5
ABCA12	0	0.0	0.1	0.0	0.0	0.0
ABCA13	0.1	0.6	0.2	0.2	0.2	0.2
ABCA2	4.5	30.7	42.0	35.1	44.1	38.0
ABCA3	5.8	42.4	41.7	52.2	76.6	75.7
ABCA4	0.1	2.7	1.8	3.3	2.7	1.5
ABCA5	1.2	1.0	4.7	5.0	5.5	3.9
ABCA6	0	0.2	1.4	0.9	1.5	1.2
ABCA7	5.2	2.1	9.6	6.9	8.4	6.2
ABCA8	0	0.0	0.1	0.2	0.0	0.0
ABCA9	1	0.5	1.1	1.4	1.5	0.9
ABCB1	0.6	0.0	0.1	0.1	0.1	0.1
ABCB10	7.1	17.7	14.2	15.5	21.3	19.1
ABCB11	0	0.0	0.0	0.1	0.1	0.0
ABCB4	0.5	0.0	0.2	0.0	0.2	0.0
ABCB5	0.4	0.3	0.3	0.8	1.2	0.7

Gene expression within the Gene Ontology (GO) cluster "vasculature development" (GO:0001944), ranked by average TPM (iPSC-ECs).

Gene.ID	iPSC	2D (TCP)	Day 1	Day 2	Day 3	Day 5
ANXA2	652.7	3775.3	3215.9	3015.4	3192.6	3485.1
CTGF	193.7	4315.4	1094.6	1286.0	2072.2	2413.0
THBS1		2522.4	1775.4	1726.1	2216.4	2010.7
CDH5		1259.8	1347.4	1252.5	1454.3	1401.8
EGFL7		577.2	1227.3	1468.3	1489.7	1415.6
GPX1	401.9	1094.1	1372.0	1324.0	1164.9	1061.2
ENG		1489.4	903.4	1030.0	1182.7	1195.8
MMP14	104.4	972.8	1411.9	1338.9	1176.7	807.5
MYH9	281.6	1476.6	989.9	924.8	1189.4	1112.7
COL18A1	320.4	682.0	940.0	1096.6	1318.5	1190.5
ANGPTL4		515.1	1374.0	870.3	810.5	970.3
ATP5B	1138.9	960.7	597.5	669.8	662.6	693.1
PLXND1		419.3	744.9	704.6	856.4	766.9
CAV1	88.7	690.8	701.5	624.2	604.9	749.0
RTN4	374.5	549.2	645.1	614.1	690.5	673.2
ECSCR		585.1	577.1	645.8	641.7	619.1
MMP2		613.9	608.8	580.6	510.1	430.4
COL5A1		764.4	454.6	399.6	508.1	603.7
PGF		279.3	824.4	723.7	550.5	283.6
CXCR4		158.2	605.4	846.9	656.2	378.3
TGFBR2		484.6	437.7	446.9	579.4	608.3
RHOB		579.9	438.0	497.6	483.5	518.9
NCL	1676.0	645.7	322.9	409.8	419.2	470.4
FLT1	45.5	208.6	539.5	428.8	522.8	484.1
BAX	306.0	357.9	416.2	443.3	484.6	443.5
CTNNB1	392.8	330.8	424.9	394.8	438.2	368.6
CYR61	199.0	809.2	146.3	176.6	227.7	334.4
EDN1		759.7	201.2	195.1	212.2	312.9
ACVRL1		250.7	302.9	285.5	344.9	336.7
LAMA4		241.7	317.0	285.9	326.3	292.1
ROBO4		421.7	203.8	213.9	275.6	248.0
KDR		165.3	219.8	277.9	331.5	292.0
ID1	287.5	111.8	212.4	237.8	318.4	286.7
AKT1	56.0	225.7	202.4	218.8	252.4	236.1
NRP2	45.0	245.2	234.9	195.5	231.3	220.3
CD44		334.7	223.5	166.6	175.3	211.5
EFNB2		87.3	196.7	218.9	305.6	285.9
NRP1		139.4	226.6	242.4	234.5	214.8
GPI	205.5	186.3	249.3	205.3	209.6	205.5
ATPIF1	299.4	202.3	216.4	211.0	191.8	214.1
COL1A1	118.6	27.5	97.1	136.3	255.0	446.6
TNFRSF12A	124.6	343.2	107.9	132.5	177.6	237.0
TGM2		270.7	146.5	124.1	186.0	254.8
JUN		139.2	208.0	204.0	207.7	191.5
EPAS1		134.2	176.2	173.4	215.5	245.6

Gene expression within the Gene Ontology (GO) cluster "biological adhesion" (GO:0022610), ranked by average TPM (iPSC-ECs).

Gene.ID	iPSC	2D (TCP)	Day 1	Day 2	Day 3	Day 5
FN1	2.0	8100.7	8039.7	6787.5	7789.6	7898.4
RPSA	3903.1	2571.9	2447.6	2000.0	1718.1	1852.7
APP	622.6	1321.2	2467.4	2681.0	2871.1	2600.0
CTGF	193.7	4315.4	1094.6	1286.0	2072.2	2413.0
THBS1		2522.4	1775.4	1726.1	2216.4	2010.7
CD99	28.9	1580.7	2199.6	2136.9	2084.7	2026.8
ITGB1	348.5	1774.2	1909.6	1561.7	1832.4	1878.8
HSPG2		1227.0	1481.8	1215.0	2038.9	1781.7
ITGA5		1883.6	1216.9	1205.8	1625.1	1637.9
CDH5		1259.8	1347.4	1252.5	1454.3	1401.8
MCAM		1407.8	982.2	1234.1	1434.3	1231.4
MSN	249.1	1757.2	948.4	979.8	1145.5	1089.0
MYH9	281.6	1476.6	989.9	924.8	1189.4	1112.7
ENG		1489.4	903.4	1030.0	1182.7	1195.8
COL18A1	320.4	682.0	940.0	1096.6	1318.5	1190.5
RHOA	561.0	838.4	798.4	854.3	917.3	878.4
CD151	55.4	956.3	641.5	647.6	900.9	974.5
CD93		496.5	641.0	815.4	971.4	808.2
CD9	158.2	743.0	788.5	652.7	648.1	582.8
TGFBI		1324.7	738.7	385.1	345.2	616.4
SRPX		566.2	542.9	633.4	752.5	873.7
LAMB1		545.9	653.4	652.6	761.1	687.0
ESAM		402.1	498.3	619.6	836.8	857.3
ZYX	380.6	730.5	407.9	470.5	568.9	542.8
COL5A1		764.4	454.6	399.6	508.1	603.7
RHOB		579.9	438.0	497.6	483.5	518.9
IGFBP7		813.0	583.1	305.9	314.6	452.2
ACTN1	327.6	778.0	224.7	239.9	346.6	449.2
CTNNB1	392.8	330.8	424.9	394.8	438.2	368.6
RAB13	360.4	177.3	445.0	482.1	405.4	395.9
PECAM1		277.7	487.5	499.6	520.7	475.7
LAMC1	83.6	347.5	361.1	387.6	516.6	494.1
CTNNA1	352.4	355.0	314.7	361.0	393.5	386.0
RAC1	292.7	322.3	355.6	359.8	374.1	366.5
CYR61	199.0	809.2	146.3	176.6	227.7	334.4
ICAM2		317.4	318.6	390.3	414.3	402.9
JUP	152.8	324.7	369.0	318.4	354.6	319.5
FBLIM1	56.2	377.9	311.9	320.3	370.7	350.0
CD24	1767.8					
STAB1		327.2	279.8	304.0	401.7	386.4
VCL	495.7	347.3	152.8	179.0	223.5	237.8
IL32		227.6	281.4	328.0	389.4	365.8
LOXL2	50.2	373.9	290.3	214.1	299.1	370.9
PXN	145.7	300.5	253.3	257.1	295.7	284.3
LAMA4		241.7	317.0	285.9	326.3	292.1

Table S5.1 Normalized gene expression (TPM) for undifferentiated iPS cells and iPSC-ECs in 2D or 3D culture. Normalized gene expression in transcripts per million (TPM) for human induced pluripotent stem (iPS) cells and iPS cell-derived endothelial cells (iPSC-ECs) cultured on tissue culture polystyrene (TCP) or in 50% crosslinked PEG hydrogels for up to 5 days. Normalized gene expression is reported as "transcripts per million" (TPM), where the value for each gene is scaled such that the sum of expression for all 19,084 genes equals one million. **Columns I-O**: Gene expression within the Gene Ontology (GO) cluster "vasculature development" (GO:0001944), ranked by average TPM (iPSC-ECs). **Columns Q-W**: Gene expression within the Gene Ontology (GO) cluster "biological adhesion" (GO:0022610), ranked by average TPM (iPSC-ECs).

To view the whole table please go to:
https://www.ncbi.nlm.nih.gov/pmc/articles/PMC4829480/bin/NIHMS768241-supplement-2.xlsx

B	C	D	E	F	G	H	I	J	K	L	M	N	O	P
Upregulated (iPSC-EC > iPS cells)								**Downregulated (iPS cells > iPSC-EC)**						
TCP	Day 1	Day 2	Day 3	Day 5	All 3D	ALL samples		TCP	Day 1	Day 2	Day 3	Day 5	vs ALL 3D	vs ALL
974	1047	1052	988	1096	852	732		943	761	851	722	909	583	554
A2M	A2M	A2M	A2M	A2M	A2M	A2M		A2ML1	A2ML1	AASS	A2ML1	A2ML1	AASS	AASS
AADAC	AADAC	AADAC	AADAC	AADAC	AADAC	AADAC		AADACL3	AADACL3	ACAP1	AASS	AADACL3	ACAP1	ACAP1
ABCA13	ABCA2	ABCA2	ABCA2	ABCA2	ABCA2	ABCA2		AASS	AASS	ACAT2	ACAP1	AASS	ACAT2	ACOXL
ABCA2	ABCA3	ABCA3	ABCA3	ABCA3	ABCA3	ABCA3		ACAP1	ACAP1	ACOXL	ACAT2	ACAP1	ACOXL	ACTA1
ABCA3	ABCA4	ABCA4	ABCA4	ABCA4	ABCA4	ABCA4		ACOXL	ACAT2	ACSS3	ACOXL	ACAT2	ACTA1	ACTC1
ABCA4	ABCA6	ABCA6	ABCA6	ABCA6	ABCA6	ABCC3		ACSS3	ACOXL	ACTA1	ACTA1	ACOXL	ACTC1	ACTN3
ABCC3	ABCC3	ABCC3	ABCC3	ABCC3	ABCC3	ABCG1		ACTA1	ACTA1	ACTC1	ACTC1	ACSS3	ACTN3	ADAMTS19
ABCG1	ABCG1	ABCG1	ABCG1	ABCG1	ABCG1	ABI3		ACTC1	ACTC1	ACTN3	ACTN3	ACTA1	ADAMTS19	ADAMTS20
ABI3	ABI3	ABHD6	ABI3	ABHD6	ABI3	ABLIM3		ACTN3	ACTN3	ADAM33	ADAMTS15	ACTC1	ADAMTS20	ADAMTS8
ABI3BP	ABLIM3	ABI3	ABLIM3	ABI3	ABLIM3	ACSL5		ACVR2B	ADAM33	ADAMTS19	ADAMTS19	ACTN3	ADAMTS8	ADCY2
ABLIM3	ACE	ABLIM3	ACE	ABLIM3	ACE	ACTA2		ADAM22	ADAMTS19	ADAMTS20	ADAMTS20	ADAM22	ADCY2	ADCY5
ACSL5	ACSL5	ACE	ACSL5	ACE	ACSL5	ACVRL1		ADAM33	ADAMTS20	ADAMTS5	ADAMTS5	ADAM33	ADCY5	ADCY8
ACTA2	ACTA2	ACSL5	ACTA2	ACSL5	ACTA2	ADAM12		ADAMTS16	ADAMTS8	ADAMTS8	ADAMTS8	ADAMTS15	ADCY8	ADD2
ACVRL1	ACVRL1	ACTA2	ACVRL1	ACTA2	ACVRL1	ADAM9		ADAMTS19	ADCY2	ADCY1	ADCY2	ADAMTS19	ADD2	ADRA2B
ADAM12	ADAM12	ACVRL1	ADAM12	ACVRL1	ADAM12	ADAMTS6		ADAMTS20	ADCY5	ADCY2	ADCY5	ADAMTS20	ADRA2B	AFP
ADAM15	ADAM32	ADAM12	ADAM15	ADAM12	ADAM32	ADAMTS9		ADAMTS4	ADCY8	ADCY5	ADCY8	ADAMTS5	AFP	AIF1L
ADAM9	ADAM9	ADAM15	ADAM32	ADAM15	ADAM9	ADCY4		ADAMTS5	ADD2	ADCY8	ADD2	ADAMTS8	AIF1L	AIM1L
ADAMTS18	ADAMTS6	ADAM32	ADAM9	ADAM32	ADAMTS6	ADCY7		ADAMTS8	ADRA2B	ADD2	ADORA1	ADCY1	AIM1L	ALPL
ADAMTS6	ADAMTS9	ADAM9	ADAMTS6	ADAM9	ADAMTS9	AFAP1L1		ADCY2	AFP	ADRA2B	ADRA2B	ADCY2	ALPL	ANK1
ADAMTS9	ADCY4	ADAMTS6	ADAMTS9	ADAMTS6	ADCY4	AGPAT3		ADCY5	AIF1L	ADRBK2	ADRA2C	ADCY5	ANK1	ANKRD24
ADAMTSL1	ADCY7	ADAMTS9	ADCY4	ADAMTS9	ADCY7	AHNAK		ADCY8	AIM1L	AFP	AFP	ADCY8	ANKRD24	AP1M2
ADCY4	ADRA1B	ADCY4	ADCY7	ADAMTSL1	AFAP1L1	AHRR		ADCYAP1R1	ALPL	AIF1	AGAP4	ADD2	AP1M2	AP3B2
ADCY7	AFAP1L1	ADCY7	AFAP1L1	ADCY4	AGFG2	ALOX5AP		ADD2	ANK1	AIF1L	AIF1L	ADORA1	AP3B2	APOC1
ADRA1B	AGFG2	ADRA1B	AGFG2	ADCY7	AGPAT3	AMY1C		ADRA2A	ANKRD24	AIM1L	AIM1L	ADRA2A	APOC1	APOE
ADRA1D	AGPAT3	AFAP1L1	AGPAT3	ADRA1B	AGTR1	ANGPT2		ADRA2B	AP1M2	ALPL	ALPL	ADRA2B	APOE	ARHGAP8
ADTRP	AGTR1	AGFG2	AGTR1	AFAP1L1	AHNAK	ANGPTL4		ADRBK2	AP3B2	AMPH	AMPH	ADRA2C	ARHGAP44	ARHGEF35
AFAP1L1	AHNAK	AGPAT3	AHNAK	AGFG2	AHRR	ANKRD1		AFP	APOC1	ANK1	ANK1	ADRBK2	ARHGAP8	ARHGEF5
AGPAT3	AHNAK2	AGTR1	AHNAK2	AGPAT3	ALOX5AP	ANKRD44		AGAP4	APOE	ANK2	ANK2	AFP	ARHGEF35	ART5
AHNAK	AHRR	AHNAK	AHR	AGTR1	AMY1C	ANKRD52		AIF1	ARHGAP44	ANKRD24	ANK3	AGAP4	ARHGEF5	ASS1
AHNAK2	AK1	AHR	AHRR	AHNAK	ANGPT2	ANKRD55		AIF1L	ARHGAP8	ANO5	ANKRD24	AIF1	ART5	ATP1A2
AHRR	AKAP12	AHRR	AK1	AHNAK2	ANGPTL4	ANPEP		AIM1L	ARHGEF35	AP1M2	ANO5	AIF1L	ASS1	ATP1A3
AKAP12	ALOX5AP	AK1	ALOX5AP	AHR	ANKRD1	ANTXR2		ALPL	ARHGEF4	AP3B2	AP1M2	AIM1L	ATP1A2	B3GALT1
AKAP2	AMY1C	ALOX5AP	AMY1C	AHRR	ANKRD44	ANXA2R		AMT	ARHGEF5	APOC1	AP3B2	ALPL	ATP1A3	B3GALT5
ALOX5AP	ANGPT2	AMY1C	ANGPT2	ALOX5AP	ANKRD52	APBA1		ANK1	ARSI	APOE	APOC1	ANK1	B3GALT1	B3GNT7
AMY1C	ANGPTL4	ANGPT2	ANGPTL4	AMY1C	ANKRD55	APLN		ANKRD24	ART5	ARHGAP44	APOE	ANK2	B3GALT5	B4GALNT3
ANGPT2	ANKRD1	ANGPTL4	ANKRD1	ANGPT2	ANPEP	ARHGAP24		ANKS1B	ARTN	ARHGAP8	ARHGAP44	ANK3	B3GNT7	BAIAP2L1
ANGPTL4	ANKRD33	ANKMY1	ANKRD33	ANGPTL4	ANTXR2	ARHGAP29		ANO2	ASS1	ARHGEF35	ARHGAP8	ANKRD24	B4GALNT3	BEX1
ANKRD1	ANKRD37	ANKRD1	ANKRD44	ANKRD1	ANXA2R	ARHGAP31		ANO5	ATCAY	ARHGEF5	ARHGEF35	ANO5	BAIAP2L1	BMPR1A
ANKRD20A3	ANKRD44	ANKRD33	ANKRD52	ANKRD44	APBA1	ARHGDIB		ANO9	ATP1A2	ARNT2	ARHGEF5	ANO9	BEX1	BSPRY
ANKRD44	ANKRD52	ANKRD44	ANKRD55	ANKRD52	APLN	ARHGEF15		AP1M2	ATP1A3	ARSI	ARNT2	AP1M2	BMPR1A	C10orf82
ANKRD52	ANKRD55	ANKRD52	ANPEP	ANKRD55	APOLD1	ARPC4-TTLL3		AP3B2	ATRNL1	ART5	ART5	AP3B2	BSPRY	C19orf46
ANKRD55	ANPEP	ANKRD55	ANTXR2	ANPEP	AQP1	ARRB1		APOC1	AURKB	ASPM	ASS1	APOC1	C10orf82	C1orf106
ANPEP	ANTXR2	ANPEP	ANXA2R	ANTXR2	AQP7	ARSD		APOE	B3GALT1	ASS1	ATP1A2	APOE	C15orf42	C1orf116
ANTXR2	ANXA2R	ANTXR2	APBA1	ANXA2R	ARHGAP24	ARSJ		ARHGAP8	B3GALT5	ATCAY	ATP1A3	ARAP2	C19orf46	C1orf172

R	S	T	U	V	W	X	Y	Z	AA	AB	AC	AD

iPSC-ECs UPREGULATED vs. iPSC (Overlapping genes for ALL 2D and 3D samples, see full list in column H).

Category	Term	Count	%	PValue	Genes	List Total	Pop Hits	Pop Total	Fold Enrichment	Bonferroni	Benjamini	FDR
GOTERM_BP_FAT	GO:0001944~vasculature development	58	8.1	4.4E-27	NRP1, ACVRL	6E+02	3E+02	1E+04	6E+00	1E-23	1.3E-23	8E-24
GOTERM_BP_FAT	GO:0001568~blood vessel development	57	8.0	8.9E-27	NRP1, ACVRL	6E+02	2E+02	1E+04	6E+00	3E-23	1.3E-23	2E-23
GOTERM_BP_FAT	GO:0048514~blood vessel morphogenesis	46	6.4	2.0E-20	EMCN, ACVRL	6E+02	2E+02	1E+04	5E+00	6E-17	2.0E-17	4E-17
GOTERM_BP_FAT	GO:0051270~regulation of cell motion	41	5.7	8.2E-18	DLC1, PLXNA3	6E+02	2E+02	1E+04	5E+00	2E-14	6.1E-15	1E-14
GOTERM_BP_FAT	GO:0030334~regulation of cell migration	38	5.3	2.2E-17	DLC1, ACVRL	6E+02	2E+02	1E+04	5E+00	6E-14	1.3E-14	4E-14
GOTERM_BP_FAT	GO:0040012~regulation of locomotion	39	5.5	2.8E-16	DLC1, ACVRL	6E+02	2E+02	1E+04	5E+00	7E-13	1.1E-13	4E-13
GOTERM_BP_FAT	GO:0001525~angiogenesis	34	4.8	7.8E-16	EMCN, ACVRL	6E+02	1E+02	1E+04	6E+00	2E-12	3.3E-13	1E-12
GOTERM_BP_FAT	GO:0009611~response to wounding	66	9.2	1.2E-15	F2RL2, F2RL3,	6E+02	5E+02	1E+04	3E+00	4E-12	4.5E-13	2E-12
GOTERM_BP_FAT	GO:0035295~tube development	38	5.3	1.8E-13	DLC1, CAV2, N	6E+02	2E+02	1E+04	4E+00	5E-10	5.8E-11	3E-10
GOTERM_BP_FAT	GO:0042127~regulation of cell proliferation	79	11.0	1.9E-13	DLC1, NOG, S	6E+02	8E+02	1E+04	2E+00	6E-10	5.6E-11	3E-10
GOTERM_BP_FAT	GO:0042060~wound healing	35	4.9	3.2E-13	F2RL2, F2RL3,	6E+02	2E+02	1E+04	4E+00	9E-10	8.6E-11	6E-10
GOTERM_BP_FAT	GO:0009792~embryonic development ending in birth or egg hatchi	46	6.4	1.5E-12	DLC1, NOG, A	6E+02	3E+02	1E+04	3E+00	4E-09	3.7E-10	3E-09
GOTERM_BP_FAT	GO:0043009~chordate embryonic development	45	6.3	4.2E-12	DLC1, NOG, A	6E+02	3E+02	1E+04	3E+00	1E-08	9.6E-10	8E-09
GOTERM_BP_FAT	GO:0001763~morphogenesis of a branching structure	21	2.9	9.4E-12	NRP1, TBX3, C	6E+02	7E+01	1E+04	7E+00	3E-08	2.0E-09	2E-08
GOTERM_BP_FAT	GO:0001501~skeletal system development	43	6.0	1.8E-11	NOG, PTGS2, I	6E+02	3E+02	1E+04	3E+00	5E-08	3.6E-09	3E-08
GOTERM_BP_FAT	GO:0007155~cell adhesion	69	9.7	2.0E-11	DLC1, NRP1, I	6E+02	7E+02	1E+04	2E+00	6E-08	3.8E-09	4E-08
GOTERM_BP_FAT	GO:0022610~biological adhesion	69	9.7	2.1E-11	DLC1, NRP1, I	6E+02	7E+02	1E+04	2E+00	6E-08	3.7E-09	4E-08
GOTERM_BP_FAT	GO:0048754~branching morphogenesis of a tube	19	2.7	6.6E-11	NRP1, TBX3, F	6E+02	7E+01	1E+04	7E+00	2E-07	1.1E-08	1E-07
GOTERM_BP_FAT	GO:0007389~pattern specification process	38	5.3	6.8E-11	NOG, MFNG, T	6E+02	3E+02	1E+04	3E+00	2E-07	1.1E-08	1E-07
GOTERM_BP_FAT	GO:0060429~epithelium development	34	4.8	2.1E-10	DLC1, PGF, H(	6E+02	2E+02	1E+04	4E+00	6E-07	3.1E-08	4E-07
GOTERM_BP_FAT	GO:0035239~tube morphogenesis	25	3.5	2.9E-10	DLC1, NRP1, F	6E+02	1E+02	1E+04	5E+00	8E-07	4.0E-08	5E-07
GOTERM_BP_FAT	GO:0048598~embryonic morphogenesis	40	5.6	2.9E-10	DLC1, NOG, T:	6E+02	3E+02	1E+04	3E+00	9E-07	3.9E-08	5E-07
GOTERM_BP_FAT	GO:0051094~positive regulation of developmental process	37	5.2	8.4E-10	IL6ST, HOXA1	6E+02	3E+02	1E+04	3E+00	2E-06	1.1E-07	2E-06
GOTERM_BP_FAT	GO:0009891~positive regulation of biosynthetic process	64	9.0	2.0E-09	MEF2C, ACVR	6E+02	7E+02	1E+04	2E+00	6E-06	2.5E-07	4E-06
GOTERM_BP_FAT	GO:0008284~positive regulation of cell proliferation	46	6.4	2.0E-09	NOG, S100A6,	6E+02	4E+02	1E+04	3E+00	6E-06	2.4E-07	4E-06

iPSC-ECs UPREGULATED vs. iPSC (TCP ONLY, see column B for full list).

Category	Term	Count	%	PValue	Genes	List Total	Pop Hits	Pop Total	Fold Enrichment	Bonferroni	Benjamini	FDR
GOTERM_BP_FAT	GO:0001944~vasculature development	70	7.4	8.3E-31	NRP2, ACVRL	7E+02	3E+02	1E+04	5E+00	3E-27	2.7E-27	2E-27
GOTERM_BP_FAT	GO:0001568~blood vessel development	69	7.3	1.2E-30	NRP2, ACVRL	7E+02	2E+02	1E+04	5E+00	4E-27	2.0E-27	2E-27
GOTERM_BP_FAT	GO:0048514~blood vessel morphogenesis	57	6.0	2.4E-24	NRP2, NRP1, A	7E+02	2E+02	1E+04	5E+00	8E-21	2.7E-21	4E-21
GOTERM_BP_FAT	GO:0051270~regulation of cell motion	46	4.9	2.0E-17	DLC1, PLXNA3	7E+02	2E+02	1E+04	4E+00	7E-14	1.7E-14	4E-14
GOTERM_BP_FAT	GO:0001525~angiogenesis	40	4.2	3.4E-17	NRP2, EMCN,	7E+02	1E+02	1E+04	5E+00	1E-13	2.2E-14	6E-14
GOTERM_BP_FAT	GO:0009611~response to wounding	80	8.5	4.8E-17	F2RL2, F2RL3,	7E+02	5E+02	1E+04	3E+00	2E-13	2.6E-14	9E-14
GOTERM_BP_FAT	GO:0030334~regulation of cell migration	42	4.4	1.2E-16	DLC1, ACVRL	7E+02	2E+02	1E+04	5E+00	4E-13	5.2E-14	2E-13
GOTERM_BP_FAT	GO:0007155~cell adhesion	94	9.9	2.4E-16	DLC1, PVR, NI	7E+02	7E+02	1E+04	2E+00	7E-13	9.1E-14	4E-13
GOTERM_BP_FAT	GO:0022610~biological adhesion	94	9.9	2.6E-16	DLC1, PVR, NI	7E+02	7E+02	1E+04	2E+00	7E-13	8.1E-14	4E-13
GOTERM_BP_FAT	GO:0042127~regulation of cell proliferation	100	10.6	7.2E-16	DLC1, NOG, S	7E+02	8E+02	1E+04	2E+00	2E-12	2.2E-13	1E-12
GOTERM_BP_FAT	GO:0040012~regulation of locomotion	43	4.5	3.3E-15	DLC1, ACVRL	7E+02	2E+02	1E+04	4E+00	1E-11	1.0E-12	6E-12
GOTERM_BP_FAT	GO:0006928~cell motion	71	7.5	8.2E-15	NRP2, PVR, PI	7E+02	5E+02	1E+04	3E+00	3E-11	2.3E-12	1E-11
GOTERM_BP_FAT	GO:0051094~positive regulation of developmental process	49	5.2	4.9E-13	MSR1, IL6ST, I	7E+02	3E+02	1E+04	3E+00	2E-09	1.2E-10	9E-10
GOTERM_BP_FAT	GO:0001501~skeletal system development	53	5.6	5.3E-13	NOG, PTGS2, I	7E+02	3E+02	1E+04	3E+00	2E-09	1.2E-10	1E-09
GOTERM_BP_FAT	GO:0016477~cell migration	48	5.1	1.4E-12	NRP2, PVR, C/	7E+02	3E+02	1E+04	3E+00	5E-09	3.2E-10	3E-09
GOTERM_BP_FAT	GO:0042060~wound healing	39	4.1	1.6E-12	F2RL2, F2RL3,	7E+02	2E+02	1E+04	4E+00	5E-09	3.3E-10	3E-09
GOTERM_BP_FAT	GO:0035295~tube development	42	4.4	2.0E-12	DLC1, CAV2, N	7E+02	2E+02	1E+04	4E+00	7E-09	3.9E-10	4E-09
GOTERM_BP_FAT	GO:0048870~cell motility	50	5.3	5.7E-12	NRP2, PVR, NI	7E+02	3E+02	1E+04	3E+00	2E-08	1.0E-09	1E-08
GOTERM_BP_FAT	GO:0051674~localization of cell	50	5.3	5.7E-12	NRP2, PVR, NI	7E+02	3E+02	1E+04	3E+00	2E-08	1.0E-09	1E-08
GOTERM_BP_FAT	GO:0045597~positive regulation of cell differentiation	41	4.3	3.1E-11	MSR1, IL6ST, I	7E+02	2E+02	1E+04	3E+00	1E-07	5.4E-09	6E-08

AF	AG	AH	AI	AJ	AK	AL	AM	AN	AO	AP	AQ	AR

iPSC-ECs DOWNREGULATED vs. iPS cells (Overlapping genes for ALL 2D and 3D samples, see full list in column P).

Category	Term	Count	%	PValue	Genes	List Total	Pop Hits	Pop Total	Fold Enrichmen	Bonferroni	Benjamini	FDR
GOTERM_BP_FAT	GO:0007155~cell adhesion	52	9.665427509	2.25E-09	PCDHA6, COL	402	700	13528	2.499843639	4.97E-06	4.97E-06	3.91E-06
GOTERM_BP_FAT	GO:0022610~biological adhesion	52	9.665427509	2.31E-09	PCDHA6, COL	402	701	13528	2.496277528	5.11E-06	2.56E-06	4.02E-06
GOTERM_BP_FAT	GO:0016337~cell-cell adhesion	25	4.646840149	2.47E-06	PCDHA6, CLD	402	276	13528	3.048164972	5.46E-03	1.82E-03	4.30E-03
GOTERM_BP_FAT	GO:0032989~cellular component morphogenesis	30	5.576208178	7.42E-06	SHROOM3, LF	402	397	13528	2.542952743	1.63E-02	4.10E-03	1.29E-02
GOTERM_BP_FAT	GO:0048666~neuron development	26	4.832713755	2.71E-05	LPPR4, ERBB3	402	339	13528	2.580959509	5.83E-02	1.19E-02	4.72E-02
GOTERM_BP_FAT	GO:0030030~cell projection organization	27	5.018587361	3.92E-05	LPPR4, ERBB3	402	368	13528	2.469013628	8.30E-02	1.43E-02	6.81E-02
GOTERM_BP_FAT	GO:0030182~neuron differentiation	30	5.576208178	4.64E-05	LPPR4, TUBB2	402	438	13528	2.304913787	9.76E-02	1.46E-02	8.06E-02
GOTERM_BP_FAT	GO:0000902~cell morphogenesis	26	4.832713755	6.07E-05	SHROOM3, LF	402	356	13528	2.457711443	1.26E-01	1.67E-02	1.05E-01
GOTERM_BP_FAT	GO:0031175~neuron projection development	21	3.903345725	7.82E-05	LPPR4, GNAO	402	256	13528	2.760494403	0.158902692	1.90E-02	1.36E-01
GOTERM_BP_FAT	GO:0007268~synaptic transmission	23	4.275092937	8.10E-05	DLGAP1, PLP1	402	298	13528	2.597282046	0.164157894	1.78E-02	0.140804043
GOTERM_BP_FAT	GO:0019226~transmission of nerve impulse	25	4.646840149	1.23E-04	CLDN19, GABI	402	350	13528	2.403695807	0.238223028	2.44E-02	0.213584511

iPSC-ECs DOWNREGULATED vs. iPS cells (TCP ONLY, see column J for full list).

Category	Term	Count	%	PValue	Genes	List Total	Pop Hits	Pop Total	Fold Enrichmer	Bonferroni	Benjamini	FDR
GOTERM_BP_FAT	GO:0007155~cell adhesion	79	8.577633008	2.03E-11	PCDHA6, LYPI	682	700	13528	2.238609133	5.31E-08	5.31E-08	3.59E-08
GOTERM_BP_FAT	GO:0022610~biological adhesion	79	8.577633008	2.11E-11	PCDHA6, LYPI	682	701	13528	2.235415682	5.54E-08	2.77E-08	3.75E-08
GOTERM_BP_FAT	GO:0007268~synaptic transmission	41	4.451682953	1.31E-08	SYT4, GABRB3	682	298	13528	2.72908343	3.43E-05	1.14E-05	2.32E-05
GOTERM_BP_FAT	GO:0019226~transmission of nerve impulse	45	4.885993485	1.82E-08	CLDN19, SYT4	682	350	13528	2.550314202	4.77E-05	1.19E-05	3.23E-05
GOTERM_BP_FAT	GO:0016337~cell-cell adhesion	35	3.800217155	1.24E-06	PCDHA6, CLD	682	276	13528	2.51540652	0.003248707	6.51E-04	0.002202644
GOTERM_BP_FAT	GO:0007267~cell-cell signaling	58	6.297502714	2.62E-06	GABRB3, SYT4	682	600	13528	1.917458456	0.00685039	0.001145004	0.004652958
GOTERM_BP_FAT	GO:0031175~neuron projection development	30	3.25732899	3.71E-05	LPPR4, ERBB3	682	256	13528	2.324505132	0.092623507	0.013789445	0.065772714
GOTERM_BP_FAT	GO:0048666~neuron development	36	3.908794788	4.38E-05	LPPR4, ERBB3	682	339	13528	2.106454208	0.108514693	0.014255702	0.077724153
GOTERM_BP_FAT	GO:0006836~neurotransmitter transport	15	1.628664495	6.15E-05	SYT4, ATP1A2	682	83	13528	3.584778999	0.14891139	0.01775592	0.109085067
GOTERM_BP_FAT	GO:0006816~calcium ion transport	20	2.17155266	9.10E-05	TRPM3, JPH4,	682	142	13528	2.793771426	0.21206791	0.023552543	0.161207371
GOTERM_BP_FAT	GO:0030182~neuron differentiation	42	4.560260586	9.54E-05	LPPR4, TUBB2	682	438	13528	1.90206082	0.221171924	0.022467839	0.169061167
GOTERM_BP_FAT	GO:0030030~cell projection organization	37	4.017372421	1.05E-04	LPPR4, ERBB3	682	368	13528	1.994358026	0.239750803	0.022583505	0.185375599
GOTERM_BP_FAT	GO:0032989~cellular component morphogenesis	39	4.234527687	1.07E-04	S100A4, SHRC	682	397	13528	1.948602791	0.244938687	0.021380158	0.190001928
GOTERM_BP_FAT	GO:0006811~ion transport	63	6.840390879	1.44E-04	JPH4, JPH3, SI	682	768	13528	1.627153592	0.313923656	0.026552985	0.254712669
GOTERM_BP_FAT	GO:0006936~muscle contraction	20	2.17155266	2.46E-04	MYL7, ACTC1,	682	153	13528	2.592912043	0.475032452	0.042051495	0.4352647
GOTERM_BP_FAT	GO:0000902~cell morphogenesis	35	3.800217155	2.55E-04	S100A4, SHRC	682	356	13528	1.950146628	0.487025191	0.04086221	0.450838626
GOTERM_BP_FAT	GO:0007409~axonogenesis	23	2.497285559	2.87E-04	LPPR4, ERBB3	682	193	13528	2.363849088	0.528305329	0.04323873	0.507355963
GOTERM_BP_FAT	GO:0032940~secretion by cell	24	2.605863192	3.06E-04	NKD2, SRCIN1	682	207	13528	2.299800247	0.55178371	0.043603007	0.541735079
GOTERM_BP_FAT	GO:0030001~metal ion transport	42	4.560260586	3.39E-04	JPH4, SLC38A	682	465	13528	1.791618579	0.588623685	0.045673894	0.599460843
GOTERM_BP_FAT	GO:0048667~cell morphogenesis involved in neuron differentiation	24	2.605863192	3.52E-04	LPPR4, ERBB3	682	209	13528	2.277792589	0.602413161	0.045069862	0.622399174
GOTERM_BP_FAT	GO:0051350~negative regulation of lyase activity	11	1.194353963	3.66E-04	GRM4, GNAL,	682	55	13528	3.967155425	0.616297432	0.044589029	0.646307834
GOTERM_BP_FAT	GO:0031280~negative regulation of cyclase activity	11	1.194353963	3.66E-04	GRM4, GNAL,	682	55	13528	3.967155425	0.616297432	0.044589029	0.646307834
GOTERM_BP_FAT	GO:0007194~negative regulation of adenylate cyclase activity	11	1.194353963	3.66E-04	GRM4, GNAL,	682	55	13528	3.967155425	0.616297432	0.044589029	0.646307834
GOTERM_BP_FAT	GO:0030802~regulation of cyclic nucleotide biosynthetic process	16	1.737242128	3.96E-04	GUCA1A, ADC	682	110	13528	2.885203946	0.645982316	0.046103766	0.700446304
GOTERM_BP_FAT	GO:0030808~regulation of nucleotide biosynthetic process	16	1.737242128	3.96E-04	GUCA1A, ADC	682	110	13528	2.885203946	0.645982316	0.046103766	0.700446304

iPSC-ECs DOWNREGULATED vs. iPS cells (Overlapping genes for ALL 3D samples, see full list in column O).

Category	Term	Count	%	PValue	Genes	List Total	Pop Hits	Pop Total	Fold Enrichmer	Bonferroni	Benjamini	FDR
GOTERM_BP_FAT	GO:0007155~cell adhesion	55	9.717314488	5.93E-10	PCDHA6, CAD	423	700	13528	2.51279973	1.36E-06	1.36E-06	1.04E-06
GOTERM_BP_FAT	GO:0022610~biological adhesion	55	9.717314488	6.10E-10	PCDHA6, CAD	423	701	13528	2.509215137	1.41E-06	7.03E-07	1.07E-06
GOTERM_BP_FAT	GO:0016337~cell-cell adhesion	27	4.770318021	5.26E-07	PCDHA6, CAD	423	276	13528	3.128584644	0.001211425	4.04E-04	9.20E-04
GOTERM_BP_FAT	GO:0032989~cellular component morphogenesis	31	5.477031802	7.14E-06	SHROOM3, LF	423	397	13528	2.497263757	0.016307217	0.004101975	0.012475985
GOTERM_BP_FAT	GO:0048666~neuron development	28	4.946996466	8.02E-06	LPPR4, ERBB3	423	339	13528	2.64150575	0.01830773	0.003688658	0.01402061
GOTERM_BP_FAT	GO:0019226~transmission of nerve impulse	28	4.946996466	1.43E-05	CLDN19, GABI	423	350	13528	2.558486998	0.0324351	0.00548039	0.025018307

Table S5.2 Differentially expressed genes for iPSC-ECs and iPS cells. Differential gene expression determined by EBSeq analysis (FDR ≤ 0.005) for iPSC-ECs relative to undifferentiated iPS cells. See Leng et. al. *Bioinformatics*. 2013; 29:1035-43. **Columns B-H**: Genes upregulated by iPSC-ECs relative to iPS cells. **Columns J-P**: Genes downregulated by iPSC-ECs relative to iPS cells. **Columns R-AR**: Top 25 Gene Ontology (GO) terms for iPSC-ECs upregulated (R-AD) or downregulated (AF-AR) compared to undifferentiated iPS cells. GO terms were identified using the DAVID Functional Annotation Tool (see manuscript for references). Settings used in DAVID: EASE = 0.001; ≥10 genes. Some lists for iPS cells were less than 25 GO terms, since only those with a Benjamini score ≤ 0.05 were included.

To view the whole table please go to:

https://www.ncbi.nlm.nih.gov/pmc/articles/PMC4829480/bin/NIHMS768241-supplement-2.xlsx

B	C	D	E	F	G	H	I	J	K	L	M	N
Upregulated genes for 3D (synthetic EMC) relative to 2D (TCP) culture (FDR ≤ 0.005).							Upregulated genes for 2D (TCP) relative to 3D (synthetic EMC) culture (FDR ≤ 0.005).					
Day 1	Day 2	Day 3	Day 5	3D > 2D ALL	At least 1		Day 1	Day 2	Day 3	Day 5	2D > 3D ALL	At least 1
304	349	370	354	141	612		378	387	309	203	104	577
ABCA5	ABCA5	ABCA5	ABCA5	ABCA5	ABCA5		AARS2	ABAT	ABAT	ABAT	ABAT	MARCH4
ABCA6	ABCA7	ABCA6	ABCC3	ACE	ABCA6		ABAT	ACAT2	ACAT2	ABCA13	ADAMTSL1	SEPT3
ABCA7	ABCC3	ABCA7	ACE	ACP5	ABCA7		ABCB8	ACTN1	ACTN1	ADAMTS18	ANKRD1	AARS2
ACE	ACE	ABCC3	ACER2	ADM	ABCC3		ACAT2	ADAMTS18	ADAMTS18	ADAMTSL1	APLN	ABAT
ACP5	ACP5	ACE	ACP5	ADORA2A	ACE		ACTN1	ADAMTSL1	ADAMTSL1	ADD2	ARSJ	ABCA13
ACSS1	ACSM3	ACER2	ADAMTS4	ADSSL1	ACER2		ADAMTSL1	ADAMTSL3	ADD2	ADTRP	ASF1B	ABCB8
ADM	ADAM32	ACP5	ADAMTS9	AGFG2	ACP5		ADTRP	ADD2	AHNAK2	AHNAK2	AURKB	ACAT2
ADORA2A	ADAMTS10	ACSM3	ADAMTS10	AGTR1	ACSM3		ANKRD1	ADRA1D	ALCAM	ANKRD1	BUB1	ACTN1
ADSSL1	ADAMTS9	ACSS1	ADM	AK4	ACSS1		ANKRD20A3	ADTRP	ANKRD1	APLN	BUB1B	ADAMTS18
AGFG2	ADM	ADAM32	ADORA2A	AMT	ADAM32		ANLN	AHNAK2	ANLN	APLP1	CCNB1	ADAMTSL1
AGTR1	ADORA2A	ADAMTS4	ADSSL1	AMY2B	ADAMTS10		AOX1	AJUBA	APLN	ARHGDIG	CCNB2	ADAMTSL3
AK4	ADSSL1	ADAMTS9	AGAP5	ANGPTL2	ADAMTS4		APLN	ALCAM	ARHGAP11A	ARSJ	CD274	ADD2
ALDOC	AFAP1L1	ADAMTS10	AGAP9	APBB3	ADAMTS9		ARHGAP11A	ANKRD1	ARHGDIG	ASF1B	CDC20	ADRA1D
AMT	AGAP9	ADM	AGFG2	APOLD1	ADM		ARHGAP11B	ANLN	ARSJ	AURKB	CDC45	ADTRP
AMY2B	AGFG2	ADORA2A	AGPAT9	AREG	ADORA2A		ARSJ	ANO4	ASF1B	BASP1	CDCA2	AHNAK2
ANGPTL2	AGTR1	ADSSL1	AGTR1	ARL10	ADSSL1		ASF1B	APLN	ASPM	BUB1	CDCA8	AJUBA
ANKRD12	AHR	AFAP1L1	AHR	ARRDC3	AFAP1L1		ASPM	APOBEC3B	ATAD2	BUB1B	CDH2	ALCAM
ANKRD33	AHSA2	AGAP9	AHSA2	BAALC	AGAP5		ATAD2	ARHGAP11A	AURKA	CARD11	CDH6	ANKRD1
ANKRD37	AK4	AGER	AK4	BCL2L11	AGAP9		ATIC	ARHGDIG	AURKB	CCNA1	CENPF	ANKRD20A3
ANKZF1	AMN1	AGFG2	AMT	BMF	AGER		ATP5G1	ARSJ	AXL	CCNB1	CIT	ANLN
APBB3	AMT	AGTR1	AMY2B	BNIP3L	AGFG2		AURKA	ASF1B	BASP1	CCNB2	CLDN11	ANO4
APOLD1	AMY2B	AHR	ANGPT1	BST2	AGPAT9		AURKB	ASPM	BDNF	CD163L1	CNTNAP2	AOX1
AREG	ANGPTL2	AHSA2	ANGPTL2	C10orf10	AGTR1		AXL	ATAD2	BIRC5	CD274	COL17A1	APLN
ARG2	ANKRD10	AK4	ANKRD10	C4orf3	AHR		BAG2	ATP5J2-PTCD	BMP4	CDC20	CORO1A	APLP1
ARHGEF37	ANKRD33	AMT	ANKRD37	CA12	AHSA2		BDNF	AURKA	BOP1	CDC45	CYR61	APOBEC3B
ARL10	APBB3	AMY2B	APBB3	CADM1	AK4		BIRC5	AURKB	BRCA1	CDCA2	CYTL1	ARHGAP11A
ARRDC3	APLNR	ANGPTL2	APLNR	CALCRL	ALDOC		BLM	AXL	BTBD11	CDCA8	DHCR24	ARHGAP11B
ATP6V0D2	APOLD1	ANKRD10	APOLD1	CD109	AMN1		BMP4	BCL9L	BUB1	CDH2	DLGAP5	ARHGDIG
AXIN2	AREG	ANKRD33	AREG	CDH7	AMT		BOP1	BDNF	BUB1B	CDH6	EBNA1BP2	ARSJ
B3GALNT1	ARHGAP27	APBB3	ARGLU1	CLK1	AMY2B		BRCA1	BIRC5	C3orf78	CENPF	EDN1	ASF1B
B3GALT4	ARHGAP28	APLNR	ARHGAP4	COLEC12	ANGPT1		BRI3BP	BMP4	C15orf42	CENPV	FAM64A	ASPM
BAALC	ARHGAP4	APOLD1	ARHGAP27	CPXM1	ANGPTL2		BTBD11	BOP1	CABLES1	CHAF1B	FAM83D	ATAD2
BAIAP3	ARHGEF37	AREG	ARHGEF37	CREBRF	ANKRD10		BUB1	BRCA1	CARD11	CIT	FBN2	ATIC
BCL2L11	ARL10	ARGLU1	ARL10	CXCL16	ANKRD12		BUB1B	BRI3BP	CASC5	CLDN11	FEN1	ATP5G1
BEX2	ARPC4-TTLL3	ARHGAP4	ARRDC3	CYP1A1	ANKRD33		BYSL	BTBD11	CCNA1	CLU	FERMT1	ATP5J2-PTCD1
BHLHE41	ARRDC3	ARHGAP27	ART4	DBNDD1	ANKRD37		C10orf2	BUB1	CCNA2	CNTNAP1	FLRT3	AURKA
BMF	ATG16L2	ARHGAP28	ATG16L2	DDIT4	ANKZF1		C15orf42	BUB1B	CCNB1	CNTNAP2	FOXM1	AURKB
BNIP3	AXIN2	ARL10	B3GAT1	DPY19L2	APBB3		C16orf74	C15orf42	CCNB2	COL13A1	FRMD6	AXL
BNIP3L	B3GALNT1	ARL17B	BAALC	EBF4	APLNR		C20orf27	C16orf74	CCNF	COL17A1	GADL1	BAG2
BST2	B3GALT4	ARPC4-TTLL3	BCL2L11	EFCAB4A	APOLD1		C22orf29	C20orf27	CD163L1	CORO1A	GAL	BASP1
BTG1	B3GAT1	ARRDC3	BIRC3	EGLN3	AREG		CABLES1	C22orf29	CD274	CRLF1	GEMIN4	BCL9L
C1orf51	BAALC	ATG16L2	BMF	EGR1	ARG2		CAD	CABLES1	CDC6	CYP2S1	GLI2	BDNF
C2orf72	BCL2L11	AXIN2	BMPER	ENO2	ARGLU1		CASC5	CALD1	CDC20	CYR61	GLIPR1	BIRC5
C4orf3	BCL6B	B3GALT4	BNIP3L	F3	ARHGAP27		CCDC99	CARD11	CDC25A	CYTL1	GREM1	BLM
C4orf47	BMF	B3GAT1	BRWD1	GAB1	ARHGAP28		CCL2	CASC5	CDC45	DACT3	HHIP	BMP4
C10orf10	BNIP3	BAALC	BST2	GABRE	ARHGAP4		CCNA2	CCDC81	CDCA2	DHCR24	IL7R	BOP1
C11orf35	BNIP3L	BAIAP3	BTNL9	GALNTL4	ARHGEF37		CCNB1	CCNA1	CDCA3	DLGAP5	KAL1	BRCA1
CA11	BST2	BCL2L11	C1orf63	GIMAP5	ARL10		CCNB2	CCNA2	CDCA5	DNAJC25-GN	KCNAB1	BRI3BP

GO terms for differentially expressed genes **3D upregulated over 2D ---->**

Day 1

Category	Term	Count	%	PValue	Genes	List Total	Pop Hits	Pop Total	Fold Enrichment	Bonferroni	Benjamini	FDR
GOTERM_BP_FAT	GO:0001666~response to hypoxia	15	5.281690141	2.43E-08	NOL3, CYP1A1	214	134	13528	7.076300739	4.43E-05	4.43E-05	4.13E-05
GOTERM_BP_FAT	GO:0070482~response to oxygen levels	15	5.281690141	4.67E-08	NOL3, CYP1A1	214	141	13528	6.724995029	8.50E-05	4.25E-05	7.93E-05
GOTERM_BP_FAT	GO:0010033~response to organic substance	30	10.56338028	3.08E-06	ADORA2A, ALI	214	721	13528	2.630303187	0.005587273	0.001865904	0.005229493

Day 2

Category	Term	Count	%	PValue	Genes	List Total	Pop Hits	Pop Total	Fold Enrichment	Bonferroni	Benjamini	FDR
GOTERM_BP_FAT	GO:0001666~response to hypoxia	13	3.915662651	4.61E-06	ACE, CYP1A1,	241	134	13528	5.445717471	0.008658402	0.008658402	0.007865566
GOTERM_BP_FAT	GO:0070482~response to oxygen levels	13	3.915662651	7.81E-06	ACE, CYP1A1,	241	141	13528	5.175362703	0.014631311	0.007342612	0.013331325
GOTERM_BP_FAT	GO:0040012~regulation of locomotion	14	4.21686747	3.84E-05	ICAM1, ADOR/	241	192	13528	4.093015214	0.0698816	0.023858571	0.065505658
GOTERM_BP_FAT	GO:0001558~regulation of cell growth	14	4.21686747	4.30E-05	PPARG, NPR1	241	194	13528	4.050819181	0.077945559	0.020083341	0.073376482
GOTERM_BP_FAT	GO:0030334~regulation of cell migration	13	3.915662651	4.81E-05	ICAM1, ENPP2	241	169	13528	4.31790616	0.086738746	0.017982999	0.082037194
GOTERM_BP_FAT	GO:0006915~apoptosis	26	7.831325301	6.91E-05	MEF2C, CADM	241	602	13528	2.424339339	0.122295202	0.021506199	0.117921627
GOTERM_BP_FAT	GO:0012501~programmed cell death	26	7.831325301	8.70E-05	MEF2C, CADM	241	611	13528	2.38862894	0.151525913	0.023200313	0.148517896
GOTERM_BP_FAT	GO:0051270~regulation of cell motion	13	3.915662651	1.71E-04	ICAM1, ENPP2	241	193	13528	3.780964462	0.276190811	0.039598098	0.291941538
GOTERM_BP_FAT	GO:0008219~cell death	28	8.43373494	1.87E-04	MEF2C, CADM	241	719	13528	2.185977528	0.2974832	0.038472174	0.318866915
GOTERM_BP_FAT	GO:0009611~response to wounding	23	6.927710843	1.90E-04	F2RL3, CYP1A	241	530	13528	2.435950834	0.30096949	0.035172634	0.323352428
GOTERM_BP_FAT	GO:0016265~death	28	8.43373494	2.07E-04	MEF2C, CADM	241	724	13528	2.170880998	0.323432122	0.034896787	0.352795913
GOTERM_BP_FAT	GO:0042127~regulation of cell proliferation	29	8.734939759	3.45E-04	VIP, TBC1D8, I	241	787	13528	2.068425187	0.478555932	0.048854958	0.587255671

Day 3

Category	Term	Count	%	PValue	Genes	List Total	Pop Hits	Pop Total	Fold Enrichment	Bonferroni	Benjamini	FDR
GOTERM_BP_FAT	GO:0006915~apoptosis	30	8.450704225	4.59E-06	MEF2C, CADM	260	602	13528	2.592895477	0.00879733	0.00879733	0.007860205
GOTERM_BP_FAT	GO:0012501~programmed cell death	30	8.450704225	6.08E-06	MEF2C, CADM	260	611	13528	2.554702254	0.011632654	0.005833341	0.010408239
GOTERM_BP_FAT	GO:0042060~wound healing	15	4.225352113	1.86E-05	F2RL3, ADOR/	260	191	13528	4.086186065	0.035145607	0.011855192	0.031822227
GOTERM_BP_FAT	GO:0008219~cell death	32	9.014084507	1.93E-05	MEF2C, CADM	260	719	13528	2.315694875	0.036505836	0.009254127	0.033076807
GOTERM_BP_FAT	GO:0040012~regulation of locomotion	15	4.225352113	1.97E-05	ICAM1, ADOR/	260	192	13528	4.064903846	0.037154623	0.00754389	0.033675821
GOTERM_BP_FAT	GO:0016265~death	32	9.014084507	2.16E-05	MEF2C, CADM	260	724	13528	2.299702507	0.040738512	0.006907959	0.03699199
GOTERM_BP_FAT	GO:0009611~response to wounding	26	7.323943662	3.02E-05	F2RL3, ADOR/	260	530	13528	2.55245283	0.056500096	0.008274011	0.051723439
GOTERM_BP_FAT	GO:0001666~response to hypoxia	12	3.38028169	5.28E-05	ACE, SMAD9, (	260	134	13528	4.659471871	0.096563139	0.012613407	0.090294733
GOTERM_BP_FAT	GO:0070482~response to oxygen levels	12	3.38028169	8.39E-05	ACE, SMAD9, (	260	141	13528	4.428150573	0.149136566	0.017784799	0.143566483
GOTERM_BP_FAT	GO:0050878~regulation of body fluid levels	12	3.38028169	8.39E-05	VIP, F2RL3, AF	260	141	13528	4.428150573	0.149136566	0.017784799	0.143566483
GOTERM_BP_FAT	GO:0030334~regulation of cell migration	13	3.661971831	9.98E-05	ICAM1, ENPP2	260	169	13528	4.002366864	0.17474246	0.019022717	0.170705748
GOTERM_BP_FAT	GO:0042981~regulation of apoptosis	32	9.014084507	1.56E-04	MEF2C, IFIH1,	260	804	13528	2.070876387	0.259536989	0.02694661	0.266942283
GOTERM_BP_FAT	GO:0043067~regulation of programmed cell death	32	9.014084507	1.86E-04	MEF2C, IFIH1,	260	812	13528	2.050473664	0.300928997	0.029392952	0.31796399
GOTERM_BP_FAT	GO:0010941~regulation of cell death	32	9.014084507	1.99E-04	MEF2C, IFIH1,	260	815	13528	2.042925908	0.317719593	0.028980581	0.33951988
GOTERM_BP_FAT	GO:0032101~regulation of response to external stimulus	12	3.38028169	2.44E-04	ZFP36, AGTR1	260	159	13528	3.926850508	0.374327848	0.032940168	0.416278564
GOTERM_BP_FAT	GO:0051270~regulation of cell motion	13	3.661971831	3.45E-04	ICAM1, ENPP2	260	193	13528	3.504663212	0.485022564	0.040628611	0.588611618

Day 5

Category	Term	Count	%	PValue	Genes	List Total	Pop Hits	Pop Total	Fold Enrichment	Bonferroni	Benjamini	FDR
GOTERM_BP_FAT	GO:0001944~vasculature development	20	5.847953216	4.30E-07	LMO2, EFNB2,	263	251	13528	4.098586642	8.83E-04	8.83E-04	7.41E-04
GOTERM_BP_FAT	GO:0040012~regulation of locomotion	17	4.970760234	1.01E-06	ICAM1, ADOR/	263	192	13528	4.554340938	0.002083035	0.00104206	0.001748601
GOTERM_BP_FAT	GO:0001568~blood vessel development	19	5.555555556	1.35E-06	LMO2, COL3A1	263	245	13528	3.989012183	0.002766256	9.23E-04	0.002322919
GOTERM_BP_FAT	GO:0030334~regulation of cell migration	15	4.385964912	5.21E-06	ICAM1, ENPP2	263	169	13528	4.565437487	0.010657683	0.002675136	0.008984899
GOTERM_BP_FAT	GO:0006915~apoptosis	30	8.771929825	5.73E-06	CADM1, ADOF	263	602	13528	2.563318722	0.011724068	0.002355888	0.009889185
GOTERM_BP_FAT	GO:0012501~programmed cell death	30	8.771929825	7.62E-06	CADM1, ADOF	263	611	13528	2.525561163	0.015560464	0.002610387	0.013150441
GOTERM_BP_FAT	GO:0010033~response to organic substance	33	9.649122807	9.97E-06	ADORA2A, OS	263	721	13528	2.35427137	0.020304282	0.002926174	0.017200551
GOTERM_BP_FAT	GO:0040017~positive regulation of locomotion	11	3.216374269	1.96E-05	ICAM1, CDH13	263	98	13528	5.773570265	0.039510439	0.005026346	0.033799324

GO terms for differentially expressed genes **2D upregulated over 3D ---->**

Day 1

Category	Term	Count	%	PValue	Genes	List Total	Pop Hits	Pop Total	Fold Enrichment	Bonferroni	Benjamini	FDR
GOTERM_BP_FAT	GO:0000279~M phase	78	21.13821138	9.62E-57	KIF23, KIFC1, I	312	329	13528	10.27963526	1.99E-53	1.99E-53	1.66E-53
GOTERM_BP_FAT	GO:0022403~cell cycle phase	84	22.76422764	1.48E-55	KIF23, E2F1, K	312	414	13528	8.797473058	3.06E-52	1.53E-52	2.55E-52
GOTERM_BP_FAT	GO:0007049~cell cycle	107	28.99728997	1.17E-54	KIFC1, PRC1, I	312	776	13528	5.978621464	2.42E-51	8.07E-52	2.02E-51
GOTERM_BP_FAT	GO:0007067~mitosis	63	17.07317073	8.82E-51	KIF23, KIF22, K	312	220	13528	12.41643357	1.83E-47	4.57E-48	1.52E-47
GOTERM_BP_FAT	GO:0000280~nuclear division	63	17.07317073	8.82E-51	KIF23, KIF22, K	312	220	13528	12.41643357	1.83E-47	4.57E-48	1.52E-47
GOTERM_BP_FAT	GO:0022402~cell cycle process	90	24.3902439	1.79E-50	KIF23, E2F1, K	312	565	13528	6.906739278	3.71E-47	7.42E-48	3.09E-47
GOTERM_BP_FAT	GO:0000087~M phase of mitotic cell cycle	63	17.07317073	3.02E-50	KIF23, KIF22, K	312	224	13528	12.19471154	6.26E-47	1.04E-47	5.22E-47
GOTERM_BP_FAT	GO:0048285~organelle fission	63	17.07317073	1.36E-49	KIF23, KIF22, K	312	229	13528	11.92845146	2.81E-46	4.01E-47	2.34E-46
GOTERM_BP_FAT	GO:0000278~mitotic cell cycle	72	19.51219512	8.11E-46	E2F1, KIF23, K	312	370	13528	8.437422037	1.68E-42	2.10E-43	1.40E-42
GOTERM_BP_FAT	GO:0051301~cell division	59	15.98915989	7.19E-38	KIF23, KIFC1, I	312	295	13528	8.671794872	1.49E-34	1.66E-35	1.24E-34
GOTERM_BP_FAT	GO:0007059~chromosome segregation	26	7.046070461	6.55E-22	KIFC1, CCDC9	312	81	13528	13.91769547	1.36E-18	1.36E-19	1.13E-18
GOTERM_BP_FAT	GO:0006259~DNA metabolic process	53	14.36314363	3.28E-20	CLSPN, KIF22,	312	506	13528	4.54155265	6.81E-17	6.19E-18	5.67E-17
GOTERM_BP_FAT	GO:0006260~DNA replication	33	8.943089431	5.29E-19	CLSPN, BLM, I	312	190	13528	7.530769231	1.10E-15	9.14E-17	9.13E-16
GOTERM_BP_FAT	GO:0051726~regulation of cell cycle	40	10.8401084	2.41E-17	E2F1, CKS1B, I	312	331	13528	5.23975521	5.00E-14	3.85E-15	4.17E-14
GOTERM_BP_FAT	GO:0007017~microtubule-based process	35	9.485094851	5.43E-17	KIF23, KIFC1, I	312	253	13528	5.998277085	1.13E-13	8.05E-15	9.38E-14
GOTERM_BP_FAT	GO:0000070~mitotic sister chromatid segregation	15	4.06504065	2.07E-14	KIFC1, CCDC9	312	36	13528	18.06623932	4.30E-11	2.87E-12	3.58E-11
GOTERM_BP_FAT	GO:0000819~sister chromatid segregation	15	4.06504065	3.27E-14	KIFC1, CCDC9	312	37	13528	17.57796258	6.77E-11	4.23E-12	5.64E-11
GOTERM_BP_FAT	GO:0008283~cell proliferation	40	10.8401084	2.81E-13	E2F1, CKS1B, :	312	436	13528	3.977887556	5.83E-10	3.43E-11	4.85E-10
GOTERM_BP_FAT	GO:0007051~spindle organization	15	4.06504065	7.57E-13	KIF23, KIF11, F	312	45	13528	14.45299145	1.57E-09	8.71E-11	1.31E-09
GOTERM_BP_FAT	GO:0010564~regulation of cell cycle process	20	5.420054201	1.20E-11	DLGAP5, EDN	312	114	13528	7.606837607	2.49E-08	1.31E-09	2.08E-08
GOTERM_BP_FAT	GO:0007346~regulation of mitotic cell cycle	22	5.962059621	3.98E-11	CDC6, CDK1, I	312	152	13528	6.275641026	8.26E-08	4.13E-09	6.88E-08
GOTERM_BP_FAT	GO:0000226~microtubule cytoskeleton organization	21	5.691056911	1.56E-10	KIF23, CCDC9	312	147	13528	6.194139194	3.23E-07	1.54E-08	2.69E-07
GOTERM_BP_FAT	GO:0051276~chromosome organization	37	10.02710027	5.05E-10	DPF3, KIFC1, (	312	485	13528	3.307798044	1.05E-06	4.75E-08	8.71E-07
GOTERM_BP_FAT	GO:0006974~response to DNA damage stimulus	32	8.672086721	5.75E-10	CLSPN, KIF22,	312	373	13528	3.719804771	1.19E-06	5.18E-08	9.92E-07
GOTERM_BP_FAT	GO:0000075~cell cycle checkpoint	16	4.33604336	2.15E-09	CDK1, CDC6, I	312	91	13528	7.623555931	4.45E-06	1.86E-07	3.71E-06

Day 2

Category	Term	Count	%	PValue	Genes	List Total	Pop Hits	Pop Total	Fold Enrichment	Bonferroni	Benjamini	FDR
GOTERM_BP_FAT	GO:0022403~cell cycle phase	78	20.8	3.93E-48	KIF23, E2F1, K	318	414	13528	8.014948501	8.73E-45	8.73E-45	6.84E-45
GOTERM_BP_FAT	GO:0000279~M phase	71	18.93333333	9.25E-48	KIF23, KIFC1, I	318	329	13528	9.180554759	2.06E-44	1.03E-44	1.61E-44
GOTERM_BP_FAT	GO:0000280~nuclear division	61	16.26666667	1.18E-47	KIF23, KIF22, K	318	220	13528	11.79542596	2.62E-44	8.75E-45	2.05E-44
GOTERM_BP_FAT	GO:0007067~mitosis	61	16.26666667	1.18E-47	KIF23, KIF22, K	318	220	13528	11.79542596	2.62E-44	8.75E-45	2.05E-44
GOTERM_BP_FAT	GO:0000087~M phase of mitotic cell cycle	61	16.26666667	3.84E-47	KIF23, KIF22, K	318	224	13528	11.58479335	8.53E-44	2.13E-44	6.68E-44
GOTERM_BP_FAT	GO:0048285~organelle fission	61	16.26666667	1.62E-46	KIF23, KIF22, K	318	229	13528	11.33185027	3.59E-43	7.18E-44	2.81E-43
GOTERM_BP_FAT	GO:0022402~cell cycle process	84	22.4	1.01E-43	KIF23, E2F1, K	318	565	13528	6.32466188	2.24E-40	3.73E-41	1.75E-40
GOTERM_BP_FAT	GO:0000278~mitotic cell cycle	69	18.4	5.82E-42	E2F1, KIF23, K	318	370	13528	7.933299337	1.29E-38	1.85E-39	1.01E-38
GOTERM_BP_FAT	GO:0007049~cell cycle	93	24.8	9.06E-41	KIF23, E2F1, K	318	776	13528	5.098327174	2.02E-37	2.52E-38	1.58E-37
GOTERM_BP_FAT	GO:0051301~cell division	59	15.73333333	2.19E-37	KIF23, KIFC1, I	318	295	13528	8.508176101	4.87E-34	5.41E-35	3.81E-34
GOTERM_BP_FAT	GO:0007059~chromosome segregation	24	6.4	3.83E-19	KIFC1, NEK2, S	318	81	13528	12.60470533	8.51E-16	8.51E-17	6.66E-16
GOTERM_BP_FAT	GO:0051726~regulation of cell cycle	40	10.66666667	4.67E-17	E2F1, CKS1B, I	318	331	13528	5.140891904	1.04E-13	9.44E-15	8.13E-14
GOTERM_BP_FAT	GO:0008283~cell proliferation	41	10.93333333	1.11E-13	E2F1, CKS1B, :	318	436	13528	4.000403901	2.48E-10	2.06E-11	1.94E-10
GOTERM_BP_FAT	GO:0000070~mitotic sister chromatid segregation	14	3.733333333	7.16E-13	KIFC1, NCAPH	318	36	13528	16.54367575	1.59E-09	1.23E-10	1.25E-09
GOTERM_BP_FAT	GO:0000819~sister chromatid segregation	14	3.733333333	1.08E-12	KIFC1, NCAPH	318	37	13528	16.09654938	2.40E-09	1.72E-10	1.88E-09
GOTERM_BP_FAT	GO:0007017~microtubule-based process	30	8	1.40E-12	KIF23, KIFC1, I	318	253	13528	5.044373182	3.11E-09	2.07E-10	2.44E-09
GOTERM_BP_FAT	GO:0007346~regulation of mitotic cell cycle	23	6.133333333	7.62E-12	EGFR, CDC6,	318	152	13528	6.437106918	1.69E-08	1.06E-09	1.33E-08
GOTERM_BP_FAT	GO:0010564~regulation of cell cycle process	19	5.066666667	1.47E-10	NEK2, DLGAP5	318	114	13528	7.090146751	3.27E-07	1.92E-08	2.56E-07
GOTERM_BP_FAT	GO:0006260~DNA replication	22	5.866666667	3.73E-09	GINS2, CDC6,	318	190	13528	4.925786164	8.30E-06	4.61E-07	6.49E-06
GOTERM_BP_FAT	GO:0007051~spindle organization	12	3.2	4.91E-09	KIF23, KIF11, F	318	45	13528	11.3443348	1.09E-05	5.75E-07	8.54E-06

Table S5.3 Differentially expressed genes for iPSC-ECs in 3D relative to 2D culture. Differential gene expression by EBSeq analysis (FDR ≤ 0.005) for iPSC-ECs cultured in 50% crosslinked PEG hydrogels (3D) relative to cells cultured on TCP (2D). See Leng et. al. *Bioinformatics*. 2013; 29:1035-43. **Columns F and M**: "3D > 2D ALL" and "2D > 3D ALL" includes differentially expressed genes that overlapped for all time points. **Columns G and N**:All genes that were differentially expressed for at least one time point. **Columns Q-AR**: Gene Ontology (GO) terms for iPSC-ECs upregulated in 3D (Q-AC) or 2D (AF-AR) culture. GO terms were identified using the DAVID Functional Annotation Tool (see manuscript for references). Settings used in DAVID: EASE = 0.001; ≥10 genes. Only Top 25 GO terms or GO terms with a Benjamini score ≤ 0.05 are shown.

To view the whole table please go to:

https://www.ncbi.nlm.nih.gov/pmc/articles/PMC4829480/bin/NIHMS768241-supplement-2.xlsx

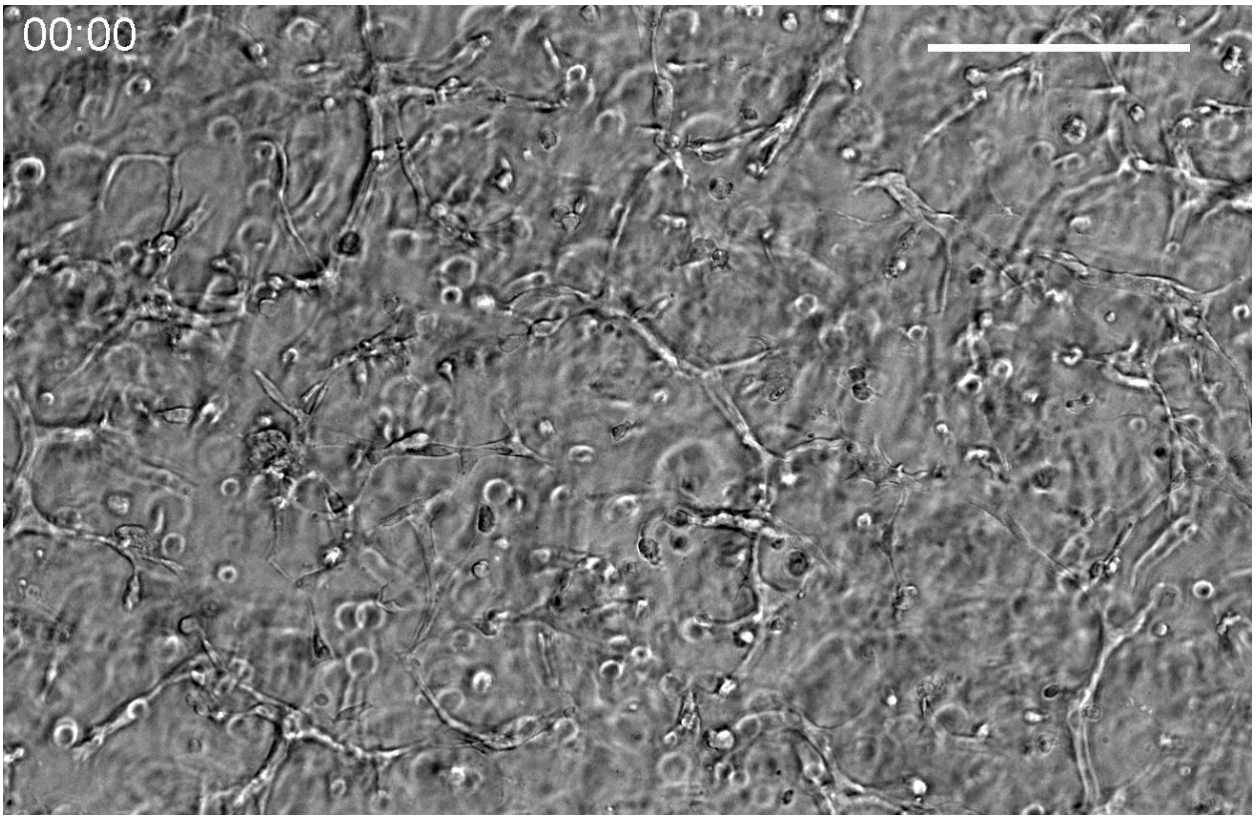

Movie S5.1 Initial network formation by iPSC-ECs cultured in synthetic ECM. Time lapse images (1 hr / frame, beginning ~12 hrs after encapsulation) illustrating initial vascular network formation by iPSC-ECs cultured in synthetic ECM. Scale bar = 100 μm. Time scale shown in Hr:Min.

To view the movie please go to:

https://www.ncbi.nlm.nih.gov/pmc/articles/PMC4829480/bin/NIHMS768241-supplement-3.avi

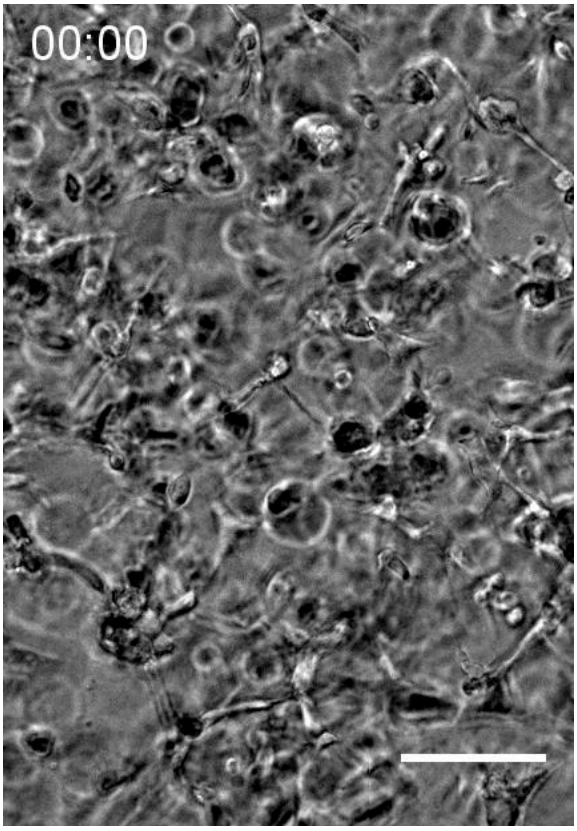

Movie S5.2 Formation of interconnected vascular networks by iPSC-ECs cultured in synthetic ECM. Time lapse images (1 hr / frame, beginning ~36 hrs after encapsulation) for iPSC-ECs cultured in synthetic ECM. Scale bar = 250 μm. Time scale shown in Hr:Min.

To view the movie please go to:

https://www.ncbi.nlm.nih.gov/pmc/articles/PMC4829480/bin/NIHMS768241-supplement-4.avi

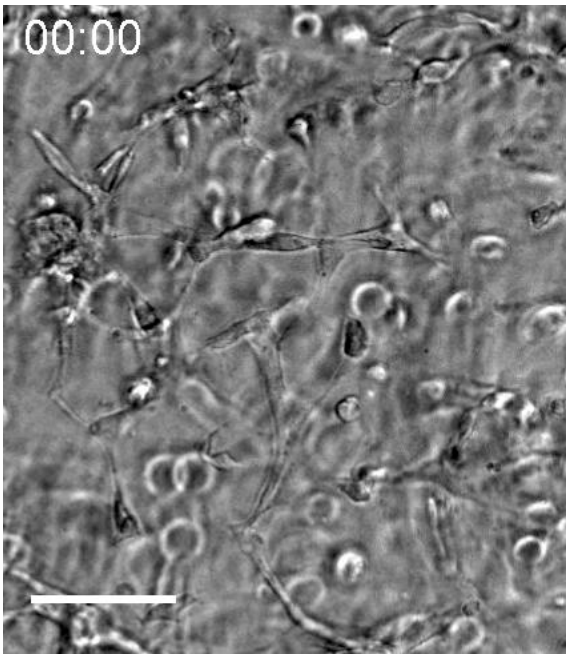

Movie S5.3 Locally transient vascular networks formed by iPSC-ECs in synthetic ECM. Time lapse images (1 hr / frame, beginning ~36 hrs after encapsulation) for iPSC-ECs cultured in synthetic ECM. The same region is shown in Supplemental Movie 2 (bottom left corner), but with different z-planes highlighted to better illustrate transient formation of networks. Scale bar = 100 μm. Time scale shown in Hr:Min

To view the movie please go to:

https://www.ncbi.nlm.nih.gov/pmc/articles/PMC4829480/bin/NIHMS768241-supplement-5.avi

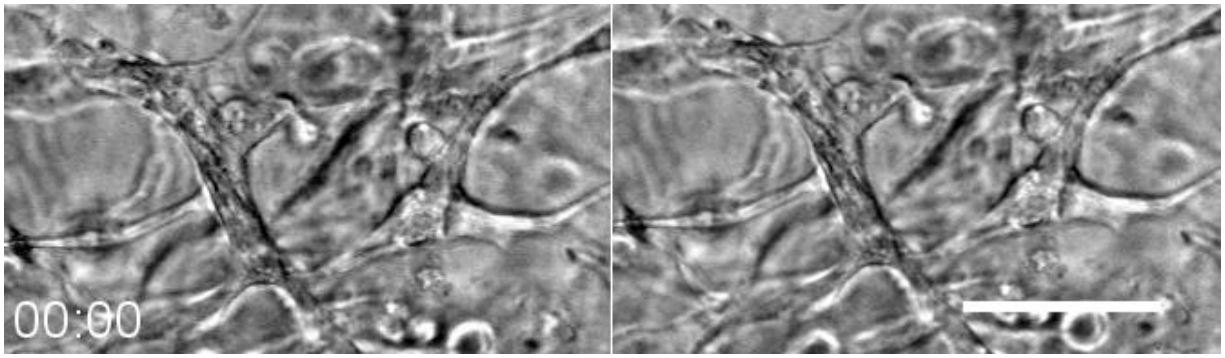

Movie S5.4 Apparent vacuole dynamics for iPSC-ECs during vascular network formation. Time lapse images (1 hr / frame, beginning ~36 hrs after encapsulation) illustrating apparent vacuole dynamics in the central region of tubules formed by iPSC-ECs. Two separate z-planes are shown to illustrate both the inner and outer regions of the tubules. The circled region illustrates apparent vacuole condensation (time points 06:00-20:00, left image), such as described in Kamei et. al. Nature. 2006; 442:453-6. The right image is more clearly in focus within the same region for some frames. Scale bar = 100 μm. Time scale shown in Hr:Min.

To view the movie please go to:

https://www.ncbi.nlm.nih.gov/pmc/articles/PMC4829480/bin/NIHMS768241-supplement-6.avi

Chapter 6: Synthetic PEG based hydrogel that supports metabolic function of iPS-derived hepatocyte in 3D

Hamisha Ardalani, James A. Thomson, William L. Murphy "Synthetic PEG based hydrogel that supports metabolic function of iPS-derived hepatocyte in 3D", In Preparation.

6.1 Preface

In Chapter 4, we developed a 3D in vitro model of iHEP cells in suspension culture in which ECs in our 3D co-cultured aggregates self-organized and formed capillary-like structures, reminiscent of sinusoidal architecture in vivo. To extend the life-span of the aggregates in vitro and to improve delivery of oxygen and nutrients to the core of the aggregates, there is a need to integrate aggregates with formed capillary networks, much like in vivo. However, the first step towards that goal is finding an ECM that not only is supportive of ECs allowing angiogenesis but is also supportive of iHEP metabolic and enzyme activity functions. In Chapter 5, we described a chemically defined synthetic PEG hydrogel tethered with RGDS and MMP-degradable crosslinker that is permissive for angiogenesis and vascular remodeling like in vivo. In this chapter, we built upon our previous findings and showed that the same PEG hydrogel formulation that allows angiogenesis is also supportive of the metabolic function and CYP450 enzyme activity of encapsulated iHEP aggregates.

6.2 Abstract

Organoid cultures are typically done in Matrigel [1,2], however due to complex, undefined nature, batch-to-batch variabilities and immunogenic response of Matrigel, there is a need to find chemically defined substrates that not only address the above challenges but also offer a great deal of control over the mechanical properties of the gel. Here, we used polyethylene glycol (PEG) as a blank substrate, which are commonly used in clinical studies. The PEG was functionalized with RGDS peptide and was crosslinked through MMP-degradable peptide sequence. We showed PEG hydrogel at intermediate crosslinking density, 50%, with the shear modulus of 785±40 Pa results in the highest albumin and urea production compared to other crosslinking densities. Moreover, encapsulated iHEP aggregates exhibited hepatocellular activity similar to Matrigel as characterized by albumin and urea production and induction of CYP450 drug metabolism enzymes. The evaluation of integrin binding peptide (RGDS) on iHEP aggregate metabolic function and enzyme activity showed effect of integrin binding peptides is more pronounced at 30% crosslinking density and has no effect on the albumin and urea synthesis at 50% crosslinking density. Overall, this study shows the fine balance between crosslinking density and integrin binding peptides on metabolic function of iHEP aggregates encapsulated in PEG hydrogel. This work lays the ground for development of better 3D *in vitro* models, specifically for liver diseases mediated by the biomechanical properties of the ECM.

6.3 Introduction

Hepatic differentiation of cells from human pluripotent stem cells (hPSC) and organoid cultures are traditionally done on/in Matrigel [1–5]. Indeed, Matrigel is considered as a standard culture condition to which many new culture systems are being compared. Matrigel is a protein extract from Engelbreth–Holm-Swarm (EHS) mouse sarcoma cells. It mainly contains laminin-

111 (~60%), collagen type IV (~30%), and entactin (~8%) together with numerous other proteins and several growth factors, like EGF, bFGF, IGF-1, TGF-β, PDGF, and NGF [6,7]. However, one of the drawbacks of Matrigel is undefined components in the product can lead to possible variations between independent cell culture experiments. Moreover, the use of animal origin matrices inhibits use of the cells for clinical applications due to the risk of pathogen transmission that could trigger immune rejection of transplanted cells [8]. Therefore, a bioengineered synthetic ECM is essential.

Here, we used polyethylene glycol (PEG) as a blank substrate. The PEG can be functionalized with select ECM proteins or varied in mechanical stiffness, also being transparent after forming gels provide an easy means of viewing cells over time [9]. We used 8 arm-PEG norbornene that arms were functionalized with RGDS peptide and were crosslinked through MMP-degradable peptide sequence. We showed PEG hydrogel at intermediate crosslinking density, 50%, with the shear modulus of 785$\pm$40 Pa results in the highest albumin and urea production compared to other crosslinking densities. Moreover, encapsulated iHEP aggregates exhibited hepatic activity similar to Matrigel as characterized by albumin and urea production and induction of CYP450 drug metabolism enzymes. The evaluation of integrin binding peptide (RGDS) on iHEP aggregate metabolic function and enzyme activity showed effect of integrin binding peptides is more pronounced at 30% crosslinking density and has no effect on the albumin and urea synthesis at 50% crosslinking density. Overall, this study shows the fine balance between crosslinking density and integrin binding peptides on metabolic function of iHEP aggregates encapsulated in PEG hydrogel. This work lays the ground for development of better 3D *in vitro* models, specifically for liver diseases mediated by the biomechanical properties of the ECM [10–17].

6.4 Materials and Methods

6.4.1 Hepatocyte cell culture

iCell Hepatocyte 2.0 (iHEP, from Cellular Dynamics International) was thawed and plated into collagen I-coated 24 and 96-well plates at a $3x10^5$ cells/cm^2. Plating volumes for 24 and 96-welll plates were 0.57 ml and 0.1 ml, respectively. Maintenance medium used for 2D culture of hepatocytes was DEME/F12 medium, no phenol red supplemented with B27 supplement (1x), Dexamethasone (0.1 μM) and Oncostatin M (20 ng/ml). On day 1 through day 4 post-plating, spent medium is replaced daily. On day 5, medium is replaced with Maintenance medium minus Oncostatin and spent medium is replaced every two days thereafter.

6.4.2 Aggregate formation and maintenance

On day 5 post iHEP 2D culture Accutase was used to dissociate iHEPs. Cells were seeded into Aggrewell plates (STEMCELL Technologies) at 500 viable cells per well and subsequently centrifuged at 100 x g for 2 min. Cells were seeded in iHEP Maintenance medium (*Section 2.2*) minus Oncostatin M. Aggregates were maintained in serum-free medium with 50% medium change every 48-72 h. The cells formed spheroids within 24-48 hours after transfer to the Aggrewell. iHEP aggregates were harvested after 2 days and passed through the 37-micron reversible strainer to filter all the single cells. Aggregates were then encapsulated in PEG hydrogels (Fig. 6.1).

6.4.3 Aggregate encapsulation and polymerization of PEG hydrogels

iHEP aggregates were re-suspended in a 2X photoinitiator solution (0.2 % wt./wt. Irgacure 2959) and mixed 1:1 with a 2X PEG monomer solution. For experiments encapsulating iHEP aggregates in PEG hydrogel using 384 multiwell plates (Corning, Cat # 3764), wells were pre-coated with a thin layer of hydrogel (~8 μL) and then 12 μL of the cell and monomer solution was pipetted on the top. Both bottom and top layers were polymerized for 2 min using ~5-10 mW/cm^2 UV light centered at ~365 nm. 384-multiwell plates were placed on the top shelf of the exposure stand for a UVP XX-15L series UV lamp, Fisher. For aggregates encapsulated in Matrigel, we used same amount (~8 μL) of Matrigel (Corning, Cat# 356231, 9.2 mg/ml)) at the bottom of each wells and polymerized for 20 minutes in 37^{o}C incubator, then Matrigel was added to pelleted iHEP aggregates and 12 μL was pipetted on the top and polymerized at 37^{o}C for 20 minutes. 80 μL of media was added to each well and half of the media was exchanged every 48 h. Each well contained 20-30 iHEP aggregates per well (Fig. 6.1).

For experiments, seeding iHEP single cells on top of PEG hydrogel, 20 μL of 2X PEG monomer solution with 2X photoinitiator solution at 1:1 ratio was pipetted in each well and polymerized as described above. For cells seeded on top of Matrigel, 20 μL of Matrigel (at 9.2 mg/ml) was pipetted in each well and polymerized as described above. Then, iHEP single cells at 500, 1000, 5000, 10000 and 20000 cells per well were seeded on the top of the polymerized hydrogel. 80 μL of media was added to each well and half of the media was exchanged every 48 h (Fig. S61).

6.4.4 Poly (ethylene glycol) (PEG) hydrogel preparation

Poly(ethylene glycol) (PEG) hydrogels were formed using thiol-ene photopolymerization chemistry [36]. 8-arm PEG-norbornene was purchased from a commercial source (JenKem USA:

20,000 MW, 8ARM (TP)-NB-20K). Stock PEG solutions were prepared by adding 0.8 mL 1X PBS to 300 mg lyophilized 8-arm PEG-NB powder (final volume = 1 mL) and filtered through a 0.2 μm nylon syringe filter (Fisher) for a final concentration of 300 mg/mL sterile monomer. Monomer solutions for cell encapsulation were prepared in 1X PBS with 40 mg/mL 8-arm PEG-NB in which 30, 50 and 70% of the available norbornene arms were cross-linked with a matrix metalloproteinase (MMP)-degradable peptide with cysteines flanking the active sequence (KCG**GPQG*IWGQ**GCK, GenScript; active sequence in bold; * = cleavage site). To promote cell adhesion, C**RGDS** (GenScript, active sequence in bold) at 0, 2 and 4 mM was incorporated as a pendant group through the terminal cysteine. Scrambled sequence (CRDGS) peptide and cysteamine at 2 and 4 mM were used as non-adhesive controls.

6.4.5 Quantification of Shear Modulus

To measure the shear modulus of PEG hydrogels, 68 μL precursor solutions were pipetted into 8.0 mm diameter, 1.2 mm depth Teflon wells and cured for 2 minutes using 365 nm UV light at a dose rate of ~5-10 mW/cm^2. The resulting hydrogels were swollen to equilibrium in 1X PBS for 24 hr. The samples were tested using an Ares-LS2 rheometer (TA Instruments). A 5 ×g force was applied to the samples via parallel plate crossheads and a strain sweep test at 1 Hz fixed frequency was performed from 0.1 to 20% strain. If the sample was not robust enough to withstand a 5 ×g force the gap between the parallel plates of the rheometer was set to 1.0 mm distance. Measurements for complex shear modulus for each hydrogel formulation were taken at 1 Hz, 2–20% strain.

6.4.6 Biochemical Assays

6.4.6.1 ALB and Urea Secretion

Albumin and urea secretion were analyzed by measuring the concentration of albumin and urea of lysed cells in the culture medium. Encapsulated aggregates in PEG or Matrigel were mechanically dissociated by pipetting up and down and supernatants were assayed for albumin and urea levels. Albumin was measured using an enzyme-linked immunosorbent assay (ELISA) kit (E88-129, Bethyl Laboratories). Urea concentration was measured using a calorimetric assay kit from Bioassay Systems (DIUR-100).

6.4.6.2 Cytochrome P450

Luminescence-based assays (Promega, Madison, WI) for CYP2C9 (luciferin-H), CYP3A4 (luciferin-IPA) and CYP1A2 (luciferin-1A2) were used to measure CYP450 activity. Briefly, cultures were rinsed in phenol red-free culture medium and incubated with luminescent substrates, diluted in same medium, for 1 hour (3μM luciferin-IPA, CYP3A4 substrate) or 3 hours (100μM luciferin-H, CYP2C9 substrate) at 37ºC. For CYP1A2 cultures were rinsed with PBS and incubated with luminescent substrate diluted in PBS for 1 hour (6μM luciferin-1A2). Following incubation, supernatant was processed according to manufacturer instructions and luminescence was measured using luminometer (Promega GloMax plate reader).

Drug dosing. For CYP450 induction studies, aggregates were pretreated with inducers for 72 h beginning at 48 h post-encapsulation. Stock solutions of inducers were prepared in dimethyl sulfoxide (DMSO) and diluted at 1:1000 for final concentration of 25 μM of Rifampicin, 100 μM fo omeprazole and 50 μM of dexamethasone. Vehicle controls were pretreated with 72 h of either 1:1000 DMSO or no drug. Since dexamethasone is a known inducer of cytochrome P450 3A4, dexamethasone was extracted from the medium to lower CYP3A4 basal activity.

6.5 Results

6.5.1 Albumin and urea secretion of encapsulated iHEP aggregates were enhanced in PEG hydrogels with intermediate crosslinking density

Rheometric analysis of PEG hydrogels showed increase (122 ± 25 to 1600 ± 40 Pa) in the shear modulus when crosslinking density was increased from 30% to 70% (Fig. 6.2a). Matrigel at 9.2 mg/mL showed similar stiffness compared to the 30% crosslinking density (Fig. 6.2a). Phase-contrast images of encapsulated iHEP aggregates showed that aggregates maintained their 3D spherical morphology at different crosslinking density (Fig. 6.2b).

Albumin and urea secretion of encapsulated iHEP aggregates showed 2-fold increase from 30% to 50% crosslinking density and 1.4-fold decrease from 50% to 70% crosslinking density (Fig. 6.2c-d). At 50% crosslinking density, the secreted albumin was 1.5-fold higher than that of aggregates encapsulated in Matrigel (Fig. 6.2c). However, no significant difference was observed for the urea secretion between iHEP aggregates encapsulated in 50% crosslinking density and Matrigel (Fig. 6.2d). These results demonstrate aggregates encapsulated at 50% crosslinking density has the highest level of albumin and urea synthesis compared to 30% and 70% crosslinking density, and the values are higher or at the same level of aggregates encapsulated within Matrigel.

6.5.2 Integrin binding peptide was not essential for metabolic function of iHEP aggregates encapsulated at intermediate crosslinking density

Presence of 2 mM RGDS for 30% crosslinking density PEG hydrogels resulted in 2-fold and 1.7-fold increase in albumin and urea production of encapsulated iHEP aggregates relative to 0 mM RGDS. Urea and albumin production of encapsulated iHEP aggregates at 50% crosslinking density were maintained at the same level in the presence of 2 mM RGDS. Conversely, presence

of 2 mM RGDS for encapsulated iHEP aggregates in 70% crosslinking density PEG hydrogel showed 1.8-fold and 1.3-fold decrease in albumin and urea production, respectively (Fig. 6.3a, b). Moreover, phase contrast images taken from aggregates showed that aggregates maintained their spherical morphology in 50% and 70% crosslinking PEG hydrogels even in the presence of adhesive integrin binding peptides (Fig. 6.3d,e) Contrary to 50% and 70% crosslinking densities, iHEP aggregate encapsulated in 30% crosslinking density PEG with 2mM RGDS showed sign of adhesion to the ECM and increase in the surface area of aggregates (Fig. 6.3c). Together, these results show that albumin and urea production of encapsulated iHEP aggregates depend on the balance between crosslinking density and integrin binding peptides. And integrin binding peptide was not essential for metabolic function of iHEP aggregates encapsulated at intermediate crosslinking density

6.5.3 Integrin binding peptide was not essential for CYP450 enzyme activity of iHEP aggregates encapsulated at intermediate crosslinking density

Since encapsulated iHEP aggregates at intermediate crosslinking density (50%) showed higher level of albumin and urea production, we then characterized the liver specific drug metabolism functions of encapsulated iHEP aggregates by assessing the basal CYP450 enzyme activity and their induction in response to known pharmacological inducers. Similar to albumin and urea synthesis results (Fig. 6.3a, b), presence of RGDS did not have any significant effect on the basal activity level of CYP 3A4, 2C9 and 1A2 of the iHEP aggregates encapsulated in 50% crosslinking density PEG hydrogels (Fig. 6.4). The basal activity of those enzymes was similar to the aggregates encapsulated in Matrigel. Encapsulated iHEP aggregates showed 2-fold and 1.5-fold increase in CYP3A4 basal activity level after induction with dexamethasone and rifampicin, respectively (Fig. 6.4a).1.8-fold increase in CYP2C9 basal activity level after induction with

rifampicin (Fig. 6.4b), and a 3-fold increase in CYP1A2 basal activity level after induction with omeprazole (Fig. 6.4c) was observed. Similarly, encapsulated iHEP aggregates in Matrigel showed 1.6-fold and 1.4-fold increase in CYP3A4 by dexamethasone and rifampicin, respectively (Fig. 6.4a), a 1.8-fold increase in CYP2C9 by rifampicin (Fig. 6.4b), and a 2.7-fold increase in CYP1A2 by omeprazole (Fig. 6.4c). Taken together, PEG hydrogels with 50% crosslinking density, maintained activity of CYP1A2, CYP2C9, and CYP3A4 (with or without pharmacological inducers) of iHEP aggregate at the same level to that of iHEP aggregates encapsulated in Matrigel. Moreover, the presence of RGDS did not have any significant effect on the induced or basal level of those enzymes.

6.6 Discussion

Though natural hydrogels have produced promising results for hepatocyte differentiation, downstream applications are limited by the use of natural hydrogels (e.g., Matrigel), which is poorly characterized, highly variable and of mouse origin [4,16]. Thus, there is a need for a well-defined, xeno-free matrix that would address the issues associated with natural hydrogels. Synthetic hydrogels are appealing because not only their chemistry and properties are controllable and reproducible but also are structurally similar to the extracellular matrix of many tissues. They can be produced with defined molecular weight, block structures, degradable linkages and crosslinking modes. Properties of hydrogels such as degradability, mechanical stiffness, crosslinking densities and gel formation dynamics can be easily tuned in synthetic hydrogels. However, there are very few publications that have studied the effect of synthetic hydrogels properties on iPS/ES derived hepatocyte metabolic function and CYP450 enzyme activities [18–20] and such studies were often done in a 2D culture format. Here we used synthetic MMP-

degradable PEG hydrogel functionalized with integrin binding peptide, RGDS, to study the effect of crosslinking density and integrin binding peptide concentration on the function of 3D iHEP aggregates in a 3D context.

By examining the function of iHEP aggregates encapsulated in PEG hydrogels with different crosslinking density, we found that hydrogels at 50% crosslinking density secret highest level of albumin and urea and the values are higher or at the same level to iHEP aggregates encapsulated in Matrigel (Fig. 6.2). It's worth to mention that the shear modulus of healthy liver is between 400-600 Pa [10,21] and shear modulus of PEG hydrogels at 50% crosslinking density was 785±40 Pa. Since PEG is biologically inert and is not functionalized with adhesive peptide, the secreted ECM molecules attached to the iHEP aggregates may act as transmitters to transfer the matrix biomechanical signal to the iHEP cells located on the periphery of the iHEP aggerates. Previous SEM data demonstrated the deposition of ECM on the surface of iHEP aggregates [22]. Alternatively, varying crosslinking density alters the mesh size for these networks, which can impact the diffusional properties of the hydrogel. It is not possible to uncouple mechanical properties from diffusional properties examined in this study.

Integrin ligation by RGDS peptide has been reported to confer survival to isolated hepatocytes through the Akt pathway [23]. In addition, cellular response to RGD can depend on how the peptide is presented (e.g., concentration). To show that iHEP cells used in this study express the integrin that can specifically recognize the RGD sequence, we seeded single iHEP cells at different cell density on top of the 50% crosslinking hydrogels with adhesive RGDS (at 2 and 4mM) and non-adhesive controls (no RGDS, scrambled RGDS sequence and Cysteamine at 2 and 4mM) (Fig. S6.1). The results showed when cells are seeded on PEG hydrogels with 2 and 4 mM RGDS the iHEP single cells attached to the ECM and spread. However, in the presence of

non-adhesive controls, single iHEP cells self-organized and formed small aggregates. The size of the aggregates increased as the seeding cell density increased. Further, rheometric analysis of hydrogels with different adhesive and non-adhesive moieties showed no change in shear moduli of 50% crosslinking hydrogels (Fig. S6.2a). After stablishing that iHEP cells could recognize the RGD sequence tethered to the PEG hydrogel and there are no non-specific bindings to non-adhesive sequences (RDGS and cysteamine), we studied the effect of RGD concentration on iHEP aggregates in a 3D context.

Notably, further functionalizing of the PEG hydrogels with adhesive RGDS peptide did not have a significant effect on albumin and urea production (Figs. 6.3, S62b-c) and CYP450 enzyme activities (Fig. 6.4) of encapsulated iHEP aggregates at 50% crosslinking density. While the presence of RGDS in 30% crosslinking density enhanced the albumin and urea production by 2-folds, it caused a 2-fold decrease in 70% crosslinking density (Fig. 6.3). It is likely the balance between outside-in signals (e.g., stiffness, crosslinking density, integrin binding density) and inside-out signals (e.g., cell-cell contact) that affects the iHEP cell metabolic function and its interaction with the ECM. Steinberg and co-workers established that the formation of tissue self-assemblies is essentially a “tug-of-war” between substrate adhesiveness and cellular cohesion [24]. In the case of 50% crosslinking density with RGDS the cohesion forces (coming from cell-cell contact) established during the spheroid formation were sufficient to alleviate the need for any cell-matrix contacts in 3D (Figs. 6.3, S63), as the PEG hydrogel background is biologically inert, and presence of adhesive peptides at different density did not have any significant effect in ALB and urea production (Fig. 6.3). Li and co-workers also showed that RGDS was not necessary for optimal rat hepatocyte function encapsulated in 10% polyethylene glycol (PEG) diacrylate,

however, they did not study the effect of adhesive ligands at different stiffness on the function of hepatocytes [25].

The fine balance between the substrate adhesiveness and cellular cohesion forces was evident when single iHEP cells at different density were seeded on top of the 50% crosslinking PEG hydrogels functionalized with adhesive and non-adhesive peptides at different concentration (Fig. S6.1). Self-assembly of iHEP cells in the case of scrambled non-adhesive peptide (RDGS), Cysteamine and 0 mM RGDS demonstrate that the cohesive forces were bigger than adhesive forces. However, the addition of RGDS peptide tips the balance towards the opposite side and results in the spread of the iHEP single cells on PEG substrate. In the case of Matrigel, the cells did not form aggregates like what we observed in the PEG conditions (Fig. S6.1); however, the cells agglomerated together and formed a dense network of cells, which shows cohesive forces are bigger than the adhesive forces on Matrigel substrate. This is perhaps due to the way Matrigel forms gel, as Hakkinen et al. showed that Matrigel forms a gel without discernable fibers at the cellular level compared to collagen and fibrin gels, and thus fibroblasts failed to spread or generate adhesion [26,27]. iHEP cells after forming 3D aggregates were seeded on top of the same hydrogel and the result were similar to when the aggregates were encapsulated inside the hydrogel (Fig. 6.2 and 6.3), suggesting that cohesive forces due to increased cell-cell contact established after aggregate formation is higher than the adhesive forces when cells are seeded in aggregate format. Together, this study demonstrates that adhesion to matrices is different if cells are seeded in 2D or 3D format.

6.7 Conclusions

Our current understanding of the effect of mechanical properties of ECM is derived primarily from studies of cellular adhesions formed on two-dimensional (2D) substrates in vitro. Yet the rules of cell-ECM interactions and mechano-sensing in three-dimensional microenvironments are more complex under both in vitro and in vivo conditions [26,28]. Here, we presented a well-defined synthetic substrate for 3D culture of iHEP aggregates that can substitute Matrigel. Having a great deal of control over the mechanical and biochemical properties of the PEG hydrogels can help us to unravel the mechano-transduction signal that the ECM sends to hepatocyte and its role in maturation and differentiation of iPS/ES-derived hepatocytes. We showed that iHEP aggregates encapsulated in PEG hydrogels with intermediate crosslinking density, where the shear modulus is close to the healthy liver shear modulus produces the highest level of albumin and urea. Moreover, at that crosslinking density, the RGDS integrin binding peptides did not have any effect on iHEP aggregates metabolic function. Our study also revealed the difference between interaction of iHEP cells with the ECM in a 2D and 3D context. We can use this in vitro model for making a more predictive 3D in vitro models to study liver diseases that are associated with the mechanical property of the liver environment. Moreover, in contrasts to the suspension culture of the iHEP aggregates, where uncontrolled aggregation often results in large spheroid with necrotic cores [29], iHEP aggregates encapsulated in PEG are protected from the shear stress and aggregates can be cultured in small volumes without such consequences. The aggregates here were cultured under the static condition; however, they can be adapted to the microfluidic platforms where the physiological dynamic flow can be established. Finally, aggregates containing different cell types could be combined to explore signaling or metabolic interaction between aggregates of varying cell types.

6.8 Disclosure of Potential Conflicts of Interest

The authors declare no competing financial interests.

6.9 Acknowledgments

The authors thank Victoria Harms (UW-Madison) for preforming the rheometric analysis on hydrogels. This research was funded by the Environmental Protection Agency (STAR Grant no. 83573701) and the National Institutes of Health (1U01TR002383-01).

6.10 References

[1] T. Takebe, K. Sekine, M. Kimura, E. Yoshizawa, S. Ayano, M. Koido, S. Funayama, N. Nakanishi, T. Hisai, T. Kobayashi, T. Kasai, R. Kitada, A. Mori, H. Ayabe, Y. Ejiri, N. Amimoto, Y. Yamazaki, S. Ogawa, M. Ishikawa, Y. Kiyota, Y. Sato, K. Nozawa, S. Okamoto, Y. Ueno, H. Taniguchi, Massive and Reproducible Production of Liver Buds Entirely from Human Pluripotent Stem Cells, Cell Reports. 21 (2017) 2661–2670. doi:10.1016/j.celrep.2017.11.005.

[2] M.A. Lancaster, J.A. Knoblich, Organogenesis in a dish: Modeling development and disease using organoid technologies, Science. 345 (2014) 1247125–1247125. doi:10.1126/science.1247125.

[3] K. Si-Tayeb, F.K. Noto, M. Nagaoka, J. Li, M.A. Battle, C. Duris, P.E. North, S. Dalton, S.A. Duncan, Highly efficient generation of human hepatocyte-like cells from induced pluripotent stem cells, Hepatology. 51 (2010) 297–305. doi:10.1002/hep.23354.

[4] D.C. Hay, J. Fletcher, C. Payne, J.D. Terrace, R.C.J. Gallagher, J. Snoeys, J.R. Black, D. Wojtacha, K. Samuel, Z. Hannoun, A. Pryde, C. Filippi, I.S. Currie, S.J. Forbes, J.A. Ross, P.N. Newsome, J.P. Iredale, Highly efficient differentiation of hESCs to functional hepatic endoderm requires ActivinA and Wnt3a signaling, Proceedings of the National Academy of Sciences. 105 (2008) 12301–12306. doi:10.1073/pnas.0806522105.

[5] N.R.F. Hannan, C.-P. Segeritz, T. Touboul, L. Vallier, Production of hepatocyte-like cells from human pluripotent stem cells, Nature Protocols. 8 (2013) 430–437. doi:10.1038/nprot.2012.153.

[6] C.S. Hughes, L.M. Postovit, G.A. Lajoie, Matrigel: A complex protein mixture required for optimal growth of cell culture, PROTEOMICS. 10 (2010) 1886–1890. doi:10.1002/pmic.200900758.

[7] BD Matrigel Matrix, (n.d.). http://fscimage.fishersci.com/cmsassets/downloads/segment/Scientific/pdf/BD/bd_cellculture_matrigel_faq.pdf.

[8] M.J. Martin, A. Muotri, F. Gage, A. Varki, Human embryonic stem cells express an immunogenic nonhuman sialic acid, Nature Medicine. 11 (2005) 228–232. doi:10.1038/nm1181.

[9] M.P. Lutolf, Synthetic matrix metalloproteinase-sensitive hydrogels for the conduction of tissue regeneration: Engineering cell-invasion characteristics, Proceedings of the National Academy of Sciences. 100 (2003) 5413–5418. doi:10.1073/pnas.0737381100.
[10] W.-C. Yeh, P.-C. Li, Y.-M. Jeng, H.-C. Hsu, P.-L. Kuo, M.-L. Li, P.-M. Yang, P.-H. Lee, Elastic modulus measurements of human liver and correlation with pathology, Ultrasound Med Biol. 28 (2002) 467–474.
[11] Daniel Deegan, Effects of Liver Extracellular Matrix Gel Stiffness on Primary Hepatocyte Function, Dissertation, Wake Forest University, 2016. http://hdl.handle.net/10339/57438.
[12] R.G. Wells, The role of matrix stiffness in regulating cell behavior, Hepatology. 47 (2008) 1394–1400. doi:10.1002/hep.22193.
[13] R.G. Wells, Cellular Sources of Extracellular Matrix in Hepatic Fibrosis, Clinics in Liver Disease. 12 (2008) 759–768. doi:10.1016/j.cld.2008.07.008.
[14] J. Schrader, T.T. Gordon-Walker, R.L. Aucott, M. van Deemter, A. Quaas, S. Walsh, D. Benten, S.J. Forbes, R.G. Wells, J.P. Iredale, Matrix stiffness modulates proliferation, chemotherapeutic response, and dormancy in hepatocellular carcinoma cells, Hepatology. 53 (2011) 1192–1205. doi:10.1002/hep.24108.
[15] K.S. Jung, S.U. Kim, S.H. Ahn, Y.N. Park, D.Y. Kim, J.Y. Park, C.Y. Chon, E.H. Choi, K.-H. Han, Risk assessment of hepatitis B virus-related hepatocellular carcinoma development using liver stiffness measurement (FibroScan), Hepatology. 53 (2011) 885–894. doi:10.1002/hep.24121.
[16] H. Tsukuma, T. Hiyama, S. Tanaka, M. Nakao, T. Yabuuchi, T. Kitamura, K. Nakanishi, I. Fujimoto, A. Inoue, H. Yamazaki, T. Kawashima, Risk Factors for Hepatocellular Carcinoma among Patients with Chronic Liver Disease, New England Journal of Medicine. 328 (1993) 1797–1801. doi:10.1056/NEJM199306243282501.
[17] T.R. Cox, J.T. Erler, Remodeling and homeostasis of the extracellular matrix: implications for fibrotic diseases and cancer, Disease Models & Mechanisms. 4 (2011) 165–178. doi:10.1242/dmm.004077.
[18] B.L. Villarin, K. Cameron, D. Szkolnicka, H. Rashidi, N. Bates, S.J. Kimber, O. Flint, S.J. Forbes, J.P. Iredale, M. Bradley, D.C. Hay, Polymer Supported Directed Differentiation Reveals a Unique Gene Signature Predicting Stable Hepatocyte Performance, Advanced Healthcare Materials. 4 (2015) 1820–1825. doi:10.1002/adhm.201500391.
[19] B. Lucendo-Villarin, K. Cameron, D. Szkolnicka, P. Travers, F. Khan, J.G. Walton, J. Iredale, M. Bradley, D.C. Hay, Stabilizing Hepatocellular Phenotype Using Optimized Synthetic Surfaces, Journal of Visualized Experiments. (2014). doi:10.3791/51723.
[20] Y. Luo, C. Lou, S. Zhang, Z. Zhu, Q. Xing, P. Wang, T. Liu, H. Liu, C. Li, W. Shi, Z. Du, Y. Gao, Three-dimensional hydrogel culture conditions promote the differentiation of human induced pluripotent stem cells into hepatocytes, Cytotherapy. 20 (2018) 95–107. doi:10.1016/j.jcyt.2017.08.008.
[21] S.S. Desai, J.C. Tung, V.X. Zhou, J.P. Grenert, Y. Malato, M. Rezvani, R. Español-Suñer, H. Willenbring, V.M. Weaver, T.T. Chang, Physiological ranges of matrix rigidity modulate primary mouse hepatocyte function in part through hepatocyte nuclear factor 4 alpha: Matrix rigidity modulates hepatocyte function, Hepatology. 64 (2016) 261–275. doi:10.1002/hep.28450.
[22] H. Ardalani, S. Sengupta, V. Harms, V. Vickerman, J.A. Thomson, W.L. Murphy, 3-D Culture and Endothelial Cells Improve Maturity of Human Pluripotent Stem Cell-Derived

Hepatocytes, Acta Biomaterialia. (2019) S1742706119305367. doi:10.1016/j.actbio.2019.07.047.
[23] G.G.M. Pinkse, R. Jiawan-Lalai, J.A. Bruijn, E. de Heer, RGD peptides confer survival to hepatocytes via the β1-integrin-ILK-pAkt pathway, Journal of Hepatology. 42 (2005) 87–93. doi:10.1016/j.jhep.2004.09.010.
[24] P.L. Ryan, R.A. Foty, J. Kohn, M.S. Steinberg, Tissue spreading on implantable substrates is a competitive outcome of cell-cell vs. cell-substratum adhesivity, Proceedings of the National Academy of Sciences. 98 (2001) 4323–4327. doi:10.1073/pnas.071615398.
[25] C.Y. Li, K.R. Stevens, R.E. Schwartz, B.S. Alejandro, J.H. Huang, S.N. Bhatia, Micropatterned Cell–Cell Interactions Enable Functional Encapsulation of Primary Hepatocytes in Hydrogel Microtissues, Tissue Engineering Part A. 20 (2014) 2200–2212. doi:10.1089/ten.tea.2013.0667.
[26] A.D. Doyle, K.M. Yamada, Mechanosensing via cell-matrix adhesions in 3D microenvironments, Experimental Cell Research. 343 (2016) 60–66. doi:10.1016/j.yexcr.2015.10.033.
[27] K.M. Hakkinen, J.S. Harunaga, A.D. Doyle, K.M. Yamada, Direct Comparisons of the Morphology, Migration, Cell Adhesions, and Actin Cytoskeleton of Fibroblasts in Four Different Three-Dimensional Extracellular Matrices, Tissue Engineering Part A. 17 (2011) 713–724. doi:10.1089/ten.tea.2010.0273.
[28] B.M. Baker, C.S. Chen, Deconstructing the third dimension - how 3D culture microenvironments alter cellular cues, Journal of Cell Science. 125 (2012) 3015–3024. doi:10.1242/jcs.079509.
[29] E. Curcio, S. Salerno, G. Barbieri, L. De Bartolo, E. Drioli, A. Bader, Mass transfer and metabolic reactions in hepatocyte spheroids cultured in rotating wall gas-permeable membrane system, Biomaterials. 28 (2007) 5487–5497. doi:10.1016/j.biomaterials.2007.08.033.

6.11 Figures

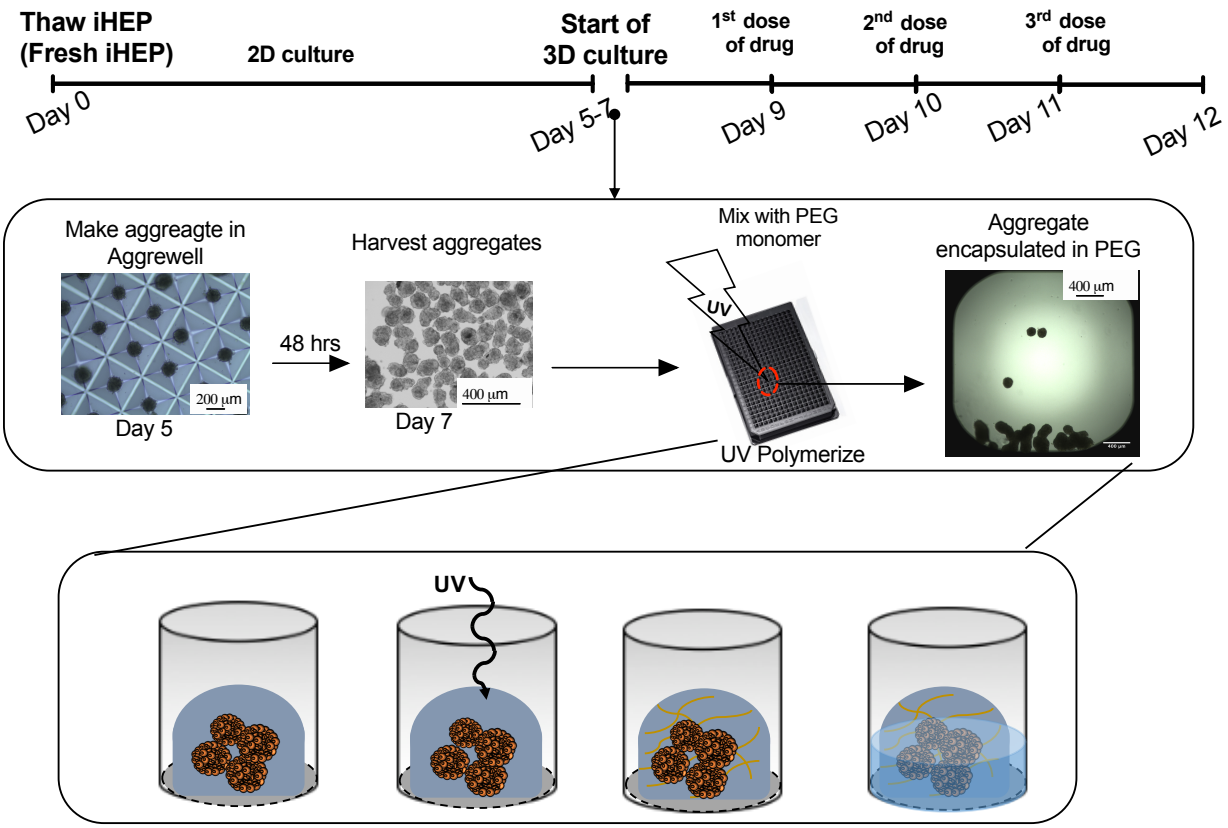

Figure 6.1 Schematic depicting the experimental procedure for iHEP culture and 3D aggregate formation and aggregate encapsulation in PEG hydrogel

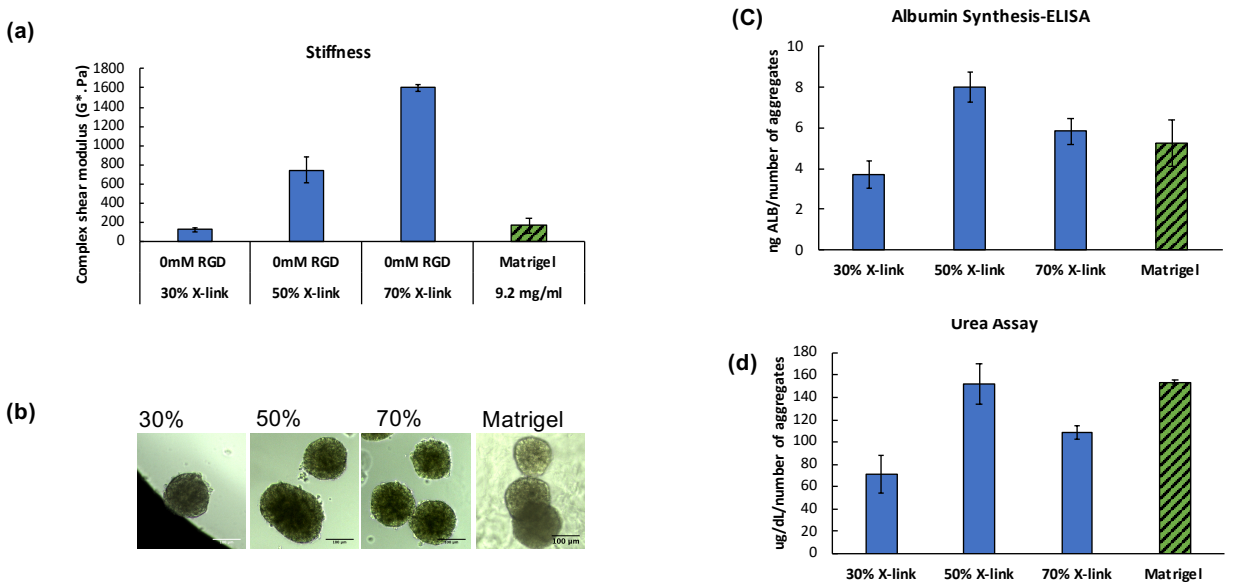

Figure 6.2 Effect of hydrogel crosslinking density on Albumin and Urea secretion (a) Rheometric analysis of PEG hydrogel formulation**.** The PEG hydrogel shear modulus was tuned from 122 ± 25 – 1600 ± 40 Pa by maintaining a constant PEG-norbornene concentration while varying the crosslinking density from 30-70% molar ratio thiol:norbornene. **(b)** Morphology of aggregates in hydrogel with different stiffness after 10 days. Scale bar is 100 µm. **(c, d)** Comparison of albumin and urea secretion for iHEP aggregates encapsulated in PEG hydrogels with different crosslinking density versus Matrigel.

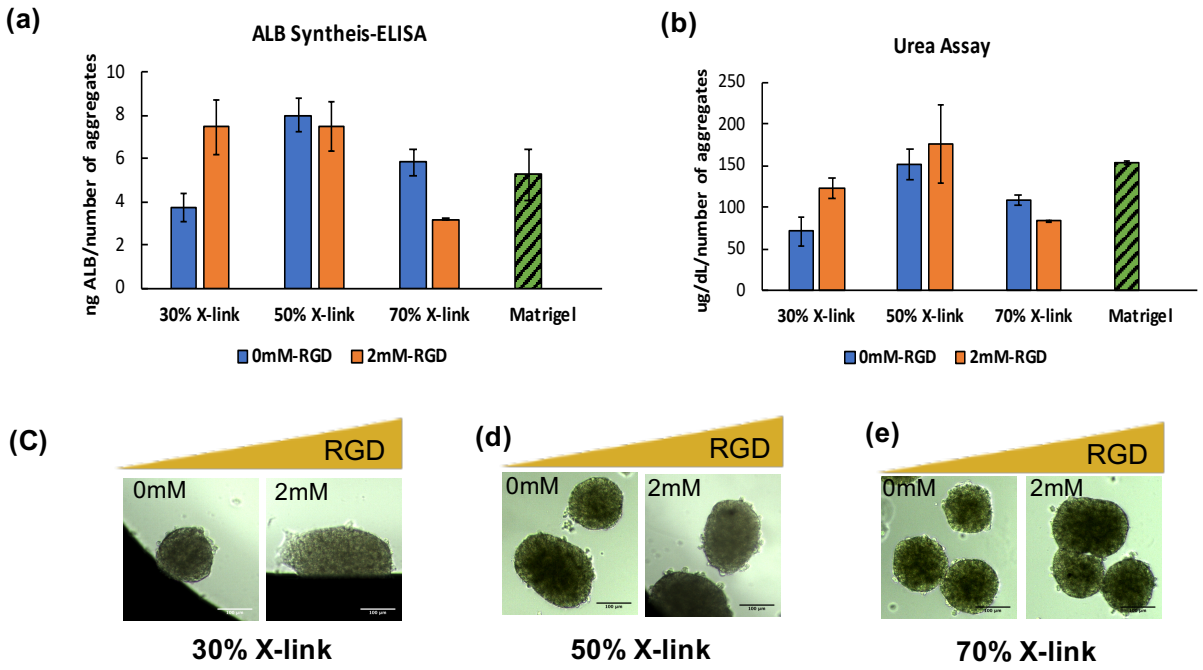

Figure 6.3 Effect of integrin-binding peptide on albumin and urea secretion of encapsulated iHEP aggregates at different crosslinking density (a, b) Comparison of albumin and urea secretion with and without RGDS for iHEP aggregates encapsulated in PEG hydrogels with different crosslinking density versus Matrigel **(c-e)** Gross morphology of aggregates in PEG hydrogels with(out) adhesive moieties after 10 days. Scale bar is 100 μm

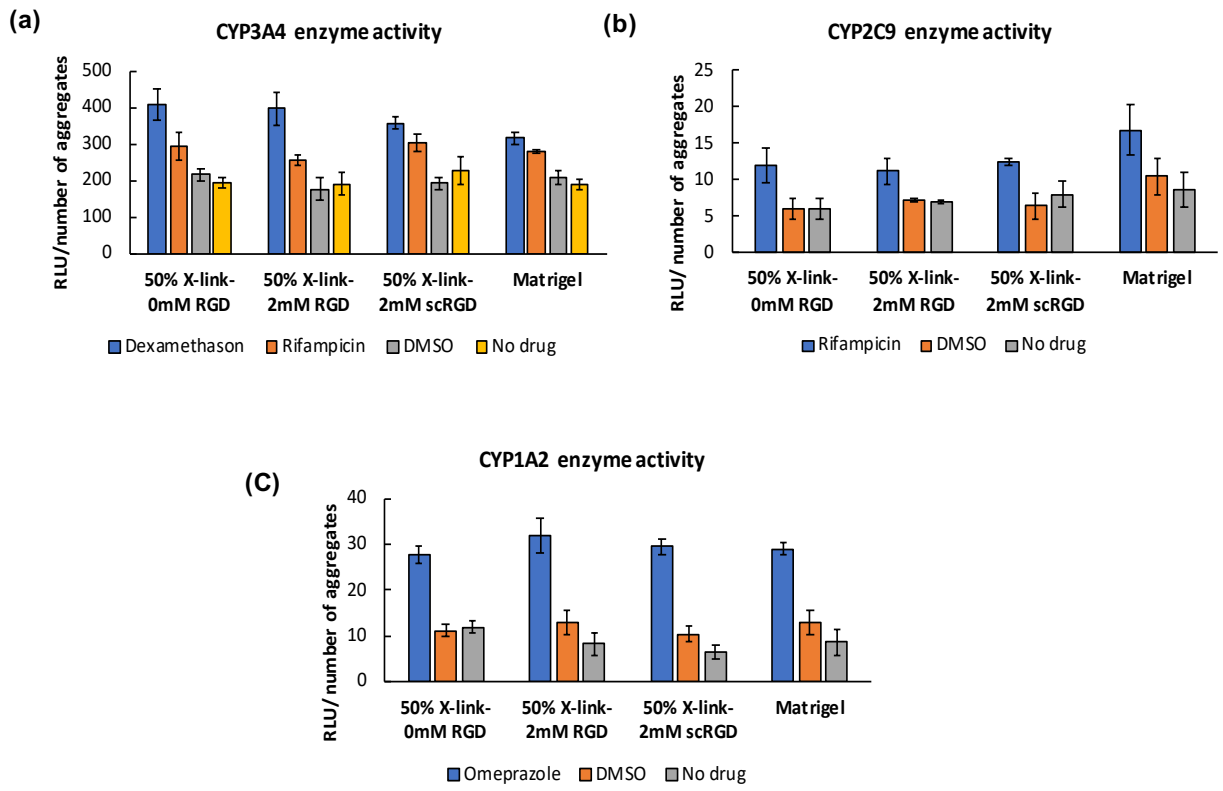

Figure 6.4 Effect of integrin-binding peptide on drug metabolism enzyme activity of 3D iHEP aggregates encapsulated in PEG hydrogels with intermediate crosslinking density (a) CYP3A4 basal activity and induction with dexamethasone and rifampicin **(b)** CYP2C9 basal activity and induction with rifampicin **(c)** CYP1A2 basal activity and induction with omeprazole

6.12 Supplemental Figures

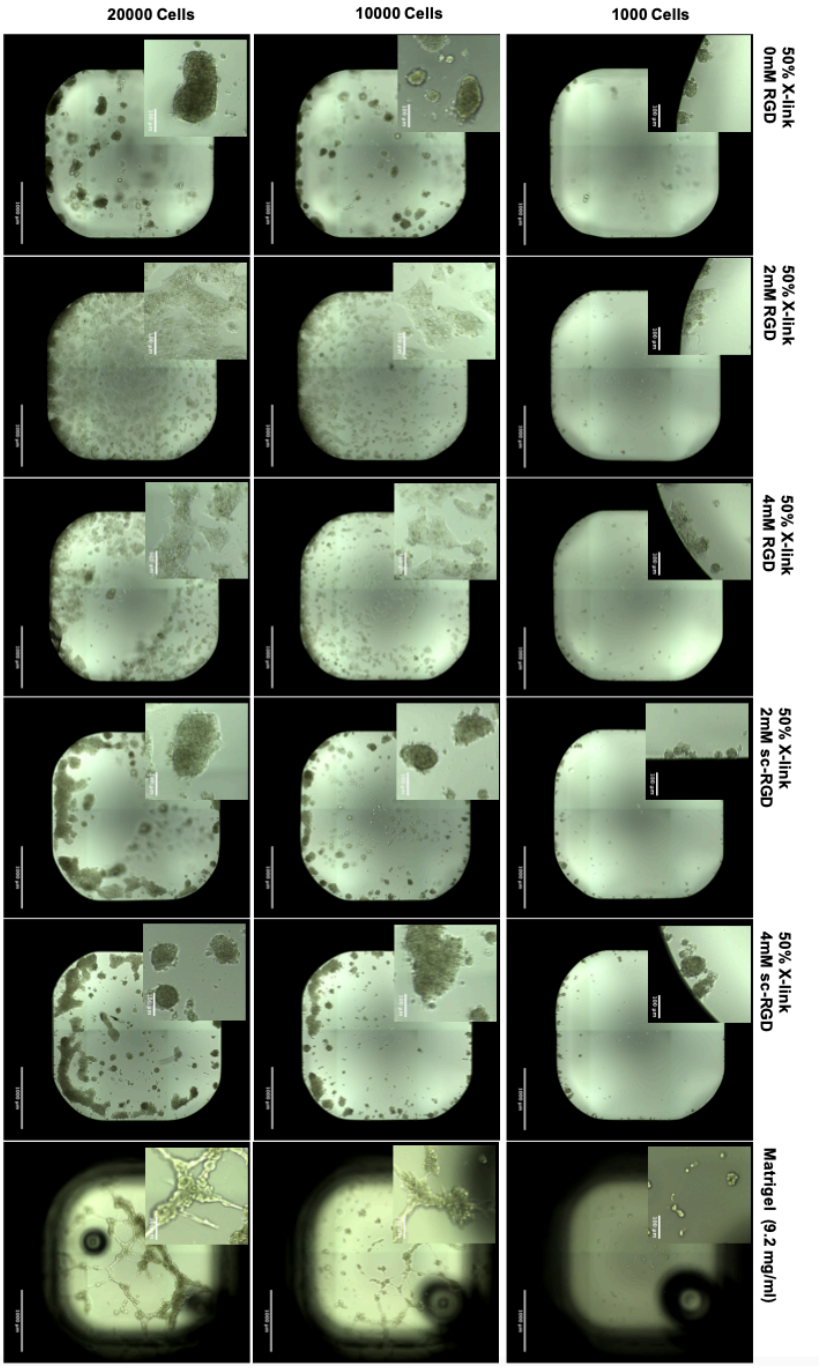

Figure S6.1 Effect of integrin binding peptide on iHEP at single cell. Morphology of iHEP cells seeded as single cells at different cell density on top of the 50% crosslinking PEG hydrogels with adhesive peptide (RGDS, at 2 and 4mM) and non-adhesive controls (no RGDS, scrambled RGDS sequence and Cysteamine at 2 and 4mM). Scale bar for the outside image is 1000 μm and for the inside image is 100 μm.

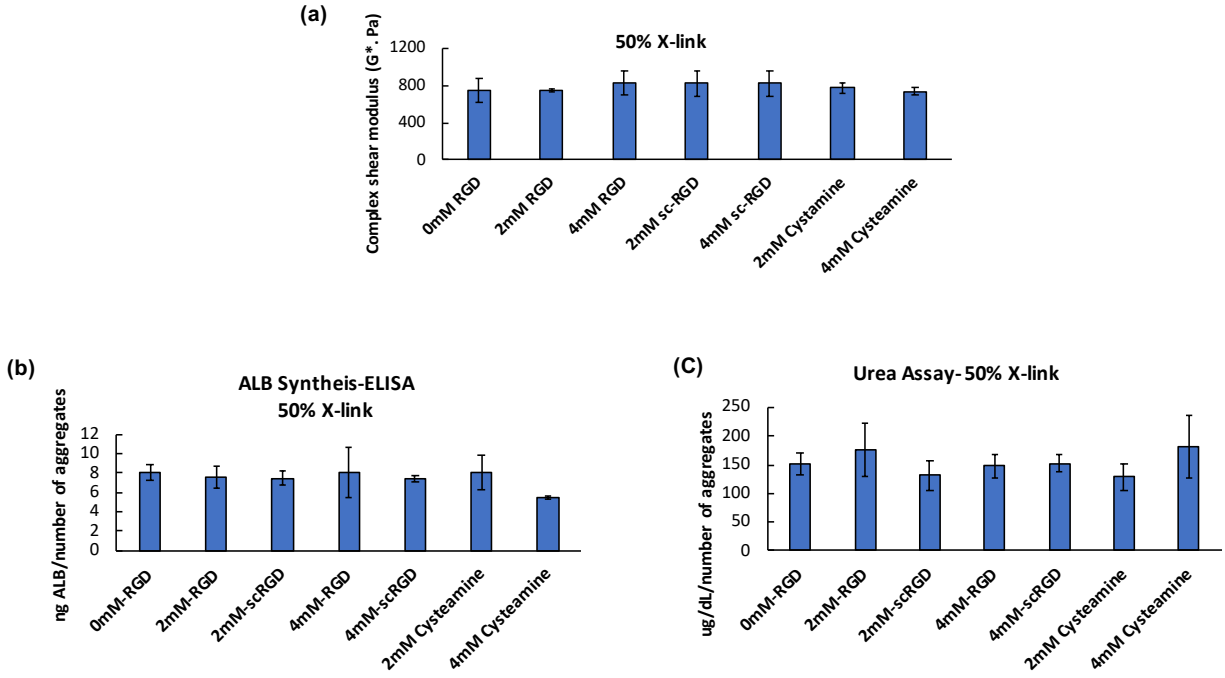

Figure S6.2 Effect of integrin-binding peptide and non-integrin binding peptides (controls) on albumin and urea secretion for iHEP aggregates encapsulated in 50% crosslinking density (a) Comparison of shear moduli of hydrogels with adhesive and non-adhesive controls at 50% crosslinking density. **(b, c)** Comparison of albumin and urea secretion with adhesive and non-adhesive controls at 50% crosslinking density.

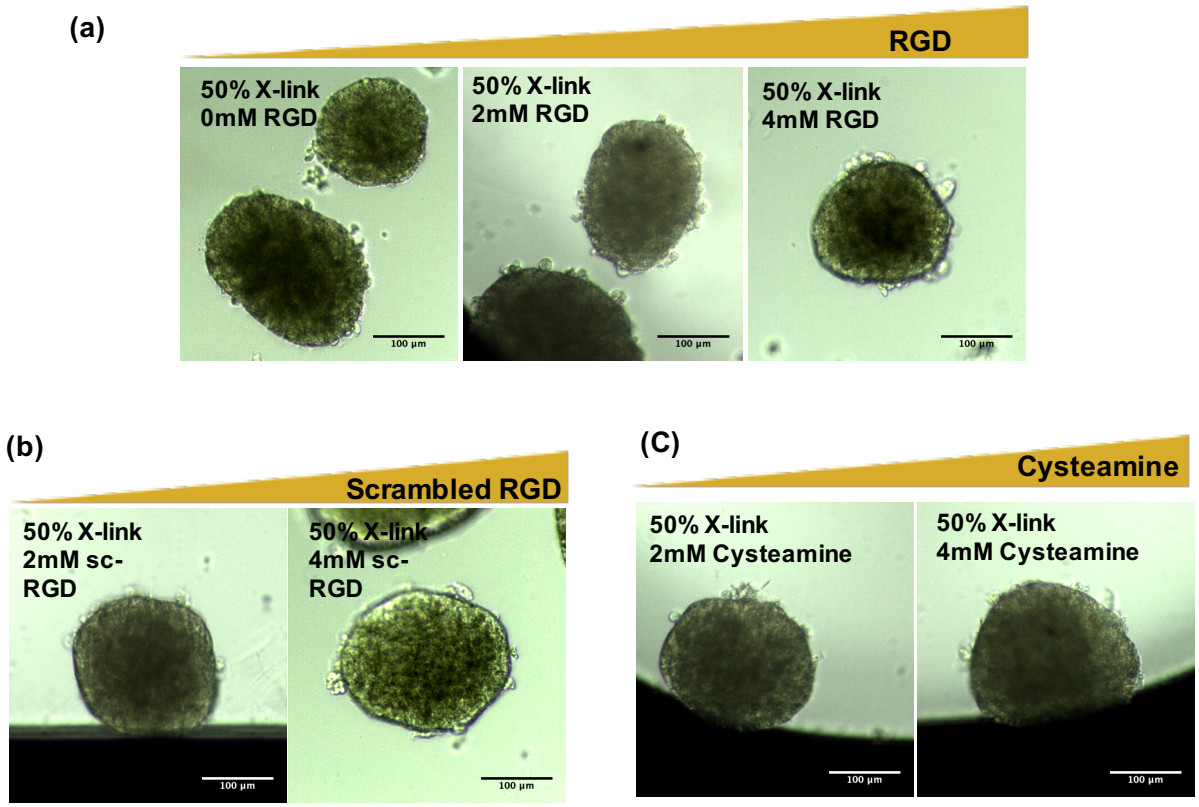

Figure S6.3 Effect of integrin binding peptide concentration on iHEP aggregate morphology. (a) Gross morphology of encapsulated iHEP aggregates in hydrogels with 50% crosslinking density at 0, 2 and 4 mM RGD concentration. **(b-c) Effect of non-integrin binding peptide (controls) concentration on iHEP aggregate morphology. (b)** Morphology of encapsulated iHEP aggregates in hydrogels with 50% crosslinking density at 2 and 4 mM scrambled RGD concentration. **(c)** Morphology of encapsulated iHEP aggregates in hydrogels with 50% crosslinking density at 2 and 4 mM Cysteamine.
Images were taken after 10 days. Scale bar is 100 µm

Chapter 7: Conclusions and recommendations for future work

7.1 Conclusions

Although the advent of iPS/ES-derived hepatocytes in the past decade has helped to bridge the gap between clinical demands and primary human hepatocyte (PHH) availability, those cells exhibit a fetal phenotype rather than a mature phenotype and therefore is not entirely on par with PHH [1]. In order to create the mature iPS derived hepatocytes, we created an in vitro model that can recapitulate the complex 3D structure of the liver during liver development. Creating such in vitro model needs a wholistic approach to encompass all the factors that impact liver organ development. To simplify the problem, we focused on two significant areas known to play an important role on iHEP maturation: (i) cell-cell interaction (both homotypic and heterotypic) (in Chapter 4) and (ii) cell-ECM interactions (in Chapter 5 and 6).

Chapter 4 focuses on the effect of 3D culture and liver non-parenchymal cells on maturation of iPS derived hepatocytes. We show that 3D culture of iPS-derived hepatocytes and their co-culture with human sinusoidal endothelial cells (sECs) to improve their maturity. In addition, co-culture of ECs formed endothelial networks within the hepatic 3D cultures, mimicking aspects of an *in vivo* architecture. Although iHEPs in 3D co-cultured with ECs were significantly more mature than iHEPs in monoculture, they still express fetal markers and do not approach the maturity of adult PHHs. To further promote iHEP differentiation towards the adult PHH phenotype, alternative approaches should be explored, such as stimulation with small molecules or culturing iHEP aggregates in ECMs. The ECM should be supportive of both ECs and iHEPs.

Chapter 5 then describes a chemically defined synthetic PEG hydrogel, that allows iPS-derived endothelial cells to self-assemble into capillary networks through mechanisms consistent with *in vivo* vascular morphogenesis. We showed that capillary tubules with patent lumens were stable for at least 14 days when endothelial cells, without the support of mural cells were encapsulated in PEG hydrogels and were polymerized within a passive flow microfluidic device. This suggests that lack of mural cells does not entirely account for regression of vascular networks in vitro.

Extending the concept of chemically defined synthetic ECM in 3D culture geometries, Chapter 6 described how cross-linking density and integrin binding peptide concentration affect iHEP metabolic function and CYP450 enzyme activity. We showed that PEG hydrogels at 50% crosslinking density with the shear modulus of 785$\pm$40 Pa and no adhesive peptides supports iHEP aggregate metabolic functions and enzyme activities, similar to naturally derived ECM such as Matrigel. Altogether, this thesis describes methods to improve metabolic function and enzyme activity of iPS derived hepatocyte, and highlights how 3D culture, cell-cell and cell-ECM interactions can affect the metabolic function of iPS-derived hepatocytes.

7.2 Recommendations for future work

7.2.1 Understanding the mechanisms through which non-parenchymal cells affect iHEP maturation

The 3D based approach developed in Chapter 4, showed how heterotypic cell-cell interaction can affect the metabolic function and enzyme activity of the iPS-derived hepatocytes. In particular, this approach described how both human sinusoidal endothelial cells and iPS-derived

endothelial cells among all the liver non-parenchymal cells play an important role in maturation of the hepatocytes, however, the mechanisms through which these cells affect iHEP maturation yet to be determined. Future work should specifically aim to understand such mechanisms. Moreover, the aggregate co-cultures described here may be used to evaluate the reciprocal interactions between endothelial cells and iHEPs in physiological and pathophysiological conditions. For example, some drugs like azathioprine are known to be more toxic to sECs, which can lead to downstream effects in PHH cells due to release of apoptotic factors from sECs [1–3]. Our co-cultures have the potential to study such cellular cross-talk during and after drug exposure.

Contrary to ECs, addition of cholangiocytes (CC) to iHEPs resulted in a diminished metabolic activity, urea and albumin secretion, likely because of CC overgrowth and activation. Our data suggests that cholangiocyte containing aggregates become activated. Activation of CCs has been reported in cholestatic liver diseases, such as inherited diseases (Agile syndrome and cystic fibrosis), autoimmune cholangitis, and primary biliary cirrhosis [4–6]. Activated cells typically lose their cell-cell contact and acquire a motile phenotype, similar to what we observed in iHEP/CC aggregates Future study into how CC get activated is critical before using this model for any cholestatic liver disease modeling.

7.2.2 Understanding the mechanisms through which ECM properties affect iHEP metabolic function in 2D versus 3D

The mechanical properties of a cell's surrounding environment play a critical role in modulating cell function [7–14]. In Chapter 6, we evaluated the effect of crosslinking density and integrin binding ligands on metabolic function of iHEP cells in 3D and 2D format. We show that 3D iHEP aggregates encapsulated in PEG hydrogels with 50% cross-linking density behave different than that of single cell iHEP cells seeded on top of the same PEG hydrogels. While iHEP

single cells attach and spread to the PEG substrate that is modified with RGD peptide, the 3D iHEP aggregates did not show any sign of attachment and kept their 3D morphology. Perhaps the increased cell-cell contact in 3D iHEP aggregates can explain such difference. Although considerable progress has been made already to deconstruct the difference between 2D and 3D cell culture, much work remains to shed new light on the complex interplay between materials, mechanics and biological function in 3D versus 2D.

Our study showed that single cell iHEP cells on PEG hydrogels with no adhesive moieties tend to spontaneously self-assemble and form aggregates. Aggregate formation from 2D to 3D on a synthetic ECM provides better imaging capabilities compared to the 3D aggregates and is easier to adapt to automation and high throughput applications. We showed that based on cell seeding density, size of the aggregates differs. Matrigel is widely used as a scaffold for organoid culture [15,16], but varies between batches and is a poorly defined mixture of proteins, including many potent growth factors and extracellular matrix components [17]. In contrast to previous studies, self-assembly of cells into 3D construct occurred on minimally complex PEG hydrogels with only bioactive component being matrix metalloproteinase (MMP)-degradable crosslinker permissive to proteolytic remodeling. Future studies into the effect of synthetic substrate on 3D aggregates formation would be an interesting avenue to pursue.

Moreover, effect of integrin binding peptide on iHEP aggregates function was significant at 30% crosslinking density. Varying crosslinking density alters the mesh size for these networks, which can impact the diffusional properties of the hydrogel [18]. It is not possible to uncouple mechanical properties from diffusional properties examined in this study. Thus, deciphering the complexity surrounding the interplay between matrix mechanical properties and stiffness should be another avenue to explore.

7.2.3 Potential use of microfluidic platform to create perfusable liver-on a chip

Unlike other tissues like cornea and skin that can absorb nutrients and oxygen from their environments by diffusion, liver tissues are highly vascularized and metabolically more demanding, making diffusion insufficient for delivery of nutrients and oxygen to all the cells. In fact, the liver contains more than 100 billion hepatocytes positioned within 50 μm of the sinusoids [19]. Thus, incorporating endothelial cells that can form connected, perfusable vasculature is an important aspect often underscored in developed *in vitro* liver models.

A variety of approaches have been developed to promote vascularization in *in vitro* human liver models. As described in Chapter 2, those approaches can be categorized into three different categories: 1) self-assembled spheroids/organoids, 2) bio-printed livers, and 3) engineered liver tissues or liver-on-a-chip. Our 3D iHEP aggregates cocultured with sECs, described in Chapter 4 displayed endothelial organization into a network of capillary-like structures, reminiscent of liver sinusoids. To the best of our knowledge, this is the first demonstration of self-assembly of endothelial networks within 3D iHEP aggregates. Our aggregates can potentially be integrated with perfusable vascularized networks using microfluidic platforms, which may further improve the nutrient and oxygen delivery to the core of the aggregates and create larger-sized aggregates. The perfusion in such a system would expose endothelial cells to shear stress while protecting the iHEP cells from shear stress, much like an in vivo environment.

Our initial data (Fig. 7.1a, b) on integrating iHEP aggregates with capillary network using a microfluidic device indicate successful engagement of aggregates with capillary networks in Matrigel. However, Matrigel shows sign of degradation after 7-10 days, possibly due to proteolytic enzymes such as MMPs secreted by stimulated ECs and iHEPs [20,21], thus resulted in capillary regression and iHEP aggregate collapse (Fig. 7.1c). Our findings described in Chapter 5 and 6, for

the synthetic PEG based hydrogel that is supportive of capillary network formation (for over 14 days) and metabolic function of iHEP aggregates, lay the ground for an ECM that can substitute Matrigel in the microfluidic platform. We can modify the degradability of the PEG hydrogels by replacing the crosslinker with less degradable crosslinkers to circumvent the early degradation and instability of naturally derived ECM (e.g., Matrigel). Implementing our findings inside a microfluidic platform and the potentials that microfluidics offer should be an avenue for continued research.

Finally, as discussed in Section 2.2.2, liver acinus has three different zones with different oxygen tensions. There are very few *in vitro* liver models that can recapitulate the metabolic zonation and gradient in oxygen tension [20–22]. Such *in vitro* liver models with the ability to recapitulate the complex cellular microenvironment and structural organization of the liver are useful for investigating the role of zonation in physiology, toxicology, and disease progression. Thus, developing such in vitro models should be another avenue for future investigation.

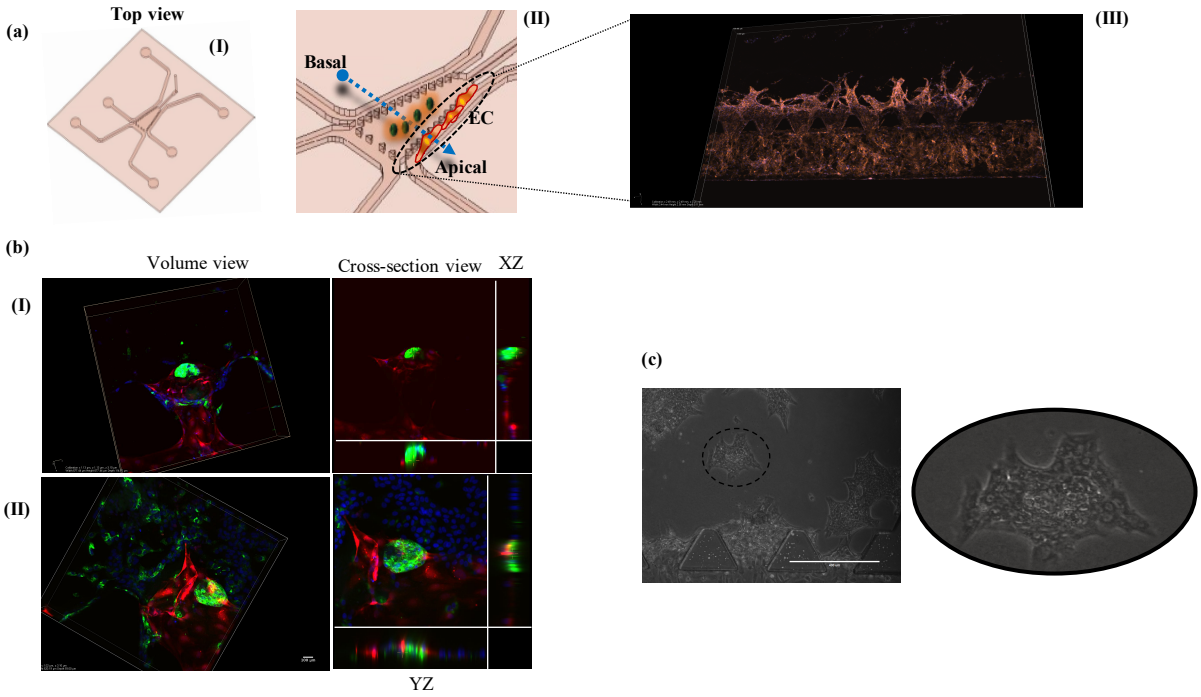

Figure 7.1. Integration of iHEP aggregates with capillary networks inside a microfluidic device (a-I) Top view of microfluidic device **(a-II)** iHEP aggregates and Matrigel are mixed together and injected into the middle chamber of the microfluidic device, endothelial cells are then added to the side channel and device is rotated 90º angle for 10-20 minutes to allow ECs attach to the Matrigel in the middle channel, then basal to apical flow is established in the device by creating hydrostatic pressure **(a-III)** Confocal image of successful capillary network formation and angiogenesis inside the middle chamber **(b)** Successful integration of capillary network (red, mcherry reporter EC line) with iHEP aggregates (green, anti-albumin) **(b-I)** Volume view and cross section view shows ECs' sprouts wrapped around the iHEP aggregates **(b-II)** Volume view and cross section view shows ECs' sprouts perfused inside the iHEP aggregates **(c)** Matrigel degradation in the microfluidic device results in 3D iHEP aggregates collapse and spread like in 2D culture.

7.3 References

[1] Z. Kmieć, Cooperation of liver cells in health and disease, Adv Anat Embryol Cell Biol. 161 (2001) III–XIII, 1–151.
[2] L.D. Deleve, Dacarbazine toxicity in murine liver cells: a model of hepatic endothelial injury and glutathione defense, J. Pharmacol. Exp. Ther. 268 (1994) 1261–1270.
[3] L.D. DeLeve, X. Wang, J.F. Kuhlenkamp, N. Kaplowitz, Toxicity of azathioprine and monocrotaline in murine sinusoidal endothelial cells and hepatocytes: The role of glutathione and relevance to hepatic venoocclusive disease, Hepatology. 23 (1996) 589–599. doi:10.1002/hep.510230326.
[4] S. Priester, Involvement of cholangiocyte proliferation in biliary fibrosis, World Journal of Gastrointestinal Pathophysiology. 1 (2010) 30. doi:10.4291/wjgp.v1.i2.30.
[5] C. Yin, K.J. Evason, K. Asahina, D.Y.R. Stainier, Hepatic stellate cells in liver development, regeneration, and cancer, Journal of Clinical Investigation. 123 (2013) 1902–1910. doi:10.1172/JCI66369.
[6] G. Xie, A.M. Diehl, Evidence for and against epithelial-to-mesenchymal transition in the liver, AJP: Gastrointestinal and Liver Physiology. 305 (2013) G881–G890. doi:10.1152/ajpgi.00289.2013.
[7] R.G. Wells, The role of matrix stiffness in regulating cell behavior, Hepatology. 47 (2008) 1394–1400. doi:10.1002/hep.22193.
[8] R.G. Wells, Cellular Sources of Extracellular Matrix in Hepatic Fibrosis, Clinics in Liver Disease. 12 (2008) 759–768. doi:10.1016/j.cld.2008.07.008.
[9] D.E. Discher, Tissue Cells Feel and Respond to the Stiffness of Their Substrate, Science. 310 (2005) 1139–1143. doi:10.1126/science.1116995.
[10] D. Mitrossilis, J. Fouchard, D. Pereira, F. Postic, A. Richert, M. Saint-Jean, A. Asnacios, Real-time single-cell response to stiffness, Proceedings of the National Academy of Sciences. 107 (2010) 16518–16523. doi:10.1073/pnas.1007940107.
[11] M. Cavo, M. Fato, L. Peñuela, F. Beltrame, R. Raiteri, S. Scaglione, Microenvironment complexity and matrix stiffness regulate breast cancer cell activity in a 3D in vitro model, Scientific Reports. 6 (2016). doi:10.1038/srep35367.
[12] V. Natarajan, E.J. Berglund, D.X. Chen, S. Kidambi, Substrate stiffness regulates primary hepatocyte functions, RSC Advances. 5 (2015) 80956–80966. doi:10.1039/C5RA15208A.
[13] S. Nasrollahi, C. Walter, A.J. Loza, G.V. Schimizzi, G.D. Longmore, A. Pathak, Past matrix stiffness primes epithelial cells and regulates their future collective migration through a mechanical memory, Biomaterials. 146 (2017) 146–155. doi:10.1016/j.biomaterials.2017.09.012.
[14] A.M. Cozzolino, V. Noce, C. Battistelli, A. Marchetti, G. Grassi, C. Cicchini, M. Tripodi, L. Amicone, Modulating the Substrate Stiffness to Manipulate Differentiation of Resident Liver Stem Cells and to Improve the Differentiation State of Hepatocytes, Stem Cells International. 2016 (2016) 1–12. doi:10.1155/2016/5481493.
[15] T. Takebe, R.-R. Zhang, H. Koike, M. Kimura, E. Yoshizawa, M. Enomura, N. Koike, K. Sekine, H. Taniguchi, Generation of a vascularized and functional human liver from an iPSC-derived organ bud transplant, Nature Protocols. 9 (2014) 396–409. doi:10.1038/nprot.2014.020.

[16] M.A. Lancaster, J.A. Knoblich, Organogenesis in a dish: Modeling development and disease using organoid technologies, Science. 345 (2014) 1247125–1247125. doi:10.1126/science.1247125.
[17] C.S. Hughes, L.M. Postovit, G.A. Lajoie, Matrigel: a complex protein mixture required for optimal growth of cell culture, Proteomics. 10 (2010) 1886–1890. doi:10.1002/pmic.200900758.
[18] L.M. Weber, C.G. Lopez, K.S. Anseth, Effects of PEG hydrogel crosslinking density on protein diffusion and encapsulated islet survival and function, J. Biomed. Mater. Res. 90A (2009) 720–729. doi:10.1002/jbm.a.32134.
[19] R.P. Visconti, V. Kasyanov, C. Gentile, J. Zhang, R.R. Markwald, V. Mironov, Towards organ printing: engineering an intra-organ branched vascular tree, Expert Opinion on Biological Therapy. 10 (2010) 409–420. doi:10.1517/14712590903563352.
[20] G. Taraboletti, S. D'Ascenzo, P. Borsotti, R. Giavazzi, A. Pavan, V. Dolo, Shedding of the Matrix Metalloproteinases MMP-2, MMP-9, and MT1-MMP as Membrane Vesicle-Associated Components by Endothelial Cells, The American Journal of Pathology. 160 (2002) 673–680. doi:10.1016/S0002-9440(10)64887-0.
[21] S.R. Calabro, A.E. Maczurek, A.J. Morgan, T. Tu, V.W. Wen, C. Yee, A. Mridha, M. Lee, W. d'Avigdor, S.A. Locarnini, G.W. McCaughan, F.J. Warner, S.V. McLennan, N.A. Shackel, Hepatocyte produced matrix metalloproteinases are regulated by CD147 in liver fibrogenesis, PLoS ONE. 9 (2014) e90571. doi:10.1371/journal.pone.0090571.
[22] J.W. Allen, In Vitro Zonation and Toxicity in a Hepatocyte Bioreactor, Toxicological Sciences. 84 (2005) 110–119. doi:10.1093/toxsci/kfi052.
[23] F.T. Lee-Montiel, S.M. George, A.H. Gough, A.D. Sharma, J. Wu, R. DeBiasio, L.A. Vernetti, D.L. Taylor, Control of oxygen tension recapitulates zone-specific functions in human liver microphysiology systems, Experimental Biology and Medicine. 242 (2017) 1617–1632. doi:10.1177/1535370217703978.
[24] X. Li, S.M. George, L. Vernetti, A.H. Gough, D.L. Taylor, A glass-based, continuously zonated and vascularized human liver acinus microphysiological system (vLAMPS) designed for experimental modeling of diseases and ADME/TOX, Lab on a Chip. 18 (2018) 2614–2631. doi:10.1039/C8LC00418H.